Chemical Engineering Approaches to the Fabrication of Uniform Polymeric Particles and Structures

Alroaithi, Mohammad Sami

Awarding institution:
King's College London

KING'S College LONDON

University of London

Chemical Engineering Approaches to the Fabrication of Uniform Polymeric Particles and Structures

by

Mohammad Sami Alroaithi

A thesis submitted in fulfilment of the requirements for the degree of Doctor of Philosophy in Chemical and Process Engineering

to

KING'S COLLEGE LONDON

OCTOBER 2017

Declaration of Authorship

I, Mohammad S. Alroaithi, declare that this thesis, titled " Chemical Engineering Approaches to the Fabrication of Uniform Polymeric Particles and Structures", and the work presented in it are my own, and that the word limit prescribed in the College regulations is not exceeded. I further confirm that where I have consulted or quoted from the published work of others, this is always clearly attributed and referenced accordingly.

Sign: _____ 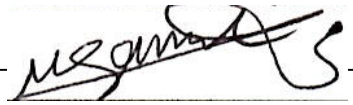 _____

Date:
_____12/10/2017_____

﴿ وَفَوْقَ كُلِّ ذِي عِلْمٍ عَلِيمٌ ﴾

Acknowledgements

In the name of Allah, the Most Gracious, the Most Merciful. All praise is due to Allah for the strength he has granted and blessed me with in allowing me to complete this thesis.

First of all, I would like to acknowledge my debt to everyone at King's College London and elsewhere whom have assisted, taught and helped me acquire a greater knowledge base in order to write this doctoral thesis in chemical engineering. First and foremost, I pay my deepest gratitude and respect to Dr. Shahriar Sajjadi for his patience, motivation, encouragement and immense knowledge. I have been extremely fortunate to have known Dr. Sajjadi who cared and gave me a greater insight into the subject, responded to my questions and queries so promptly throughout my time as his student.

I also would like to extend my thanks and gratitude to Dr. Ankur Chaurasia for the insightful discussions during this research. Special thanks and appreciations are also extended to the two senior technicians Mr. Julian Greenberg and Mr. William Luckhurst for their highest level of technical support and extraordinarily response in resolving issues that arose during my research.

I also gratefully acknowledge the generous financial sponsorship provided by the government of Saudi Arabia during the past four years to be able to complete this research in its current form.

And, my heartiest thanks and appreciation go to all members of my family and friends, where the completion of this thesis would not have been accomplished without their support, especially my patents whose constant love, support and guidance are with me in wherever I am.

Last, but in no way least, my deepest immense gratitude goes to my beloved wife Ebtihal for her endless love, care, prayers and encouragement. I also must not forget to appreciate the great comfort to know that you were willing to manage our household activities while I have been continuously distracted with my work. Your reminders that I should stop playing with Tamim and do some works are appreciated. My heartfelt thanks.

Mohammad S. Alroaithi

Abstract

This thesis aims to investigate different approaches to fabricate well-defined and uniform polymeric materials, with sizes ranging from micrometre to nanometre.

We first developed a simple approach via which the size of polymer microparticles resulting from conventional suspension polymerisation could be satisfactorily controlled. The approach employed a two-stage stirring protocol in which a conventional emulsification was conducted in the first stage at a higher agitation speed, followed by polymerisation at reduced stirring speed. The proposed policy led to the formation of more uniform particles, depending on the stabiliser concentration, than those obtained from the one-stage conventional method.

The two-stage stirring protocol was extended to include membrane emulsification as the precursor to polymerisation. The use of a stirred-vessel membrane emulsification, by which the size of drops could be controlled with more accuracy, followed by a shear-controlled suspension polymerisation significantly improved the uniformity of products. The effects of various governing parameters in membrane emulsification, such as the feeding policy, stirring speed, stabiliser concentrations, and flowrates were studied in order to find the optimum conditions under which the one-to-one copy of the initial drops and polymer microparticles could be achieved.

In the next stage, both emulsification and polymerisation stages were replaced by the state of art microfluidics and UV polymerisation, respectively, to produce complex microparticles with highly ordered and well-defined interconnected windows. Uniform water/oil/water (w/o/w) double emulsion, with controlled number of inner water droplets, was first produced and then used as precursor before it was consolidated into porous

microparticles through UV photopolymerisation. The sizes and number of cores, porosity and the morphology of the porous microparticles were precisely tuned by the flowrate, confinement offered by the geometry of the channel and packing structure of the inner droplets.

The study was then extended to fabricate 3D porous structures known as polyHIPE. Uniform w/o, in which the internal phase ratio (water phase) occupies more than 74.05% of the total volume of the emulsion, was produced by co-flow microfluidics device. A centrifugal-step was also attempted to further increase the phase ratio and thus the resultant porosity of the structure. Polymerisation of the external oil phase resulted in the formation of open polyHIPE structures with distinctive morphology and porosity.

The final aim of this thesis was to synthesis uniform polymer nanoparticles with a high solids content. Emulsifier-free emulsion polymerisation was chosen as the technique, but a mixture of acetone and water was used as the reaction media to increase the solubility of the monomer phase. The particle size, number of particles and the uniformity were controlled by the concentration of acetone as well as the monomer concentrations. The combined effects of co-monomer and acetone were also investigated and sub-100nm uniform nanoparticles with high solids content were obtained.

Table of Contents

List of Figures

Nomenclature

CHEMICAL COMPONENTS

Abbreviation	Component
DVB	Divinylbenzene
EHA	2-Ethylhexyl acrylate
HDODA	1, 6 Hexanediol diacrylate
IBOA	Isobornyl acrylate
KCl	Potassium chloride
KPS	Potassium persulfate
LPO	Lauryl peroxide
MMA	Methyl methacrylate
NaSS	Sodium p-styrenesulfonate
PDMS	Poly(dimethylsiloxane
PEG-PPG-PEG	Poly (ethylene glycol)-block-poly (propylene glycol)-block-poly (ethylene glycol)
PMMA	Poly(Methyl methacrylate
PS	Polystyrene
PTFE	Polytetrafluoroethylene
PVA	Poly (vinyl alcohol)
SDS	Sodium dodecyl sulfate
St	Styrene
TMPTA	Trimethylolpropane triacrylate

GENERAL NOTATIONS

Symbol	Meaning
A	Area
CMC	Critical Micellar Concentration
CV	Coefficient of Variation
D	Diameter
D_v	Volume average diameter
D_{32}	Sauter- mean diameter
DSD	Droplet Size Distribution
DLS	Dynamic Light Scattering
d_{min}	Minimum stable drop size
d_{max}	Maximum stable drop size
d_w	Size of the window
EFEP	Emulsifier-free emulsion polymerisation
F	Force
ε	relative magnitude of opening area on the surface
ϕ	Phase ratio
f	Asphericity
GPC	Gel permeation chromatography
HIPE	High Internal Phase Emulsion
I	Initiator
γ	Interfacial tension
k	Reaction Rate Constant
ω	Rotational speed

L	Length
m	Mass
M	Monomer
M_c	Co-monomer
MDC	Micropore Dispersion Cell
n	Number of pore
N	number of drops/particles counted
N_A	Avogadro number.
N_p	number of particle
NPs	Nanoparticles
ρ	Density
PDI	Polydispersity index
P	Plug-like shapes
PSD	Particle Size Distribution
Q	Volumetric flowrate
RCF	Relative Centrifuge Force
r	Radius
R^*	Radicals
R_c	Rate of coalescence
R_b	Rare of break-up
R	Reaction rate
τ	Shear stress
σ	Standard deviation
Surfactant	Surface active agent
SPG	Shirasu Porous Glass

S	Spherical
SS	Semi-spherical
SEM	Scanning Electron Microscope
SCFM	Stirred Vessel Membrane Emulsification
t_f	Droplet formation time
T	Temperature
TEM	Transmission Electron Microscopy
μm	Micrometre
η	viscosity
v	velocity
UV	Ultraviolet

Chapter 1 Introduction

1.1. OVERVIEW

Polymers, which are large molecules of repeating subunits known as monomers, shape up a wide range of materials around us and have become an integral part of our everyday lives. The field of polymer science is rapidly expanding and playing a vital role in a variety of areas ranging from catalyst, medicine, and pharmaceutical, biotechnology, conducting materials, environmental technology and many other applications. The polymer materials, which may readily occur in nature or be artificially synthesised, exist in a wide range of shapes, sizes and compositions. These include solid/porous spherical particles, microcapsules, 2D-sheets and 3D-structures. However, polymeric particles have particularly been the focus of an intensive research since the beginning of the 20th century due to their numerous applications. The term 'particle' usually refers to an individual chunk of polymer, having a small aspect ratio, which can vary in shape and composition. Great efforts and advances have been engaged in researching, modelling and testing to synthesise polymer particles in a convenient, simple and reproducible manner at relatively large quantities in order to comply with the increase in demand of polymer particles.

In general, polymer particles are conventionally synthesised by a family of different polymerisation techniques such as suspension, dispersion, conventional emulsion, microemulsion, miniemulsion, and precipitation polymerisation [1]. Each approach aims to produce polymer particles with different physical and chemical properties. For example, particles in nanometre scale are used for applications such as adhesives, binders, plastic pigments, coatings, rubbers as well as polymeric supports for the purification of proteins [2,3,4,5], whereas polymeric particles with larger diameter (10-1000μm) are

ideal for ion exchange resins [6,7]. It is, therefore, very crucial to choose the appropriate approach for obtaining polymeric particles that fulfil the requirement of a certain application. Nowadays, obtaining highly uniform polymeric particles are progressively becoming an interesting area of research due to their outstanding performance in applications including drug delivery [8,9], disease diagnoses, chromatography [10,11], biotechnology and other medical and pharmaceutical applications [12]. Ever since, researchers have been developing various approaches to synthesise well-defined polymer particles that are uniform in size and shape. The importance of particles being uniform is to determine the physical and chemical properties, dealing with stability and dynamic behaviour of individual particles of the particular system and correlate it as a one unit.

With increasing attention focused on preparation of polymer particles, many methods are still being developed that can produce polymer particles of uniform size. Herein, a state of art will be engineered to diminish the margin for further improvements in the preparation of uniform polymer particles that best suits the purpose of the specific needs.

1.2. RESEARCH OBJECTIVES

Although intensive and extensive studies have been done in the preparation of polymer particles, this thesis aims to narrow the research gap and conduct empirical research toward obtaining uniform polymeric particles within nano to micro scale. The reasons behind undertaking this project is the importance of the uniform polymeric materials in various applications. The main aim of this research will be accomplished by fulfilling the following research objectives:

a) Review the literature concerning all emulsification and polymerisation techniques that can be employed to obtain polymeric particles.

b) Investigate various polymerisation techniques to obtain well-defined uniform polymer particles, with different sizes ranging from nanometre to micrometre.

c) Identify if any alterations or improvements are required to further maximise the particles uniformity or creating different polymeric structures.

1.3. THESIS STRUCTURE

The current Chapter 1 is presented to give an overview, motivation and the main objectives of the work. Chapter 2 covers an extensive literature review to describe and compare emulsification and polymerisation approaches to synthesis polymer particles. Furthermore, the review would highlight the fundamentals and development of the ultimate microfluidics approach and how is integrated to fabricate uniform and more complex forms of microparticles

Chapter 3 describes materials, equipment set-up and polymerisation techniques used to fabricate a wide range of polymeric materials, along with their characterisation techniques.

Chapter 4 considers the feasibility of improving the uniformity of polymer particles, within the means of conventional suspension polymerisation, by developing a two-stage stirring protocol. This chapter includes some fundamental understanding of liquid-liquid dispersion and how stirring is related to drop/particle size and size distribution. The effects of different stabiliser concentrations and stirring speeds were also investigated.

Chapter 5 focuses on obtaining uniform polymer microparticles by membrane emulsification-assisted suspension polymerisation. Highly uniform droplets were produced by a stirred-vessel membrane emulsification device followed by a shear-controlled suspension polymerisation. The effects of various process parameters

including feeding policy, agitation speed, stabiliser concentration, and flowrate were examined.

Chapter 6 introduces a microfluidics approach for the fabrication of uniform porous microparticles with highly ordered and well-defined interconnected windows. Three different porous microparticles shapes, defined based on the shape of the external drop, namely spherical, semi-spherical and plug-like shape, are presented. The effect of flow conditions on the size and number of cores, porosity, shapes and structures of the microparticles, is also explored. The formation mechanism of windows, during polymerisation, is investigated.

Chapter 7 aims to extend the use of microfluidics technique to fabricate 3D- porous structures with a well-defined morphology. A wide range of relative centrifuge force is explored in attempt to increase the phase ratio of HIPE and thus the porosity of the resultant polyHIPE structures.

Chapter 8 considers emulsifier-free emulsion polymerisation (EFEP) approach to obtain uniform nanoparticles with a high solids content. The addition of solvent and ionic comonomer on the kinetic of emulsifier-free emulsion polymerisation is investigated.

Chapter 9 presents the key points derived from the thesis and provide some recommendations and suggestions for future research.

Chapter 2 Literature Review

This chapter presents a review of the literature concerning emulsification and polymerisation methods used to produce uniform polymeric materials, providing background information about this research. Moreover, it will shed light on the recent advances in microfluidics in developing a wide range of polymeric materials. The governing parameters to achieve this goal, such as the role of surfactants, are discussed first.

2.1. BACKGROUND

The fabrication of almost any polymer particle starts when two immiscible liquids are brought into contact with each other [13]. When the liquid-liquid system is agitated, the single-liquid drops (known as a dispersed phase) will be dispersed in the other liquid medium (continuous phase) to form emulsions, namely oil-in-water (o/w) or water-in-oil (w/o). This is the simplest type of emulsions and are usually referred to as "single emulsion". The emulsion can also be produced in different forms, such as double or triple emulsions. Double emulsion is a more complex form of an emulsion and is obtained when the single emulsion is dispersed into a third liquid phase, which can either be o/w/o or w/o/w. Higher-order emulsions such as w/o/w/o or w/o/w/o/w can also be obtained by further repeating the process steps. Figure 2.1 shows the schematic illustration of a typical preparation of emulsions. The stability of the emulsion, which refers to the ability to resist changes in the emulsion's physicochemical properties over a period of time, is a responsible factor for controlling the final structure of the polymer particles. Emulsions are thermodynamically unstable and there are many instability phenomena that might modify the properties of the emulsion and thus the resulting polymer material.

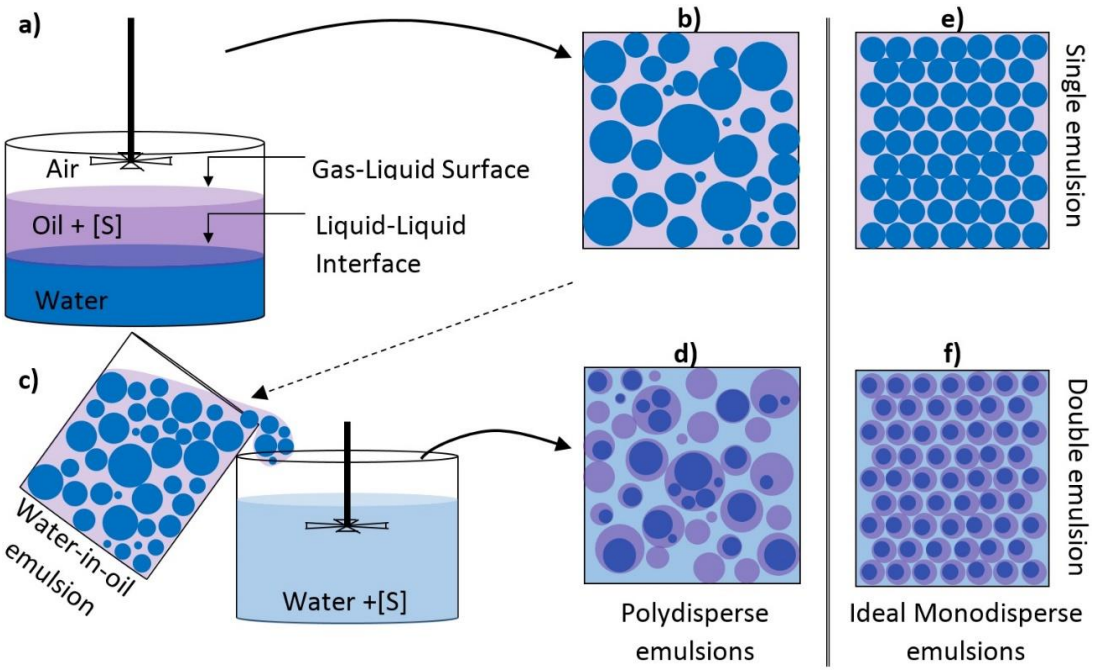

Figure 2.1 **a)** The schematic represents the formed gas-liquid and liquid-liquid interfaces when a layer of oil is added on top a water phase. When this oil-water system is agitated, it results in the formation of a polydisperse, single (water-in-oil) emulsion **b). c)** The single emulsion can be dispersed into a third aqueous phase to obtain a non-uniform double emulsion. **e)** and **f)** depict the ideally monodisperse single and double emulsions, respectively. Reprinted with permission from ref. [14].

Therefore, the addition of a surface active agent (*surfactant*), emulsifier or stabiliser is a key to obtain a stable emulsion [15]. The surfactant is a third component which adsorbs at the interface between the two phases and helps to reduce the surface tension of a liquid in which it is dissolved. Typical surfactant molecules consist of two parts: head (hydrophilic) and tail (hydrophobic) (see Figure 2.2a). One part is attracted to the dispersed phase (oil) while the other part attracts the continuous phase (water), which cover the surface of the dispersed-phase droplets, formed by mixing, to suppress the destabilisation of the emulsion [16]. Surfactant concentration is also another factor to consider when preparing an emulsion. Figure 2.2b shows a schematic illustration on how the surfactant concentration alters the surface tension.

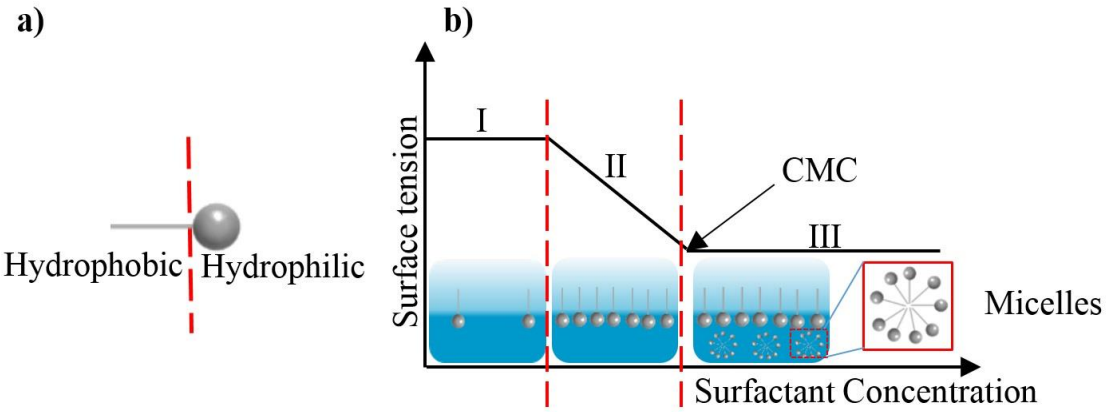

Figure 2.2 **a)** Structure of the amphiphilic molecule. **b)** Surface tension against surfactant concentration (logarithmic scale).

At a very low surfactant concentration, the surfactant molecules arrange on the surface and result in a slight, or no, decrease in surface tension (**Stage I**). At a moderate addition of surfactant (**Stage II**), as shown in Figure 2.2b, more molecules will be adsorbed at the interface which helps to rapidly decrease the surface tension. Further increase in the surfactant concentration, beyond which the interface becomes fully saturated by the surfactant molecules, does not change surface tension. This point in surface chemistry is known as critical micellar concentration (CMC) [17]. CMC is the concentration above which the surfactant molecules self-aggregate and arrange themselves in different geometries to form *micelles (***Stage III**). The knowledge of CMC is practically important as the addition of more surfactant above CMC may have an effect on the properties of the continuous phase, like viscosity [18]. Micelles should also be avoided in some polymerisation techniques because they can act as the locus of micellar nucleation [19,20].

There are three different classes of surfactants that can be used to stabilise the emulsions including anionic (negative charge), cationic (positive charge) and non-ionic surfactants. An ionic surfactant, such as sodium dodecyl sulfate (SDS), has the functional group at

the head. Therefore, when two drops approach each other, a repulsive force occurs due to the charges at both drops interface. Nonionic surfactants, such as polymeric surfactants, have also shown to be a promising choice to stabilise the emulsion. For nonionic surfactants, the stability of the drops is achieved via ‘steric effects’.

Figuring out what surfactant to use that best suits the purpose, could be a major challenge. William C. Griffin developed a very useful tool to characterise the surfactant based on the ratio of the hydrophobic to the hydrophilic amount of the molecule [21]. This system is referred to as Hydrophile Lipophile Balance, (HLB) number. The HLB number of a surfactant is directly related to its solubility. Surfactants having low HLB values (typically between 4-6) indicate a good solubility in non-polar systems, such as oil, which assists the stabilisation of w/o emulsions. In contrast, high HLB values (typically between 8-18) are indicative of a great solubility in water or any other polar solvent, which tends to stabilise o/w emulsions.

There are many forms of emulsion instability including coalescence, creaming/sedimentation, flocculation, phase inversion and Ostwald ripening, that result from the absence of surfactant, little surfactant or poor mixing. The various mechanisms of emulsion instability, as named above, are schematically presented in Figure 2.3. One of the most common breakdown phenomena of the emulsion is coalescence, which refers to the process when two or more drops merge to form a larger drop [22]. Creaming and sedimentation is a result of an external force (gravitational or centrifugal), making the droplets move more rapidly either to the top or to the bottom depending on the density differences between the two phases [23].

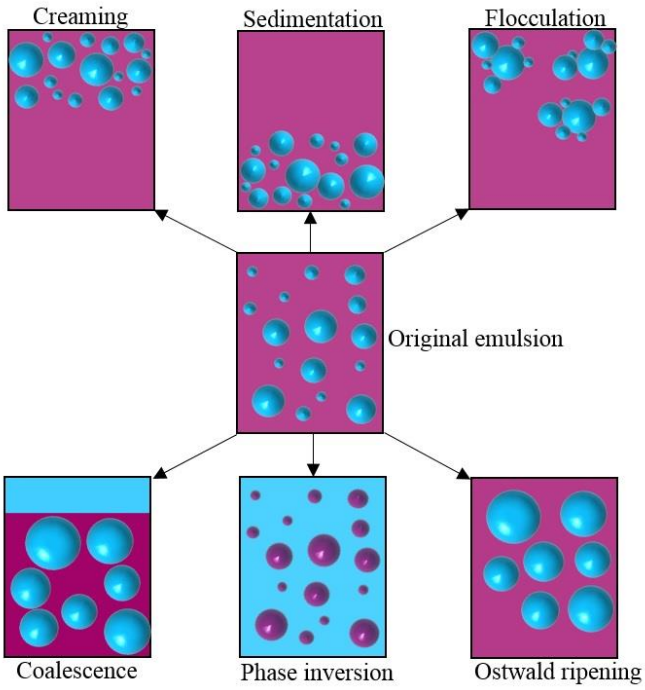

Figure 2.3 Breakdown phenomena of emulsion.

The aggregation of droplets into large unit, without any change in the initial droplet size, is called flocculation, which occurs when there is no enough repulsion to keep the droplets separate. Phase inversion is characterised by an exchange or inversion between the two phases, for example, o/w emulsion may become w/o emulsion with time. Ostwald ripening, in the case of non-uniform drops, is when smaller droplets migrate toward the larger drop, shifting the drop size distribution to large values [24].

The aim of this chapter is not to give an exhaustive description of surfactants and their behaviours. However, it was very useful to have a brief overview of surfactant types, characterisations and mechanisms of emulsion instability that could potentially be used or observed, throughout this research.

2.2. FABRICATION OF MICROPARTICLES

The term ‘microparticle’ refers to a particle with a diameter of micrometre range (typically 1-1000 μm). The preparation of polymer microparticles starts with an

emulsification process. The emulsification process can significantly affect the kinetics of polymerisation, as well as the properties of resulting microparticles such as the size and uniformity. Hence, it is essential to choose the appropriate techniques to obtain polymer microparticles that comply with the applications required. The following sub-headed sections are intended to describe the most common emulsification and polymerisation approaches that are used to make polymer microparticles.

2.2.1 Emulsification techniques

2.2.1.1. Conventional techniques

Traditionally, an emulsion is prepared by mechanical disruption of the disperse phase into the continuous phase. Stirred vessel, colloidal mill, homogeniser, static mixer or high pressure are among the most common types of emulsion preparation, due to their high throughput (see Figure 2.4) [25]. While these conventional techniques are capable of yielding a large output, they require a significant amount of energy and suffer from a high mechanical stress. The major drawback of these approaches is also the ability to control the drop size and uniformity which might cause an adverse effect on the end product. This is because the emulsion is forced through a different region of shear and thus the resulting emulsion is polydisperse. [26,27]. It also encounters several issues including foaming, alteration of product hardness and the requirement of subsequent purification [2]. In Chapter 4 we will investigate methods using stirred vessel, which is mainly used in the industry, to improve the uniformity of drops and therefore polymer microparticles.

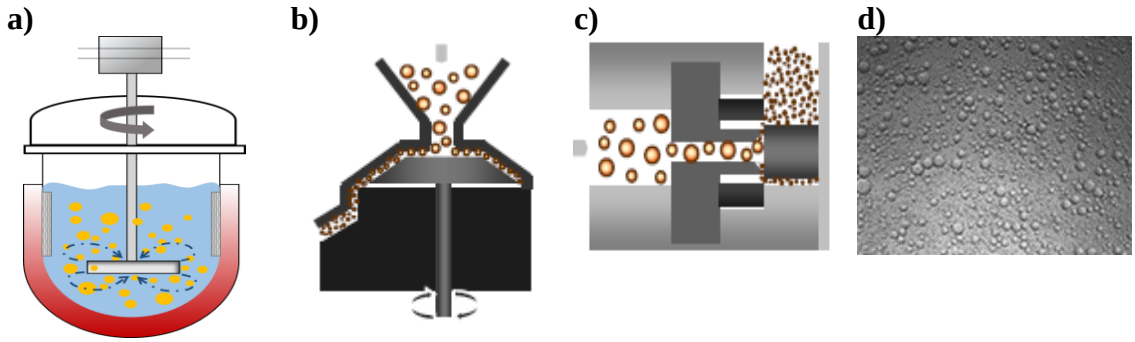

Figure 2.4 Schematic illustration of **a)** Stirred vessel, **b)** Colloidal mill; **c)** High pressure homogeniser and **d)** micrograph image shows drops produced by a conventional technique.

2.2.1.2. Membrane emulsification

To overcome issues encountered with the conventional techniques, it is necessity to develop techniques to control the drop size and uniformity. Microstructured systems, such as membrane emulsification, are examples of techniques built to have a better control over the drop size and uniformity. In membrane emulsification, the dispersed phase is passed through the uniform pores of microporous membrane into the continuous phase. The drops then grow at the pore and detach after reaching a certain size. The formation of drops is determined by the balance between cohesive and detaching forces. Several parameters, such as emulsion formulation, hydrodynamic condition and pore size are key to controlling the drop size and size distribution [28,29,30]. In addition to this, the surface treatment is also important; for example a hydrophilic membrane is used to produce oil-in-water (o/w) emulsion whereas a hydrophobic membrane is required for water-in- oil (w/o) emulsion.

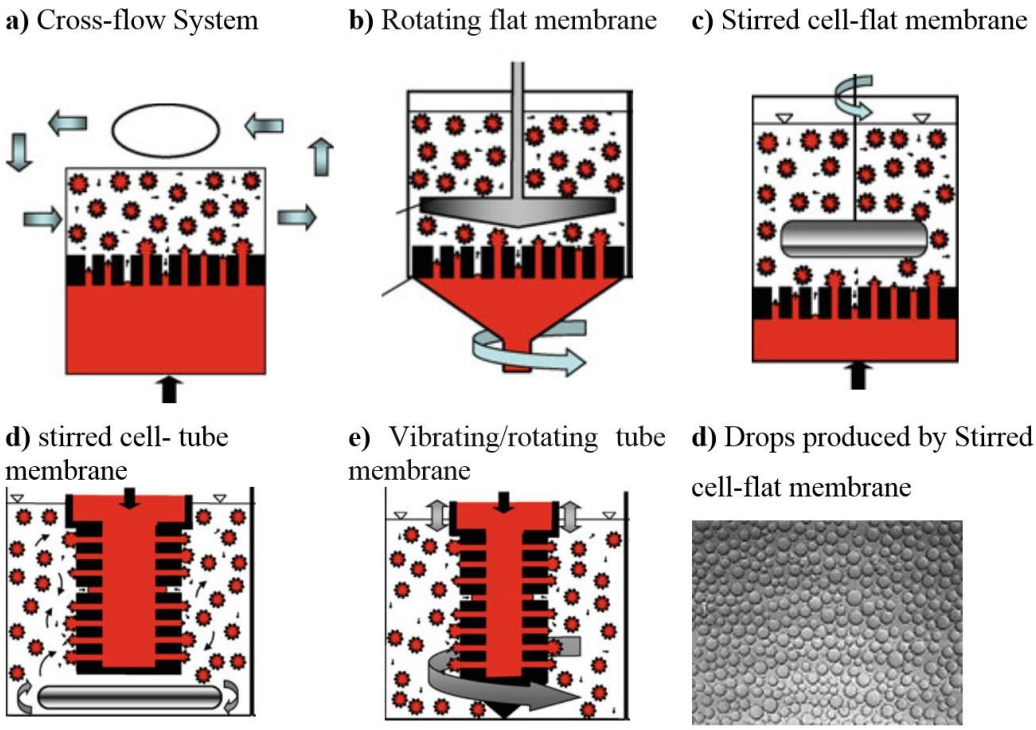

Figure 2.5 several membrane emulsification techniques.

There are numerous membrane emulsification devices, as shown in Figure 2.5, such as cross flow system, rotating flat membrane, stirred cell-flat membrane, stirred cell- tube membrane, and vibrating/rotating tube membrane. A cross flow system (Figure 2.5a), more commonly known as SPG (Shirasu Porous Glass), is the first type of membrane emulsification that was developed in 1981. In such a system, the shear stress is generated by the cross pump to recirculate the flow at the surface of the membrane [28]. While cross-flow systems benefit from a constant shear stress at membrane surfaces and a reliable scale-up [28], they suffer from complexity. It has always been a trend in industry to use one of the common stirring systems as they are easier to operate and much simpler to apply a moderate control of the drop size and size distributions. It is also believed that they overcome many of the disadvantages associated with cross-flow system, such as the purification after each experiment and the cost of maintenance [27,31,32].

In the rotating membrane system (see Figure 2.5b), there is no a detachment force as the shear stress applied is only to transfer the droplet away from the module. This is controlled by the frequency of membrane oscillation or by the speed of rotation of membrane [33]. Moreover, vibrating membranes and vibrating tubular membranes (Figure 2.5d and Figure 2.5e) have also been designed to control the drop size and improve the degree of uniformity [34].

On the other hand, Kosvintsev [29] modified a Weissenberg 'plate and cone' rheometer to obtain uniform droplets. The impervious plate underneath the cone was replaced by the membrane to allow the dispersed phase to pass through the pore into the continuous phase. Uniform drops were produced under a constant shear stress. This approach was compared when a simple paddle-stirred cell was used instead. It has been proved that, the degree of uniformity was similar to that obtained by the modified Weissenberg rheometer under the same operating conditions [29].Therefore, it was concluded that using a paddle-stirred cell was much simpler and more reliable (see Figure 2.5c). This is the most recent type of membrane emulsification that has received increasing attention as a viable alternative to other membrane emulsification systems. We leave a detailed discussion on paddle-stirred cell membrane emulsification for the synthesis of the uniform of polymer particles to Chapter 5.

2.2.1.3. Microfluidic-based technique

Microfluidic approach is defined as a technique to process and produce a monodisperse emulsion in a microchannel that has at least one dimension in sub-millimetre scale [35]. The science behind microfluidics has received extensive attention in recent years due to its precise control over the drop size as well as the achievement of producing highly monodisperse emulsions with a coefficient of variation (CV) as low as 3% [35].

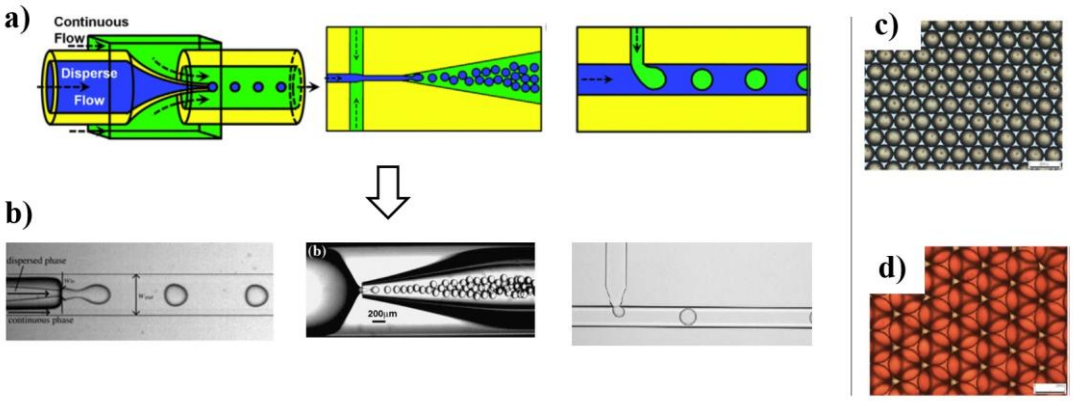

Figure 2.6 **a)** Schematic illustration of the microfluidic devices for the generation of uniform single emulsion, (from left to right), co-flow; flow-focusing and T-junction geometries, respectively. **b)** Optical images showing the single drop formation flowing inside the microchannel for each system. **c)** and **d)** Monodisperse o/w and w/o emulsions from microfluidics device, respectively. Scale bars are 200 μm [36].

There are two different types of microfluidics devices; two-dimensional and three-dimensional. The two-dimensional device which is also known as planar microfluidic has channels etched on a substrate which carry the liquid. It also suffers from wetting issues (i.e. the surface property of the device) [37,38]. However, the three-dimensional device is an axisymmetric device that overcomes the issues in planar microfluidics. The device is fabricated by inserting a microcapillary tube (inner channel) which carries the dispersed phase into another capillary. The drop is formed at the tip of the inner channel and is detached by the outer flow. The drop size is controlled by the variation of channel dimensions and the flow rate of both the dispersed and continuous phase. There are three kinds of 3D microfluidic devices depending on the direction and nature in which the continuous phase flows around the drop. It can be co-flow, flow-focus or T-junction as illustrated in Figure 2.6a.

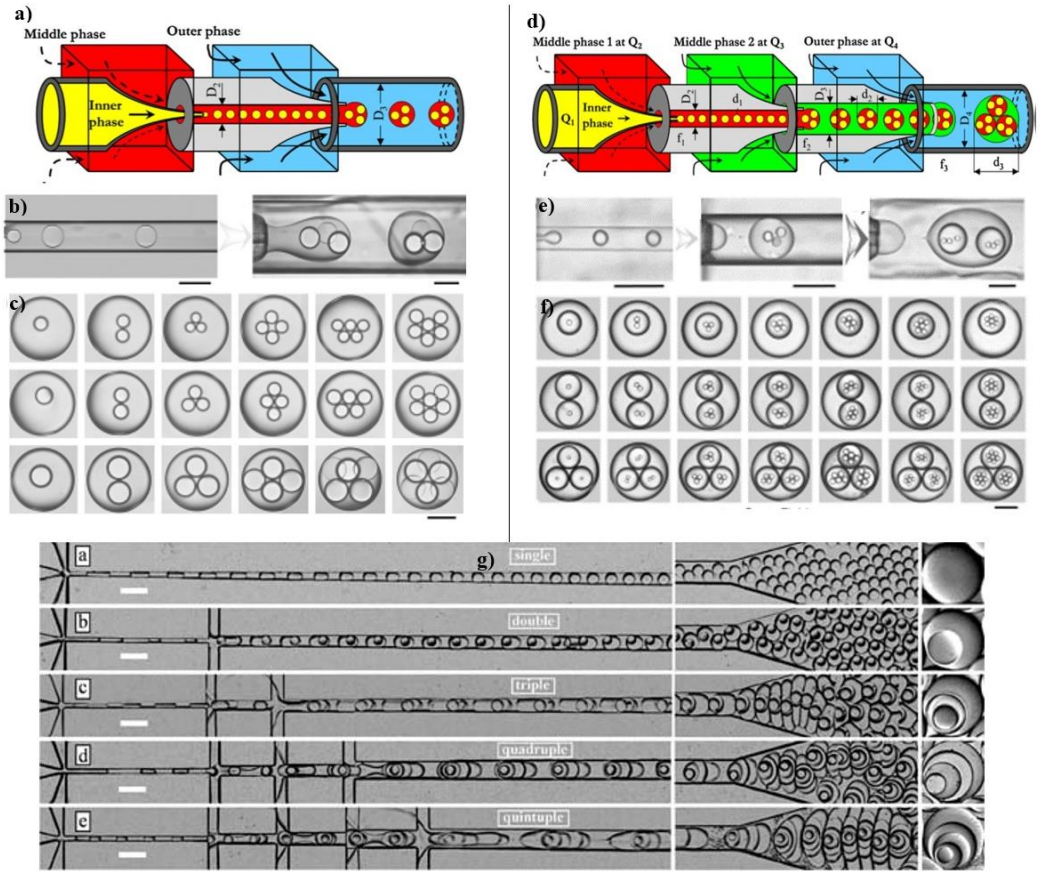

Figure 2.7 a) Schematic illustration of the microfluidic devices for the generation of uniform double emulsions. **b)** and **c)** optical micrograph images show the first and second emulsification stages and the final uniform double emulsions with controlled number of inner droplets, respectively. **d)** Microfluidic devices for the generation of uniform triple emulsions. **e)** and **f)** optical micrograph images show the first, second and third emulsification stages and the final uniform triple emulsions, respectively [39,40]. **g)** The multiple emulsions, with increasing order of complexity, produced by the arrays in a PDMS device [41].

For all types, the drops are detached from the tip with the help of the continuous phase acting as a dragging force. In a co-flow geometry, as shown in Figure 2.6, one fluid flows inside the inner capillary and the outer fluid flows through in the same direction. In contrast to flow-focusing devices, the two fluids are introduced from opposite directions. The inner fluid is focused by the outer fluid through a narrow hole of a tapered glass capillary. Drop formation through a T-junction system, has also been reported.

In 2005, Utada et al [39,40] introduced a microfluidic device to produce uniform double emulsions. In this study, the formed single emulsion was dispersed into a third immiscible liquid, with a controllable number of internal core droplets (see Figure 2.7a). It was observed that the size of the core droplets and the overall drop size were dependent on the flowrates as well as the viscosity ratio of outer and middle phase. They also showed the capability of microfluidics to form a triple emulsion, while maintaining uniformity at all levels. (Figure 2.7b). The production of a triple emulsion was obtained by introducing the double emulsion into another immiscible liquid. Similarly, the number of internal droplets and the drop size were individually controlled by the flow condition of all phases. Even more complex form of emulsion, like quintuple emulsion (five-layered drops), was also reported [41]. The formation of quintuple emulsions, shown in Figure 2.7c, was achieved by forming a stabilised multi-layered compound jet in a PDMS. The surface affinity of the device was desirably modified for the formation of a stable quintuple emulsion.

2.2.1.4. Physics of drops

In the physics of drop formation in microchannel/membrane, there are a number of forces, namely interfacial tension, kinetic, and drag force, acting on a drop during its formation. These forces are divided into cohesive and disruptive forces, which hold the drop to the pore or tip of the capillary and detach the drop from tip of the capillary, respectively. The interfacial tension force, which is the force due to the interfacial tension at the liquid-liquid interface, is a cohesive force and expressed as:

$$F_\gamma = \pi\, d_t\, \gamma \tag{2.1}$$

where γ is the interfacial tension and d_t is the diameter of the tip/pore.

The detaching forces, on the other hand, are the summation of kinetic, buoyancy and drag force.

The kinetic force is defined as:

$$F_k = \rho_i Q_i v_i \quad (2.2)$$

where $\rho_i, Q_i, and\ v_i$ are density, flow rate and velocity of the inner phase ($v_i = Q/A$) , respectively. A is the cross sectional area of the tip which is $\pi d^2/4$, therefore, equ.2 gives:

$$F_k = \rho_i \frac{{Q_i}^2}{A} \quad (2.3)$$

The buoyancy force which is the upward force is calculated by

$$F_B = \Delta\rho\, V g \quad (2.4)$$

where $\Delta\rho$ is the density difference between the continuous phase and dispersed phase and V is the volume of dispersed drop.

The drag force is defined below in terms of Stokes's drag expression:

$$F_d = 3\,\pi\,\eta_c\,\Delta v\,d_d \quad (2.6)$$

where η_c is the viscosity of the continuous phase, Δv is the relative velocity between the drop and the continuous phase, and d_d is the diameter of the droplet.

Several dimensionless numbers are usually used to quantify the relative effect of forces involved in drop detachment process. These dimensionless numbers, namely *Capillary*, *Bond* and *Weber* number are calculated as the ratio of inertia, buoyancy and kinetic force to the surface tension force.

2.2.2 Polymerisation techniques

Following one of the emulsification techniques explained above, the polymerisation process of the resulting emulsion can either be thermal or photo-polymerisation. Both approaches convert the discrete drops into solid polymer particles, mainly through free-radical polymerisation. The following sub-section describes the kinetic of free-radical polymerisation as well as polymerisation techniques to obtain polymer particles within the micrometre range.

2.2.2.1. Kinetic of free-radical polymerisation

The process of free radical polymerisation passes through a sequence of three fundamental reaction steps: *initiation, propagation and termination* [42]. The initiation step involves two reactions. The first one is the decomposition of an initiator (either thermally or photochemically), *I*, to generate a pair of radicals, R^*:

$$I \xrightarrow{k_d} 2R^* \tag{2.7}$$

The second step following the generation of radical is the addition of initiator radical to the first monomer molecules, *M*, to produce a chain radical, *M**.

$$R^* + M \xrightarrow{k_{Pi}} M^* \tag{2.8}$$

where the kinetic parameters k_d and k_{pi} are the decomposition rate constant of initiation and the initial rate constant for the primary radical, respectively. The rate of initiation, R_i, is the same as the rate of initiation decomposition, R_d and it is proportional to the concentration of initiators [I]. Therefore, from equation (2.7) and (2.8) we get the following expression:

$$R_i = \mathrm{d[M]/dt} = 2fk_d[I] \tag{2.9}$$

where *f* is the initiation efficiency and the factor 2 is derived from each initiator molecule.

Propagation is the second step and is a rapid reaction, in which the polymer chain is growing by the addition of monomer unit, *M*, during propagation, to produce the same identity as free radical with n monomer unit, M^*_{n+1} , where (n=1,2,3,..), except that it is larger by one unit :

$$M^* + M \xrightarrow{k_P} {M_1}^* \quad (2.10)$$

$${M_1}^* + M \xrightarrow{k_P} {M^*}_{n+1} \quad (2.11)$$

The rate of polymerisation, in the propagation step, is equal to the consumption of monomer with respect to time, -d[M]/dt. This depletion is due to both initiator-monomer reaction and the propagation reaction:

$$R_p = -\mathrm{d[M]/dt} = k_p[M^*][M] \quad (2.12)$$

where k_p is the propagation rate constant.

Theoretically, the propagation step continues until all monomers are consumed. However, at some point, the chain propagation at the end of the polymer chain would stop growing and terminate either by combination or disproportionation. The two different forms of termination can be represented as:

$${M_n}^* + {M_m}^* \xrightarrow{k_{tc}} \mathrm{M}_{n+m} \quad (2.13)$$

$${M_n}^* + {M_m}^* \xrightarrow{k_{td}} \mathrm{M}_n + \mathrm{M}_m \quad (2.14)$$

where k_{tc} and k_{td} are the rate constants for termination by combination and disproportionation, respectively. Both of forms of termination can be combined to one rate expression:

$$R_t = 2k_t[M^*]^2 \quad (2.15)$$

As the concentration of free radical is assumed to reach a steady state, the following expression may be written as:

$$R_d = 2fk_d[I] = 2k_t[M^*]^2 \quad (2.16)$$

Simplifying and re-arranging equation (2.16), gives:

$$[M^*] = \left(\frac{fk_d[I]}{k_t}\right)^{0.5} \quad (2.17)$$

From equation (2.12) and (2.17), the overall rate of polymerisation (R_p) can be written as:

$$R_p = k_p[M]\left(\frac{fk_d[I]}{k_t}\right)^{0.5} \quad (2.18)$$

2.2.2.2. Conventional suspension polymerisation

Suspension polymerisation is a well-established process for the synthesis of polymer microparticles that has been existed in the industry for many years. [43,44]. It is the least complex heterogeneous polymerisation in terms of its mechanism. A typical process requires the use of mechanical agitation to mix the monomer phase, containing oil soluble initiator with the continuous phase (containing stabiliser) to form discrete drops. The continuous mixing is necessary to keep the monomer drops suspended in the continuous phase and prevent creaming or settling. During the mixing, the size of the drops is the result of two competing effects, the continuous drop break up and coalescence. Coalescence is predominated in the region where the shear stress is least while breakup occurs in the high region of shear stress [45,46].

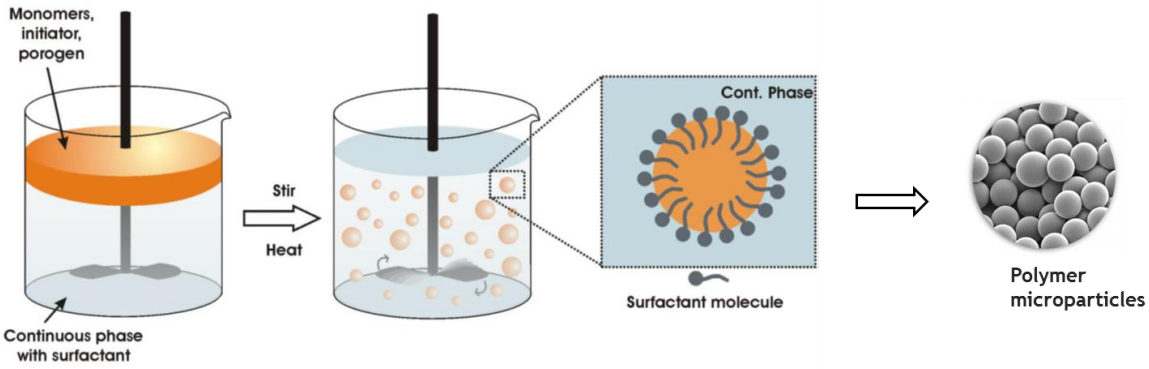

Figure 2.8 **a)** Schematic illustration of typical preparation of polymer microparticles via conventional suspension polymerisation. Reprinted from [47].

The phase ratio of the monomer is typically between 0.1-0.5. Above the optimum volume fraction, the continuous phase might be insufficient to accommodate the space between drops whereas is not feasibly economic at lower phase ratio [48]. The polymerisation proceeds in the drop phase at an appropriate reaction temperature to yield polymer beads. Figure 2.8 shows the schematic illustration of a typical preparation of particles via suspension polymerisation.

Suspension polymerisation is mostly preferred in industries due to its vast advantages including temperature control, low level of impurities and low separation cost compared to other polymerisation techniques [49]. However, the main drawback involved in the production of polymer particles by suspension polymerisation is that often produces particles with a wide size distribution.

There has been a tremendous amount of research on suspension polymerisation and its reaction mechanism involving different parameters, such as amount of initiator, stabiliser concentration, volume fraction of the monomer, reaction temperature, and stirring speed, as the manipulating factors to control the average particle size [50,51], but only a little attention has been paid on improving the uniformity of the polymer microparticles

[52,53,54]. This research gap has inspired us to develop an experimental approach to improve the uniformity of microparticles within means of suspension polymerisation.

2.2.2.3. UV polymerisation

This section overviews the microfluidic technique for the fabrication of a wide range of microparticles. It was previously mentioned that the polymer microparticles obtained by conventional techniques produce a wide size distribution. With the advent of new technologies such as microfluidics, fabricating polymeric particles on a rather small scale, and with high precision and accuracy, has become possible. Microparticles generated by microfluidics resemble those by conventional suspension polymerisation but the difference lies in the formation of one microparticles at a time.

Two systems can be employed to obtain different structures of polymer microparticles; a) a single-phase system and b) multiphase system. In a single-phase system, the monomer drops are dispersed in a continuous phase followed by a subsequent polymerisation and form a single microparticle. In the multiphase system, however, the monomer drops encapsulate a pure liquid (usually water) to form core-shell microparticles after solidification. These microparticles are generally produced through free-radical polymerisation. Polymer microparticles produced by microfluidics were first reported by Nisisako et. al. [55]. By using a T-junction microfluidic device, the monomer phase was flown inside the channel and was detached by the aqueous phase flow to form droplets. Following the emulsification step, the resulting droplets were collected in a beaker and converted to polymer particles by UV free-radical polymerisation for 1-2 min. The resulting particles have a coefficient of variation below 2.0 %.

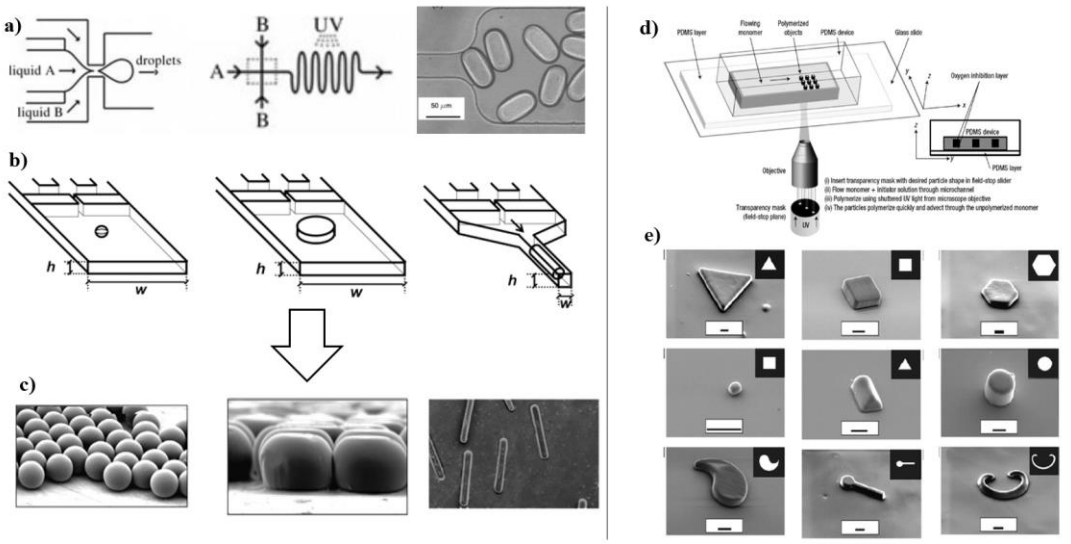

Figure 2.9 **a)** Schematic illustration of T-junction microfluidics device, the wavy microchannel where drops are cured under the UV irradiation and micrograph image of the non-spherical shape of the microparticles; **b)** Sketch of the confined microchannel where different shapes are obtained depending on the height(h) and width (w) of the microchannel; **c)** SEM images of the corresponding non-spherical shape microparticles [56].**d)** Schematic illustration of continuous- flow lithography device; **e)** SEM images of the different shapes of polymer microparticles. Inset images shows the feature on the transparency mask [57].

Kumacheva et. al. further developed a continuous microfluidic device to synthesise polymer microparticles [37]. In their work, the monomer droplets travelled in an extension wavy microchannel where they were cured under the UV irradiation to produce polymer microparticles. The role of the wavy channel was to provide enough time to solidify the droplets. It is important to stress that the continuous microfluidics device did not have any impact on the uniformity and the resultant microparticles were well-preserved. They also used the continuous microfluidic system to produce non-spherical microparticles with different morphologies (see Figure 2.9a-c). The first step to synthesising non-spherical microparticles is to form non-spherical droplets in the microchannel. The non-spherical shape is mainly determined by a relation between the size of spherical droplet and dimension of the microchannel. Thus, a droplet which has at least one dimension bigger than the width of the microchannel results in a non-spherical

shape. Following the polymerisation of the droplets, non-spherical microparticles were obtained (Figure 2.9c). During polymerisation, the size of the droplets was reduced by 5.0 -10.0 % due to the shrinkage. This results in a thin layer of lubricant aqueous phase between the inner wall and the moving microparticles and that prevents the blockage of the microchannel. A similar approach to forming non-spherical microparticles was also conducted by [58]. Later, the same conceptual approach was employed by other researchers to fabricate variety of different shapes of polymer microparticles such as triangular, square, hexagon and non-symmetrical objects (Figure 2.9d and 9e). In brief, the shape of the microparticles was determined by a transparent mask of a certain shape so that when the flowing monomer travelled inside the channel, the UV was only exposed to the transparent mask. [57]. Tae et. al used similar approach to create 3D polymeric microstructures with controlled shape and composition. [59].

Microfluidics does not lend itself easily to a mass production of particles, compared to conventional techniques, due technical difficulties and limitation in scaling up [60]. It is not economically viable to produce commodity microparticles using microfluidics. Therefore, the production of commodity or single-phase polymeric particles via microfluidics was not considered in this research. Instead, we attempted to investigate production of highly-value added particles for which the economy of scale is more favourable towards microfluidics. Examples of such particles are those generated from two-phase systems (double emulsion). Great efforts and advances have been engaged to synthesise a wide range of polymer microparticles produced from the double emulsions. These microparticles are often referred to as microcapsule or core-shell microparticles. It is at the higher range of this hierarchy, highly-packed drops, that are interests lie. Highly-packed multi-core drops, which contain more than core encapsulated by a polymeric shell, of great interest to many applications [61]

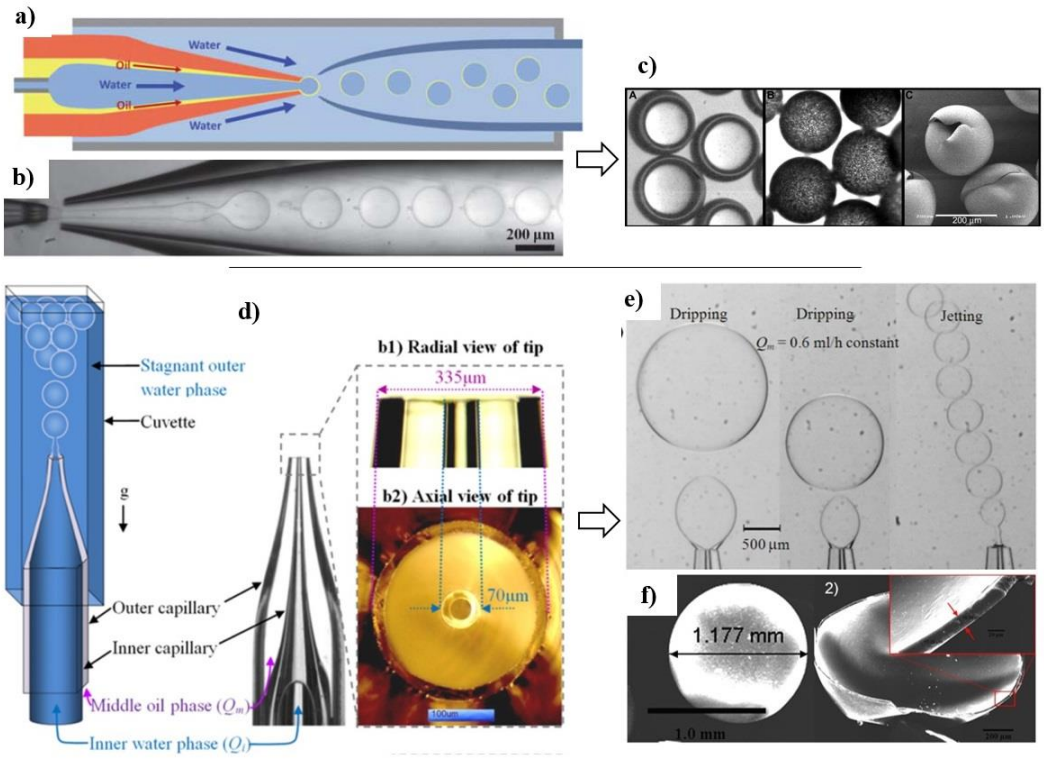

Figure 2.10 a) Schematic illustration of the microfluidics device for generation of double-emulsion drops with an ultra-thin shell**; b)** Optical images showing the double drop formation flowing inside the microchannel and **c)** SEM images of the core-shell microparticles with different shell-thickness. **d)** Schematic illustration of non-confined microfluidics device for preparation of ultra-thin core-shell with and the radial, along with the radial and axial view of the aligned capillary tips. **e)** Optical images shows the formation of the double drop at different flow regimes as indicated in the inset image. ; **f)** SEM images shows 1) the core-shell microparticle and 2) the shell thickness of the microparticle [65].

The production of microcapsule involves three streams; an inlet stream to form the core, a middle stream to form the shell and an outer stream which acts as a carrier of the double drops. The double drop can only act as precursor for the preparation of microcapsule. The transformation of drops into microcapsules mainly occurs via UV polymerisation. The size of the core and shell, phase ratio, shell thickness and the number of cores can be manipulated by varying the flowrate of the three phases.

The first novel microfluidic technique to produce precursor double emulsions and eventually core-shell microparticles was reported by Utada et al. [62]. Figure 2.10a

shows the schematic illustration of the microfluidic device that was used for the preparation of the core-shell microparticles. Water was used as the inner phase (core of the droplet) whereas the shell was a 30% solution of polymer. After the generation of a double drop, the shell was exposed to the UV to obtain a core-shell structure as shown in Figure 2.10c.

Furthermore, Kim et. al produced double emulsion drops with an ultra-thin layer using a biphasic flow and confined microchannel as a technique to reduce the shell thickness to submicron [63]. Such ultrathin core-shells can be programmed to release the content within the core as proved by Abbaspourrad et al. [64].

Recently, Ankur et. al produced large ultrathin shelled drops via non-confined microfluidics (Figure 2.10). In this approach, two capillaries were placed at the same tip and introduced vertically intro a stagnant outer water phase. The ultra-thin shell was achieved by lowering the interfacial tension of the outer interface and having an inner flowrate at least 10 times the middle phase flowrate. The ultra-thin core-shell drops were produced by photopolymerisation in a stagnant condition (Figure 2.10f) [65].

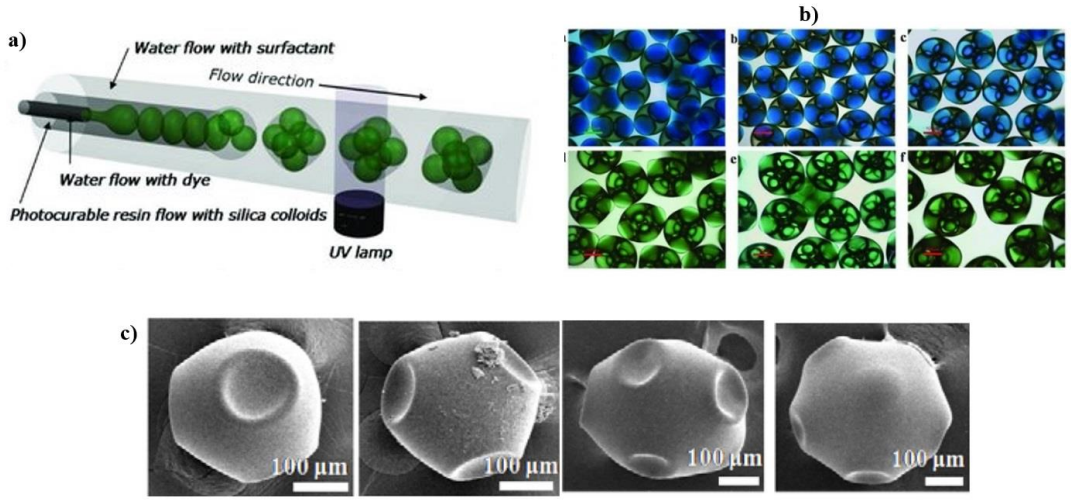

Figure 2.11 a) Schematic illustration of co-flow microfluidics device for the preparation of multi-core double drops; **b)** optical microscope images of the uniform microcapsules with different number of cores for *N*=2 to 7 and **c)** SEM images shows the unique configuration of microcapsules for *N* =3, 4, 7 and 8 [66].

Kim et. al also reported a simple, single-step double emulsion techniques to encapsulate a certain number of cores in photocurable shell drops [66]. Figure 2.11a shows the schematic illustration of the co-flow microfluidic device used for the preparation of double emulsion with multi-cores. They showed, for the first time, that the densely-packed core droplets within the oil shell rearrange into a distinctive configuration depending on the number of core droplets (Figure 2.11b). This is because the spherical core droplets were in contact with the adjacent droplets and the wall of the shell drops (the core volume becomes bigger than a critical volume). These unique configurations were solidified into multi-core microcapsules through photopolymerisation, as shown in Figure 2.11c.

Inspired by Kim et. al work, Zhang et. al. used the uniform double emulsions, as a template, to obtain porous microparticles with highly interconnected, hierarchical, porous structures using the set-up shown in Figure 2.12a.

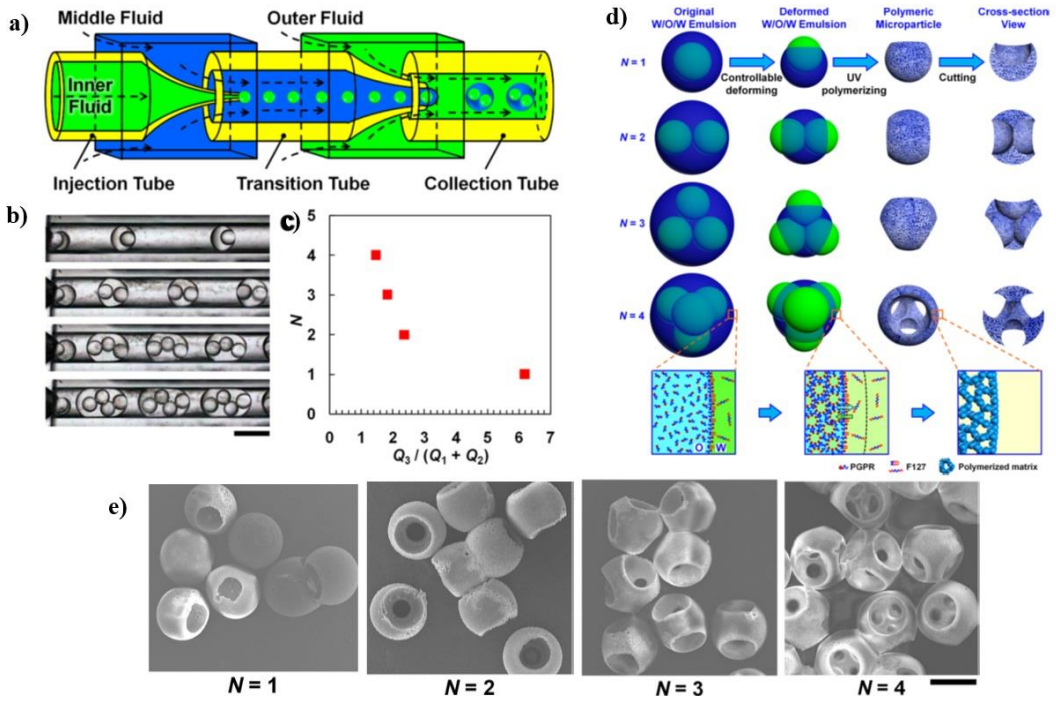

Figure 2.12 **a)** Schematic illustration of co-flow microfluidic device for the preparation of multi-core double drops; b) optical micrograph images of the uniform double drop; **c)** the effect of flowrates on the number of inner cores. **d)** The fabrication procedure for obtaining porous microparticles and **e)** SEM images of the porous microparticles with tunable number (N = 1−4) of highly of interconnected micrometer-sized pores. Scale bar is 200 μm [67].

In their work, the partially miscible oil phase with the inner and outer aqueous phases deformed the w/o/w emulsions into different shapes depending on the packing structure of the number of cores (see Figure 2.12d). The deformation process squeezes the inner core droplets, forming a thin oil film between the core droplets and the outer aqueous phase, which was ruptured after UV polymerisation as the SEM shows in Figure 2.12e [67]. Similarly, the same authors attempted to dissolve the thin shell layers, formed after polymerisation, of the tightly packed encapsulated cores to form porous microparticles for 3D cell culture. The schematic illustration and the final results are shown in Figure 2.13 [68].

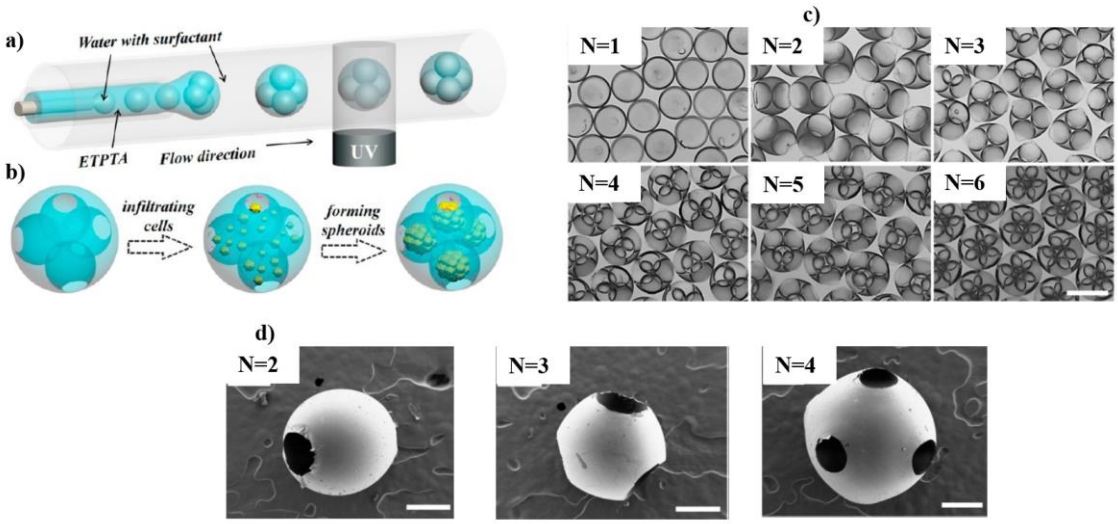

Figure 2.13 **a)** Schematic illustration of co-flow microfluidic device for the preparation of multi-core double drops; b) optical micrograph images of the uniform double drop; c) the effect of flowrates on the number of inner cores and d) SEM images of the porous microparticles withtunable number (N = 1−4) of highly of interconnected micrometer-sized pores. Scale bar is 200 μm [68].

These porous polymer microparticles, which have a solid polymer shell and a hollow interior, are also of interests to both academia and industry can be viewed as an interesting area of research due to its distinctive combination of porous structure within a polymer matrix. This unique structure of porous polymer is designed to benefit from the ease of processability, the well-defined porosity, light weight [69] and high surface area [70,71]. Such a porous structure can be produced in a format of thin film [72], monoliths, and beads [73,74,75]. The functional porous polymers can also take advantage of reversibly changing the pore structure [76]. In another words, it can switch between open and closed porous state in accordance with environmental stimulation [77]. Porous polymers are developed for a wide range of applications including food, ion exchange, separation and filtration membranes [78], encapsulation agents for controlled release of drugs [79], catalysts [80], supports for catalysts [81] petroleum and pharmaceutical industries [82,83,84,85]. Recently, they have shown to be potentially important for a series of new

applications involving gas storage [86], nanostructured carbon materials [87], electrode materials for energy storage [88,89], tissue engineering [90,91] and packing materials in chromatography [92].

In addition to the previous techniques on the preparation of solid microparticles, porous microparticles are conventionally synthesised via a number of techniques including solvent evaporation, polymerisation or seed swelling method [93]. While porous microparticles are easy to fabricate through solvent evaporation method, the diffusion of the internal phase or oil phase during evaporation, which is difficult to control, has dramatic effects on the porosity and window size of the final products [93]. Porous microparticles resulting from polymerisation techniques (i.e. suspension) suffer from the low uniformity of both window and final particles sizes, whereas seed swelling method, which benefits from a facile generation of uniform particles, cannot produce microspheres over 10 μm [94].

Given that many publications deal with fabricating porous microparticles, only a few recent works demonstrated the use of microfluidics to produce uniform porous microparticles. Although highly-packed drops have been reported in the literature, the mechanism of window opening has not been explored yet. Also window opening has been carried out by dissolution method, which does not lend itself to microfluidics easily. Furthermore, the number of windows has been always limited to a few and the morphology of microparticles has been always spherical, due to the relative ease in their fabrication. Currently there is no on-the-fly approach that facilitates drop transformation into non-spherical porous microparticles, despite potential use for anisotropic porous micropartilcles, and that will be the highlight of the presnt.

2.3. FABRICATION OF NANOPARTICLES (NPs)

The term "nanoparticles" is defined as particles (or latexes) with diameter of 10-1000 nm. Within the broad available techniques to synthesise nanoparticles (NPs), this thesis will only focus on emulsion polymerisation. The term emulsion polymerisation encompasses various related processes such as conventional emulsion polymerisation, microemulsion polymerisation, miniemulsion polymerisation and emulsifier-free emulsion polymerisation. The aim of this section is not to give a comprehensive overview about the method of NPs preparation through the emulsion polymerisation approaches, but to highlight and explain factors and vital criteria involved in the preparation of uniform NPs. In particular, only emulsifier-free emulsion polymerisation approach will be the focus of the present study.

2.3.1. Kinetic of free-radical polymerisation in disperse medium

Emulsion polymerisation is a process which involves the emulsification of a hydrophobic monomer in an aqueous medium (typically water), containing a water soluble initiator, to form a latex. The main difference between suspension and emulsion polymerisation is the locus of initiator. In suspension polymerisation, an initiator soluble in the dispersed phase (monomer) will start the initiation inside the monomer drop while in emulsion polymerisation the initiator is soluble in the aqueous continuous phase [95]. The minor change in the locus of initiator has a dramatic effect on the polymerisation mechanism [96].

The formation of latexes in emulsion polymerisation passes through three distinct intervals. The first interval is particle nucleation, which can be carried out either by micellar nucleation (heterogeneous) or homogenous nucleation process. Figure 2.14 shows the schematic illustration of both processes. The kinetic mechanism of micellar

nucleation was first proposed by Harkins and Smith and Ewart [97]. Their works state that the free-radical first reacts with the monomer phase dissolved in the aqueous phase to form oligomeric radicals. These oligomers, which are hydrophobic, are captured by monomer-swollen micelles to form particle nuclei. The particle nucleation stage (Interval I) ends when all micelles are consumed.

In the homogenous nucleation, Priest [98], Roe [99] and Fitch and Tsai [100,101] proposed a completely different mechanism. According to their theories, the homogenous nucleation process for the formation of particle nuclei in the continuous aqueous phase starts after the decomposition of initiator to generate radicals. The radicals resulting from the decomposition of a water-soluble initiator react with monomer dissolved in the aqueous water phase to form surface-active oligomeric radicals, which can continue to propagate in the aqueous phase until they reach a critical size, J_{crit}, and precipitate as a primary particle. These primary particles grow by coagulation with other primary particles and also by absorption of monomer from monomer drops until they become sufficiently large and stable (Interval I).

Interval I is relatively short and is considered to be the most important stage in terms of controlling the particle size and size distribution [97]. After interval I (the particle nucleation) ends, the particle growth stage begins (interval II). The particles will continue to grow by acquiring more monomer from the monomer drops. The second stage (Interval II) terminates when all monomers drops are consumed in the polymerisation system.

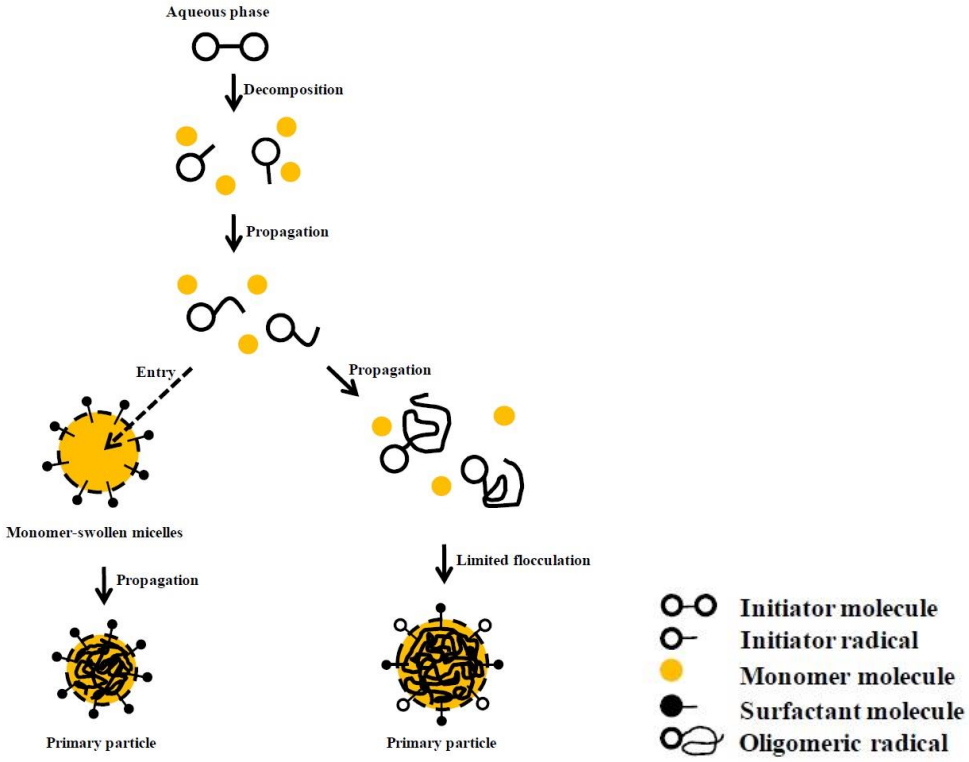

Figure 2.14 Schematic representation of both micellar nucleation and homogeneous nucleation models [102].

The completion stage (interval III) is the final stage of the reaction. In this stage, the polymerisation continues within monomer-swollen polymer particles that formed during interval I. The monomer concentration in the polymer particles is continues to decrease until the end of the reaction and usually 100% conversion is achieved.

Smith and Ewart theory has been widely used to calculate the rate of emulsion polymerisation R_p:

$$R_p = k_p[M^*](\mathrm{n}N_p/\,N_A) \qquad (2.19)$$

where *kp* is the rate constant of propagation, $[M^*]$ the concentration of monomer in the particles, *n* the average number of free radicals per particles, N_p number of particle and N_A the Avogadro's number.

2.3.2 Conventional emulsion polymerisation

Conventional emulsion polymerisation, accounts for the majority of world's production of nanoparticles (NP) and has attracted interests from both academics and industries due to its several advantages over other polymerisation types such as high molecular weight, rapid polymerisation rate, and high conversion through environmentally-friendly process [103]. In conventional emulsion polymerisation, the formation of particles follows the micellar nucleation. The kinetics of conventional emulsion polymerisation (micellar nucleation) is described above. In conventional emulsion polymerisation, both monomer and the initiator are in different phases from the beginning of the reaction. Furthermore, with applying thermal energy and mixing, the water-soluble initiator decomposes in the continuous phase and generates free radicals molecules that diffuses into monomer-swollen micelles and initiate them to form polymer particles [104,105]. It is important to stress that particle formed by conventional emulsion polymerisation only results in a wide particle size distribution. Therefore, conventional emulsion polymerisation will not be further considered herein as this thesis seeks to put forward possible ways for obtaining uniform polymer particles.

2.3.3 Emulsifier-free emulsion polymerisation

The presence of the stabiliser during the synthesis of polymer particle is the major drawback in emulsion polymerisation. Eliminating the surfactant from the final product is tedious and length process that can escalate the production cost. Therefore, extensive attention has been paid to the production of polymer latexes without the addition of surfactant. Emulsifier-free emulsion polymerisation (EFEP) is a technique that has the ability of producing latexes with a narrow size distribution.

Emulsifier-free emulsion polymerisation follows a homogenous nucleation process. In brief, the decomposed water-soluble initiator molecules react with monomer molecules dissolved in the water phase to from surface-active oligomeric radicals. The reaction takes place in the water phase and the monomer is supplied from the monomer drops by diffusion through the medium phase. The mechanism of the EFEP largely depends on the solubility of the monomer in the water phase . However, the monomer concentration should be kept minimal to avoid particle agglomeration during the course of polymerisation [106].

In the absence of the surfactant, the stability of the colloidal dispersion in such a system is achieved by electrical charges induced by one of the following component (i) ionisable initiator, (ii) hydrophilic comonomer; and (iii) ionic comonomer. Several researches have intensively studied the mechanism of particle nucleation and growth to form a stable latex particles during the EFEP [106].

Tauer et al. [107] investigated the emulsifier free emulsion polymerisation of styrene initiated by potassium persulfate. It was found that that nucleation aggregation mechanism controlled the latex particle size and its distribution. It was also noted that during particle nucleation that the number of particles per unit volume of water increased and more than one polymer chain per particle is formed.

Other investigators [108] studied the addition of small amount of functional co-monomer such as acrylic acid, methacrylic acid to improve the stability of particles during polymerisation. Wang and Pan [109] prepared EFEP of styrene with the water soluble comonomer 4-vinylpyridine. It was found that at the beginning of the reaction, more surface active oligomers from 4-vinylpyridine were generated resulting in monomer-swollen micelles that were available for subsequent particle nucleation. Also, it was found

that, the addition of these functional commoners enhanced the stability of the monomer droplet resulting in monodispersed latexes.

Ni et. al [110] examined the particle nucleation mechanism by studying the effect of adding 8% of ethyl acetate in the copolymerisation of styrene and 4-vinylpyridinealong along with reducing the agitation speed (100-200 rpm). They reported that the nucleation and growth of particles were directly related to the monomer drops stemming from the oil-water interface formed by the agitation speed and/or the condensation of monomer molecules dissolved in the aqueous phase. It was also noticed that the number of particle per unit volume of water increased with the agitation speed. In addition to monomer drop, the diffusion of monomer molecules through the medium phase and coalescence among the particles assist in the transportation of monomer to the reaction loci.

Ou et al. [111] reported the effect of hydrophilic comonomer (methyl methacrylate or vinyl acetate) on particle nucleation. An interesting analysis by Gel Permeation Chromatography (GPC) showed oligomers population with a molecular weight of approximately1000 g/mol of was generated at the very beginning of the polymerisation.

Yan et al. also prepared the emulsifier free emulsion copolymerisation of styrene, acrylic acid and methyl methacylate initiated by ammonium persulfate. Similar results were found in comparison with other studies. The rate of polymerisation and particle nucleation increased with increasing concentration of initiator or acrylic acid [112]. Moreover, Mahdavian and Abdollahi examined the addition of various concentration of acrylic acid together with copolymerisation of styrene and butadiene. As expected a small amount of comonomer increase the number of latex particles per unit volume of water as well as the rate of polymerisation [113].

Surfactant-free emulsion polymerisations have traditionally been performed in water as a medium and often produces large particles with a limited solids content, particularly in the case of partially water-soluble monomers. However, some investigators have reported the addition of a water miscible co-solvent (i.e. alcohol) to the medium phase. It was reported that the addition of alcohol has a dramatic influence on the kinetics of emulsifier-free emulsion polymerisation. A high monomer solubility in water can increase the number of particles. In contrast it could also enhance the solubility of growing chains and delay their precipitation resulting in a fewer numbers of nuclei. Others studies noticed that the final particles are influenced by variation in the composition of the medium phase containing co-solvent. It was observed that the presence of alcohol (i.e. methanol) would improve the uniformity and surface charge [111].

The addition of solvent on the kinetics of emulsifier-free emulsion polymerisation has been extensively studied. However, most works reported in the literature focused on particle size, but little attention has been paid toward increasing the solids content. Furthermore, there are still several controversial issues unresolved regarding the effect of solvent on the particle size. There also appears to be a significant research gap in the literature to investigate the addition of solvent togather with a water-soluble co-monomer on the kinetics of emulsifer-free emulsion polymerisation.

2.4. CONCLUSIONS FROM LITERATURE REVIEW

From the extensive literature review, an overview was given of the common approaches involved in the production of polymer particles. The average diameter, uniformity, shape, porosity and economic evaluation as well as applications should accordingly be taken into consideration prior to the selection of the appropriate method. The literature points to the fact that the highly uniform polymer particles/structures are shown to be potentially

useful for numerous applications. The main conclusions drawn from the literature study are as follows:

a) To identify and examine potential ways by which particle size and size distribution can be controlled within the means of conventional suspension polymerisation, with the focus being on the impeller speed as the main parameter on controlling particle size and size distribution.

b) To further maximise the particles uniformity and product scalability by using stirred-vessel membrane emulsification followed by a controlled-shear suspension polymerisation and investigating various process parameters including shear stress, stabiliser concentration and flow rate.

c) To explore the possibility of using a microfluidic approach for the production of more complex forms of microparticles such as non-spherical microparticles, core-shells and porous microparticles.

d) To extend the microfluidic technique to the fabrication of 3D- porous structures with a well-defined morphology.

e) To examine potential ways to synthesise uniform polymer nanoparticles via emulsifier-free emulsion polymerisation in the presence of solvent.

Chapter 3 Experimental

This chapter presents all materials, equipment set-up, methods and polymerisation techniques used to fabricate a wide range of polymeric materials, ranging from micro to nanometre size. This chapter also describes different characterisation techniques that have been to characterise the polymeric materials. The techniques used to characterise the emulsion properties are also described. Further details for specific materials used, equipment set-up and sample measurement/characterisation techniques used will be explained in detail where appropriate (see Appendix **A** for supplementary details on the experimental set-up as well as a list of instruments used throughout this study).

3.1. MATERIALS

Monomers: Methyl methacrylate (MMA, 99%), styrene (St, 99.9%), divinylbenzene (DVB), 2-ethylhexyl acrylate (EHA, 98%), isobornyl acrylate (IBOA, 98.5), trimethylolpropane triacrylate (TMPTA, 80%), 1, 6 hexanediol diacrylate (HDODA, 80%), and co-monomer sodium p-styrenesulfonate (NaSS) were purchased from Sigma Aldrich and used as received, expect for MMA and St, which were purified with ion-exchange resins to remove inhibitors prior to use.

Surfactants: poly (ethylene glycol)-block-poly (propylene glycol)-block-poly (ethylene glycol) **(**PEG-PPG-PEG) (Pluronic L-81) (average Mw ~ 2800 g mol^{-1} and HLB ~ 2.0) and sorbitan monooleate; Arlacel 80; Sorbitan, mono-(9Z)-9-octadecenoateor (Span 80, HLB ~ 4.3) were used as *oil-soluble surfactant*. Oil-soluble surfactants, such as, Sorbitan trioleate (span 85), Sigma Aldrich (HLB ~ 1.8), Hypemer B246, CRODA (HLB ~ 5.5) and Hypermer 2296, CRODA (HLB ~ 6) were also tested for stabilising w/o emulsions.

Poly (vinyl alcohol) (PVA) (*M*w = 85,000- 146,000 g mol^{-1}; degree of hydrolysis 87-89% and HLB ~ 18.0) and (poly (ethylene glycol)-block-poly (propylene glycol)-block-poly (ethylene glycol) (Pluronic F-127) (average Mw ~12,500 g mol^{-1} and HLB ~ 22) were used as *water-soluble surfactant.* Both types of surfactants were also purchased from Sigma Aldrich and dissolved in appropriate phases at a given concentration, prior to use.

Initiators: Depending on the polymerisation technique, lauryl peroxide (LPO, Sigma Aldrich) or α-Aminoketone. 2-Methyl-1-[4-(methylthio) phenyl] (Irgacure 907, BASF) were used as thermal or photo initiator, respectively. Both types are oil-soluble initiator whereas potassium persulfate (KPS, Sigma Aldrich) was used as a thermal water-soluble initiator for emulsifier-free emulsion polymerisation.

Auxiliary chemicals: Potassium chloride (KCl), Acetone (99.9%), Methanol (99.8%), Ethanol (95%) and 1-Propanole (99.7%) were obtained from Sigma Aldrich and used as received.

3.2. EXPERIMENTAL SET-UP

3.2.1 Reactor vessel

For polymer beads produced by a conventional technique (suspension polymerisation), both emulsification and polymerisation were simultaneously carried out in a 0.5-L jacketed glass reactor with a diameter of 10 cm equipped with four 90° baffles (see Figure 3.1b). A four-bladed flat turbine impeller with diameter and width of 3.8 cm and 1.1 cm, respectively, was installed inside the reactor for agitation. The temperature of the reactor content was controlled by passing water with the desired temperature (75.0± 0.5°C) through the reactor jacket. Also, nitrogen purging was carried out for 15.0 min before the monomer phase was added to the aqueous phase. The impeller speed was also set at the desired speed before the start of experiments.

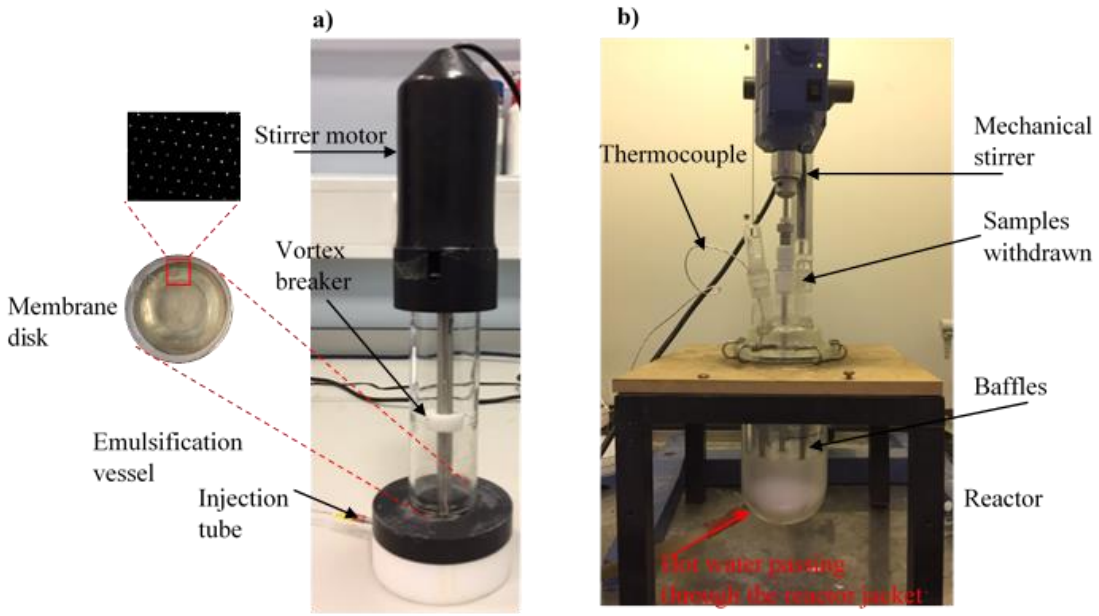

Figure 3.1 Experimental set-up of **a)** the stirred vessel membrane emulsification, with a micrograph image showing the regular array of pores in the membrane used, and **b)** the polymerisation reactor units used.

3.2.2 Stirred cell-flat membrane vessel

In the second part of the thesis, a stirred vessel membrane emulsification (SCFM) was used to improve the uniformity of drops and thus the resulting polymer beads. The emulsions were produced using a stirred vessel membrane device provided by Micropore Technology Ltd. The Micropore Dispersion Cell (MDC), shown in Figure 3.1a, consisted of a polytetrafluoroethylene (PTFE) base with an injection tube (PEEK/stainless steel), an emulsification vessel (3.5 cm in a diameter), a sealing gasket to prevent the leaking, a stirrer motor (24 Volts) and a shaft unit (stainless steel) with power supply and vortex breaker made of PTFE/stainless steel. The paddle impeller with length 3.1 and width 1.2 cm, respectively, was installed inside the emulsification vessel for agitation. A hydrophilic-ringed membrane with an array of 10 µm pore size and 200 µm pitches (distance between pore centres) was used. The membrane was made of nickel with glass based coating with a total area and porosity of 2.8 cm^2 and 0.20%, respectively. The

uniform drops produced via SCFM were transferred to a shear-controlled suspension polymerisation reactor and polymerised there (Figure 3.1).

3.2.3 Glass-capillary-based microfluidics set-up

Before making a microfluidic device, the surface of the microcapillaries should be treated in order to avoid any wetting issue during drop formation. For example, for producing w/o/w emulsions where the water phase (inner capillary) is moving through the oil phase (middle capillary) into another aqueous continuous phase (outer capillary), the inner surface of the inner capillary should hydrophobic while the outer surface should be hydrophilic. The inner surface of capillaries where water went through was made hydrophilic by plasma treatment (Femto Plasma cleaner, Diener), for few min, while the surface of the capillary where the oil was flown through was made hydrophobic by treatment with n-octadecyltrimethoxysilane at 120°C.

Note that the outer surface of the middle capillary (oil phase), which is introduced in the outer capillary, was made hydrophilic. This was done by gluing both ends to protect the treated inner surface from further changes during the hydrophilisation treatment by plasma. The glued ends of the capillary were then broken off to retrieve the open-ended capillary with the selected treatment (hydrophobic inner and hydrophilic outer surface). The capillaries were then introduced into each other with axisymmetric alignment and placed on a microscope slide. The ports were placed on the coupled capillaries, which are resting on the microscope slides, glued (Devcon 5-minute epoxy) and left to harden completely (see the inset in Figure 3.2).

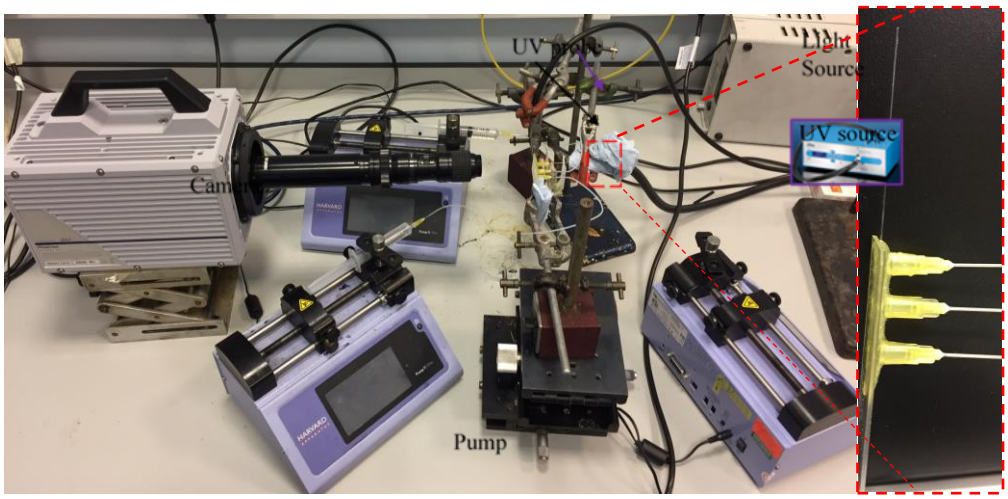

Figure 3.2 Microfluidic experimental set-up for the preparation of uniform polymeric microparticles, with a magnified image of the co-flow microfluidic device showing the ports where the flowrate of the inner, middle and outer phase (Q_i, Q_m, and Q_o), respectively, were introduced.

The generation of double drops with various morphologies was precisely manipulated by varying the flow rates of inner, middle and outer phases (Q_i, Q_m, and Q_o, respectively). Drops were formed at the tip of the capillary and detached by the high shear forces generated by the external continuous phase. The generated drops were photopolymerised by the UV (Honle UV technology) irradiation and converted to polymer microparticles. The experimental set-up of the glass-capillary-based microfluidics is shown in Figure 3.2

3.3. MEASUREMENTS AND CHARACTERISATIONS

Different standard techniques were employed to characterise different types of polymer particles. Each measurement and characterisation technique will be explained where appropriate.

3.3.1 Conversions

Conversions were measured gravimetrically. Approximately 3.0 g of the dispersion/latex was withdrawn from the reactor and placed into a weighted aluminium foil dish. The

samples were dried in an oven at 75°C for 24 h. The monomer conversions were calculated as the weight ratio of the polymer produced to the total monomer in the recipe.

$$x = \frac{\text{weight of polymer formed} - \text{residual weight}}{\text{weight of monomer in the recipe}} \quad (3.1)$$

The residue weight accounts for the weight of initiator and stabiliser in the sample.

3.3.2 Particle size analysis

The average particle size was calculated by a direct measurement on the micrographs obtained from the microscopy imaging techniques (i.e. optical, SEM or TEM) or by using particle sizing techniques, such as laser diffraction or DLS.

3.3.2.1 Optical

Drops/particles were imaged using a calibrated optical microscope (Kyowa Tokyo, Japan) with a camera (Moticam 2300) connected to a computer. For the microfluidic research, drop formation was monitored using a high-speed video camera (Photron FastCam Ultima APX—monochrome typically operated at 1000fps).

3.3.2.2 Scanning Electron Microscope (SEM)

A Scanning Electron Microscope is a tool that utilises a focused beam of high-energy electrons to scan the surface of a sample to provide details on its morphology. The working principle of SEM starts with an electron beam, typically with an energy ranging from 0.2 keV to 40 keV, generating from the electron gun (electron source) at the top of column. The electron beam then passes down through a series of scanning coils (electromagnetic lenses) and is deflected in the final lens in the *x* and *y* axes to provide a focused electrons beam so that it scans in a raster scan pattern to hit a specific area of the sample surface. The beam, magnification and the surface area to be scanned are controlled via computer. In SEM, the sample is prepared on specialized aluminium studs coated with

a conductive material, such as gold or carbon, to create a conductive thin layer on the sample in order to inhibit charging, reduce thermal damaging and improve the quality of image.

In this work, the morphology and surface features of polymer particles/ structures were detected by scanning electron microscope (SEM; Hitachi, S4000). Samples were coated with approximately 10.0 nm of gold before analysis. Then, the sample was placed on a stud and mounted by an aluminium tape. The SEM was operated at 5.0 kV which was found to inhibit the charging.

3.3.2.3 Transmission Electron Microscopy (TEM)

Transmission electron microscope (TEM) operates on the same basic principles as scanning electron microscope (SEM). Both TEM and SEM use electron beam to view and examine the features of the sample. However, the major difference lies in the fact that the electron beam is transmitted through a samples in TEM in order to give more characteristics of their internal features of the sample while the SEM is only based on scattered electrons (shows only the morphology of samples). TEM operates with much higher energy than SEM (typical energy ranging from 100 keV to 300 keV). The result in TEM is presented in a two-dimensional picture and the image produced by the microscope is via fluorescent screen. In this work, samples for TEM (TEM; Nippon Denshi Co., Japan, 200 kV) measurements were prepared by placing a drop of the diluted sample on a specialized 200-mesh carbon film supported by a copper grid, and allowed to dry at room temperature.

3.3.2.4 Laser Diffraction

Laser diffraction is generally used to determine the size and size distribution profile of particles size in the range of 1.0 to 2000 μm. The working principle starts when the laser

beam passes through a media and the angular variation in intensity of light scattered to measure. The collected data of the angular scattering intensity, responsible for this diffraction, is then analysed to correlate the size of the particles using the Mie theory of light scattering. The diffraction light pattern is inversely proportional to the particle size (i.e. the larger the particle size, the smaller the angles of the light scattering). In this work, the particles size and their distributions were analysed by laser diffraction particle sizer (Malvern, Coulter LS130).

3.3.2.5 Dynamic Light Scattering

Dynamic Light Scattering (DLS) is generally used to determine the size and size distribution profile of submicron particles suspended in solution. As the small particles in suspension continuously undergo random motion known as "*Brownian motion*", DLS connects the measured diffusion coefficient and relates it to the hydrodynamic diameter of the particles using the Stokes-Einstein equation:

$$D_h = \frac{k_B T}{3\pi\eta D_t} \tag{3.2}$$

where D_h is the hydrodynamic diameter, D_t is the translational diffusion coefficient, k_B is Boltzmann's constant, T is temperature and η is dynamic viscosity. The resulting hydrodynamic diameter measured by DLS is the diameter of sphere that diffuses as the same speed as the particle being measured.

In order to have an accurate measurement of the particle size, the concentration of the sample must be carefully adjusted. The use of a very concentrated sample results in an inaccurate particle size. This is because of particle interactions as they cannot freely diffuse through the media. A multiple scattering, which is when the light scattered by one particle is scattered by another one, also occurs. A low concentration of particles in the

sample, on the other hand, results in insufficient light scattering to make a measurement. A slightly cloudy appearance of samples is the optimum condition in order to have an accurate estimation of the particle size. This was experimented with various concentrations until a constant size was obtained. In this work, the particle sizes of selected samples were examined by dynamic laser light scattering (DLS, Malvern sizer) and we found out that a small quantity of latexes diluted in deionised water (~1% mass) is the optimum condition.

Also, note that the weighted average hydrodynamic size of the ensemble collection of particles (z-average size) obtained by DLS measurement is weighted according to the scattering intensity. This means that the z-average measured by DLS can be deceptive as a small amount of large particles can prejudice toward the larger particle. As a results, the z-average diameter will always be larger than the actual diameter measured by the TEM.

3.3.2.6 Uniformity

The term "monodisperse" is often used to explain a group of drops/particles having a uniform size and shape while the antonym is "polydisperse", indicating a wide range of particle sizes. There are two common statistical quantities that are used to describe the uniformity of drops/particles; the coefficient of variation (*CV*) and the polydispersity index (*PDI*). The classification of the coefficient of variation (*CV*) and polydispersity index (*PDI*) to describe the degree of uniformity is given in Table 3.1.

Table 3.1 Classification of *CV* and *PDI*

Degree of uniformity	*CV* range	*PDI* range
Very high	< 3.0 %	1.0
High	3.0-10.0 %	1.0-1.07
Intermediate	10.0-20.0%	1.07-1.1
Low	> 20.0 %	> 1.1

The CV is a normalized measure of the dispersion of a sample and defined as the ratio of standard deviation σ to the the number-average diameter (D_n).

$$CV = \frac{\sigma}{D_n} \times 100 \qquad \text{Where; } \sigma = \sqrt{\frac{\sum(D_i - D_n)^2}{N}} \qquad (3.3)$$

The *PDI*, on the other hand, is widely used in polymer science to indicate the size distribution of particles and defined as the weight average diameter D_w to the number-average diameter D_n.

$$PDI = \frac{D_{43}}{D_n} \qquad \text{where} \qquad (3.4)$$

$$D_w = \frac{\sum_{i=1}^{n} n_i D_i^{\,4}}{\sum_{i=1}^{n} n_i D_i^{\,3}} \quad ; \quad D_n = \frac{\sum_{i=1}^{n} n_i D_i}{N} \qquad (3.5)$$

where n_i is the number of particles with diameter D_i and $N = \sum_{i=1}^{n} n_i$ is the total number of particles counted.

3.3.3 Particles stability

3.3.3.1. Zeta potential

Zeta potential gives an indication of potential stability of the colloidal systems. The magnitude of the zeta potential is estimated when an electrical field is applied to zeta potential cell. The stable nanoparticles will repel each and avoid fluctuation when they have a positive or negative zeta potential of around ± 30.0 mV. In this research, the measurement of zeta potentials was considered for submicronic particles produced by emulsifier-free emulsion polymerisation. The zeta potential was detected zetasizer (DLS, Zetasizer, Malvern) at 25°C by injecting an approximately 1.0 ml of the diluted colloid into the zeta potential cell.

3.3.3.2. Conductivity meter

The conductivity meter is used to measure the electrical conductivity in a solution. The conductivity is measured by applying an electric current to two electrodes immersed in the solution and measured the resulting voltage. During this process, the anions migrate to the positive electrode and the cations migrate to the negative electrode whereas the continuous phase acts as an electrical conductor. The conductivity of the latex was measured by meter (MeterLab, CDM230). The device was first calibrated using KCl solution with known conductivity. The probe of the conductivity metre was immersed in the latex during the course of the reaction at given conditions.

3.3.4 Porosity

The mercury porosimetry is an instrument that utilises the non-wetting property of mercury combined with its high surface tension to measure the pore size and volume and other porosity-related properties of a porous material. The working principles begins when the non-wetting mercury is bridged across the opening of the pore creating a force-resisting entry until a sufficient pressure is applied. The pore size is inversely proportional to the pressure (i.e. the smaller the diameter of the pore, the more pressure is required to force entering the mercury into the pore). Assuming the pore with a circular opening at the surface, the resisting force F_R is expressed as:

$$F_R = \pi D \gamma \cos\theta \qquad (3.6)$$

where D is the diameter of the pore and γ is the surface tension.

The external force $F_{ext.}$ which is the product of the pressure P and area A over which the pressure is applied, for a pore of circular cross-section, is given by:

$$F_{ext.} = PA = P\pi D^2/4 \qquad (3.7)$$

At equilibrium, just before the resistive force is overcome (by setting eq. 3.6 to eq. 3.7) the equation is:

$$-\pi D g \cos\theta = \pi D^2 P/4 \quad (3.8)$$

Solving and re-arranging the above equation gives:

$$D = -4g\cos\theta /P \quad (3.9)$$

The above equation known as "Washburn equation". At a given pressure, the mercury will intrude the pores only if the diameter D of the pore is greater than that predicted by eq.3.9.

The volume of the mercury that enters the pores is also measured by mercury penetrometer. The mercury filled in the penetrometer, which acts as a reservoir for the analytical volume of mercury, will be forced out into the sample as the pressure increases. As a result, the volume of the mercury in penetrometer decreases. This decrease, therefore, is equal to the volume of the mercury contained in the porous structure. In this work, the physical properties of the porous polyHIPEs were analysed using mercury intrusion porosimetry (Micromeritics AutoPore III 9420). Intrusion and extrusion mercury contact angles of 130 degree were used. Intrusion pressures for the PolyHIPEs never exceeded 60.0×10^3 psi.

3.3.5 Interfacial tension measurement

The Surface tensions of some selected experiments were measured using Du-Nouy ring method.

Chapter 4 Improving the Uniformity of Polymer Beads in Suspension Polymerisation via using a Two- Stage Stirring Protocol*

4.1. ABSTRACT

This work introduces a two-stage stirring protocol for improving the uniformity of polymer beads produced in suspension polymerisation reactions. Methyl methacrylate (MMA) and a specific grade of polyvinyl alcohol (PVA) were used as monomer and stabiliser, respectively. In a typical suspension polymerisation, both emulsification and polymerisation occur simultaneously in a single stirred vessel reactor at a constant agitation speed (rpm) and stabiliser concentration. In the two-stage stirring protocol proposed, the emulsification stage was carried out at an appropriate rpm followed by the polymerisation stage at a reduced rpm. This policy led to the drop coalescence being suppressed. The particles average size reduced, and their distributions narrowed when compared with particles from conventional suspension polymerisation. This PSD narrowing was more significant at a low stabiliser concentration and when there was a large difference between the stirring speeds used in the two stages. The two-stage stirring protocol was extended to include a two-stage stabiliser-addition policy. The hybrid two-stage protocol improve the quality of particles by producing a narrower particle size distribution than the conventional suspension polymerisation, while improving the energy efficiency of the process. The technique can be equally used in conventional suspension polymerisation with simultaneous emulsification and polymerisation.

* To be submitted

4.2. INTRODUCTION

Suspension polymerisation is a well-established process in industry for making polymer beads [114]. In this process, the monomer phase containing an initiator is suspended as drops via mixing in a continuous phase (water) containing a stabiliser or surface active agent (surfactant) [115]. The monomer drops are transformed into polymer beads via free radical polymerisation initiated by an initiator. A wide variety of commercial products such as poly (vinyl acetate PVAC), poly (Methyl methacrylate, PMMA) and poly(styrene, PS) are manufactured by suspension polymerisation processes. Suspension polymerisation is mostly preferred in industries due to its vast advantages including good temperature control, low level of impurities and low separation cost.

One of the major challenges in suspension polymerisation is the ability to produce polymer beads with a narrow size distribution [114]. Many parameters have been investigated to improve the uniformity of polymer beads in suspension polymerisation including stabiliser type and concentration [116], initiator concentration, reaction temperature [117], and internal design of the reactor like stirrer [118] and reactor geometry [119]. Advanced technologies have also been employed, including membrane emulsification and microfluidic techniques, to generate uniform drops that can deliver uniform polymer beads when polymerised [120,121,122,123]. Although these technologies have potential to produce polymeric beads with a good control over their size and uniformity, they are limited by their high manufacturing costS and difficulties involved in their scale up. To control the size distribution of polymer beads produced by suspension polymerisation, one would require a better understanding of the main parameters affecting drop/particle size distributions.

Typically, the evolution of average drop size during a suspension polymerisation passes through four characteristic intervals [53]. The first interval is known as a “transition

stage" during which the average size of drops decreases as a result of extensive rate of break up. The second interval is the "*quasi-steady state stage*" during which the average drop size remains constant due to the rate of break up being equal to that of coalescence. The most sensitive stage during suspension polymerisation that leads to the enlargement of drops is the "*growth or sticky stage*" in which the rate of drop break-up falls below the rate of drop coalescence due to the increase in the drops viscosity. Finally, in the last interval, the viscous drops resulting from the growth stage reach their "*identification point*" beyond which they cannot be further ruptured nor undergo coalescence, and therefore remain stable and keep their identity. The sequence of these four intervals often leads to particles size distributions becoming much wider than that of the initial monomer drops, which could affect the quality of the final polymer beads [124]. This suggests controlling the rate of drop break up and coalescence during these characteristic intervals is critical for producing beads of narrow size distribution.

Drop break up and coalescence are strongly influenced by mixing conditions as well as by stabiliser type and concentration [125]. There has been much work on the effect of stirring speed on the average particle size, but only few used a stirring protocol as a means to improve the uniformity of the drop/particle size distribution. Yang et. al. adopted a coreverse rotation with different periodic intervals to supress the rate of coalescence during mixing and thus control the particle size distribution. The experimental results showed that the final particles size decreased and the uniformity of particles was improved compared to the steady stirring method [126]. However, they did not explore the underlying reason for this.

In this paper, we present a facile methodology to improve the uniformity of polymer beads by employing a two-stage stirring protocol; the emulsification of monomers was conducted in the first stage at a high impeller speed (rpm), while the polymerisation stage

was carried out using a lower impeller speed. Conventional suspension polymerisation, in which both emulsification and polymerisation stages occurred using the same impeller speed, was also conducted for comparison.

4.3. EXPERIMENTAL

4.3.1. Materials

Methyl methacrylate (MMA), lauryl peroxide (LPO) and polyvinyl alcohol (PVA) (Mw = 85000- 146000; degree of hydrolysis 87-89%) were purchased from Sigma Aldrich. The monomer was purified with ion-exchange resins (Sigma Aldrich) to remove inhibitors prior to use.

4.3.2. Set up

The experiments were carried out using a 0.5-L jacketed glass reactor equipped with four 90◦ baffles. A four-bladed flat turbine impeller with diameter and width of 3.8 cm and 1.1 cm, respectively, was installed inside the reactor for agitation. The temperature of the reactor content was controlled at the desired temperature (75.0± 1.0 ^{o}C) by passing water with appropriate temperature through the reactor jacket. Nitrogen purging was carried out for 15.0 min before the monomer phase was added to the aqueous phase. The impeller speed was set at the desired stirring speed before the start of experiments. The setup for the experiment is shown in Figure 4.1

4.3.1. Procedure

A total of 40.0 ml of methyl methacrylate (MMA) containing 1.0 % of lauryl peroxide (LPO) as initiator was poured into 200 ml of the continuous aqueous phase (distillate water) containing polyvinyl alcohol (PVA) as stabiliser. The recipe for suspension polymerisation is shown in Table 4.1.

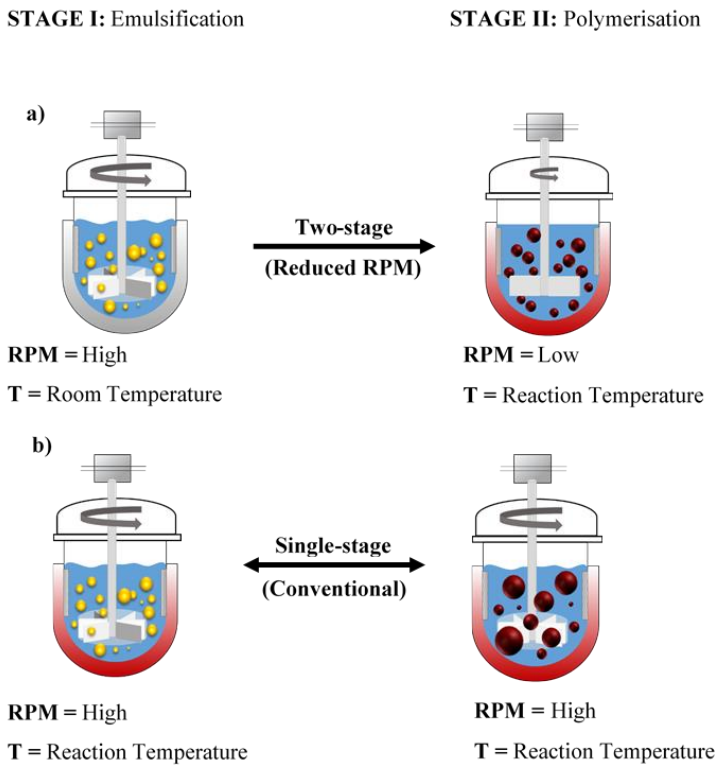

Figure 4.1 Schematic illustration of the experimental set up of **a)** The two-stage protocol and **b)** Corresponding single-stage conventional suspension polymerisation.

The mixture was stirred for 1.0 h during the emulsification stage, which was carried out at room temperature to ensure that viscosity of drops does not change with time due to the polymerisation rate being negligible at low temperatures. The agitation speed was then reduced after 60.0 min and the reaction started by pumping hot water at 75^{o}C through the jacket. Samples were withdrawn at appropriate times to measure the conversion and size of drops/particles.

Table 4.1 Recipe for suspension polymerisation.

Ingredients	Quantity
Water (g)	200
MMA/water (ϕ)	0.20
PVA (g l^{-1})	0.25-1.0
LPO/MMA (%)	1.0
LPO (g)	0.4
Temperature (◦C	75 ^{o}C ± 0.5
Impeller speed (rpm)	250-700

4.3.2. Characterisation of emulsion drops and polymer particles

Conversions were measured gravimetrically. Approximately 3.0 g of the dispersion was withdrawn from the reactor and placed in an aluminium foil dish. The samples were dried in an oven at 75°C for 24 h. The monomer conversions were calculated as the weight ratio of the polymer produced to the total monomer in the recipe.

$$x = \frac{\text{weight of polmer formed}}{\text{weight of monomer in the recipe}} \quad (4.1)$$

Drops/particles sizes were visualised by using an optical microscope (Kyowa Tokyo, Japan) with a camera (Moticam 2300) connected to a computer. The Sauter mean diameter (D_{32}) of particles and their size distributions were measured using a laser diffraction particle sizer (Malvern, Coulter LS130).

4.4. RESULTS AND DISCUSSION

4.4.1. Development of the concept

The size of monomer drops in suspension polymerisation reactors is the result of two opposing effects in the course of reaction, the continuous drop breakup and coalescence. During the transition period in a typical stirred-vessel emulsification, the driving force is the rate of break up, which is much greater than that of coalescence, $R_b >> R_c$, as a result drops continuously but quickly reduce in size until they reach a so-called "*steady-state drop size*". This average size is within the two limits known for liquid-liquid dispersions in stirred vessels.

Above the upper bound, which is called the *maximum stable drop size* d_{max}, drops are extremely unstable and will rupture immediately [127]. Drops with size below the lower bound, *the minimum stable drop size* d_{min}, are doomed to coalesce. Both d_{max} and d_{min} depend on the impeller diameter and speed, as well as stabiliser concentration and oil phase ratio (ϕ).

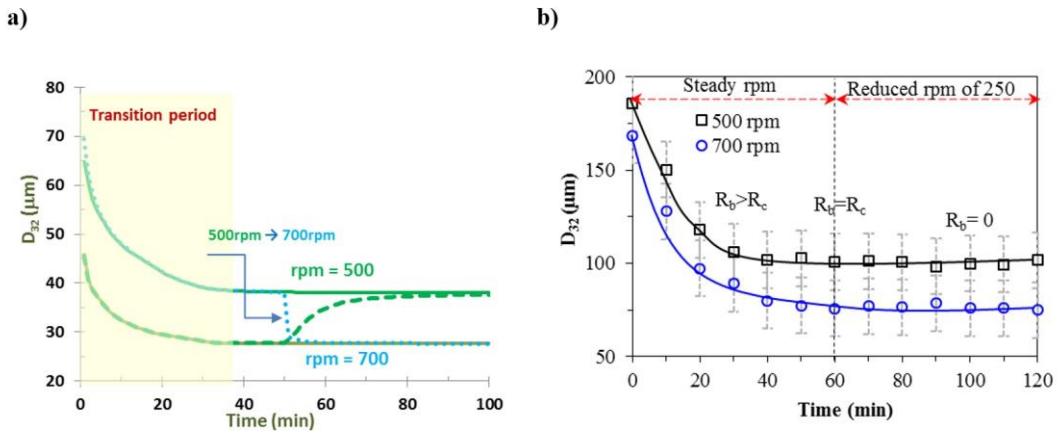

Figure 4.2 a) The theoretical time evolution of D_{32} in a MMA-water dispersion at rpm =500 and 700 rpm and when stirring speed was altered from 500 to 700 rpm or vice versa after 50.0 min in rpm (T =75.0°C, ϕ=0.20, [PVA] =0.1%, see ref [128] for modelling parameters). **b)** Experimental time evolution of D_{32} at =500 and 700 rpm and when stirring speed was reduced to 250 rpm after 60.0 min (T =25°C, ϕ=0.20, [PVA] =0.1 %).

Only drops undergoing coalescence and surpassing the d_{max} can be ruptured again during the steady state. This usually occurs under *dynamic steady state* conditions where a low concentration of stabiliser is used [124]. In this case the number of drops experiencing coalescence is almost equal to those experiencing break up, leaving the average drop size constant. If the stabiliser is effective and its concentration is high, then coalescence is prohibited and a *static steady state* is established, meaning that drops remain intact [124]. Any decrease in the impeller speed, after achieving a steady state, will theoretically increase the average drop size until a new steady state is established after sometime.

Both R_b and R_c will decrease with decreasing rpm. R_b decreases because the shear stress generated in the reactor, which acts to break up drops, is proportional to rpm. R_c is composed of two components, the frequency of drops collision and collision efficiency [129,130] The drop–drop collision frequency decreases, but the efficiency of drop coalescence increases with decreasing agitation speed due to a rise in the contact time. The net result, however, is a decrease in R_c with decreasing stirring speed.

It has been shown that the steady-state drop size in liquid-liquid dispersions is independent of the emulsification path [131]. This means that the average size of drops eventually reaches the steady-state value corresponding to the new rpm after going through a transition period. The transition period, which is the time required to reach the new steady state, may vary with conditions. The transition time following a rise in rpm, such as the one in the initial stage of emulsification, is governed by the rate of break up (i.e., $R_b > R_c$).. However, the transition time following a decrease in rpm is mainly determined by the rate of coalescence as the dominant driving force (i.e, $R_c > R_b$).

The concept behind this research is that if drops produced at a high rpm are maintained at a low rpm during polymerisation, where drops are too small to be further ruptured and then get involved in a cycle of coalescence/break-up events, polymer beads with narrower size distributions will be achieved compared to the case when both emulsification and polymerisation (i.e., conventional suspension polymerisation) occur at a constant rpm. As a matter of fact, such policies are already in use, but they are not explicitly recognised. For example, we recently reported membrane-emulsification assisted suspension polymerisation where uniform monomer drops were produced at a high shear stress in a membrane emulsification vessel, and then were polymerised in a low shear stress stirred tank reactor. This methodology, when optimised, delivered polymer beads with the same uniformity as the initial monomer drops [132]. Similar works have also been reported in the literature [126,133,134] This discussion has been illustrated in Figure 4.2a that shows how the Sauter mean drop diameter responds to an alteration in rpm. It should be mentioned that this numerical analysis is not aimed at the modelling of this process, but just to demonstrate the underlying conceptual design for this research. For the analysis purpose, we considered an emulsification system as defined in the caption of Figure 4.2a and used exactly the same modelling parameters explained elsewhere [124]. The steady-

state Sauter mean drop diameter for this system is 30.0 μm at rpm = 700, which is reached 40.0 min after the onset of stirring.

The stirring speed was reduced to 500 rpm after one hour, when the steady state was already established. Drops showed a continuous, but slow, growth in size soon after rpm being reduced. At a lower rpm of 500, drops were less vulnerable to break up because of the reduced shear stress, as stated before, but drop coalescence could still occur. However, the rate of growth of drops after reduction in the impeller speed is a function of many parameters such as the stabiliser concentration and monomer phase ratio. Figure 4.2a clearly shows how a lower rate of coalescence can supress the rate of growth of drops.

One should note that the opposite alteration in rpm, from low to high, results in a steep decrease in the size of drops. The rate of change in drop size in response to alteration in rpm from at a low rpm 500 to the high rpm 700 seems to be very fast as predicted in Figure 4.2a. This is similar to the events occurring during the transition stage (interval I) of typical suspension polymerisations when the stirring is switched on and R_b becomes the driving force for rupturing drops and reducing their size. The time scale of break up is often much shorter than coalescence. This is because break up is a single-body event but coalescence is a double-body event meaning that coalescence highly depends on the number of drops and collision rate. This delayed response provides a time window during which monomer drops can be converted to polymer beads before too much coalescence can happen.

We now verify the concept developed above for the emulsification stage of MMA. Figure 4.2a shows the variations of drop diameter with time for emulsions made using two different agitation rates of 700 and 500 rpm. These experiments were conducted in

the presence of 1.0 g l^{-1} PVA, which was found to be an optimum stabiliser concentration for suspension polymerisation of MMA under conditions used in this work [124]. The emulsification process took 60.0 min by then the steady-state drop size was achieved. For simplicity, we refer to the impeller speed during the emulsification stage by N_E and to that during post-emulsification stage (i.e., polymerisation) by N_P. The steady-state drop size at the impeller speed N_E = 500 rpm was larger than that at 700 rpm (see Figure 4.2b). These profiles are in agreement with results previously reported [135]. We then reduced the impeller speed to 250 rpm and closely monitored the subsequent change in the average drop size with time for further 60.0 min, which is a typical time for suspension polymerisation to complete. From Figure 4.2b one could see that the size of drops only slightly increased with time and drops identity was almost maintained at the reduced speed, suggesting that the methodology can be extended to the polymerisation stage. In a previous investigation we found that drops formed under similar conditions to those here did not undergo significant break up when exposed to the stirring speeds within the range of ≤ 250 rpm [132]. However, lower stirring speeds than 200 rpm found to be impractical because of creaming and phase separation of the drops, and heat transfer issues.

4.4.2. Finding the operational range of agitation speed

Before proceeding with the main aim of the present study, we first investigated the effect of agitation rate on the final particle size in a typical suspension polymerisation. It is important not only to identify the range of stirring speeds where the reduced impeller speed protocol can be fully examined, but to be able to extend such ranges. Normal operation of suspension polymerisation reactors is generally constrained by two impeller speed limits. The low speed, rpm_{min}, marks the minimum speed that can be used to disperse the monomer phase in the water phase. Below this speed mixing is poor and a stratified layer of monomer may be formed. Advantage of this monomer layer has been

taken in conducting *in-situ* mass polymerisation inside a suspension polymerisation reactor [136].

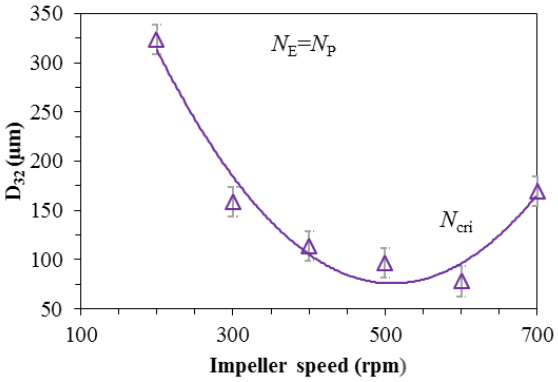

Figure 4.3. Variation in D_{32} of polymer bead with agitation speed ([PVA] = 0.5 g l^{-1}, N_E=N_P (conventional suspension polymerisation).

It is a common practice to increase stirring speed in suspension polymerisation to achieve smaller particles. However this relation breaks down above a critical rpm, N_{cri}, beyond which the use of a more intensive mixing becomes inefficient as particle size increases. The N_{cri} marks the maximum impeller speed (i.e., corresponding to the minimum average particle size achievable) that should be used for any polymerisation setting. When exceeding $N_{cri,}$ a U-shape behaviour in drop/particle size versus rpm could emerge, which has been previously reported and theoretically predicted [135]. The reason for such a behaviour beyond N_{cri} has been attributed to the increased rate of coalescence, so that R_c > R_b, because of formation of too many drops. The stabiliser concentration also plays an important role in the emergence of this feature. As the agitation rate increases, the drops surface area generated increases and thus the coverage of drops by the stabiliser molecules becomes increasingly more difficult. This facilitates drop coalescence and therefore increases the size of (polymerising) drops. One point worthy of note is that conventional polymerisations are always run using an rpm significantly lower than *N*.

Figure 4.3 shows the effect of agitation rate on the final particle size in the presence of 0.5 g l^{-1} PVA. At a low stirring rate (< 200 rpm), a massive coagulation occurred and polymer lumps were created due to the poor mixing in the reactor and the associated phase separation. As the agitation rate was increased, the final particles size initially decreased until 500-600 rpm after which particles started to increase, demonstrating a U-shape curve.

Interestingly, the critical stirring speed of 500-600 rpm obtained in this work is similar to the critical range of 600-700 rpm reported in the literature [135] as a turning point where the minimum particle size was achieved for polymerisation reaction conditions similar to those used in this work. In the next section, we tend to explore the feasibility of polymerisation beyond the critical rpm for two-stage suspension polymerisations.

4.4.3. Application of two-stage agitation protocol

4.4.3.1. Reduction in particle size

Having verified the credibility of the approach for the reaction-free emulsification stage, we extended the work to the polymerisation stage. We used two model rpms; one being rpm = 500 which represents the normal range of stirring and the second one being rpm = 700 which is beyond the normal range of operation for the current conventional system. In this work, the emulsifications were conducted at assigned rpm (700 and 500 rpm) until the drops reached the mode of steady state conditions (t = 60.0 min). Then, the rpm was reduced to the desired level (250 rpm) and the polymerisation was initiated, by increasing the temperature, to convert the discrete drops into polymer beads.

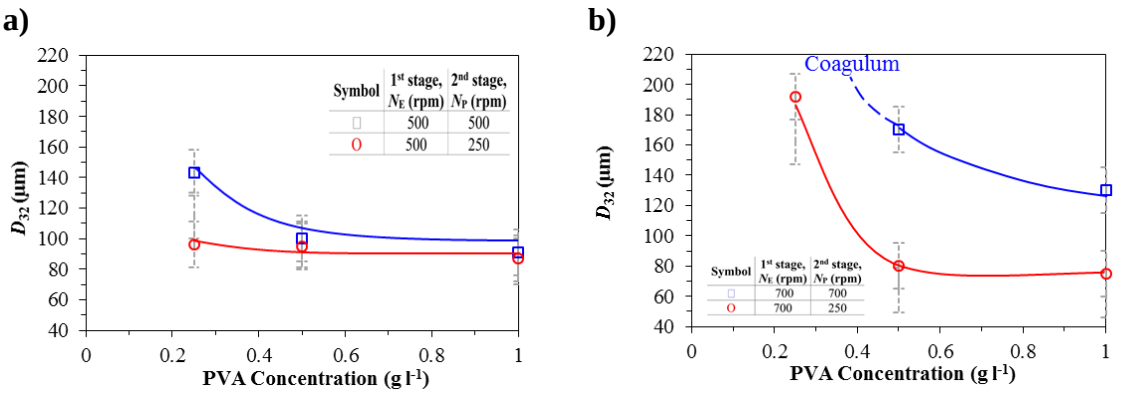

Figure 4.4. Variations in the final Sauter mean diameter of polymer beads with PVA concentrations for two-stage agitation protocol and corresponding single-stage conventional suspension polymerisation. a) N_E=500 rpm, b) N_E= 700 rpm. The polymerisation impeller speed, is N_p=250 rpm, for both studies.

Figure 4.4a and Figure 4.4b illustrate the comparison of particle sizes (D_{32}) obtained when emulsification was carried at N_E=700 and N_E=500, respectively, followed by polymerisation at the reduced stirring speed N_P=250 rpm at different PVA concentrations. The size data from corresponding conventional suspension polymerisation featured by N_p=N_E are also shown for comparison. At both rpms (700 and 500 rpm) the particle size decreased with increasing stabiliser concentration due to the associated decrease in interfacial tension. The results clearly show that the two-stage agitation protocol produces smaller particles than the conventional single-stage process, depending on PVA concentration. The advantage becomes more significant with decreasing PVA concentration.

The cross examination of Figure 4.4a and Figure 4.4b indicates that the size of particles resulting from conventional single-stage suspension polymerisation at 700 rpm is greater than those at 500 rpm. The lack of stabiliser at high rpm and [PVA] = 0.25 g l^{-1}, where large drop surface area was developed, led to gross coagulation of particles. This is in line with the finding from Figure 4.3 that particle size increased with agitation speed above

the critical range of 500-600 rpm. If the same comparison is made for the two-stage protocol, one can see that particles formed at N_E= 700 rpm are smaller than those made at N_E= 500 rpm, except for the lowest PVA concentration used; 0.25 g l^{-1}. This suggests that the two-stage protocol can be used in suspension polymerisation to extend the operational range of rpm as a means to reduce the size of particles.

4.4.3.1. Narrowing PSD

The uniformity of particles obtained using two-stage protocol is best reflected by their size distributions. Figure 4.5a and Figure 4.5b illustrate the comparison of size distribution of particles obtained at N_E=500 and N_E =700, respectively, followed by polymerisation at the reduced stirring speed N_P=250 rpm at different PVA concentrations.

The two-stage protocol always produced narrower size distributions compared with those from conventional single-stage suspension polymerisation. The difference, however, widened with decreasing stabiliser concentration, in a very similar way to the change in the average size of particles with stabiliser concentration.

The cross examination of Figure 4.5a and Figure 4.5b also indicates that the size distribution of particles from conventional single-stage suspension polymerisation at 700 rpm is broader than those at 500 rpm, which is consistent with the concomitant increase in the size of particles above the critical range. We also attempted to further maximise the uniformity of the resulting particles by reducing the polymerisation speed N_P to 150 rpm, but this did not significantly improved the uniformity of the resulting particles for an obvious reason.

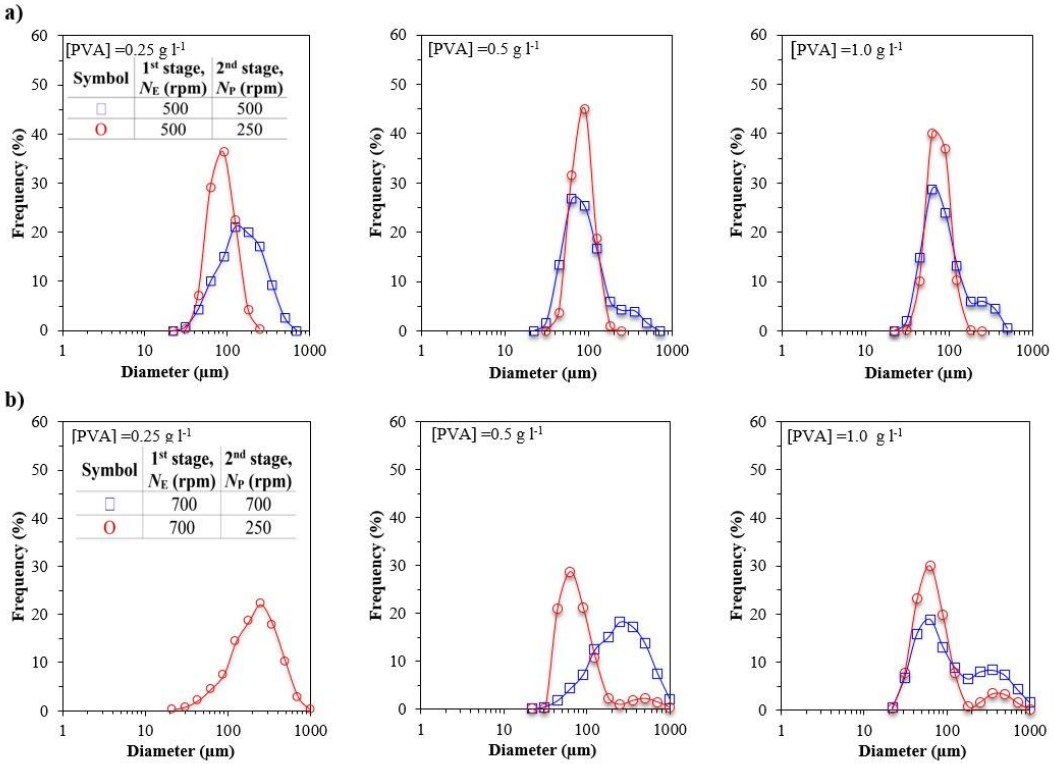

Figure 4.5 Comparison of particles size distributions obtained using two-stage protocol at **a)** N_E = 500 rpm, and **b)** N_E = 700 rpm at different PVA concentration with those from the conventional single-stage suspension polymerisation. The reduced impeller speed of N_p =250 rpm was used for both series.

4.4.4. Application of the two-stage (agitation and stabiliser addition) hybrid protocol

In this section we show how stabiliser partitioning can be used along with the two-stage agitation protocol to improve uniformity of particles. In a recent paper, it has been demonstrated that if a part of stabiliser is added to the reactor prior to the onset of the growth stage, where particles are viscous and cannot be ruptured, polymer beads with smaller size and more uniform distribution may be produced [128]. It was shown that the addition of secondary PVA, which occurred at the onset of the growth stage where particles were robust against creak-up but vulnerable against coalescence, could lead to the narrowing of PSD.

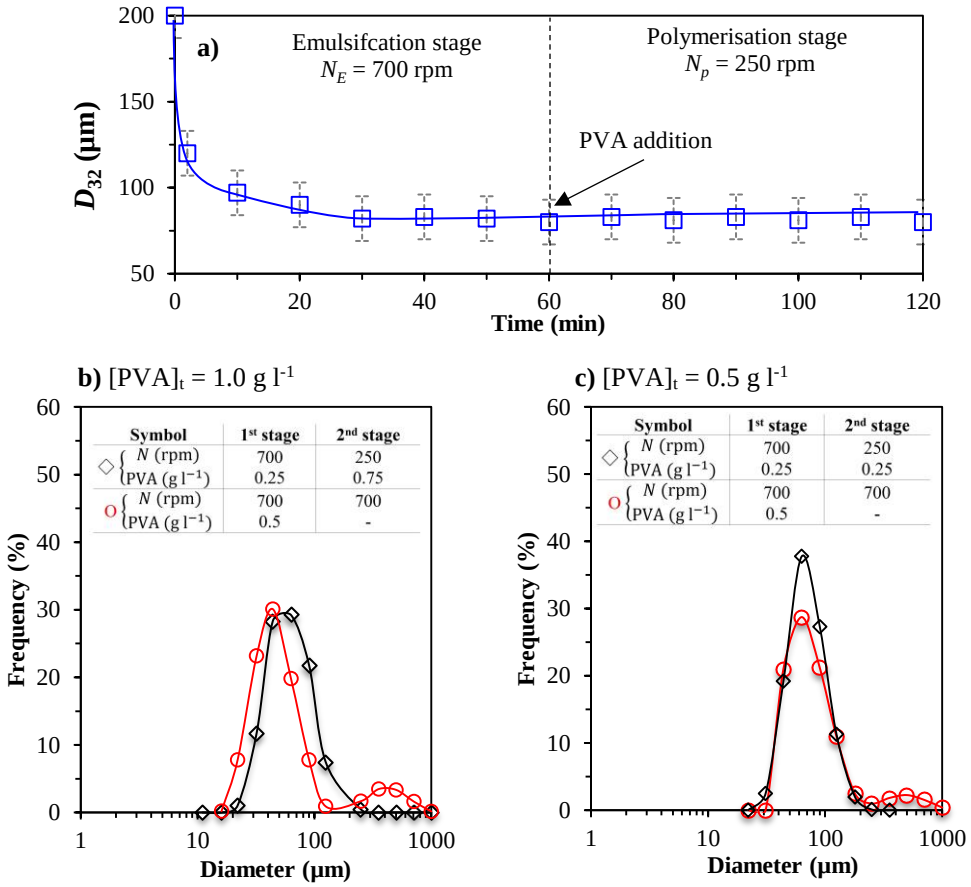

Figure 4.6 a) Effect of the two-stage (agitation and stabiliser addition) hybrid protocol on variation of D_{32} of the drops with time (Total [PVA] = 1.0 g l^{-1}). Comparison of the size distribution of particles formed using the hybrid two-stage (stabiliser addition) at **b)** [PVA]$_t$ = 1.0 g l^{-1} and **c)** [PVA]$_t$ = 0.5 g l^{-1} with simple two-stage protocol.

Following the same line of thought, we explored if the emulsification stage could be conducted at a higher rpm using only a portion of PVA from the main recipe, followed by polymerisation at a low rpm using the reminder of PVA, in order to produce more uniform particles. We divided the stabiliser into two parts, with the first part being added in the beginning of the emulsification stage and the second part at the start of polymerisation stage when the agitation speed was reduced.

To show the addition of PVA at the onset of polymerisation stage will not affect the rate of break-up, we carried out the following analysis. The Sauter diameter in a typical liquid-liquid dispersion in its simplest form is related to Weber number as:

$$D_{32} = k_1 We^{-0.6} = k_1 (d^3 N^2 \rho / \sigma)^{-0.6} = k_2 (\sigma / N^2)^{0.6} \quad (4.2)$$

where d is the impeller diameter, N is the impeller speed, ρ is the density and σ is the interfacial tension. A decrease in N by almost one third from 700 to 250 rpm, as happens as we shift from emulsification to polymerisation stag, will increase D_{32} by 87.0%, while the increase in PVA concentration from 0.25 to 0.50 g l^{-1} for example, assuming half of PVA is added at the beginning of the emulsification and the other half at the polymerisation stage, will decrease the interfacial tension σ by 31.0% (the interfacial tensions at [PVA] = 0.25 and 0.50 g l^{-1} are 6.05 and 4.12 dyn/cm, respectively) and D_{32} by 25.0 % [132]. The net effect is that the decrease in σ is easily compensated by a larger decrease in the shear stress, suggesting that the drops in the 2nd stage of the hybrid two-stage protocol remain robust against break up and thus the additional PVA can only serve to further stabilise them against coalescence. We monitored drop evolution with time when the secondary PVA addition and the reduction in rpm occurred as seen in Figure 4.6a for a typical emulsification. There was no sign of reduction in drop size with time. This validated the statement made before and allowed us to put the hypothesis into practice.

Two series of experiments were carried out at total PVA concentration of 0.5 and 1.0gl^{-1}. In both runs, 0.25 g l^{-1} of PVA was used at the beginning of the emulsification stage. The remainder of PVA concentration (to make the final PVA concentration equal to 0.5 or 1.0 g l^{-1}) was added to the reaction vessel in one shot after the beginning of the second stage when the stirring speed was also reduced.

Figure 4.6b and Figure 4.6c shows the comparison of particle size distributions obtained using simple and hybrid two-stage protocol at 1.0 wt. % and 0.50 wt. % stabiliser concentrations, respectively. We can see from Figure 4.6b that the average size of

particles is similar but their distribution is narrower when the hybrid two-stage protocol is used, compared with the case of two-state agitation protocol. The use of the small portion of the PVA from the recipe in the initial charge at the start of the emulsification stage produced large drops, because of the associated increase in the interfacial tension, but these drops were more efficiently covered by the remainder of PVA during the polymerisation stage. This provided an enhanced stability to growing drops/particles during the growth stage against coalescence and produced particles with a narrower distribution.

At the overall PVA concentration of 0.5 g l^{-1}, the hybrid protocol continued to produce more uniform polymer beads with relatively similar average size, as seen in Figure 4.6c, than the one produced by the two-stage protocol. We found that the hybrid protocol was unsuccessful at $[PVA]_t \leq 0.25$ g l^{-1} (not shown). The reason for this seems to be due to the lack of stability of drops at very low concentration of PVA. In general, the hybrid process was less vulnerable to coalescence due to a smaller drop surface area developed by the reduced amount of PVA used in the initial charge and a better surfactant coverage during the polymerisation stage. This suggests that the hybrid protocol tends to produce more uniform beads.

4.4.5. Coupled two-stage protocol

In this study, we deliberately decoupled emulsification and polymerisation stages in order to ensure the underlying foundation of the concept of two-stage protocol is sound. We carried out the emulsification stage at room temperature and in the absence of reaction, but the polymerisation stage at the reaction temperature (70^{o}C). This allowed drops to achieve their steady-state size before undergoing the polymerisation reaction. In another series, named as coupled protocol, we ran the experiments at the reaction temperature right from the beginning and reduced the rpm sometime, t_{rpm}, during polymerisation. This

protocol allows drops to undergo their transition stage while their viscosity being increased, because of ongoing reaction inside them. This can significantly affect the evolution of drop size during transition and steady-state stages by increasing their size [137].

We carried out the coupled two-stage suspension polymerisation of MMA with the agitation speed of 700 rpm being reduced to 250 rpm after t_{rpm} = 30.0, 20.0, or 10.0 min from the start of the reaction. Any time longer than 30 min, which corresponds to the conversion 0.30 and the onset of the growth stage as seen in Figure 4.7a, could not manage to control the growth of polymer beads. The comparison of particle size distributions obtained via the coupled two-stage agitation protocol at the reaction temperature (i.e., conventional suspension polymerisation) with that from the decoupled two-stage protocol (i.e., emulsification-stage carried out at room temperature followed by the polymerisation reaction at a higher temperature) is shown in Figure 4.7b.

The figure indicates that particles resulting from coupled protocol became larger and their distribution wider when t_{rpm} was further delayed. However, all runs produced smaller and narrower particle size distribution than the conventional MMA suspension polymerisation carried out at 700 rpm. If the same comparison is extended to the coupled two-stage protocol, one can easily see from Figure 4.7b that the decoupled protocol was able to deliver more uniform particles than the coupled and conventional processes. However, with increasing [PVA] to 1.0 g l^{-1} the decoupled protocol did not show a significant improvement over coupled (not shown).

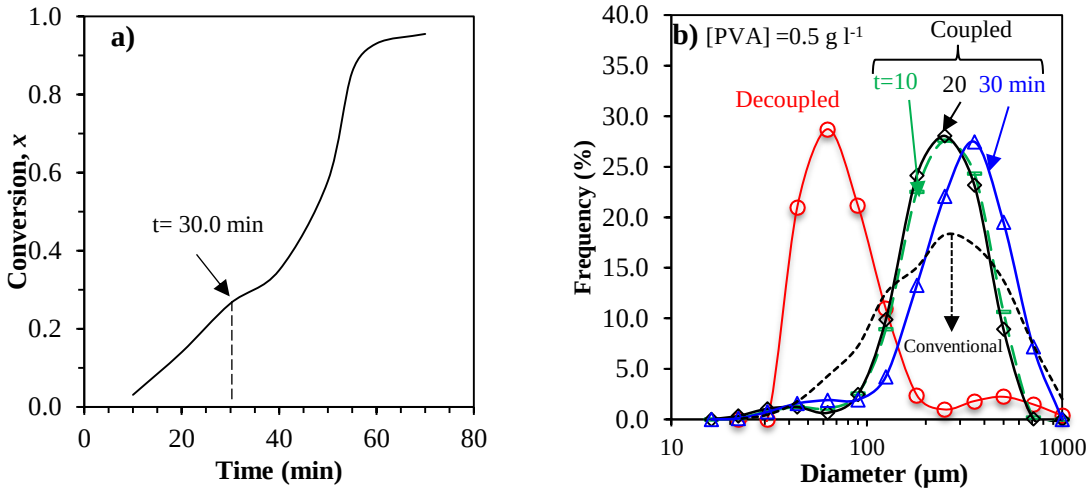

Figure 4.7 **a)** Variations in conversion versus time. **b)** Comparison of particle size distributions obtained via coupled two-stage protocols at [PVA] = 0.5 g l^{-1} at different reduction time with the corresponding decoupled and conventional suspension polymerisation (N_E = 700 rpm and N_P = 250 rpm).

The effect of sudden reduction of impeller speed at various conversions has previously been reported [137]. These investigators found that the reduction of impeller speed during the growth stage at a conversion of styrene at 0.45, produced the narrowest size distribution. It was, however, emphasised that the optimum conversion at which the impeller should be reduced may shift depending on the reaction temperature, initiator concentration and monomer types.

The reason for PSD narrowing in the coupled process lies in the fact that drops do not significantly reduce in size during transition stage because of ongoing reaction inside them, which increases their resistance against drop rupture. The larger the drops at the onset of the growth stage, at a given stabiliser concentration, the more stable they are against coalescence during the growth stage, due to a higher stabiliser surface coverage (i.e., smaller surface area for a given amount of stabiliser). This hypothesis can explain why particle size distributions became wider with increasing t_{rpm} (the longer t_{rpm} the larger

the drops at the onset of growth), but fails to explain the superiority of the decoupled protocol over the coupled one.

One may argue that the emulsification at room temperature could be the underlying reasons for this feature. Indeed, the literature has proved that PVA efficiency behaves differently depending on the molecular weight, temperature as well as the degree of hydrolysis[138]. It has been reported that PVA, similar to the one used in this study, the surface coverage and the interfacial tension decreases with increasing temperature. At low interfacial tension at the reaction temperature produce smaller drops and drops surface coverage. The reduction of the coverage of drops by the stabiliser molecules could facilitate the drops coalescence and therefore increase the size of (polymerising) drops. In contrast, the emulsification at low temperature produced larger drops and more stable and led to more uniform PSD. So the conclusion from this research cannot be generalised and depends on the stabiliser type.

4.4.6. Energy efficiency

The suggested two-stage agitation protocol benefits from a higher energy efficiency. The power required for mixing in stirred vessels is proportional to the agitation speed according to the following equation [139]:

$$P = N_{power} D^5 N^3 \rho \qquad (4.2)$$

where N_{power} is the power number, D is the agitator diameter, N is agitation speed and is ρ the fluid density. The equation above suggests that application of the two-stage suspension polymerisation with N_E =700 and N_p =250 rpm carried out for 90.0 min (30.0 min emulsification and 60.0 min polymerisation), compared with conventional suspension polymerisation carried out for 60.0 min at $N_E = N_p = 700$ rpm, would consume approximately 45.0% less power, which is a significant reduction in energy requirement.

4.5. CONCLUSION

In this work, we developed a two-stage stirring protocol to improve the uniformity of polymer beads obtained by suspension polymerisation. The concept behind this research was to produce drops at a high rpm in the emulsification stage, followed by their polymerisation at a reduced rpm (polymerisation stage). The results showed that the two-stage protocol always produced narrower size distributions than those by conventional (single-stage) suspension polymerisation. The difference, however, widened with decreasing stabiliser concentration, in a very similar way to the change in the average size of particles with stabiliser concentration. The main conclusion drawn from this finding is that the two-stage protocol can extend the range of operational rpm in suspension polymerisation. The application of the hybrid two-stage (agitation and stabiliser addition) protocol further succeeded to improve the uniformity of particles in comparison to the two-stage agitation protocol and conventional suspension polymerisation. Finally, the suggested protocol can also be implemented under isothermal conditions for both emulsification and reaction stages and can still contribute to uniformity of particles.

Chapter 5 Uniform Polymer Beads by Membrane Emulsification-Assisted Suspension Polymerisation [†]

5.1. ABSTRACT

This chapter focuses on a two-stage polymerisation process for the production of uniform polymer beads. Highly uniform droplets were firstly produced by a stirred-vessel membrane emulsification device. Methyl methacrylate (MMA) and a specific grade of polyvinyl alcohol (PVA) were used as monomer and stabiliser, respectively. The effects of various process parameters affecting the droplet size and uniformity including feeding policy, agitation speed, stabiliser concentration, and flowrate were investigated. The evolution of droplets size and their coefficient of variation (CV) were monitored in the course of emulsification. A new start-up policy, validated by monitoring droplet formation at the membrane surface, was introduced that eliminated the non-uniformity in the size of droplets formed early during emulsification. The emulsification was followed by a shear-controlled suspension polymerisation to convert the discrete droplets of MMA monomer to polymer beads. A wide range of reactor impeller speeds and PVA concentrations was studied to find the conditions under which the droplets formed via membrane emulsification would not undergo further break or coalesce during polymerisations and a one-one copy of the initial droplets with the same CV can be achieved.

[†] Alroaithi, M. and Sajjadi, S., 2016. Uniform Polymer Beads by Membrane Emulsification-Assisted Suspension Polymerisation. RSC Adv, 6, pp. 79745-79754

5.2. INTRODUCTION

Polymeric beads with a narrow size distribution have been shown to be potentially important for a wide range of applications, including ion exchange resins [140], drug delivery [141,142], support material for enzymes [143], chromatographic packing materials [144] as well as other medical and pharmaceutical applications [145]. The traditional method to produce polymer beads is based on dispersing monomers in a stirred tank containing an aqueous solution of stabilising agents; suspension polymerisation [146]. The resulting droplets are transformed to polymer beads with the help of mixing, initiator and reaction temperature [147]. The effect of important parameters on particle size including stabiliser concentration, impeller speed, reaction temperature and initiator concentration have been studied in great detail in the literature [146,147,148,149,150,151]. These studies have shown that suspension polymerisation often results in particles with wide size distributions, mainly due to varying rate of droplet breakage and coalescence in the stirred tank reactors. Because of continuous droplets coalescence, there is a significant difference between the size of initial monomer droplets and resulting polymer beads in conventional suspension polymerisation reactors [152]. The coefficient of variance as high as 35% has been reported for polymer beads resulting from conventional suspension polymerisation reactors.

Membrane emulsification, which is capable of producing droplets with a narrow size distribution, has received increasing interest over the past decades [153]. It benefits from the ability to control droplets size and lends itself easily to high throughput production [154].

Cross-flow membrane emulsification is the most common type of membrane emulsification techniques, in which the dispersed phase is directly passed into another

immiscible liquid (the continuous phase) through uniform pores. The droplets are then detached at the surface of the membrane under certain conditions [155]. Cross-flow systems benefit from a constant shear stress across the membrane surface and a reliable scalability. However, the major disadvantages associated with cross-flow systems are the cleaning requirement for membranes after each use and the associated costs of maintenance [155]. Recently a new type of membrane emulsification, which is based on stirred cell-flat membrane (SCFM), has received an increasing attention as a viable alternative to other membrane emulsification methods [155]. While in principle SCFM may be classified under cross-flow membrane emulsification, it differs in the sense that it uses the shear stress generated by a stirring impeller to rupture droplets. The device is much easier to operate, and provides good control over the droplets size and size distribution [154]

The factors controlling the size and uniformity of emulsion droplets in SCFM are the type of membranes and their characteristic properties including pore size and distance between the pores, emulsion formulation, and hydrodynamic conditions (flow rate, shear stress, viscosity of the liquid phases and interfacial tension) [156]. In addition, the surface property of the membrane is another important factor; for example, a hydrophilic membrane is required for making oil-in-water (o/w) emulsions whereas a hydrophobic membrane is required for water-in- oil (w/o) emulsions. The shear stress is the most influential parameter affecting droplets size and size distribution. Despite it is possible to obtain relatively uniform droplets in the absence of shear stress [155], several researchers concluded that a shear stress must be applied at the surface of the membrane if highly uniform droplets are desired. A simple paddle stirrer has been found to induce a uniform shear stress at the membrane surface and provide more uniform droplets[154,155,156]. Increasing the shear stress will stop the growth of the emerging droplets and result in a

faster detachment of droplets, leading to smaller droplets with a higher degree of uniformity[157,158]. Uniform emulsions can be created via SCFM using two types of membranes; standard and ringed membrane, with smaller number of pores for the latter one. A ringed membrane appears to have a remarkable advantage over a standard membrane. The degree of uniformity of droplets created by a ring membrane, expressed in terms of coefficient of variation (CV), has been reported to be approximately one-half of that of the standard membrane at the same operating condition [154].

The application of membrane emulsification to suspension polymerisation has been reported in the literature [149,159,160,161,162]. However, we are not aware of any report on the application of SCFM in suspension polymerisation. The application of SCFM to suspension polymerisation is particularly important because both processes, SCFM and suspension polymerisation reactions, occur in a similar environment (i.e. stirred vessel) via which the extent of shear can be correlated. The main aim of this chapter is to evaluate the possibility of producing highly uniform polymer beads by SCFM-assisted suspension polymerisation. Once uniform droplets are produced via SCFM, they are polymerised in a shear-controlled suspension polymerisation reactor. We used a wide range of flowrate, impeller speed and stabiliser concentration in order to arrive at the optimum conditions. We also developed a different start-up approach, from what has been used by other researchers, which led to an enhanced droplet uniformity.

5.3. EXPERIMENTAL

5.3.1. Materials

Methyl methacrylate (MMA), lauryl peroxide (LPO) and poly (vinyl alcohol) (PVA) (Mw = 85000- 146000; degree of hydrolysis 87-89%) were purchased from Sigma Aldrich.

The monomer was purified with ion-exchange resins to remove inhibitors (Sigma Aldrich) prior to use.

5.3.2. Set-up

Emulsions were produced using a stirred vessel membrane device provided by Micropore Technology Ltd. The Micropore Dispersion Cell (MDC) consisted of a Polytetrafluoroethylene (PTFE) base with an injection tube (PEEK/stainless steel), an emulsification vessel (3.5 cm in a diameter), a sealing gasket to prevent the leaking, a stirrer motor (24 Volts) and a shaft unit (stainless steel) with power supply and vortex breaker made of PTFE/stainless steel.

A hydrophilic-ringed membrane with an array of 10 µm pore size and 200 µm pitches (distance between pore centres) was used. The paddle impeller length and width were 3.1 cm and 1.2 cm, respectively. The membrane was made of nickel with glass based coating with a total area and porosity of 2.8 cm2 and 0.20%, respectively. Prior to use, the membrane disc was cleaned by the following procedure. The disc was initially cleaned with a commercial detergent and subsequently flushed thoroughly with large quantities of distilled water. The washed disc was dipped in an ultrasonic bath containing distilled water for 1 min. The disc was then subjected to a sequence of chemical treatment in the ultrasonic bath, starting with the addition of 4M NaOH solution, followed by the addition of 2.0 wt% citric acid solution (to remove the oxide layer) and methanol, and finally rinsed again with the continuous aqueous phase.

5.3.3. Procedure

A total of 20 ml of methyl methacrylate (MMA) containing 1.0 wt% of lauryl peroxide (LPO) as initiator was injected through the pores of the membrane at a constant rate, using

a syringe pump (Harvard), into 80 ml of the continuous aqueous phase (distillate water) containing a given concentration of PVA as stabiliser.

This gives a dispersed phase ratio (ϕ) of 0.20. All emulsification experiments were carried out at room temperature. Two start-up techniques were used to feed the monomer into the emulsification vessel. These will be discussed in detail in the results section. The resulting emulsions were collected in a hydrophilic borosilicate glass beaker and poured gently into the reactor vessel while being stirred at a given rpm, from a close distance to avoid any unwanted impact on the emulsion. The reactor content, kept under a blanket of nitrogen, was then heated up to the reaction temperature for polymerisation to start.

We monitored the emulsion uniformity during this transfer and ensured that there was no detectable change in the CV of droplets. The reactor used for polymerisation was a 0.5-L jacketed glass reactor with a diameter of 10 cm equipped with four 90° baffles. A four-bladed flat turbine impeller with diameter and width of 3.8 cm and 1.1 cm, respectively, was installed inside the reactor for agitation. The temperature of the reactor content was controlled at the desired temperature (75.0± 0.5°C) by water at appropriate temperature being pumped through the reactor jacket. Figure 5.1 shows the schematic illustration of the stirred vessel membrane emulsification and the polymerisation reactor units used.

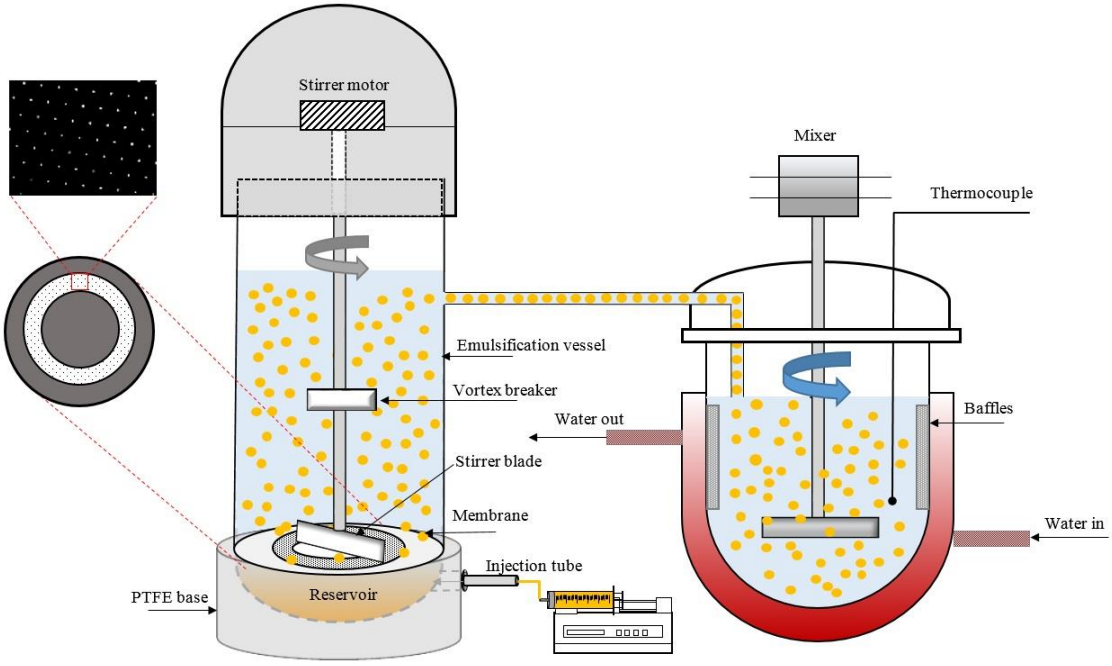

Figure 5.1 Schematic illustration of a) stirred vessel membrane emulsification with micrograph image shows the regular array of pores on membrane used. b) Polymerisation reactor units used.

5.3.4. Characterisation of emulsion drops and polymer particles.

Conversions were measured gravimetrically. Approximately 3.0 g of the dispersion was withdrawn from the reactor and placed in an aluminium foil dish. The samples were dried in an oven at 80°C for 24 hours. The monomer conversions were calculated as the weight ratio of the polymer produced to the total monomer in the recipe. Surface tensions were measured using Du-Nouy ring method. Droplets/particles sizes were measured by using a calibrated optical microscope (Kyowa Tokyo, Japan) with a camera (Moticam 2300) connected to a computer. The Sauter-mean diameter (D_{32}) of droplets/particles, the coefficient of variation (CV), standard deviation (σ) and the number-average diameter (D_n) were calculated, as defined in Eq. (5.1-5.4). A number of droplet/particles (N) were used for size measurements Particles size and size distributions of some samples were

also analysed by laser diffraction particle sizer (Malvern, Coulter LS130) to confirm the particle sizes determined by the optical microscope.

$$D_{32} = \frac{\sum D_i^3}{\sum D_i^2} \tag{5.1}$$

$$CV = \frac{\sigma}{D_n} \times 100 \tag{5.2}$$

Where;

$$\sigma = \sqrt{\frac{\sum (D_i - D_n)^2}{N}} \tag{5.3}$$

$$D_n = \frac{\sum D_i}{N} \tag{5.4}$$

5.4. RESULTS AND DISCUSSION

5.4.1. Stage one: Droplet formation by membrane emulsification

5.4.1.1. Feeding policy

Two start-up techniques were performed to feed the monomer into the emulsification vessel. In method C, the continuous aqueous phase was poured into the emulsification vessel, which was withdrawn through the pores of the membrane and pumped back repeatedly to remove the air bubbles. Afterward, the dispersed phase was injected through the membrane pores into the emulsification vessel. This start-up technique has been recommended by the manufacture of the device (Micropore Technology), and has been used by other researchers [147,154,158].

We introduce an alternative start-up method, method D, in which only to-be-dispersed phase is fed through the membrane. This policy did not allow any intermixing between the phases in the membrane reservoir. Prior to emulsification, the reservoir was void.

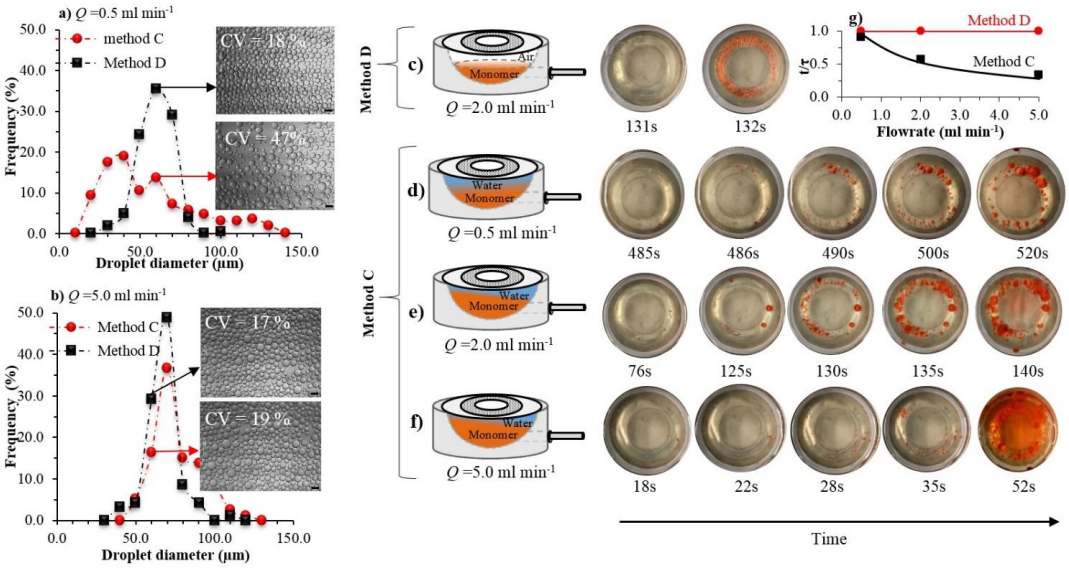

Figure 5.2 Droplet size distribution of emulsions made via methods C and D at flowrate of **a)** Q = 0.50 ml min^{-1} and **b)** Q =5.0 ml min^{-1}. Insets are corresponding micrographs. Scale bar is 100 μm (rpmE=1000; ϕ = 0.20; [PVA] = 1.0 g l^{-1}). The top view of the membrane showing the formation of droplets in the absence of stirring for **c)** method D at the flow rate of 2.0 ml min^{-1}, and **d, e, f)** for method C at the flow rates of 0.5, 2.0, 5.0 ml min^{-1}, respectively. The corresponding schematic illustrations of the filling pattern in the reservoir are also shown in c-f for methods D and C. **g)** Variations in t/τ with flowrate for methods D and C.

The water continuous phase, placed in the emulsification vessel, is prevented from drawing into the reservoir through the membrane pores during pumping if the injection tube is connected to the pump. This guaranteed smooth filling of the reservoir by the dispersed phase as air was pushed out through the membrane, and allowed monomer to come into contact with the water continuous phase only at the membrane surface and during droplet formation. We also investigated the effects of both start-up methods on droplet size in order to maximise the uniformity of droplets.

Figure 5.2a and Figure 5.2b shows the droplet size distribution (DSD) of the emulsions made at two typical feeding rates, while the average size of drops was the same for both methods at low feed rate, represented by Q = 0.5 ml min^{-1}the size distribution of drops

was significantly broader for method C. At high feed rates, represented by Q = 5.0 ml min^{-1}, the average droplet size was again similar, but the size distribution of droplets formed by method C was broader though to a lesser extent.

In order to explain these differences in droplet size distributions, we studied the filling pattern of the reservoir at different flowrates for both methods. Figure 5.2-f shows the schematic illustration of the filling pattern in the reservoir as well as the top views of the membrane surface over a period of time during feeding. The total volume of the reservoir under the membrane, is V_b = 4.40 ml. The residence time of the oil in the reservoir is simply given by $\tau = V_b / Q$, where Q is the flowrate (ml min^{-1}). The variations in t/τ versus Q, with t being the time at which the first droplet appears on the membrane, are given in Figure 5.2g. For method D (Figure 5.2c) all pores became active within a second at t/τ =1.0 regardless of Q values, as expected, indicating that the monomer had to fill the reservoir before it could pass through the pores (residence times of 528, 132 and 52s were obtained for the flow rate of 0.5, 2.0 and 5.0 ml min^{-1}, respectively). The pore activation pattern for method C differs appreciably from that for method D, depending on the flowrate. The dimensionless t/τ continuously decreased with increasing Q. Figure 5.2d-f shows the schematic illustration of the oil-water mixing pattern in the reservoir and the top view photographs of the membrane for three flowrates using method C. At a low feed rate (Q = 0.5 ml min^{-1}), the filling pattern for method C is similar to that of method D, with air being replaced by water. This appears to be due to the surface affinity of the monomer towards the hydrophobic polymeric base which exceeds the gravity effect and keeps the monomer under water. As a result, the first monomer droplet appeared almost at the same time as that in method D (t/τ = 1.0). This long exposure of the monomer phase to the water phase during filling time at low Q, which lasted around 9.0 min for Q = 0.5 ml min^{-1}, could lead to the adsorption of PVA by the monomer phase. The adsorption of

surfactants on expanding interfaces usually starts within seconds. It has been experimentally shown that even polymeric PVA molecules can be adsorbed on the surface of hydrophobic oils within a fraction of minute. Therefore, it is likely that the earlier droplets were produced at lower interfacial tension, resulting in the formation of a large number of small droplets (satellite), as shown in the micrograph images in Figure 5.2a. The formation of satellite droplet at low *Q* has been reported before, but not elucidated. It was also noticed that some of the pores were not active (dead zone), which is likely to be due to the presence of small pockets of the water continuous phase trapped underneath the membrane and across the holes at low *Q*. A smaller number of active pores (see Figure 5.2d) also implies a higher volumetric flux, and as a result larger droplets are formed later during emulsification when the effect of PVA adsorption has subsided. It has been reported in the literature and also confirmed in the following section that the size of droplets increases with increasing flux (i.e. flow rate). The formation of small and large droplets at low *Q*, at early and late emulsification time, respectively, causes a wide droplet size distribution to evolve, as shown in Figure 5.2a, with the average size remaining almost constant. At intermediate *Q*, 2.0 ml min-1, the first droplet appeared at t = 76s and more pores became active in comparison to low *Q*. At high *Q*, 5.0 ml min^{-1}, however, the monomer jet produced in the reservoir channelled through the water phase towards the membrane so that the first droplet appeared at t = 18s at the membrane surface. The PVA adsorption by the monomer during transition period in method C is of little significance at high *Q* because of low contact time. More pores became active with time until most pores became active at around 52s (see Figure 5.2f). During this transition period, the flux underwent a continuous decrease due to the increase in the number of active pores with time, which can subsequently affect the uniformity of droplets by forming increasingly smaller droplets with decreasing flux. This resulted in slight positive

skewness of droplets distribution (Figure 5.2b), but a similar average droplet size with that of method D was obtained.

We can conclude that adopting a right start-up protocol can remarkably improve the uniformity of resulting droplets. The CV of droplets produced using method D was smaller than the CV values of droplets obtained by using conventional start-sup method C in this research and in those reported by other investigators. However, the difference between the two becomes less noticeable at high *Q*, and where a large volume fraction of monomer is to be produced thus alleviating the effect of small droplets formed early during emulsification on the overall CV. Therefore, in view of the improved results, only the second method (D) was selected as the start-up policy for the rest of experiments.

5.4.1.2. Effect of flowrate

Figure 5.3a indicates the effects of flowrate on the droplet size and coefficient of variation. The droplet size increases with the flowrate, a trend which has also been reported before [154, 158]. For the conditions used in Figure 5.3, the velocity of the continuous phase (v_c) is around 160.0 cm/s at 1000rpm ($v_c = \pi ND$ where N is the impeller speed; N = 1000 rpm, and D is the impeller diameter; D = 3) while the dispersed phase velocity (v_d) ranged from 0.60 cm/s to 13.0 cm/s for the disperse phase flowrate (Q) ranging from 0.20 to 5.0 ml min^{-1}, respectively ($v_d = Q/n\pi r2$) where n is the number of pores, n= 8800, and r is the pore radius; r = 5.0 µm).This means that by increasing the flow rate, the velocity gradient ($\Delta v = v_c - v_d$) between phases always decreased. Therefore, the increase in the droplet size with flowrate can be attributed to the decrease in the velocity gradient between the dispersed and continuous phases. A smaller velocity gradient between the phases reduces the shear stress on the forming droplet and results in an increase in the droplet size.

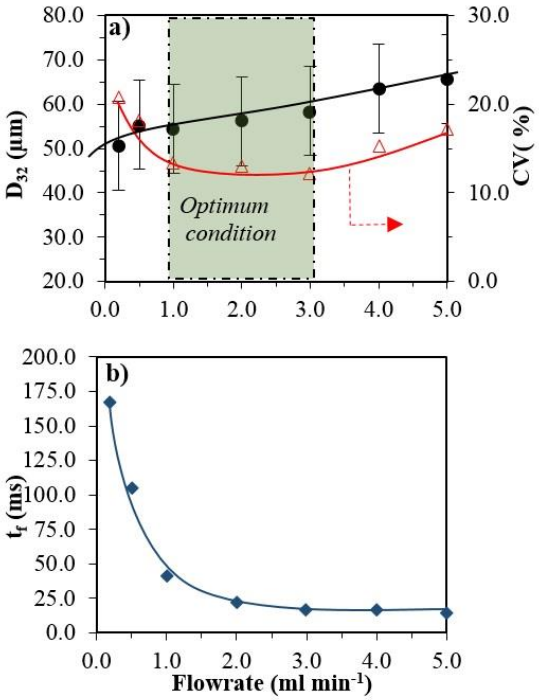

Figure 5.3 a) Effect of flowrate on the Sauter-mean droplet diameter (D_{32}) and the CV. b) The droplet formation time at different flowrates (method D; rpm_E =1000; ϕ = 0.20; [PVA] = 1.0 g l^{-1}).

Another factor that can contribute to the increase in the droplet size with increasing flowrate is the dynamic interfacial tension. Fresh interfaces are created as a droplet expands during formation. The rate of surface expansion increases with the flowrate. The transport of surfactant molecules from the aqueous phase to the surface of droplets is controlled by diffusion. The higher is the flow rate, the shorter is the droplet formation time, calculated by $t_f = nV/Q$, where n is the number of pores, V is the volume of the droplet and Q is the flowrate. The droplet formation time versus flowrate is shown in Figure 5.3b, which indicates that at low flow rates the emerging droplets remained in contact with water during their formation for relatively long time. However, at higher rates droplets formed rather quickly, leaving little time for PVA adsorption on droplets. The lower the amount of surfactant adsorbed at the expanding droplet interface, the larger the dynamic interfacial tension will be at the moment of droplet detachment. The

increased dynamic interfacial tension augments the cohesive force on the forming droplet, resulting in a larger droplet size [156].

The CV initially decreased with increasing flowrate (Figure 5.3a). The high CV at low *Q* is possibly due to the longer contact time between the monomer droplets and the surfactant and the resulting reduced interfacial tension, as stated before, which favours the formation of droplets with non-uniform sizes. Increasing the flowrate to 1.0 ml min^{-1} improved the uniformity of the droplets, and kept CV almost constant until the flowrate of 3.0 ml min^{-1}. A further increase in the flowrate slightly increased the CV. The optimum conditions therefore were found to be within the flow rate of 1.0 - 3.0 ml min^{-1}. We therefore selected the flowrate of 2.0 ml min^{-1} for the rest of this study.

5.4.1.3. Effect of impeller speed

The effect of impeller speed within 500-2500 rpm on the resulting droplets diameter, CV and DSD are shown in Figure 5.4. The droplets form at the pore spacing of the membrane and are detached by the dragging force. Increasing the impeller speed therefore shortens the droplet formation time on the membrane, due to the higher shear stress acting on the droplets at the surface, and as a result reduces their average size (see Figure 5.4a) [157]. The DSD remained almost constant within rpm = 500 – 1500, but broadened with further increase in the impeller speed (see Figure 5.4b).

In order to find the reason for the DSD broadening with increasing rpm, we monitored droplets size and CV with emulsification time; at t = 2.0 min into emulsification and at final emulsification time of t = 10.0 min. The average droplet sizes obtained at t = 2.0 and 10.0 min for rpm_E = 500 – 1500 were similar and within the experimental error.

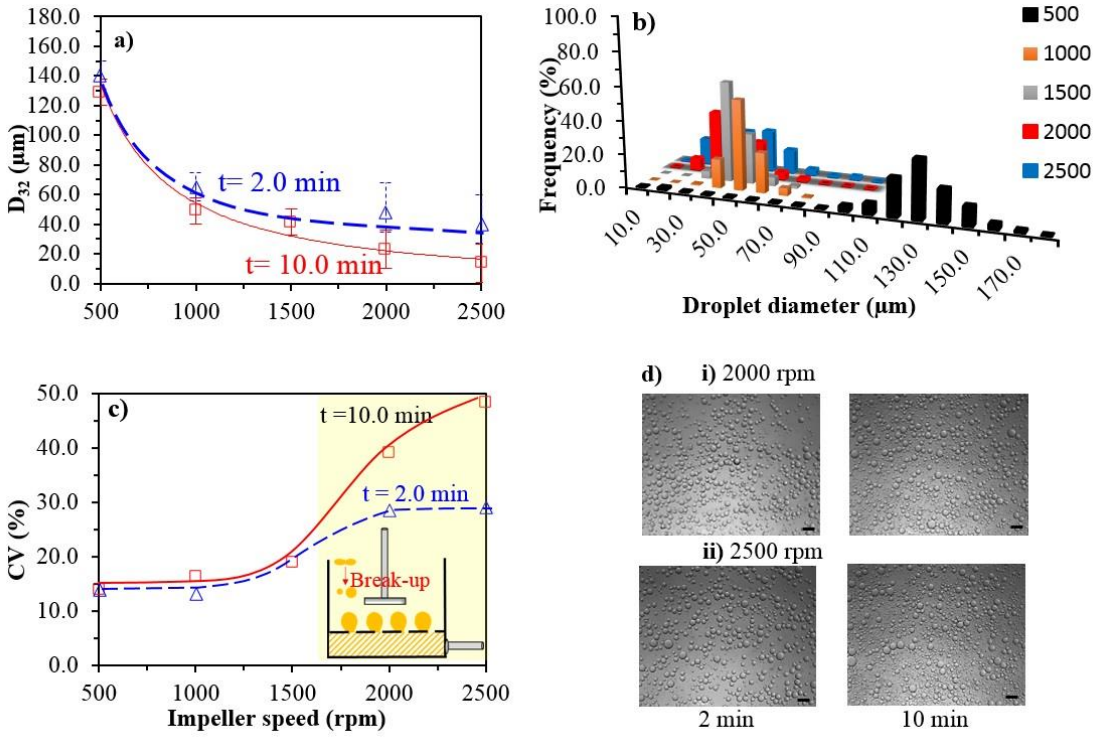

Figure 5.4 Variations in a) the Sauter-mean droplet diameter (D_{32}) and b) the droplet size distribution with the emulsification impeller speed (rpm_E). c) The variations in the CV with impeller speed for emulsification times of 2.0 min and 10.0 min. The inset illustrates the increase in CV due to drop break up in the emulsification vessel. d) Micrographs of the emulsions obtained with emulsification time at i) 2000 rpm and ii) 2500 rpm. Scale bar is 100 μm (method [D]; Q = 2 ml min^{-1}; ϕ= 0.20; [PVA] = 1.0 g l^{-1}).

The results for CV are shown in Figure 5.4c. It is obvious from this figure that the CVs at t =2.0 and 10 min were similar for the runs within the range of rpm_E = 500 - 1500, indicating that droplets formed early during emulsification were stable and remained so. However, one could see the effect of high shear stress, repsented by rpm_E = 2000-2500, on CV with time (Figure 5.4c and Figure 5.4d). The initial CV at t = 2.0 min mainly represents the droplet formation mechanism and the interaction of the droplets on the membrane surface, whereas the final CV embeds information regarding drops interaction in the course of emulsification.

The comparison implies that the uniformity of the droplets degraded with emulsification time due to a continuous break-up and coalescence in the emulsification vessel. The shear

stress at the membrane surface, where droplets are formed, is only a fraction of the maximum shear stress generated at the vicinity of the impeller. With increasing rpm, the likelihood of droplet rupture at the impeller tip increases, leading to the formation of droplets with a wide size distribution.

5.4.1.4. Effect of stabiliser concentration

Stabilisers play a major role in balancing the rates of droplets break-up and coalescence in the process [163,164,165,166,167]. Studies have suggested polymeric water-soluble stabilisers, such as Poly Vinyl Alcohol (PVA), for use in suspension polymerisation processes. The stability of the droplets by PVA depends largely on its degree of hydrolysis. The optimum droplets stabilisation in suspension polymerization process is usually achieved when the degree of hydrolysis of PVA is between 80-90% and molecular weight is of above 70,000. Using PVA with a different degree of hydrolysis may adversely affect the polymer morphology [146, 147,168,]. We used a PVA with a molecular weight and degree of hydrolysis between = 85000 - 146000 and 87-89%, respectively in this research. The effects of PVA concentration on the droplets size and CV were studied within a wide range at 0.25, 0.5, 1.0, 2.0 and 4.0 g l^{-1}. As shown in Figure 5.5a and Figure 5.5b the droplets size and CV initially decreased with increasing PVA concentration, but both reached a plateau at the PVA concentration of around 1.0 g l^{-1}. The decrease in droplet size with increasing stabiliser concentration could be easily explained by the associated decrease in the interfacial tension (see Figure 5.5c), which assists droplet rupture from the membrane.

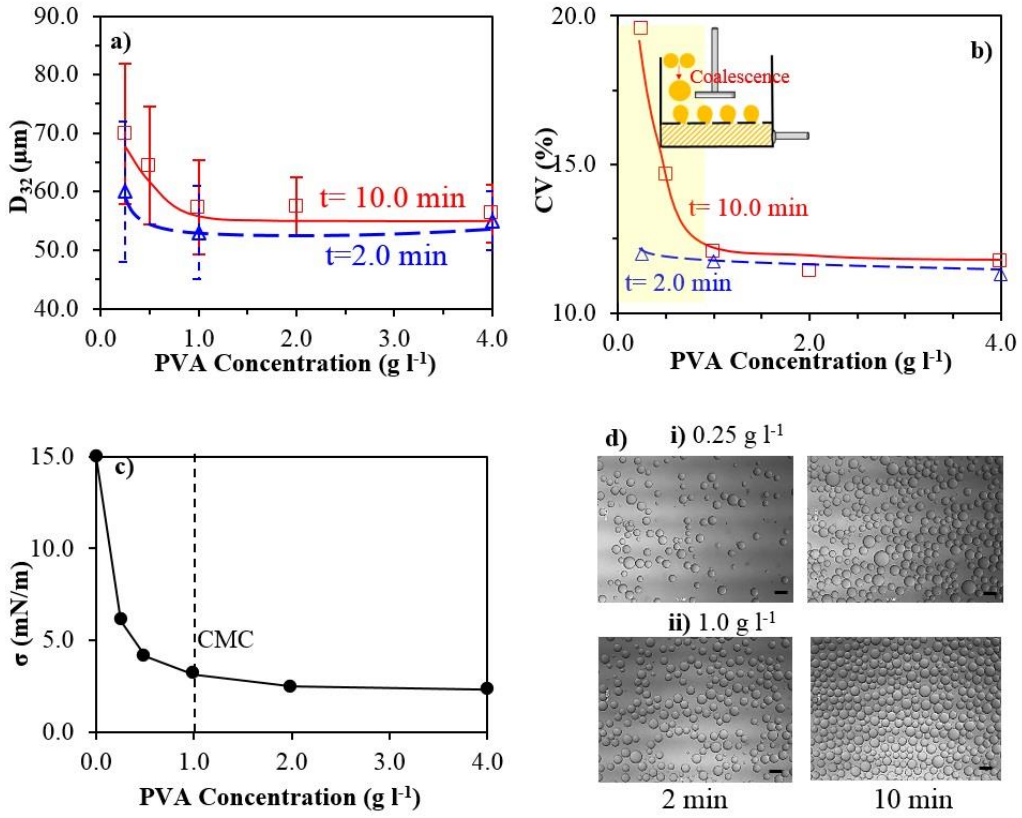

Figure 5.5 a) Effects of PVA concentration on the Sauter-mean diameter of droplets (D_{32}). b) CV of the droplets obtained at emulsification time of 2.0 min and 10.0 min. The inset illustrates the increase in CV due to droplet coalescence in the emulsification vessel. c) Interfacial tension versus PVA concentration. d) Micrographs of the droplets obtained at emulsification time of 2.0 min and 10.0 min using i) 0.25 g l^{-1} and ii) 1.0 g l^{-1} PVA. Scale bar is 100 µm (method D, rpm_E =1000; ϕ = 0.20; Q = 2 ml min^{-1}).

The concentration of PVA at the onset of the plateau for the Sauter-mean droplet diameter (D_{32}) is around 1.0 g l^{-1}, which is close to the critical micellar concentration (CMC) of the PVA. We should note that increasing the concentration of the stabiliser will improve the stability of the droplets against coalescence only if they are not yet fully covered by the stabiliser. A full surface coverage is usually attained at the condition of CMC in the aqueous phase. Any further increase above the CMC will only form micelles (aggregation of stabiliser molecules in the liquid phase), with no significant effect on droplet coverage

by the surfactant. The presence of micelles should be avoided in suspension polymerisation as they can act as the locus of micellar nucleation [146,147].

In order to find the reason for DSD broadening with decreasing stabiliser concentration, we monitored the size and CV of droplets with emulsification time. The results for t = 2.0 and 10 min are also shown Figure 5.5b. It is evident from Figure 5.5b and the micrographs shown in Figure 5.5d for the two typical stabilizer concentrations that the CVs of droplets were similar for all stabiliser concentrations at early time (i.e. when they just formed) but a difference gradually developed which widened with time and decreasing PVA concentration, particularly when PVA concentration was below 0.50g l^{1}. The increase in CV for [PVA] = 0.25 $g.l^{-1}$ was associated with an increase in the Sauter mean diameter of droplets from approximately 60.0 µm at *t* = 2.0 min to 70.0 µm at *t* = 10.0 min, as seen in Figure 5.5d. An increasing CV with time for the lower PVA concentrations, associated with an increase in D_{32}, implies that coalescence occurred during stirring in the emulsification vessel and probably at the membrane surface. Droplets were stable at stabiliser concentrations equal to or greater than 1.0 g l^{-1} and as a result their CV did not change significantly with time.

5.4.2. Stage 2: Suspension polymerisation of resulting droplets

5.4.2.1 Pre-polymerisation stage

Before starting with the production of polymeric particles via suspension polymerisation, it should be ensured that droplets break-up and coalescence are minimised under the mixing conditions employed in the reactor. The emulsification vessel and polymerisation reactor featured different vessel and impeller diameters, and baffling systems and as a result they had different flow regimes. Mixing in the polymerisation reactor occurred under turbulent conditions at rpm >100. Two common policies for scale-up in turbulent

mixing of liquid-liquid dispersions are constant power input per unit mass of fluid (which is proportional to N^3D^2 with N as the impeller speed and D the impeller diameter) and constant impeller tip speed (ND). It has been also reported that the maximum energy dissipation rate occurring at the vicinity of the impeller, which can be 100 times greater than the average value, should be used for scale up. However, the membrane emulsification occurred under laminar or transitional conditions as indicated by the formation of vortices, making it difficult to perform a theory-guided comparative analysis. Therefore, we experimentally studied a wide range of polymerisation reactor impeller speeds (rpmR) to find the optimum mixing condition, which would not degrade the degree of uniformity of droplets resulting from the membrane emulsification during polymerisation. An intermediate concentration of PVA, 1.0 g l^{-1}, from the range of PVA concentrations used in this study, was chosen. A dispersion formed in the emulsification vessel at 1000 rpm and 2.0 ml min^{-1} flowrate and was gently placed inside the reactor vessel. The impeller speed was raised stepwise at the rate of 50 rpm per 10 min (drpm/dt =5 s^{-1}). Droplets size data were recorded at the end of each stage.

Figure 5.6 indicates the effect of the reactor impeller speed on the CV of the droplets with time. As one can see there is a little change in the CV when the impeller speed is lower than 300 rpm, however, the degree of uniformity of droplets started to degrade with further increase in the impeller speed beyond the critical speed of 300 rpm.

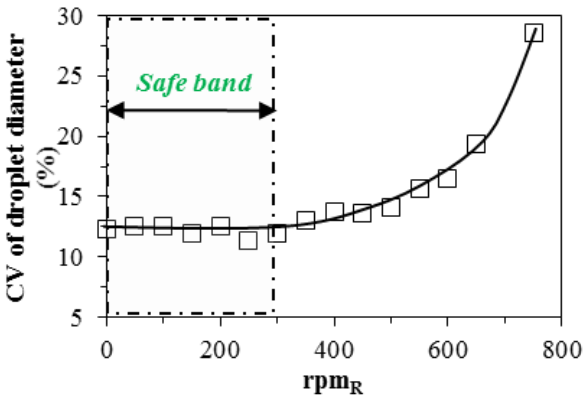

Figure 5.6 The effects of the reactor impeller speed (rpmR) on the CV of droplets formed by membrane emulsification (method D, rpmE =1000, Q = 2.0 ml min-1; ϕ = 0.20; [PVA] = 1.0 g l^{-1}).

In a typical suspension polymerisation, an optimum rpm is usually required not only to preserve droplet sizes during the reaction but to provide rapid heat transfer from the reactor too. An impeller speed of lower than 100 rpm was found to be impractical because of creaming and phase separation of the droplets, and lack of control on the reaction temperature. We concluded from Figure 5.6 that the safe band for conducting polymerisation reactions is within 100-300 rpm, from which we select rpm = 250. This prudent rpm provides a minimum drop break-up and coalescence in the polymerisation reactor. It is also sufficient to enhance mixing and heat transfer during reactions so that the reaction temperature could be easily controlled.

5.4.2.2 Polymerisation stage

After the optimum impeller speed was identified, the reaction was carried out at the same rpm in order to study the effect of PVA concentration on the size of monomer droplets and final polymer particles. Our aim was to be able to control the growth of droplets during polymerisation and obtain similar droplet/particle size distributions. A suspension polymerisation reaction typically passes through four stages which are; transition, quasi steady state, growth or sticky and identification stages [152]. In the current work, the

transition stage did not exist, as droplets had already been formed. The conversions were measured versus time for polymerisation runs using a low and high concentration of PVA, and are plotted in Figure 5.7a. From this figure it is clear that the rate of polymerisation was not affected by the PVA concentration and droplet size, which agrees with the literature.39 It also shows that there is a dramatic increase in the rate of polymerisation around the conversion of 0.30, which is known to be due to the gel effect. The onset of the gel effect occurred at about 40 min and the as a result conversion reached a value as high as 90% in few minutes. So we can conclude that the kinetics of polymerisation, and as a result droplets properties such as viscosity, were not influenced by the PVA concentration used.

Figure 5.7b illustrates the comparisons of the D_{32} of monomer droplets and final polymer particles versus PVA concentration. As can be clearly seen, the average size of droplets was slightly above that of particles when [PVA] $\geq$ 1.0 g l^{-1}. We take a note that droplets shrink around 10% in diameter when they transform from MMA monomer droplets to PMMA particles ($\rho_{\mathrm{MMA}} = 0.940\ \mathrm{g\ cm^{-3}}, \rho_{\mathrm{PMMA}} = 1.18\ \mathrm{g\ cm^{-3}}$). This suggests that there was no significant droplet coalescence or break up during polymerisation within this range of PVA concentration and as a result a similar CV was obtained for polymer particles and monomer droplets.

However, for [PVA] < 0.5 g l^{-1}, particles size became larger than their initial droplet size, despite their shrinkage, and their CV being increased, indicating a significant coalescence occurring in the course of polymerisation in the reactor, as shown in Figure 5.7c. The droplet/particle size distributions shown in Figure 5.7d and Figure 5.7e confirm that wide and narrow PSDs were obtained at typical low and high concentrations of PVA, respectively.

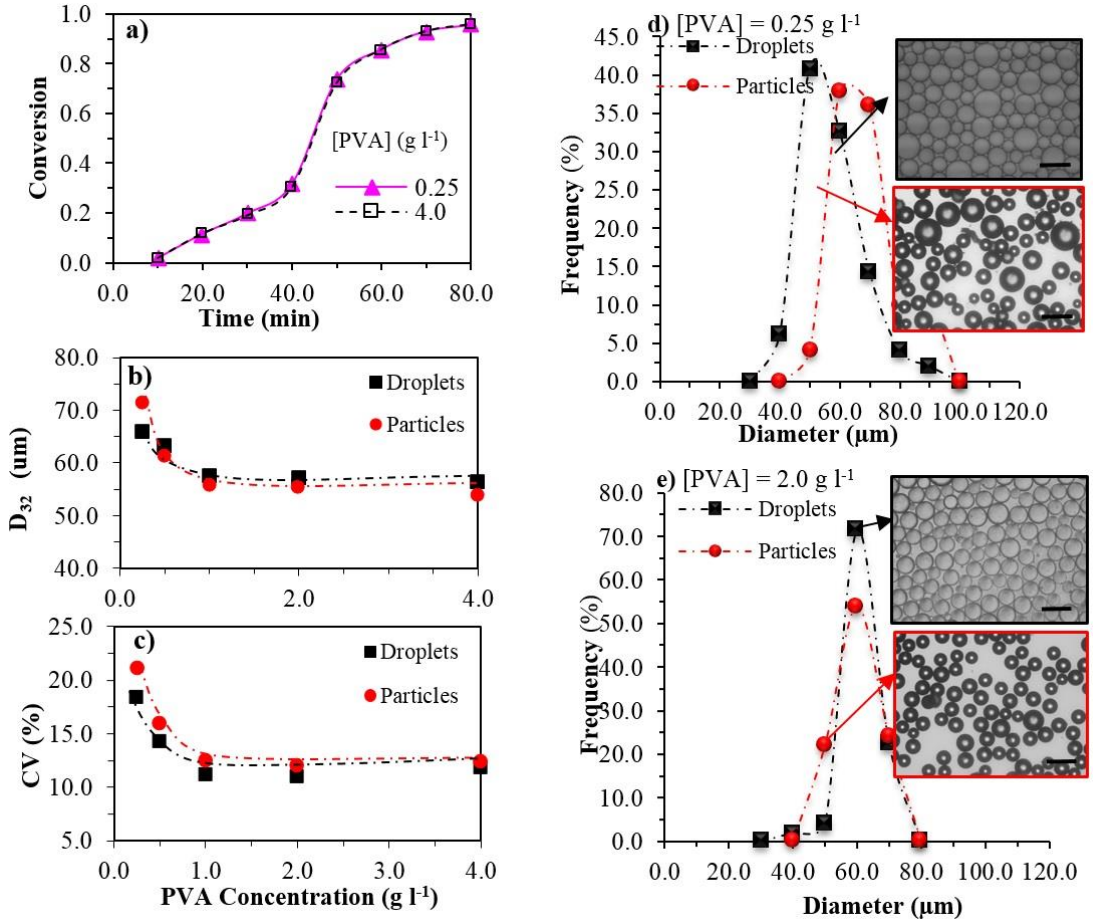

Figure 5.7 a) Variations in conversion versus time for two different PVA concentrations. b,c) The sauter-mean diameter (D_{32}) and CV of monomer droplets/final particles at versus PVA concentration, respectively. d,e) Droplet size distribution of monomer droplets and final particles at two PVA concentrations of 0.25 g l^{-1} and 2.0 g l^{-1}, respectively. Insets are corresponding micrographs. Scale bar is 100 µm (method D, rpm_E=1000, rpm_R = 250, Q = 2.0 ml min^{-1}; ϕ = 0.20).

This clearly suggests that the degree of uniformity of droplets was effectively maintained during polymerisation if a sufficient amount of stabiliser, via which the growth stage could be hindered, was used. This minimum or critical concentration was found to be 0.5 g l^{-1} for the current polymerisation system. We showed in a previous section that in the absence of reaction in the membrane emulsification vessel, the critical PVA concentration is 1.0 g l^{-1} and droplets formed using PVA concentrations lower than this value underwent coalescence.

Figure 5.7c shows that the CV of polymer beads from assisted-suspension polymerisation is smaller than 20%, which shows a significant improvement over that from conventional polymerisation, which is usually greater than 30%[169,170]. To confirm this, we also made polymer beads using a similar formulation to that used in this research via a conventional polymerisation system in which both emulsification and polymerisation occurred simultaneously in the reactor ([PVA] = 1.0 g l^{-1}, ϕ = 0.20, T = 75.0± 0.5°C, rpm = 700). The CV of the final beads was 42.0%, which is much greater than the CV of those obtained from the membrane-assisted polymerisation.

5.5. CONCLUSION

Highly uniform monomer droplets obtained via stirred cell-flat membrane (SCFM) were successfully converted to uniform polymer beads via suspension polymerisation. The similarity between the environments where droplets form in the SCFM vessel and those of the polymerisation reactors where droplets undergo polymerisation facilitates the controllability of droplets uniformity. We introduced a novel start-up method that did not allow intermixing of phases prior to emulsification and any associated mass transfer involved, thereby enhancing the uniformity of resulting droplets.

Highly uniform droplets were obtained via membrane emulsification at an impeller speed range 500 -1500 rpm and flowrates within 1.0-3.0 ml min^{-1}. The size distribution of monomer droplets underwent broadening at high impeller speed due to droplet break up in the emulsification vessel. The monomer droplet size and CV increased with further increase in the flowrate above the optimal range. PVA helped to stabilise the droplets; however, there was not any apparent advantage in increasing the amount of stabiliser above its CMC. The CV significantly increased at low PVA concentration due to droplet coalescence in the emulsification vessel during circulation. Safe ranges of the reactor

impeller speed and PVA concentration, within which the degree of uniformity of monomer droplets formed by membrane emulsification could be preserved during polymerisation, were found. One important highlight of this research is that we were able to decouple factors responsible for degradation of droplets uniformity during circulation (in the emulsification vessel) from those affecting droplets during formation at the membrane surface from the outset. The main conclusion drawn is that to achieve maximum droplet uniformity, the phase ratio of dispersed droplets should be kept at minimum and droplets leave the emulsification vessel as soon as they are formed. This suggests that an optimum range of operations for the SCFM device will be achieved in a continuous mode.

Chapter 6 Fabrication of Highly-Ordered Interconnected Porous Microparticles ‡

6.1 ABSTRACT

Herein, we present a facile and versatile route for the fabrication of uniform porous microparticles with well-defined interconnected windows. Three different porous microparticle shapes, defined based on the shape of the external drop, namely spherical, semi-spherical, and plug were produced. We used a microfluidic platform to first produce monodisperse w/o/w double emulsions. The uniform double drops with controlled number of encapsulated inner water droplets were then consolidated into porous microparticles through UV photopolymerisation of the oil (monomer). The size and number of cores, porosity, shape and structure of the microparticles could be precisely tuned by the flowrate, confinement offered by the geometry of the channel, and by packing structure of the inner droplets. We tracked the evolution of drops morphology and the resulting microparticles with alteration in the flowrates. We concluded that the shell thickness of the monomer phase should be minimised in order to produce interconnected windows. The proposed strategy provides a key advantage for the fabrication of uniform porous microparticles over many existing technologies.

‡ To be submitted

6.2 INTRODUCTION

Porous polymeric materials have attracted a great attention due to their distinctive properties. They are characterised by the presence of external pores on the surface as well as inner interconnected windows. Porous materials enjoy several mechanical advantages over impermeable substances, such as light weight [171], well-defined porosity, high surface area [172,173], and excellent absorption capacity. Porous polymeric microparticles, which are miniature porous entities, are extensively developed for a wide range of applications including ion exchange resin, separation and filtration [174], encapsulation agents for controlled release of drugs [175], catalysts [176], supports for catalysts [177], and packing materials in chromatography industries [178,179,180,181]. A recent highly regarded application is scaffold for tissue engineering [182,183]. For this application, highly porous microparticles with interconnected windows are required to facilitate the transport of nutrients within the scaffold.

Most porous microparticles are conventionally synthesised thorough a number of techniques including solvent evaporation, polymerisation or seed swelling method [184]. While porous microparticles are easy to fabricate through the solvent evaporation method, the diffusion of the internal phase or oil phase during evaporation, which is difficult to control, has dramatic effects on the porosity and window size of the final products [93]. Similarly, porous microparticles resulting from polymerisation techniques (i.e. suspension) suffer from a low uniformity in both window and final particles sizes, whereas seed swelling method, which benefits from a facile generation of uniform nano or micro particles, cannot produce microspheres over 10 µm [185].

Literature clearly indicate that the porosity, window size and surface functionality of porous microparticles have directly influenced their applications. Controlling these

parameters are therefore very crucial. Any non-homogeneity in these parameters can have an adverse effect on absorption or release kinetics of the porous materials [186,187]. Therefore, the developments of procedures to rationally control the porosity, window size, and particle shape to obtain well-defined porous microparticles are highly desired. Recently, microfludics have been utilised to produce highly uniform single or double emulsion drops in a reproducible manner, which can subsequently be polymerised, usually by photopolymerisation, to obtain a wide range of materials such as simple microparticles and microcapsules with well-defined morphologies and properties. However, the fabrication of uniform porous microparticles using such emulsions with a controlled number of windows, window size, and porosity in a single step is still a challenge. A recent paper [188] has employed a high internal phase emulsion (HIPE) in conjunction with microfluidics to produce uniform particles but with polydisperse windows.

Currently there is no on-the-fly approach that facilitates drop transformation into a porous structure with interconnected windows during polymerisation. An offline method, which used dissolution of the thin shell layers of the tightly-packed encapsulated cores to from a porous particle, however, has been reported [189,190].

To date, most microparticles produced by microfluidics have been spherical in shape due to the relative ease in their fabrication. Non-spherical microparticles are generally challenging to produce due to the domination of surface tension force between two immiscible phases, which resists the formation of non-spherical shapes [191]. Non-spherical microparticles, however, can be produced by compressing a drop in a confined channel with diameter smaller than that of the drop [192]. Non-spherical particles can be packed more densely than spherical particles [193]. They also benefit from a light weight

and behave differently, from spherical particles, under the same hydrodynamic [194], magnetic [195], and electric conditions [196]. Non-spherical microparticles can also help to simulate the molecules shape in their self-assembly studies, as most molecules are non-spherical [197].

In this work, we demonstrate a simple and versatile microfluidic approach for the fabrication of spherical and non-spherical porous microparticles with highly-ordered and well-defined interconnected windows. The size, shape, and internal structures of particles were manipulated in a single step, using a microfluidic set-up. Typical experiments consisted of producing water/oil/water (w/o/w) double emulsions, with controlled number of encapsulated inner droplets, which were used as templates for the production of porous microparticles. We examined different configurations of drops and their evolution from critically packed to highly packed morphology. Plug-like porous particles were also obtained by polymerising large double drops confined within narrow capillaries, which is reported for the first time.

6.3 EXPERIMENTAL

6.3.1. Materials

2-ethylhexyl acrylate (EHA, 98.0%, Sigma-Aldrich), isobornyl acrylate (IBOA, 85.0% Sigma-Aldrich), trimethylolpropane triacrylate (TMPTA, 80.0 %, Sigma-Aldrich) were used as monomers. Poly (ethylene glycol)-block-poly (propylene glycol)-block-poly (ethylene glycol) **(**PEG-PPG-PEG) (Pluronic L-81) (average Mw ~ 2800 g mol^{-1} and HLB ~ 2) and Irgacure 907 (BASF) were used as surfactant and photoinitiator respectively, in the middle (monomer) phase. Poly (ethylene glycol)-block-poly (propylene glycol)-block-poly (ethylene glycol) (Pluronic F-127) (average Mw ~12,500 g mol^{-1} and HLB ~ 22) was used as surfactant in the inner or outer aqueous phase.

6.3.2. Microfluidic device fabrication

For the generation of w/o/w emulsions, four micro-capillaries were used as the inner (ID: 50.0 µm, OD: 80.0 µm), middle (ID: 150.0 µm, OD: 250.0 µm), outer (ID: 300.0 µm, OD: 400µm) and an extension capillary (ID: 500 µm, OD: 1000 µm), all introduced and aligned axisymmetrically. The capillaries were then placed on a microscope slide and the ports were placed on the coupled capillaries, which are resting on the microscope slides, glued (Devcon 5-minute epoxy) and left to harden completely. All capillary surfaces were selectively treated. The capillaries through which oil was flown were made hydrophobic by treatment with n-octadecyltrimethoxysilane while the surface of the capillary where the water went through was made hydrophilic by plasma treatment (Femto Plasma cleaner, Diener).

6.3.3. Procedure

The uniform w/o/w drops were generated by pumping the inner water phase, having 1.0 wt% of Pluronic F-108, through the middle phase containing 91.0 wt% of the monomer mixture (composed of 75.0 wt. % EHA, 20.0 wt. % IBOA, and 5.0 wt. % TMPTA based on the total weight of monomer phase), 5.0 wt. % of surfactant Pluronic F-127, and 4.0 wt. % irgacure 907 photoinitiator dissolved in the monomer phase prior to the experiments. The middle phase, engulfing the inner phase, was then pumped into the external aqueous solution of 1.0 wt. % F-108 (outer phase), which was pumped before the monomer phase to avoid wetting the external channel. The syringe containing the monomer was wrapped in an aluminium foil to avoid light penetration. All phases were pumped through the microcapillaries using Harvard pump 11 Elite. The schematic illustration of the device used for the fabrication of various w/o/w compound drops is shown in Figure 6.1.

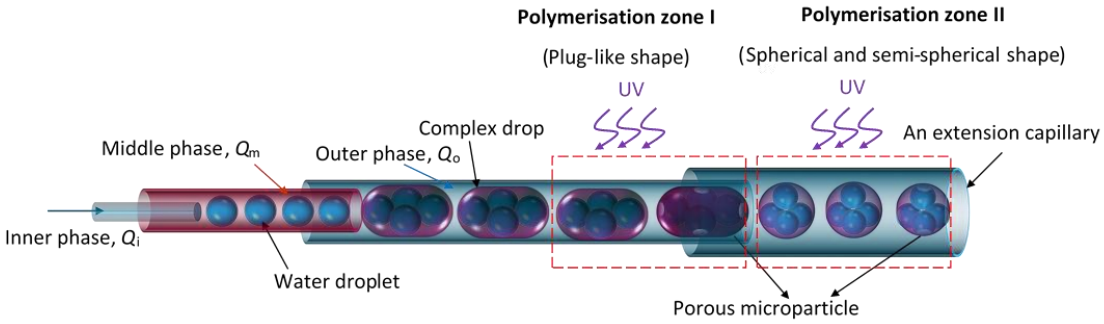

Figure 6.1 Schematic illustration of the 3D co-flow microfluidic device designed for the preparation of porous interconnected microparticles.

The generation of drops with various morphologies with a controlled number of inner core droplets was precisely manipulated by varying the flow rates of the inner, middle and outer phases (Q_i, Q_m, and Q_o, respectively) as well as the geometry and size of the outer channel. Drops were formed at the tip of the capillary and detached by the high shear forces exerted by the external continuous phase. These compound drops travelled downstream first through a narrow outer channel where they were forced to adopt non-spherical shape (zone I), and later through a wider outer microcapillary (zone II) where they were relaxed to regain the spherical shape (Figure 6.1). The generation of emulsions in the microfluidic device was observed by a high-speed video camera (Photron FastCam Ultima APX—monochrome).

The generated w/o/w emulsions were photopolymerised by the UV irradiation and converted to polymer microparticles. The polymerisation zone determined the shape of the microparticles. Non-spherical plug-like microparticles were obtained when drops were polymerised in the outer confined microcapillary (Polymerisation zone I; ID: 300 µm, OD: 400µm), while spherical/semi-spherical microparticles were obtained when the polymerisation zone was shifted downstream to the wider extended capillary

(Polymerisation zone II; ID: 500 µm, OD: 1000µm). The polymer microparticles were collected and left to dry before characterisation.

6.3.4. Morphological Characterisation

Drops/particles with various shapes and structures were observed and sized by an optical microscope (Kyowa Tokyo, Japan, with a camera Moticam 2300 connected to the PC). The morphology, diameter of the windows, and surface features of the microparticles were assessed by scanning electron microscope (SEM; Hitachi, S4000). For SEM, samples were coated with a thin layer of approximately 5.0 nm of gold and placed on a stud before analysis. The SEM was operated at 5.0 kV.

6.4 RESULTS AND DISCUSSION

6.4.1. Study of chemical formulations

A careful selection of monomers is essential for successful fabrication of polymeric materials via UV polymerisation. A droplet moving in a microchannel will have only a small fraction of a second to polymerise by the UV light and therefore it should be highly reactive. We investigated monomers that can be used for fast polymerisation, in order to provide a comprehensive guide and source of information for those wishing to join the field of rapid UV-based synthesis of polymeric materials via microfluidics.

We started with styrene, which is used as a model monomer in various polymerisation techniques. We exposed styrene drops to UV under static condition (no moving drop) and monitored the progress of reaction with time. The drops showed little absorbance of UV light and proved to be poorly reactive even within the exposure time of longer than 20.0 min.

We then tested methacrylate-based monomers such as methyl methacrylate (MMA), glycidyl methacrylate (GMA), butyl methacrylate, and crosslinkers like ethylene glycol dimethacrylate (EGDMA). The polymerisation time for these monomer drops took few minutes in a static condition before they are sufficiently solidified. There is no report in the literature that has managed to produce polymeric particles using these monomers on the fly within a short span of time. Chaurasia et. al produced methacrylate-based ultrathin shelled drops via microfluidics, but the polymerisation reaction was conducted under static conditions for 10.0 min [198]. Serra et. al. used methacrylate-based monomers and managed to produce polymeric particles on the fly by increasing the exposure length and intensity (wrapping the outer channel with aluminium foil), but an exposure time of 2.0 min was required [199]. As the objective of this research was to achieve instant polymerisation of the moving drops in microchannel, styrene and methacrylate-based monomer did not appear to be ideal choices and thus were not further considered in this research for the fabrication of polymeric materials.

Acrylate-based monomers are highly reactive and form closely cross-linked networks, in the presence of a cross-linker, when undergo radical polymerisation; particularly photopolymerisation. There are a number of studies reported in the literature based on the fly polymerisation of acrylic monomers. It has been demonstrated that drops of acrylate-based monomers can be polymerised within 200 ms [56, 57]. Our preliminary experiments also proved that acrylic monomers are good candidates for rapid UV polymerisation of drops to microparticles. We have verified acrylic monomers such as trimethylolpropane triacrylate (TMPTA), 1,6-hexanediol diacrylate (HDODA), tri(propylene glycol) diacrylate (TPGDA), isobornyl acrylate (IBOA), and 2-ethylhexyl acrylate (EHA) as good candidates.

However, the use of IBOA, TEMPTA, TPGDA, and HDODA failed to produce complex structures such as porous microparticles because of the lack of stability of the inner phase before polymerisation could take place (i.e. coalescence occurred few seconds after drop formation). EHA, however, was found to be a promising choice as it did not compromise emulsion stability. Yet, the polymer materials made of EHA were elastic. Hence, IBOA was used as co-monomer in order to improve the elasticity of the polymeric materials. TMPTA was used as a cross-linker to impart porosity as well as strength to the resulting polymer particles while maintaining the stability.

Stabilising multiple emulsions requires at least two different surfactants: one with a low HLB (Hydrophilic–Lipophilic Balance) for the w/o interface and another one with a high HLB for the o/w interface. We used 5.0 wt. % Pluronic L-81 (HLB ~ 2) and 1.0 wt. % Pluronic F-127 (HLB ~ 22) in the middle and outer phase, respectively. We prepared uniform w/o/w emulsions, using the set up shown in Figure 6.1, and studied their stability. The resulting w/o/w drops were stable during formation and also during flow in the microcapillary.

Despite that long-term stability of w/o/w drops is not required for instant microfluidic polymerisation, it is very useful to determine the conditions under which the core droplets begin to coalesce. When the drops were collected in the downstream and monitored, a tendency for the internal core droplets to coalesce with each other, rather than with the shell drop, emerged with time.

Figure 6.2a shows w/o/w drops containing no surfactant in the core droplets at time 0.0 and 40.0 min, suggesting that droplet-droplet coalescence may occur before droplet-drop coalescence. The inner core droplets remained stable for a longer time (Figure 6.2b) if they contained the water-soluble surfactant (Pluronic F-127).

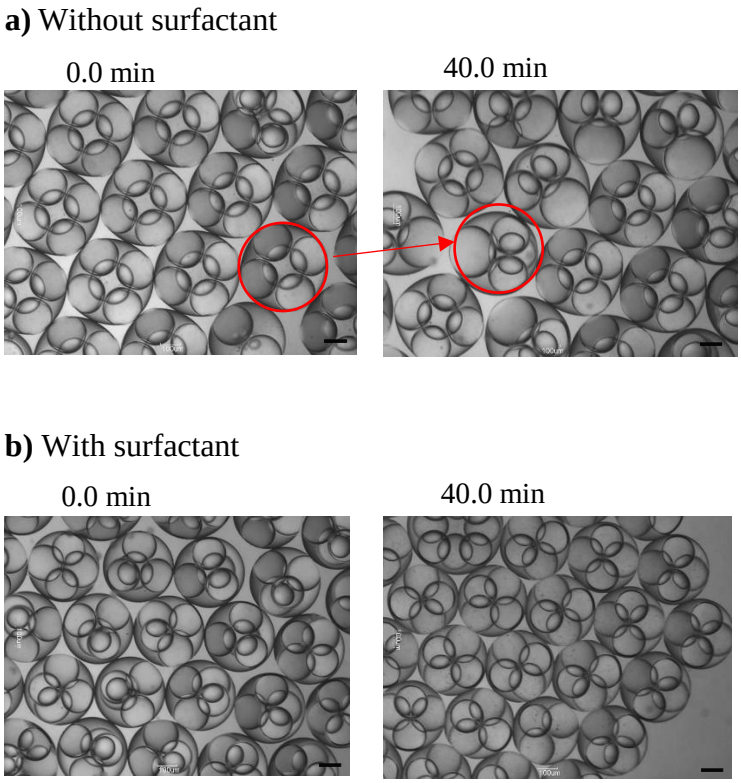

Figure 6.2 Optical micrographs images showing the stability of a typical w/o/w emulsion, **a)** with 1.0 wt% Pluronic F-127 and **b)** without surfactant in the core phase, at 0 min and 40 min, respectively. Scale bar is 100 μm.

Now let us turn our attention to polymerisation of w/o/w drops. Ideally, the thin film separating the inner core droplets and the outer shell drop should rupture during polymerisation, leaving particles with windows. However, the resulting microparticles showed no sign of opening (see Figure 6.3a). Therefore, we added water-soluble surfactant (Pluronic F-127) into the inner phase, which may speed up the driving force for the inner phase to escape the middle phase. Figure 6.3b clearly shows this policy led to the opening of windows. Nevertheless, we cannot explain why the presence of surfactant (Pluronic F-127) prevented droplet-droplet coalescence.

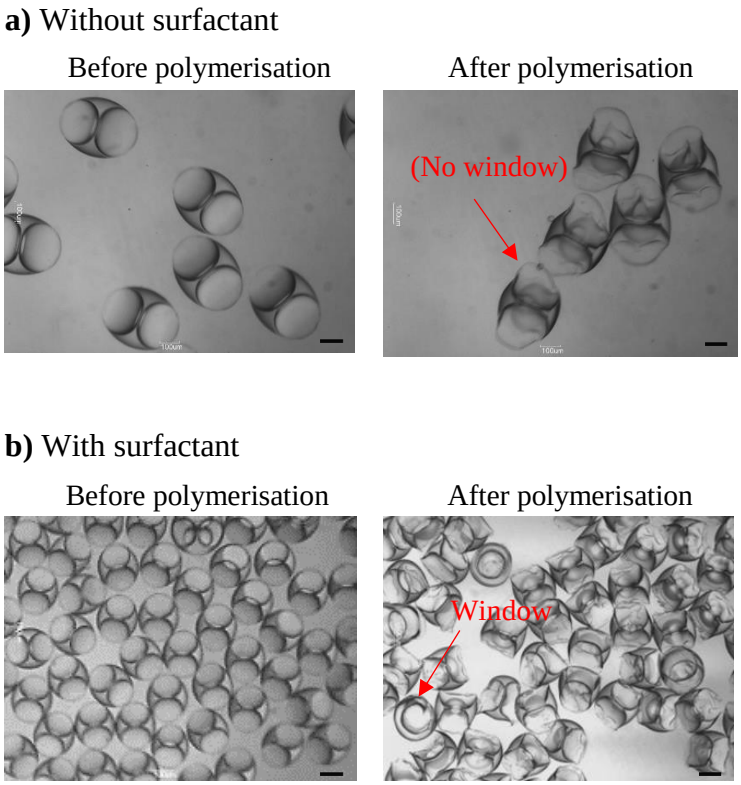

Figure 6.3 Optical micrographs images showing uniform drops and resulting polymer particles with 2 internal core droplets, **a)** without surfactant in the core phase and **b**) with 1% water-soluble surfactant (Pluronic F-127) in the core phase, respectively. Scale bar is 100 μm.

6.4.2. Evolution of drops morphology

Drops (with diameter *D*) containing internal core droplets (with diameter *d*) can come in different configurations. They are defined based on the shape of the external drops as spherical (S), semi-spherical (SS), and plug-like (P). The shape of drops was controlled either by the geometry of the channel, the phase ratio $\phi = Q_i / (Q_i + Q_m)$, or the number of internal core droplets *N*. Plug-like drops formed when their overall diameter became greater than the width of the outer capillary (300 μm), allowing the resulting drops to expand largely in the direction of flow while confined by the outer capillary (see Figure 6.1).

To produce spherical drops, an extension of a wider capillary with ID of 500 µm was attached downstream to ease the plug-like drops into their thermodynamically favoured morphology driven by minimisation of interfacial forces. However, the resulting drops could be either spherical or semi-spherical, depending on their internal phase ratio. Semi-spherical drops were obtained when they contained compact internal droplets at high phase ratio ϕ.

Figure 6.4a shows the phase map for different morphologies of drops against ϕ and N. The calculated internal phase ratio of drops (with different shapes) versus the number of internal droplets N with a constant size are shown on Figure 6.4a. In order to construct the map, three different experimental paths were considered (Figure 6.4a). The red curve in the map shows Path **C** which represents the "*critically-packed drops*". That is when the core droplets contained in an external drop start to contact with each other (adjacent droplets) and the wall of the shell drop without being deformed. This means they cannot have translational motion inside the drop anymore while they may still have rotational motion. This is analogous to critically packed uniform particles or droplets in unconfined space [200], but because of restriction in the space available within spheres, the closely packed arrangement in drops is achieved at a lower phase ratio, depending on the number of internal droplets N.

The internal phase ratio of drops under such circumstances may be called critical phase ratio ϕ_{cri}. The critical phase ratio ϕ_{cri} increases with the number of core droplets. From Figure 6.4a one could see that the ϕ_{cri} for drops containing 2, 3, 4, 5 and 6 internal droplets, for examples, are approximately 0.25, 0.29, 0.36, 0.35 and 0.42, respectively (see Appendix **B1**). The theory of packing spheres in a sphere is often based on the assumption

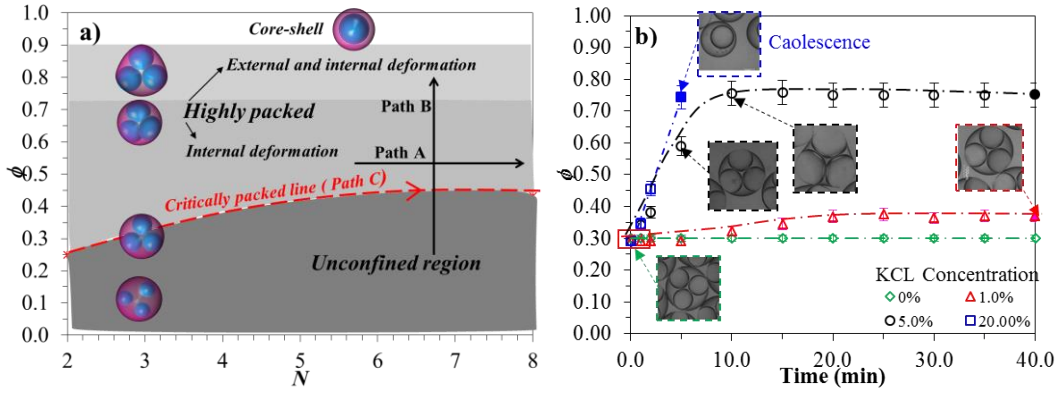

Figure 6.4. **a)** The emulsion phase ratio for different drop shapes versus number of internal droplets (N) with a constant size. The curve shows the locus of critically packed drops N=N_{cri}. The region below this curve shows unconfined region. The region above the curve shows the locus of highly packed deformed drops containing $N > N_{cri}$ internal droplets; **b)** Time-dependent change in ϕ of a drop containing three core droplets at different KCl concentrations. The filled symbols show the onset of inner droplet coalescence.

that the size of internal droplets remains constant, which implies an increase in the size of the external drop with increasing N [201]. Alternatively, a critically-packed drop with a constant size can be considered, but with decreasing size of the internal droplets as N increases. In this work, however, Path **C** could only be tracked by increasing the size of both inner droplets and external drops.

The critically-packed drops were prepared by manipulation of the three flowrates in order to accommodate the exact number of cores required at a specific ϕ_{cri}. It should also be noted that in the region below the critical packing curve, *unconfined region* (Figure 6.4a), the internal droplets are relatively small and not densely packed, which means that internal droplets do not touch the interior of the shell drop.

Path **B,** which shows a move from the unconfined region, below the critical curve, to "*highly-packed drops"* region above the critical curve, crossing the critically-packed drops curve, was also followed by manipulating the three flowrates in order to increase ϕ

while keeping the number of internal droplets N constant, as seen in Figure 6.4a. In the "*highly-packed drops*" region the shape of the internal droplets starts to transform from spherical to semi-spherical due to the compression exerted by the external drop, while the shape of the external drop remains spherical. There is also a threshold slightly above this region where the external spherical drops also started to deform because of increasing volume of the internal droplets contained (high ϕ). Further increase in ϕ above 0.90 resulted in the formation of double drops with only a single core. This is due to the formation of a stable biphasic jet at high inner phase flowrate inside the middle capillary, which emulsified at the tip into core-shell drops with an ultrathin shell [41].

From Figure 6.4a one could see that Path **A,** via which the number of cores N can be varied at constant ϕ, could be tracked by altering the flowrate of the outer phase Q_o. A reduction in Q_o would reduce the shear stress exerted on the external drops and allow more internal droplets to be contained in drops before their detachment from the tip. We also noted that deformed drops may evolve, with increasing N across Path **A,** at any given ϕ larger than ϕ_{cri}. These drops range from semi-spherical drops to spherical drops containing semi-spherical droplets. Overall, drops with different morphologies could be produced, however, there exists only one morphology that fits a given N and ϕ. (Refer to appendix **B2** for supplementary information).

6.4.2.1.Offline manipulation of drop phase ratio by "osmosis effect"

An alternative way to produce highly packed drops is to apply "osmosis effect" on drops after they are formed (post formation). This can be easily done by addition of a salt to the inner water phase to drive the continuous outer water phase to migrate towards the core water droplets through the semi-permeable membrane of the oil shell. This will increase the core droplets size as well as ϕ. We used different potassium chloride (KCl)

concentrations in the inner water phase to study its effect on the size and morphology of drops. We first tested the presence of KCl in the core phase in the absence of Pluronic F-127, and noted a major coalescence between the internal core droplets occurring. Therefore, the internal core droplets were stabilised against coalescence by adding Pluronic F-127 surfactant to the core phase.

Starting from critically packed drops containing 3 cores (ϕ_{cri} = 0.30), as an example, we can see from Figure 6.4b that the internal droplets grew with time under the influence of the osmosis effect with a rate depending on the salt concentration. Little difference was noticed in ϕ when 1.0 wt. % of KCl was used. However, it is clear from Figure 6.4b that the internal droplets were compressed against the shell drop due to their growth and became semi-spherical. By increasing KCl concentration to 5.0 wt. %, initially a constant increase in ϕ was observed. Soon after the start, the internal droplets began to grow and then deform to take a non-spherical shape. Within 10.0 min, the external drop also started to deform and gradually changed to semi-spherical but changed little afterwards until the inner droplets started to coalesce at around t = 40.0 min. The drops were sufficiently stable to undergo photopolymerisation prior to this time. A concentration of KCl as high as 20.0 wt .% led to faster swelling of the internal droplets but this was associated with a quicker destabilisation so that after 5.0 min most internal droplets were lost by coalescence. For all cases, the flux of water into the internal core droplets increased the volume of internal core droplets while the volume of the volume of the external phase remained unchanged. This transformed the spherical drops to semi-spherical ones.

This set of experiments suggests that the osmosis effect could be used as an auxiliary method to produce high internal phase complex drops. The maximum phase ratio, ϕ_{max}, obtained via osmosis effect was approximately 0.75, as drops above this value began to

coalesce, suggesting that the approach cannot currently be used to extend the limits of ϕ unless appropriate surfactants can be found.

6.4.3. Microparticles produced by polymerisation of critically packed drops

Producing critically-packed drops using a microfluidic device by increasing the number of internal droplets N without affecting their size (increasing ϕ) is a formidable task. This is because a change in the phase ratio ϕ is practically associated with a change in the internal droplet size. Therefore, the critically-packed drops were produced via Path **C** by manipulating Q_m and Q_o at a constant Q_i to adjust ϕ and N. While this path could deliver such structures, the size of the internal droplets slightly increased with increasing ϕ. The reason for this will be explained later.

Figure 6.5a-f shows micrograph images of the generated critically-packed drops with a given N (inset) and their polymerised products. Windows were formed during polymerisation due to shrinkage; and the density differences between the monomer phase and polymer gel phase [202].

It was intuitively thought that the location around the droplet-droplet and droplet-drop interfaces should rupture during polymerisation, resulting in porous microparticles with external windows and highly interconnected open windows between the neighbouring voids. However, from the SEM images in Figure 6.5a-f one could see that the critically-packed drops revealed an interesting feature when polymerised. Drops containing two internal cores droplets did not open up at all, but those with 3-5 internal droplets showed increasingly occasional opening. Generally, critically-packed microparticles showed partial opening with a small window size when $N < 5$ (as seen in Figure 6.5a-c) but showed complete window opening with $N \geq 6$ (as seen in Figure 6.5d-f).

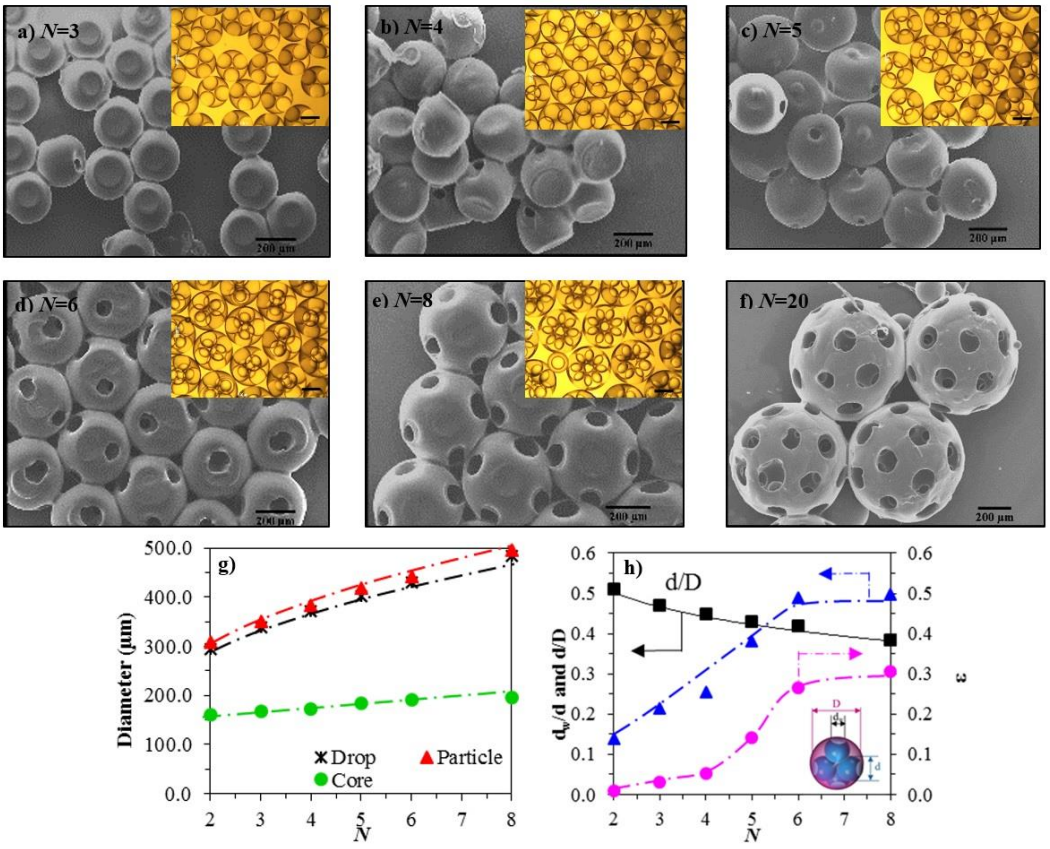

Figure 6.5 a-f) SEM images of porous microparticles, produced from the critically-packed drops, with a given number of core droplets (N) obtained at fixed Q_i =200 µl hr^{-1} ; **a)** N = 3 (Q_m =450 µl hr^{-1}, Q_o = 2000 µl hr^{-1}); **b)** N = 4 (Q_m =350 µl hr^{-1}, Q_o = 1000 µl hr^{-1}); **c)** N = 5 (Q_m =350 µl hr^{-1}, Q_o = 700 µl hr^{-1}); **d)** N = 6 (Q_m =270 µl hr^{-1}, Q_o = 400 ul hr^{-1}); **e)** N = 8 (Q_m =270 µl hr^{-1}, Q_o = 300 µl hr^{-1}); **f)** N = 20 (Q_m =270 µl hr^{-1}, Q_o = 100 µl hr^{-1}). Insets show optical micrograph images of the corresponding critically-packed drops. The scale bar is 200 µm. **g)** Diameter of the internal core, external drop and final particle versus the number of cores N and **h)** relative size of internal droplets d to the external drop D (symbols and line represent the experimental data and corresponding theoretical calculation, respectively), relative size of windows on the surface of microparticles d_w with regard to the diameter of the core (d) as well as the relative magnitude of opening area on the surface of a microparticle ε, versus the number of cores N.

Drawing the attention back to the effects of the number of internal droplets N on the initial droplet/drop size, one could see from Figure 6.5g that the external drop size increased with the number of cores. The size of the internal droplets also shows a small change with N, but this was inevitable due to the method used to fabricate such structures. One can also see that the size of the polymeric microparticles is smaller than the original drop size

approximately by 5.0 % for all cases, indicating the volume shrinkage of drops by photopolymerisation.

The ratio of the diameter of the window d_w on the surface of microparticles to the diameter of the internal droplets d, d/d_w, as well as the relative magnitude of the opening area on the surface of a microparticle, $\varepsilon = N d_w^2/D^2$, are shown in Figure 6.5h. Note that the number of external windows on the surface of the microparticles was found to be equivalent to the number of internal droplets N. A simulation model suggests that the internal droplets densely packed in a drop share the same shell (outer layer) until $N \leq 13$ [203]. Packing more internal droplets than $N = 13$ may indicate that there will be a central single droplet surrounded by the rest of droplets touching the outer shell layer (external drop). This implies there will be N-1 external windows for drops containing N droplets. However, online monitoring and counting indicated that there was 20 droplets in the drop, which had 20 windows (see Figure 6.5f).The d/d_w for $N = 20$ was 0.27, which is very close the theoretical value (0.28). This may suggest that the configuration of soft (liquid) droplets contained in a soft sphere could be different from what has been developed for hard spheres [203]. From Figure 6.5h one could see that the relative size of the windows with regard to the size of the cores d_w/d and ε increase with increasing N (i.e. increasing ϕ). This indicates that the potential of critically-packed drops to produce more and larger interconnected windows is enhanced with increasing N or ϕ. Figure 6.5h also shows that while the relative window size achievable d_w/d becomes saturated at N=6, more open area can be created by simply increasing N.

6.4.4. Microparticles produced by polymerisation of highly packed drops

This section aims to describe the method used to create highly open porous microparticles with a controlled number of openings. This was achieved by making the total volume of the core droplets larger than the critical packing volume for a given N; $\phi > \phi_{cri}$. This strategy was introduced to achieve a minimum shell thickness across neighbouring droplets/drop, enhance the film rupture, and create larger relative opening areas.

When the critical packing state is exceeded, the core droplets confined in the shell re-arrange themselves into distinct configurations to minimise the surface area, depending on the number of core droplets [200]. The shell drop may maintain its spherical shape or be deformed to semi-spherical one. A constant-ϕ trajectory (Path **A**) is well suited to fabricating a wide range of desired morphologies in this category.

A series of experiments was conducted with the phase ratio of the inner phase being maintained constant at ϕ= 0.70 and the diameter of inner droplets controlled at d=140 µm (path **A** in Figure 6.4a). Starting with highly-packed semi-spherical drops containing two internal core droplets (N=2) with $\phi > \phi_{cri}$ = 0.25, we transformed the drops to highly-packed drops (spherical drops with deformed internal droplets) containing N = 6 internal core droplets by decreasing Q_o. The conditions required to obtain these highly-packed drops are outlined in the caption of Figure 6.6.

One can see from the SEM images in Figure 6.6a-e and the measured asphericity factor f in Figure 6.6g that the external drops changed shape from ellipsoid to semi-spherical with increasing N. This also increased the size of external drops, as shown in Figure 6.6h. These complex drops were then polymerised on the fly to produce microparticles. Figure 6.6a-e shows SEM images of the resulting porous microparticles, which have as many internal droplets as external windows.

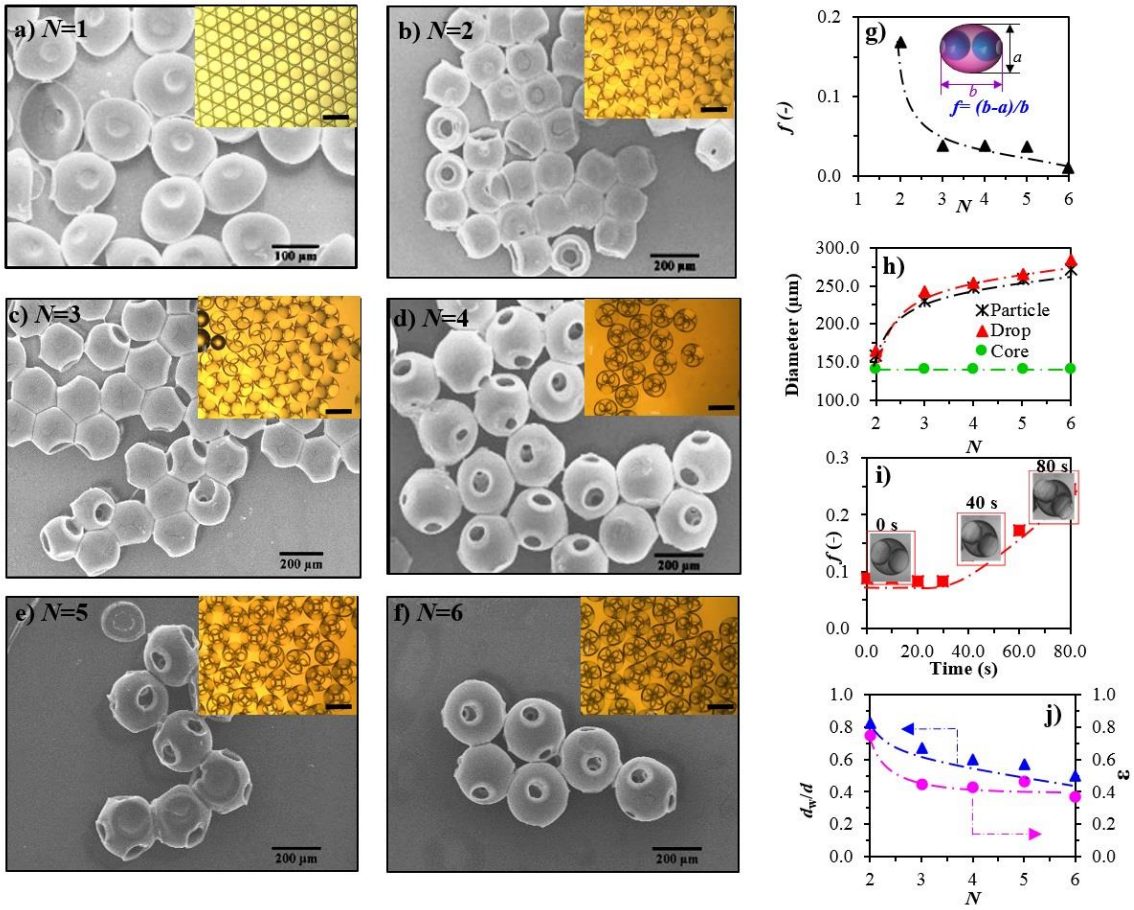

Figure 6.6 SEM images of the microparticles with different configurations obtained with **a)** N = 1 (Q_o= 5000 µl hr^{-1}) **; b)** N = 2 (Q_o= 3000 µl hr^{-1})**; c)** N = 3 (Q_o= 5000 µl hr^{-1})**; d)** N = 4 (Q_o= 1000 µl hr^{-1})**; e)** N = 5 (Q_o= 800 µl hr^{-1})**; f)** N = 6 (Q_o= 600 µl hr^{-1}). [Q_i =500 µl hr^{-1} and Q_m =200 µl hr^{-1}]. Insets show optical micrographs of the corresponding highly-packed drops. The scale bar is 200 µm.; **g)** The asphericity (f) of the external drop versus N; **h)** Diameter of the external drops **,** internal droplets and particles versus number of cores N; **i)** Time-dependent change in the asphericity (f) of the overall drop containing two core droplets during polymerisation induced by microscope light; **j)** The ratio of the size of the window d_w on the surface of microparticles to the initial size of the internal droplets d, d/d_w, as well as the relative magnitude of opening area on the surface of a microparticle ε, versus N

The semi-spherical drops opened up more consistently than the spherical ones due to a significant stress applied on their over-stretched asymmetric interfaces during shrinking.

Symmetric morphologies such as simple core-shell drops (see Figure 6.6a for N=1) did not open due the balanced forces applied on the uniform shell. During polymerisation of

asymmetric drops, defined by varying shell thickness within the drops, the thinner the shell created by the interfaces between adjacent core droplets (and between them and the outer drop) the more vulnerable was the drop to rupture. Such unassisted ruptures created particles with external and internal interconnected windows. Other studies used a supplementary dissolution method to create porous microparticles [189], which does not lend itself easily to microfluidics.

In order to fully examine the mechanism of window formation, we monitored the morphology evolution of a compound drop containing 2 internal cores with time during polymerisation, as seen in Figure 6.6i, with ϕ above the critical phase ratio ϕ_{cri}. The shape of the external drop, measured by aspherisity factor *f*, changed from semi-ellipsoid to ellipsoid with time during polymerisation. The volume of external drop decreased due to the shrinkage of the shell phase during polymerisation, which imparted a significant force on the tightly packed core droplets. The relative size of interconnecting windows and relative surface area of particles ε decreased with increasing *N*, as shown in Figure 6.6j unlike for critically-packed drops that showed an increase in d_w/d and ε with *N*.

6.4.5. Microparticles produced by polymerisation of plug-like drops

Porous plug-like microparticles, which are reported for the first time, were obtained by producing drops whose diameter was bigger than the diameter of the outer channel. This was achieved by using a low Q_o to allow drops to expand before detachment. Under such conditions drops were compressed to form a plug-like morphology. We first developed phase maps (Figure 6.7a and Figure 6.7b) to find the conditions under which plug-like multi-core drops were formed. To construct Figure 6.7a, we fixed the flowrate of the outer phase at Q_o = 300 µl $hr^{-1}$and altered Q_i and Q_m.

Drops with one or several cores were produced by precisely adjusting the flow rate of the inner Q_i and middle phase Q_m. At relatively low Q_m (<50 µl hr^{-1}), regardless of Q_i, drops were unstable and underwent coalescence (See Appendix **B6**). When the flowrates of the inner phase was high (Q_i= 100 µl hr^{-1}), and at moderate Q_m= (>100 µl hr^{-1}), a chain, defined as a linear arrangement of water droplets contained in continuous jet of oil, was formed. The reason for this will be discussed later. There was an intermediate range of the inner phase flowrate that led to the formation of stable and uniform multicore plugs. Increasing Q_i at a given Q_m led to an increase in the number of cores as well as in the internal phase ratio ϕ. The number of core droplets are shown on the phase map.

The phase map in Figure 6.7b shows the flow conditions, in terms of Q_m=Q_i and Q_o, required for incorporation of any given number of core droplets desired. In this map, unlike the map in Figure 6.7a, we allowed Q_o to vary against the other flowrates. At very low Q_i = Q_m and high Q_o, the core droplet developed very quickly because of high shear stress, resulting in drops with a core-shell morphology. Increasing Q_i = Q_m from 50 µl hr^1 to 500 µl hr^{-1}at fixed Q_o=3000 µl hr^{-1}, resulted in a small change in the number of cores contained. From the phase map, we can observe that the morphology of drops changes at specific transition points from plug-like drops to chain (See Appendix **B6**). In a co-flow system, this transition point is often correlated with the capillary number $Ca = \mu v/\gamma$ (where µ is the viscosity, v is velocity and γ is the interfacial tension). In this case, however, the correlation of the transition point is better represented in terms of velocity as the viscosity of the middle (monomer) and outer phase (water) is roughly the same.

We plotted the outer phase velocity v_o as a function of the middle phase velocity v_m (Figure 6.7c). The red dotted-line shows the equality between the two velocities or the critical transition velocity for drop formation mechanisms. This line will allow us to

estimate the counteracting forces between the outer and middle phases. In the region above the line the outer phase has a greater velocity than that of the middle phase thus rupturing the middle phase. In the region below the line the external force acts as a cohesive force, rather than a disruptive force, thus allowing the chain to form.

The data extracted from the resulting phase maps are plotted in Figure 6.7d-f. The drop size in a typical microfluidic device is determined by a competition between interfacial tension and hydrodynamic forces. When Q_m increases at given Q_i and Q_o the drag force acting on the inner phase becomes dominant, which therefore results in a shorter detachment time and smaller inner cores (Figure 6.7d). In contrast, increasing Q_m decreased the drag force acting on the outer drops and formed longer plugs (Figure 6.7e), meaning smaller core droplets contained in a longer chain. As Q_m further increased, the range of change in the droplets size became continuously smaller (Figure 6.7d), however, the axial length of the plug (L) and the number of internal droplets continued to increase, as shown in Figure 6.7e and Figure 6.7f.

On the contrary, increasing the inner flow rate Q_i increased the inner core size. This is due to a decrease in drag and the associated increase in the detachment time of the droplet from the capillary tip. The number of cores also increased with increasing Q_i at a given Q_m until a threshold value was reached beyond which the number of cores began to decrease due to an increase in their size (see Figure 6.7f). An ultra-thin core-shell drop was obtained when Q_i was increased to higher range (1000 µl hr^{-1}) (not shown on the map). Refer to Appendix **B6** and **B7** for supplementary optical images showing the formation of droplets obtained under different flow conditions).

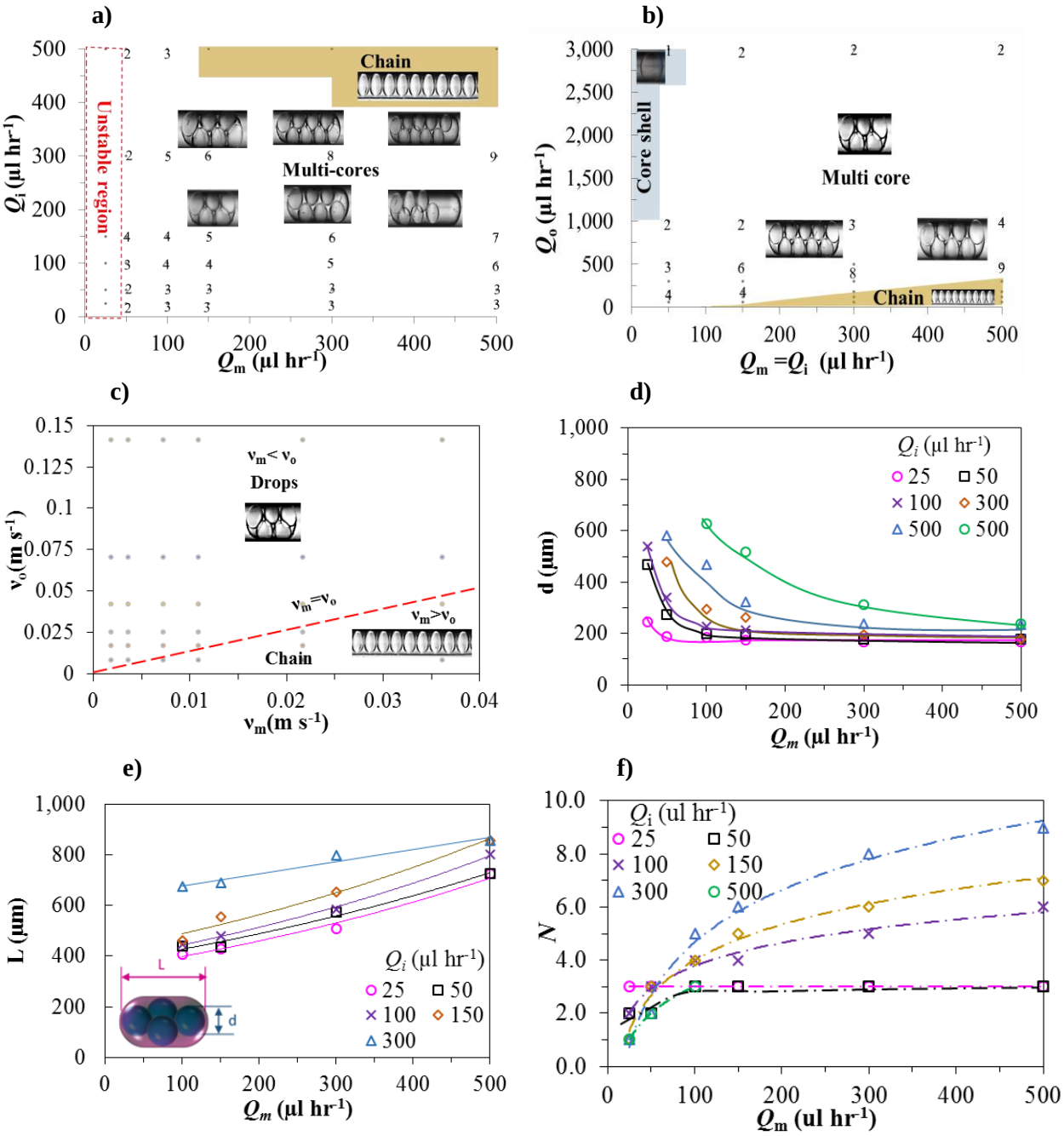

Figure 6.7 Phase maps showing different domains of double drops with controllable number of cores **a)** in terms of Q_i vs Q_m at a fixed Q_o=300 µl hr^{-1}and **b)** in terms Q_o vs Q_m = Q_i. The inset numbers represent the number of internal droplets. The ellipsoid internal droplets is just an optical effect [204]. **c)** The velocity of the outer phase v_o versus that of the middle phase v_m. The red dotted-line shows the critical transition velocity for drops formation mechanism. **d), e)** and **f)** Show variations in the diameter of core, shell axial length, and number of cores, respectively, with Q_m at different Q_i (Q_o=300 µl hr^{-1}).

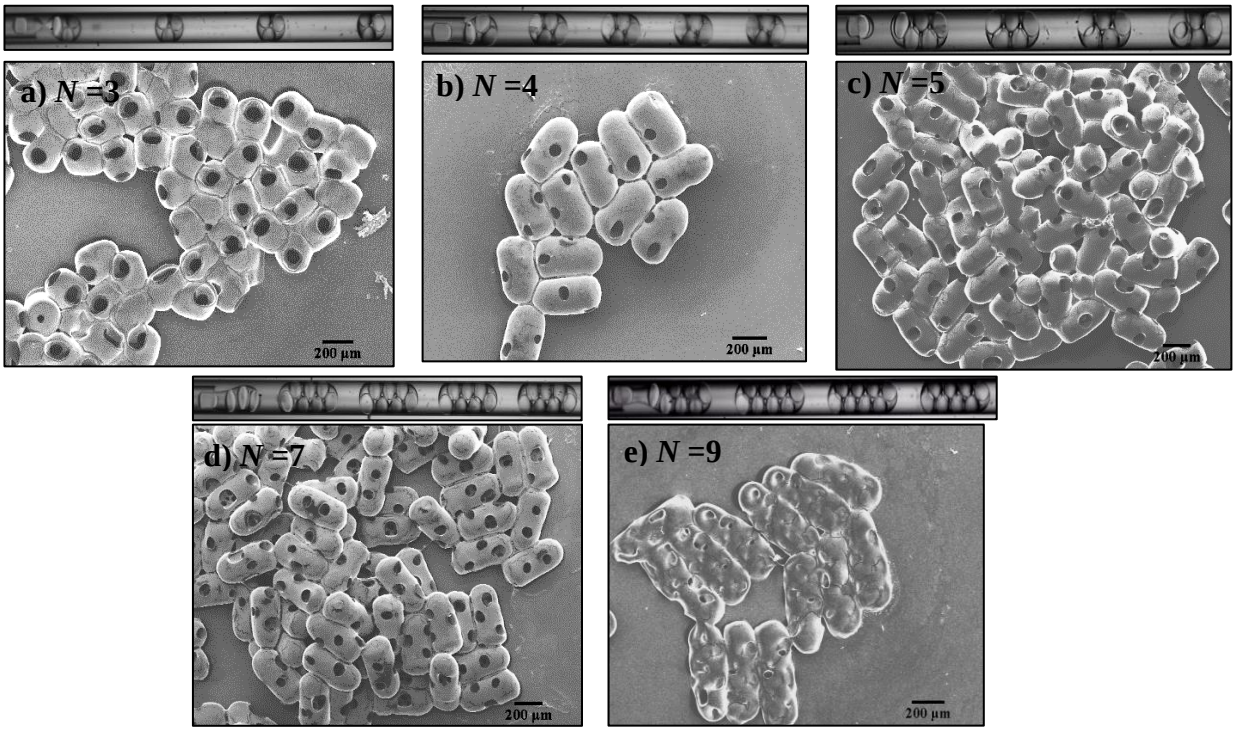

Figure 6.8 a-e) Images taken at the tip of the capillary showing the formation of droplets and SEM images of the microparticles with different configuration obtained at a fixed Q_i and Q_m=150 µl hr^{-1}and: **a)** triple cores formed at Q_o=500 µl hr^{-1}; **b)** four cores formed at Q_o=400 µl hr^{-1}, **c)** five cores formed at Q_o=300 µl hr^{-1}; **d)** seven cores formed at Q_o=200 µl hr^{-1}and **e)** nine cores formed at Q_o=50 µl hr^{-1}.

In the next stage, the polymerisation of the plug-like double emulsions was attempted. Figure 6.8a-e shows a range of plug-like microparticles with N=2 to 9 and d=150.0 µm produced at ϕ= 0.50. The size of the external drops and the number of internal droplets contained were controlled via decreasing Q_o. The double drops were punctured during UV polymerisation resulting in unique porous plug-like microparticles. The porous plug-like microparticle can also be pushed against each other to form porous fibres (see Appendix **B8**).

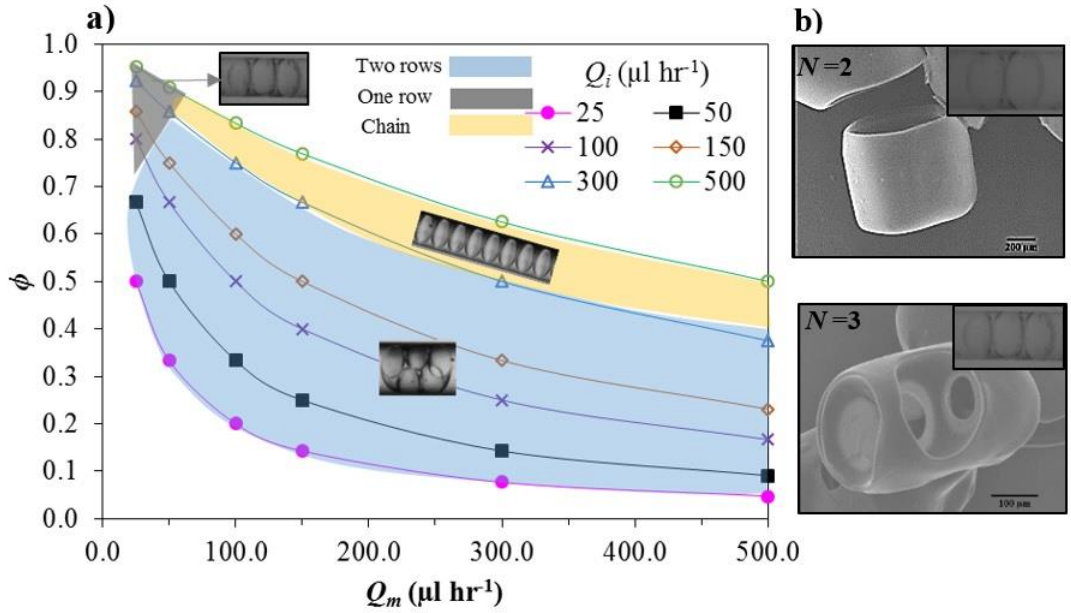

Figure 6.9 a) The phase map showing the change in the phase ratio (ϕ) as well as the droplets morphologies with varying Q_m and Q_i. **b-c)** SEM images of the one-row plugs obtained at a fixed Q_o =300 µl hr^{-1} and: b) N = 2 (Q_i=300 µl hr^{-1},Q_m=50 µl hr^{-1}) and c) N = 3 (Q_i=500 µl hr^{-1}, Q_m=100 µl hr^{-1}). Insets show images taken inside capillary showing the formation of one-row drops.

All morphologies presented so far are plugs containing two rows of internal cores. In order to make plugs with a single row of internal droplets, the size of the internal droplets should be adjusted to be equal or larger than the diameter of the outer capillary, similar to the requirement for formation of chains. This required the manipulation of both inner and middle phase flowrates to obtain a high internal phase ratio.

Figure 6.9a shows a phase map indicating the domain of one-row plugs. Two-row plugs could be produced at $\phi \leq 0.60$. Increasing Q_i at a fixed low Q_m increased the phase ratio and thus the size of the inner cores until a threshold beyond which one row plugs were obtained. There is a transition region between one- and two-row domains, within which mixed plugs were produced. One could see from the SEM images, shown in Figure 6.9b, that one-row plugs enjoy having larger windows.

6.5 CONCLUSION

We have demonstrated a facile and versatile approach to produce uniform spherical and non-spherical porous microparticles with highly ordered interconnected windows. Uniform w/o/w emulsions, produced via glass-capillary based microfluidic technique, were used as precursors to produce various shapes of porous microparticles via polymerisation. The size, porosity and morphology of the resulting microparticles were controlled by the flow rate of individual phases, geometry of the microchannels and the packing structure of the inner droplets. Windows did not consistently form when critically-packed drops ($\phi = \phi_{cri}$) with $N \leq 6$ were polymerised. In comparison, windows consistently formed during polymerisation of highly-packed drops when $\phi > \phi_{cri}$, due to a significant stress applied on the over-stretched asymmetric interfaces during shrinkage. We have also demonstrated the fabrication of plug-shaped porous microparticles, with tunable window sizes and structures, which can open new vistas for many potential applications.

Chapter 7 Microfluidic Approach for Fabrication of Highly Porous and Hierarchical polyHIPE Structures[§]

7.1. ABSTRACT

Herein, we present a facile and versatile route for the fabrication of uniform porous polyHIPE structures with highly ordered and well-defined interconnecting windows. In this study, two polyHIPE scaffolds were prepared by means of different chemical formulations: acrylic based and styrene based. These hierarchical polyHIPE structures were obtained by collecting a uniform w/o emulsion, produced by a co-axial microfluidic device, in a hydrophobic glass vial. A closed packed uniform emulsion was collected at the bottom of the vial. A centrifugation step was carried out on the resulting emulsion to produce high internal phase emulsions (HIPEs). A wide range of relative centrifuge force and times were studied to find the conditions under which the resulting uniform HIPEs, formed via microfluidic, would not undergo further coalescence during centrifugation. The polymerisation of the resulting HIPEs was then triggered by decomposition of the radical initiator, either thermally or by UV, present in the monomer phase. The polyHIPE physical properties such as cavity size (originated from water droplets), interconnecting window size and porosity could be precisely tuned either by the flowrates or the centrifugation speed. We tracked the polymerisation of HIPEs with time to reveal the mechanism of the formation of interconnecting windows formation in PolyHIPE. Conventional styrene-based polyHIPE were produced for comparison purposes.

[§] To be submitted

7.2. INTRODUCTION

The fabrication of porous polymer materials, known as polyHIPE, is an interesting area of research due to their distinctive porous structure within a polymer matrix. PolyHIPE is produced by polymerisation of high internal phase emulsions (HIPE) [205]. HIPE is a two-phase liquid-liquid system (water in oil or oil in water) in which the "internal" phase, dispersed in the continuous phase, occupies more than 74.05% of the total volume of the emulsion. The critical value of 74.05% represents the maximum closed packing limit for uniform non-deformed spheres. Most polyHIPEs are oil based meaning that water droplets are dispersed in an organic phase containing monomers, crosslinker, and surfactants. Polymerising the organic continuous phase results in an open porous morphology with a high level of porosity; namely polyHIPE. They are used as a template for a wide range of applications including food, ion exchange, separation and filtration processes, and petroleum and pharmaceutical industries [206,207]. Some of the new emerging applications include gas storage [208,209] and tissue engineering [210,211].

PolyHIPEs typically have two different types of pores within their structure: primary and secondary. There are significant differences between the primary pores that originate from the droplets and the secondary pores which are formed across interconnecting points between neighbouring droplets. Different terminologies have been coined in the literature for addressing these pores. The primary pores have been called cell, void, and cavity [212,213,214,215,216]. The term void is found to be reserved by IUPAC nomenclature for inter-particle spaces [211], whereas cell should be avoided as it is only applied for bio-medical applications [211]. The term cavity appears to be predominated in most articles for the primary level of pores. The secondary (interconnecting) pores between the cavities are referred to as hole [213], interconnecting window [213], and pore

[214,215,216]. In most articles the term interconnecting window is referred to the secondary pores. Thus, to avoid any confusion, the term cavity and interconnecting window will be used throughout this report to address the primary and secondary pores, respectively. The difference between the cavity and interconnecting windows is shown in Figure 7.1.

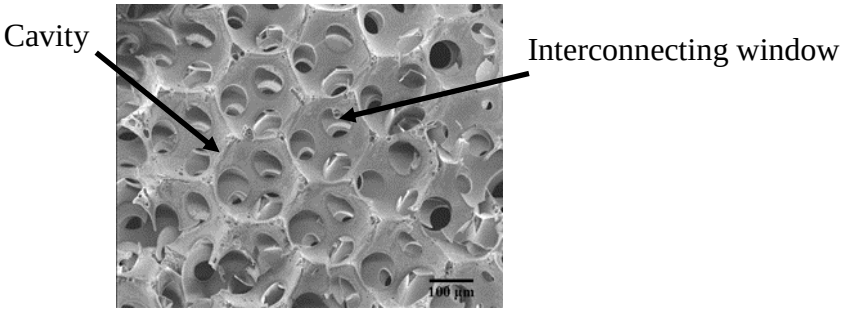

Figure 7.1 A polyHIPE prepared in this work showing the two kinds of pores.

Several attempts have been made to control the morphology of the polyHIPE structures such as varying the internal-phase volume fraction ϕ, surfactants type and concentration as well as crosslinker amount [213]. However, one of the major challenges in preparing polyHIPE is the control of the droplet size and therefore the resulting polyHIPE structures. Controlling the size of the droplets is important in order to understand and be able to tailor the property of resultant polyHIPEs (cavity size, interconnecting window size, porosity and mechanical property), for different applications. Recently, microfluidic techniques have become excellent tools for producing uniform droplets.

Given that many publications deal with fabricating conventional polyHIPEs, only a few recent works demonstrated the use of microfluidics to produce highly uniform and organised polyHIPE structures [217,218,219,220]. However, to the best of our knowledge, uniform HIPE with $\phi > 0.80$ has not been achieved using a microfluidic set-up. In this work, we investigated the production of polyHIPE scaffolds prepared by

microfluidic set-up using two different chemical formulations: acrylic based and styrene based. A centrifugal step was utilised to increase the internal water phase ratio (ϕ). The effect of ϕ on the resulting polyHIPE structures such as morphology, pores, cavities size, and porosity, were investigated. The fabrication of styrene basaed polyHIPE was conducted for comparison.

7.3. EXPERIMENTAL

7.3.1. Materials

2-ethylhexyl acrylate (EHA, 98.0%, Sigma-Aldrich), isobornyl acrylate (IBOA, 85.0%, Sigma-Aldrich), trimethylolpropane triacrylate (TMPTA, 80.0 %, Sigma-Aldrich). Poly (ethylene glycol)-block-poly (propylene glycol)-block-poly (ethylene glycol) **(**PEG-PPG-PEG) (Pluronic L-81, Sigma Aldrich) (average Mw ~ 2800 g mol^{-1} and HLB ~ 2) and Irgacure 907 (BASF) were used as surfactants and photoinitiator, respectively, in the middle (monomer) phase. Pure de-ionised water was used as the inner phase. Styrene (St, 99.9 %, VWR) and divinylbenzene (DVB, 80.0 %, Sigma Aldrich) monomers and thermal initiator lauroyl peroxide (LPO) were also used. Various stabilisers, such as sorbitan monooleate; Arlacel 80; Sorbitan, mono-(9Z)-9-octadecenoateor, Sigma Aldrich (Span 80, HLB ~ 4.3), sorbitan trioleate (span 85, HLB ~ 1.8) , Hypemer B246, CRODA (HLB ~ 5.5) and Hypermer 2296, CRODA (HLB ~ 6) were tested to find the optimum formulation for stabilising the w/o emulsions.

7.3.2. Device

An inner capillary (ID: 50.0 µm, OD: 80.0 µm) was inserted into an outer capillary (ID: 150.0 µm, OD: 250.0 µm) and aligned axisymmetrically in a coaxial arrangement. The capillaries were then introduced into each other with axisymmetric alignment and placed on a microscope slide. The ports were placed on the coupled capillaries, which are resting

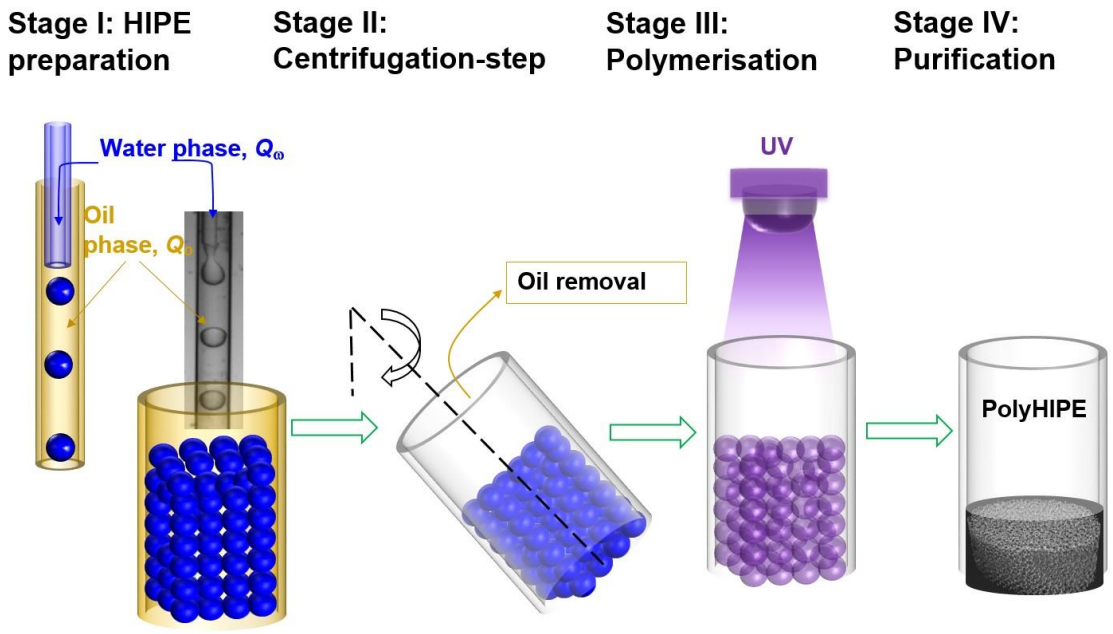

Figure 7.2 Set-up schematic for the preparation of PolyHIPE. **Stage I**: Co-flow microfluidic device consisting of two circular capillaries coupled together axisymmetrically. Uniform water droplets are formed and collected in a hydrophobic glass vial. The water and oil phases were introduced at volumetric flowrates of Q_ω and Q_o, respectively. **Stage II:** Centrifugation step. **Stage III**: Polymerisation of HIPE under the UV irradiation. **Stage IV**: The purification step.

on the microscope slides, glued (Devcon 5-minute epoxy) and left to harden completely. The capillaries through which oil is flown was made hydrophobic by treatment with n-octadecyltrimethoxysilane while the surface of capillary through which water is flown was made hydrophilic by plasma treatment (Femto Plasma cleaner, Diener).

7.3.3. HIPE preparation

Uniform w/o droplets were generated by pumping the water phase through the oil phase containing 91.0 wt. % of a mixture of monomer (composed of 55.0 wt. % EHA, 40.0 wt. % IBOA and 5.0 wt. % TMPTA, based on total monomer phase). Note that IBOA with concentrations below 40.0 wt. % was found to destabilise the HIPE during polymerisation and as a results a random polyHIPEs structures were obtained. Oil-soluble surfactant

Pluronic L-81 and irgacure 907 photoinitiator of 5.0 wt. % and 4.0 wt. %, respectively, were dissolved in the monomer phase prior to experiments.

Conventional styrene-based HIPE was made up of 84.0 wt. % monomer (90.0 wt. % styrene and 10.0 wt. % DVB, based on total monomer phase), 1.0 % initiator and 15.0 % oil-soluble surfactant.

Droplets were formed in a dripping regime at the tip of the inner capillary, by pumping the water phase by Harvard pump 11 Elite, and detached by the high shear forces exerted by the oil phase. The outer oil phase containing the monomers was introduced before the inner water phase to avoid wetting the outer channel. The syringe containing the acrylic monomers was wrapped in an aluminium foil to avoid the light penetration. The droplet size was precisely manipulated by varying the flowrates of the water phase Q_ω and oil phase Q_o. The uniform emulsions were collected in a hydrophobic glass vial (volume 1.30 ml). The schematic illustration of the preparation of PolyHIPE is shown in Figure 7.2.

7.3.4. Centrifugation step

The internal water phase ratio ϕ of the emulsions was increased by centrifugation of resulting emulsion from microfluidics set-up. After performing the centrifugation step (MiniSpin, eppendrof), the excess amount of oil formed at the top of the vial was withdrawn. The relative centrifuge force was varied from 0 to 5000 to achieve the desired internal water phase ratio ϕ.

7.3.5. HIPE characterisation

The generation of emulsion droplets in the microfluidic device was observed using a high-speed video camera (Photron FastCam Ultima APX—monochrome). Droplets sizes were measured using an optical microscope (Kyowa Tokyo, Japan) with a camera (Moticam 2300) connected to a PC.

7.3.6. Polymerisation of HIPE

Polymerisation of the resulting HIPEs, placed in a mould, were triggered by UV which decomposes the initiator present in the monomer phase. During polymerisation, both shrinkage and solidification occurred, leading to the formation a solid monolith whose shape was given by the mould. The resulting polyHIPEs were removed from the mould and washed. Styrene-based polyHIPEs were obtained through conventional thermal polymerisation; that is the HIPEs were kept in the oven at 70.0°C for 24.0h.

7.3.7. Purification

The polyHIPEs were purified via Soxhlet extraction with propanol (24.0 h) to remove the remaining monomes, crosslinker, surfactant, and initiator. After purification, the material was dried overnight in the oven at 65.0°C.

7.3.8. Characterisation of polyHIPE

Scanning electron microscope: The morphology, diameter and surface features of polyHIPEs were assessed by scanning electron microscope (SEM; Hitachi, S4000). Samples were coated with approximately 5.0 nm of gold before analysis. The samples were then placed on a stud and mounted by an aluminium tape. The SEM was operated at 5.0 kV.

Mercury intrusion porosimetry: Mercury intrusion porosimetry analysis was performed using a Micromeritics AutoPore III 9420. Intrusion and extrusion mercury contact angles of 130 degree were used. Intrusion pressures for the PolyHIPEs never exceeded 60.0×10^3 psi.

7.4. RESULTS

With the use of microfluidic set-up, two polyHIPE scaffolds were produced: acrylic based and styrene based. The HIPEs stability and the effect centrifugal step on the internal water

phase ratio (ϕ) of the resulting polyHIPE structures were studied. Similar runs were also conducted for the preparation of a typical polyHIPE via the thermal polymerisation of styrene droplets.

7.4.1. Production of stable w/o emulsions

Since the long term stability of the w/o precursor emulsion is necessary for making polyHIPEs, we extensively investigated various surfactant types and concentrations in order to stabilise the acrylic-based HIPE. The importance of surfactant and its ability to stabilise the emulsion template play a major role in the subsequent formation of open porous structure. Unlike typical emulsions, there are a limited number of surfactants that are able to stabilise high internal phase emulsions and usually large quantities of surfactants are required (typically 20 wt. % to 50 wt. %. of the external phase) [221]. Non-ionic surfactants with low HLB values (typically between 2 and 6) such as Span 80 [222], Hypermer 2296 [223,224,225] and Hypermer B246sf [224] have been found to be efficient in stabilising such emulsions.

We first tested the non-ionic surfactants sorbitan monooleate (Spans) as it is the most common surfactant used for stabilising w/o emulsions. Our preliminary results showed that Span 80 (HLB ~ 4.3), with concentration up to 30 wt. %, was not able to stabilise the acrylic-based HIPE for longer than 20.0 min, while Span 85 (HLB ~ 1.8) with similar concentration led to droplets coalescence shortly after they were formed.

Having failed to use Spans, we then shifted to polymeric surfactants as they have been found to enhance the stability of w/o emulsions [226]. We tested a small quantity (< 0.1 wt. %), of Hypermer B246 surfactant (HLB ~ 5-6) which resulted in a dramatic decrease in the interfacial tension to that extent the droplets were formed in a jetting regime. The well-known phenomenon of jetting in the microfluidic system is when the dispersed phase

flows out of the source as a jet and droplets are pinched off far from the tip resulting in a wide droplet size distribution [227]. As the formation of droplets in microfluidic devices is determined by a competition between interfacial tension and hydrodynamic forces, these two opposing factors should be tightly controlled for the generation of monodispersed droplets. Surfactants such as Hypermer B2296 (HLB ~ 5-6) and Plournic L-81 (HLB ~ 2), with concentrations up to 10 wt. %, were used but they could only improve the stability of the emulsions for 30.0 min. Increasing the concentration of both surfactants to more than 10.0 wt. % again caused a jetting mode to appear. It was found that the blend of 0.025 wt. % of Hypermer B246 and 5.0 wt. % of L-81 efficiently increased the emulsion shelf-life (stability) from approximately 30.0 min for L-81 surfactant to more than 2.0 h. One point worth of note is that the hydrophobic glass vial was found to be an additional advantage for the long term stability of w/o emulsions in comparison with a hydrophilic one.

Before starting with the production of PolyHIPE, we studied the effect of the water Q_ω and oil Q_o flowrates on droplets diameter. To construct Figure 7.3a, we fixed the flowrate of one phase while varied the other one. After few seconds from the start of pumping, the droplets became uniform and no further change in the droplet size was observed. A general trend that one may see from Figure 7.3a is that by increasing the outer oil phase flowrate Q_o at a fixed Q_ω, the droplets size decreased as a result of increasing shearing force acting on them. Increasing the water flowrate, Q_ω, at fixed Q_o, increased the droplets size. This is due to a decrease in drag, because of decreasing velocity difference between phases, and the associated increase in the detachment time of the droplet from the capillary tip.

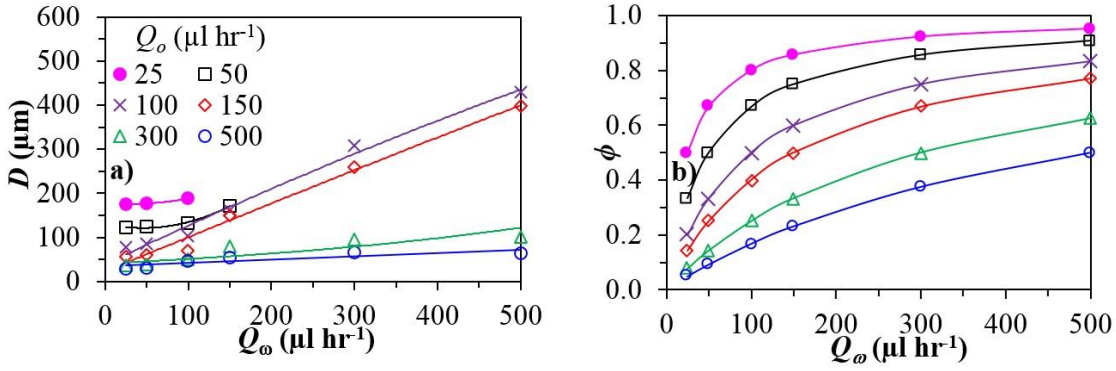

Figure 7.3 The effect of the inner water phase flowrate Q_ω and the oil phase flowrate Q_o on **a)** the water droplet size and **b)** internal water phase ratio (ϕ).

7.4.2. Increasing internal phase ratio by centrifugation

The change in flow rate of one phase is always associated with a change in the phase ratio (ϕ) (see Figure 7.3b). It was found very challenging to simultaneously control the water droplet size as well as the internal water phase ratio ϕ. This is because increasing ϕ by manipulating the flowrates always enlarges the water droplet size. It was also found that producing HIPE with extremely high Q_ω to Q_o ratio ($\phi > 0.80$) the inner phase underwent jetting, which led to the formation of water plugs via filling the outer capillary.

Therefore, we deliberately implemented a gravity-assisted phase separation policy that allows us to obtain HIPE with the desired droplet size. In the first attempt, an emulsion with $\phi = 0.50$ and D = 150$\pm$ 5.0 % was produced and allowed to settle for few min. As anticipated, a layer of the lighter phase (monomer) was formed at the top as the water droplets sank. The excess oil was removed after the phase separation between the light and heavy phases occurred. However, this policy could only increase the phase ratio by 10.0% to $\phi = 0.60$.

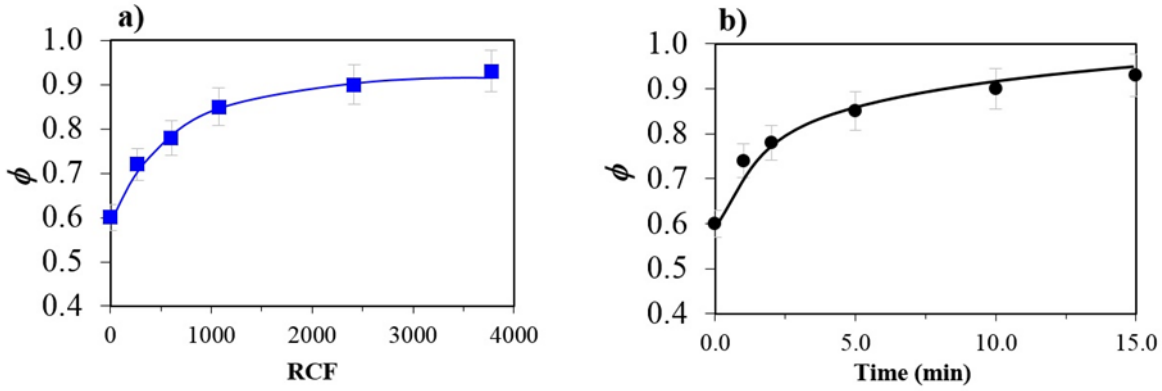

Figure 7.4 a) The effect of relative centrifuge force (RCF) on the internal water phase ratio ϕ at time = 10.0 min b) Time variation in ϕ at RCF=2400 (water droplet with D = 150. 0 ± 5.0 % were formed using $Q_\omega = Q_o$ = 150.0 µl hr-1.

We, therefore, implemented a centrifugation step on the resulting uniform emulsions to produce HIPE ($\phi > 0.74$). In this series of experiments, we first investigated the effect of relative centrifuge force (RCF) and time on water droplets behaviour. Figure 7.4a shows that at a fixed time (t= 10.0 min), internal water phase ratio ϕ increased with increasing the relative centrifuge force (RCF). The centrifuge force applied on the w/o emulsion allowed a phase separation between the water droplets and the lighter phase (continuous oil phase). This was manifested by the formation of a thicker layer of the continuous phase on the surface of emulsion when increasing RCF. One point worthy of note is that samples subjected to a speed of around 4000 RCF showed coalescence at the bottom of the mould whereas RCF and centrifugation time less than 1000 and 10.0 min, respectively, did not significantly enhance ϕ.

Figure 7.4b shows the time-dependent change in ϕ at RCF=2400. The internal water phase ratio ϕ increased with time. The ϕ increased from the initial value 0.60± 5.0 % at time= 0.0 min (i.e. no centrifuge is preformed) to approximately 0.93± 5.0 % at time = 10.0 min. However, keeping the centrifugation time longer than 10.0 min did not enhance the ϕ but instead destroyed the structure (i.e. coalescence of the droplets).

7.4.3. Polymerisation of the acrylic based HIPE

Different polyHIPEs scaffolds, with different ϕ were produced and the results are presented in Figure 7.5. The SEM micrographs in Figure 7.5a clearly show that the combined advantage of microfluidics and centrifugal step produced highly-ordered uniform porous polyHIPE structures with well-defined interconnecting windows. As one would expect by increasing ϕ above 0.74, the shape of the cavity (originated from a water droplet) changed from spherical to hexagonal. Looking carefully into the internal structure of the polyHIPEs (Figure 7.5a) we can also see that each cavity (originated from a water droplet) is connected via interconnecting windows to adjacent cavities. External windows, formed at the vial-HIPE interface, are also shown in Figure 7.5b. However, it was interesting to observe that the wall thickness between the windows on the external surface is different from the wall thickness between the windows in the internal structure, depending on ϕ. Our results revealed that the size of the internal and external windows increased with increasing ϕ (Figure 7.5a and Figure 7.5b), which implies that the wall thickness between two windows decreased.

The *relative wall thickness* δ defined as the ratio of wall thickness between the windows on the external surface to the wall thickness between the windows in the internal structure, increase with ϕ, as shown in Figure 7.5c. The relative wall thickness, δ, reached a plateau at $\phi > 0.9 \pm 5.0$ % indicating that the surface properties (ε and δ) became almost similar to the bulk properties (see Figure 7.5ac).

The *degree of openness* ε which is defined as the total surface of the windows to the total surface of the cavity $\varepsilon = N d_w^2/4D^2$, is shown in Figure 7.5c. N represents the maximum number of interconnected windows that a cavity can have.

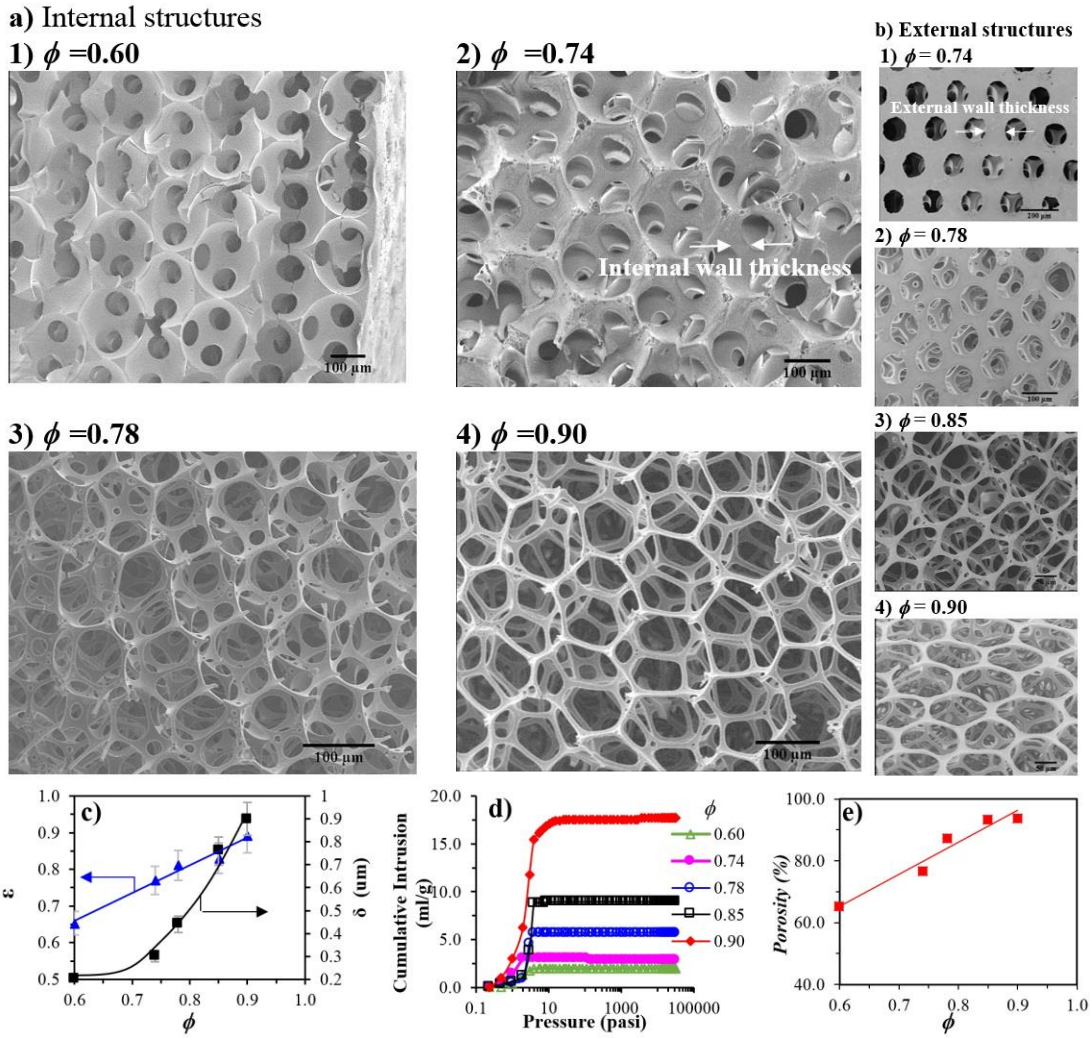

Figure 7.5 SEM images of acrylic-based polyHIPE, obtained at different phase ratio (ϕ), showing **a)** the internal structures and **b)** the surface structure; the inset arrows show the wall thickness between the two external windows; The droplet size of 150± 5.0 % was formed at $Q_w = Q_o = 150$ µl hr^{-1} ($\phi = 0.50 \pm 5.0\%$). The HIPE was centrifuged at different RCF for 10.0 min. **c)** The cumulative intrusion versus pressure at different ϕ; **d**) The measured porosity, obtained by the porositymetre, at different ϕ; **e)** The degree of openness, ε, as well as the relative wall thickness, δ, of polyHIPE at different ϕ.

Uniform droplets arrange themselves into hexagonal closed packed arrangement. This means that each droplet is in contact with other 12 droplets [220]. In order to determine the total surface of the windows, the average diameters of the windows d_w were measured using the SEM micrographs and were multiplied by the number of windows N. One would see how clearly the changes in the ϕ affected the degree of openness ε (Figure 7.5c). For

all cases, a higher degree of openness ε was observed at higher ϕ. The increase relationship between ϕ and ε is obvious because ϕ increased with decreasing the amount of polymer. As ϕ increases the surface area of the droplet increases and thus larger opening should be expected. One comment worth of note is that at $\phi > 0.74$ the droplet shape changed from spherical to hexagonal (Figure 7.5a-b). This implies that ε was estimated based on the surface area of a hexagonal window to the surface area of a hexagonal cavity ($S=L^2 \frac{3\sqrt{3}}{2}$, where L is the side length of the internal or external hexagon).

Table I: Physical property of the acrylic based polyHIPE.

Sample	RCF	ϕ^a ±5.0%	d_ω [b] (um)	V_ω (ml/g)[c]	Porosity (%)[c]	Permeability (D)[c]
PH1	0	0.60	70	2.0199	65.16	14.7
PH2	268	0.74	76	2.9078	76.80	18.8
PH3	604	0.78	90	5.7067	87.15	15.9
PH4	1073	0.85	93	8.9435	93.43	18.5
PH5	2415	0.90	102	17.6372	93.75	15.6

a: calculated water volume fraction of the HIPE before polymerisation
b: Determined by SEM.
c: Determined by mercury porosimetry.

We performed porosimetry measurements for these polyHIPE structures and the results are given in Table 1. The first data obtained by the porosimetry is the cumulative intrusion versus pressure (see Figure 7.5d). The cumulative intrusion versus pressure data are useful since they provide information about the structural strength of the sample. The intrusion volume increased in a stepwise manner, indicating that the physical structure of the sample has collapsed and the resulting cavity was replaced by the mercury. We can see that for every cumulative data point collected, there is a corresponding pressure point. Once the sufficient pressure was applied, the mercury penetrated through the surrounding interconnecting windows and filled the entire cavities. This means that windows dimeter into which the mercury penetrates is inversely proportional to the applied pressure, the larger the windows, the lower the pressure is required, as shown in Figure 7.5d. One point

worth of note is that the porosity measured by the porosimetry is slightly higher than the calculated ϕ (Figure 7.5e).

7.4.4. Styrene-based polyHIPE

So now let us turn our attention to the fabrication of styrene-based polyHIPEs. In this section, we investigated the use of the microfluidic device to form HIPE made of styrene and DVB. The stability of the w/o emulsions again was tested and the use of polymeric surfactants, similar to those used in the acrylic-based runs, failed to provide the required stability.

Also, styrene showed no absorbance to the UV irradiation and the corresponding HIPE eventually collapsed. We, therefore, shifted to the thermal polymerisation and the use of span 80, as oil soluble surfactant, was a good candidate for styrene-based polyHIPE made by thermal polymerisation. We found that surfactant concentration of 15.0 wt. % (of total oil phase) is the minimum amount required to stabilise the uniform w/o emulsion during thermal polymerisation, although it made the continuous phase very viscous. The chemical formulation of typical styrene-based HIPE made the formation of droplets by microfluidics more difficult because of the high viscosity of the continuous phase, which made it impossible to produce an emulsion with $\phi > 0.50$, when using 15.0 wt. % Span 80. This represents a serious drawback. The collected emulsions produced at $\phi = 0.50 \pm$ 5.0 % were left to settle for few min. No excess oil formed at the top of the vial unlike the acrylic-based HIPE. This means the water droplets did not properly sink under the gravity effect as expected, due to the high viscosity of the continuous phase. This was also confirmed by the SEM of the final structure of the polyHIPE (see Figure 7.6a), which shows that the cavity (originated from water droplets) did not approach each other.

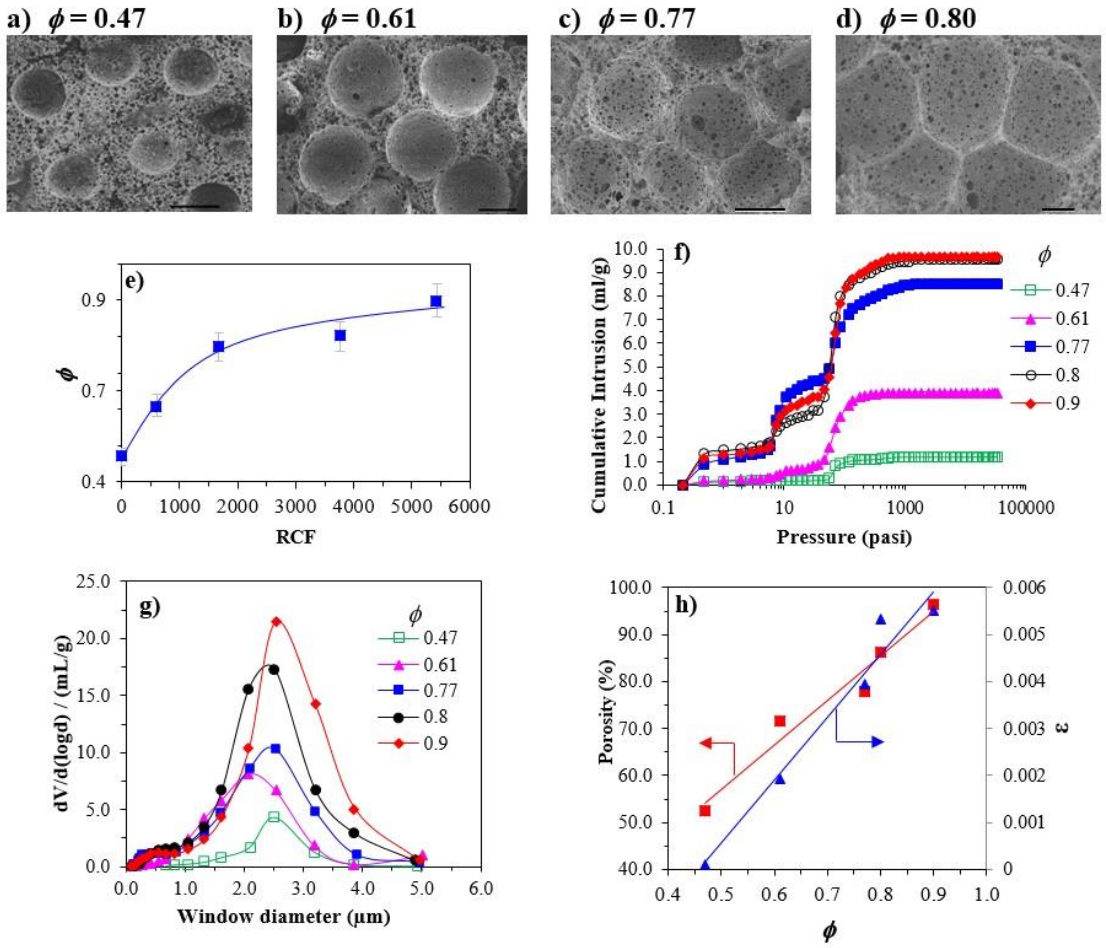

Figure 7.6 a-d) SEM images of polyHIPE obtained at different ϕ. **e)** The effect of relative centrifuge force (RCF) on the phase ratio ϕ. The HIPE was centrifuged for 10.0min. The droplet size of 150± 5.0 % were formed at Q_ω and Q_o= 200 µl hr^{-1}. **f)** The cumulative intrusion versus pressure at different ϕ. **g)** The log differential intrusion volume verses average window diameter, obtained by the porositymetre, for the styrene-DVB based PolyHIPE. **h)** The measured porosity, obtained by the porositymetre, as well as the calculated degree of openness, ε, of polyHIPE obtained at different ϕ.

Therefore, the use of a centrifuge step herein becomes even more justified. Similar to the previous case, the ϕ increased with RCF (Figure 7.6e). However, the cross examination of RCF graphs between the acrylic and styrene-based HIPE showed that for the same RCF used, the latter one has a lower ϕ, which is possibly due to the high viscosity of the continuous phase.

Table II: Physical property of the styrene based polyHIPE

Sample	(RCF)	ϕ^a ±5.0%	d_w [b] (um)	V_w (ml/g)[c]	Porosity (%)[c]	Permeability (D)[c]
PH7	0	0.47	0.668	1.1951	52.47	0.0185
PH8	604	0.61	2.406	3.9162	71.45	0.287
PH9	1677	0.77	2.430	8.4781	77.68	1.259
PH10	3773	0.80	2.448	9.4978	86.19	0.957
PH11	5433	0.90	2.49	9.6922	96.3236	1.331

a: calculated water volume fraction of the HIPE before polymerisation
b: Determined by SEM.
c: Determined by mercury porosimetry.

The styrene-based PolyHIPE structures were also tested by porositymeter, as shown in Figure 7.6f, and one could clearly see, from the cumulative intrusion graph, that much higher pressure than the previous case was required to fill the cavities. The physical properties of styrene based polyHIPEs are presented in Table II.

Figure 7.6g shows the window size distribution versus the cumulative volume of mercury. As we can see that the window diameter remained almost the same regardless of the water phase ratio ϕ. This result is also reflected by the SEM images shown in Figure 7.6a-c. Figure 7.6h illustrates the changes in ϕ on porosity and the degree of openness ε. Note that in this case, the $\varepsilon = 2N d_w^2/4D^2$, where N represents the total number of visible windows that were multiplied by 2 as the void had been cut in half. One could also see from Figure 7.6h that a similar trend was obtained with increasing ϕ; that the porosity increased whereas the calculated ε values, in this set, remains relatively the same as the ε is directly influenced by the average diameter of the windows, which is not changing.

7.4.5. Discussion

The formation of the interconnecting windows is a complex phenomenon and there is still a controversy regarding the mechanism via which they form. It depends on many parameters such as the internal phase ratio ϕ, the concentration of surfactant, droplet size and the nature of the polymer.

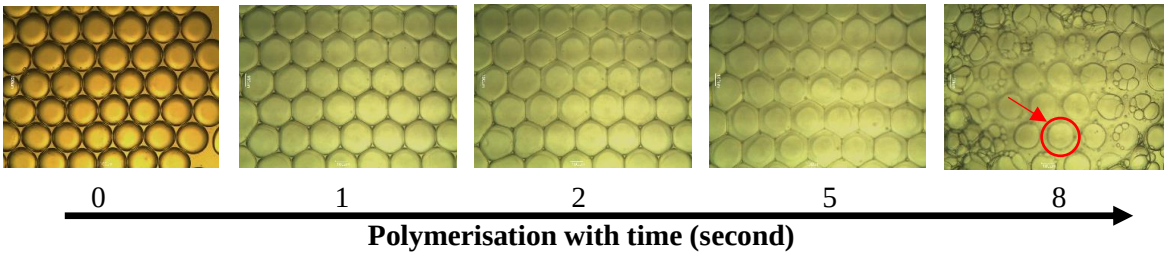

Figure 7.7 Microscope images of a one layer of uniform droplets in a hexagonal closed packing arrangement and the subsequent polymerisation. The arrow indicates the opening of the external windows after polymerisation.

In attempt to unravel the mechanism of windows formation in polyHIPE, we monitored the polymerisation of w/o emulsion (acrylic based formulations) induced by the microscope light, with time. Figure 7.7 shows the microscope images of a layer of uniform droplets in a hexagonal closed packing arrangement and the subsequent polymerisation. As can be seen from the images that the droplets got more interactive with the neighbouring droplets and an external shrinkage (expanding) was observed, forming a hexagonal structure, during polymerisation creating windows within few seconds after the exposure. Note that we have also investigated the effect of different droplet size on the windows formation and the same pattern was observed. More recently we succeeded in preparing porous microparticles by polymerisation of double emulsion drops using the same acrylic-based formulations. The results showed that the windows appeared instantly (no purification) after the double emulsion droplets were exposure to the UV while it travelled thorough the channel (estimated curing time was less than a second). The droplet-drop thin interfaces ruptured during polymerisation leaving the

microparticles with a number of windows, depending on the number of encapsulated droplets. This is consistent with the work of Cameron et. al. [228] that the formation of such windows are formed during the polymerisation due to shrinkage. This debate was supported by series of SEM which showed that the windows were formed before complete polymerisation and during the drying process [229,230].

In contrast, styrene based polyHIPEs had failed to attain porous structures as we could not observe formation of windows after the thermal polymerisation of w/o emulsion. Therefore, the styrene based polyHIPEs were subjected to purification via Soxhlet extraction with propanol (24 h) to remove the remaining residue. The purification step was suggested by Bismarck et.al [231]. They proposed that the windows are formed during the post-polymerisation (i.e. purification process- removal of surfactants residue). Their finding implies that the polymerising HIPE cannot shrink externally and the windows, after polymerisation, were still covered with the thin film, which only pop open during drying purification or drying process. Our results revealed that styrene based polyHIPEs, after purification, produced structures with a large number of irregularly interconnected window (Figure 7.6a) having roughly the same average size, regardless of ϕ, leading us to have a similar hypothesis as Bismarck et. al. This is in direct contrast with the acrylic based polyHIPE, where the window size changed with the ϕ. The difference between the two polyHIPEs was also reflected in the cumulative intrusion versus pressure graphs. The cross examination of Figure 7.5c and Figure 7.6f showed that the styrene based polyHIPE (Figure 7.6f) required much higher pressure. The pressure also increased in a step-wise manner indicating that the mercury was penetrating through smaller windows (few micrometres), compared with smooth penetration in the acrylic-based PolyHIPE which has tens of micrometres windows.

Interestingly, when comparing our results with the literature, one can argue that styrene based polyHIPE structure obtained by a conventional technique are usually more porous than the one reported here [228]. This insight can be clarified y Williams et al [232,233,234,235] investigations that the structure of styrene based polyHIPE, prepared conventionally, is mainly controlled by the amount of surfactants rather than the internal phase volume. Their argument was based on the fact that with increasing surfactant concentration the droplet size decreased and thus the overall surface area of the droplets increased, taking into account the conventional method used to prepare HIPE (highly-polydisperse droplets). The formation of induvial droplets and adjacent small droplets around the big ones can create consistent, round shaped interconnecting windows, which can be rupture during polymerisation as hypothesised by Cameron [228]. As the droplet size in this study was uniform, we infer that the windows formed in a styrene based polyHIPE was due to post polymerisation.

7.5. CONCLUSION

In conclusion, a facile microfluidic approach was introduced for fabricating highly porous and hierarchical polyHIPE structures. In this study, two polyHIPE scaffolds were prepared by means of different chemical formulations: acrylic-based and styrene-DVB polyHIPEs. The polyHIPE was produced by collecting a uniform w/o emulsion in a hydrophobic glass vial followed by a subsequent polymerisation. The long term stability of HIPE and its formation via microfluidics device, based on two different chemical formulations, were investigated. The results showed that it was experimentally challenging to simultaneously control the droplet size while alerting the internal water phase ratio ϕ. Thus, centrifugal step was implemented to achieve HIPE ratios. The conditions of relative centrifuge force (RCF) and centrifugation time under which the uniform HIPE would remain stable, during centrifugation, were identified. The combined advantage of microfluidics device and centrifugation step allowed a precise control over physical properties of the polyHIPE, such as cavity size, interconnecting window size and porosity. The maximum porosity was noted in the polyHIPE with slightly higher the internal water phase ratio ϕ. Although producing two different polyHIPEs, based on two different formulations, present a similar architecture, the resulting scaffolds differed significantly in terms of internal and external structure as well as the degree of openness ε. We also monitored the polymerisation of HIPE (acrylic based formulation) and our results indicated that the interconnecting windows can form either during or post polymerisation but this remarkably depends on the type of the surfactant, monomer and polymerisation techniques used for the preparation of polyHIPE. Finally, we believe that these hierarchical polyHIPE structures can open new vistas for many potential applications where conventional techniques fail to perform.

Chapter 8 Uniform Polymer Latexes via Emulsifier Free Emulsion Polymerisation in the presence of Solvent**

8.1. ABSTRACT

Conventional emulsifier-free emulsion polymerisation (EFEP) often produces large particles (> 500 nm) with a limited solids content, particularly in the case of partially water-soluble monomers. In the present study, the synthesis of well-defined uniform polymer nanoparticles with a high solids content was investigated through EFEP using a water-acetone mixture as the reaction medium. Styrene and an analytical grade potassium persulfate were used as monomer and initiator, respectively. A series of experiments were conducted using different acetone and styrene concentrations to examine their effects on the kinetic of emulsifier-free emulsion polymerisation. Results showed that the particle size decreases with increasing acetone concentration. The uniformity of the particles, however, depended on the concentration of acetone and monomer in the medium. The maximum number of particles was obtained at the highest acetone concentration explored and when the medium was below the saturation level with the monomer. The use of a water-soluble co-monomer sodium p-styrenesulfonate (NaSS) in the presence of acetone on the kinetic of EFEP was also investigated. The copolymerisation of styrene with NaSS in the presence of acetone allowed to generate uniform latexes with high solids content (upto 55.0%), where conventional approach failed to work.

** To be submitted.

8.2. INTRODUCTION

A great deal of research over the past few decades has been directed towards Emulsifier-Free Emulsion Polymerisation (EFEP). This technique is unique in that it can produce highly uniform, stable, and emulsifier-free polymer latexes [236,237,238,239]. Uniform latexes have been of great potential for a broad range of applications including calibration standards for light scattering [240], determination of membrane porosity in biological field [241], as well as models for studying stability, flocculation and rheological behaviour of polymeric colloidal systems [242]. A more recent application of polymer latexes is in colloidal self-assembly for the fabrication of photonic nanostructures [243].

Emulsifier-free emulsion polymerisation usually leads to the formation of uniform polymer particles with diameter ranging from 0.5 to 1.0 μm [244]. Different approaches have been adopted to reduce the particle size. One approach is to enhance nucleation by increasing the concentration of radicals via increasing the initiator concentration or raising the reaction temperature [245]. A higher initiator concentration provides more ionic end groups to the polymer particles and stabilise them against coagulation, resulting in smaller particles. Similarly, an increase in the reaction temperature causes the decomposition rate of initiator to rise, which results in a higher rate of nucleation and thus smaller particle size [245]. However, there is a limit to which particle nucleation can be enhanced by these. A very high initiator concentration can lead to the formation of large particles with a wide size distribution. This is due to an increase in the ionic strength of the aqueous phase [246]. A high reaction temperature can cause a dead-end polymerisation due to the early depletion of initiator [247].

An alternative approach to enhance the nucleation is to increase water solubility of the monomer [248]. Radicals propagate faster and precipitate sooner, prior to termination

with other radicals, if the water solubility of the monomer is significant [248]. Co-monomers with high water solubility has been used to enhance nucleation and reduce the size of particles resulting from EFEP [249,250]. While this technique is quite efficient in reducing the particle size, might adversely affect the properties of resulting particles [244]. Sajjadi and Yan have shown that smaller particles may be obtained if monomer concentration in the water phase can be maintained at or below the saturation level in order to supress the rate of particle growth/coagulation [251].

The solubility of monomer, such as styrene which has a little solubility in water, can also be increased by the addition of co-solvent to the continuous phase [252,253,254,255,256,257,258,259,260,261]. The addition of co-solvent has a dramatic influence on the nucleation in EFEP. The type of co-solvent in addition to its concentration in the continuous phase is quite important too [256]. Low carbon number alcohols (i.e. methanol or ethanol) are of primary choice, since they consist of OH group which is freely miscible with water [250,252,255,256]. Homola et. al. [252] preformed EFEP in the presence of several co-solvents (methanol, ethanol, propanediol and acetone). They showed that the particle size decreased linearly with increasing solubility of the monomer in the dispersing media for all types of solvents. However, some of the results were controversial and yet to be resolved. Homola et. al. reported that the particle size decreased slightly from 600 to 500 nm, when methanol content in the continuous phase increased from 0.0 to 100%, respectively [252] while another study showed that the use of methanol always increases the particle size regardless of the methanol content in the reaction medium [258]. Similar debate was also reported for the use of ethanol. Liu et. al. [256] showed that the particles obtained in pure water were actually smaller than those obtained in the presence of ethanol, contradicting the results obtained by Ou et. al [257] and Homola et. al. [252].

However, acetone has been found unanimously in the literature as the most efficient solvent in reducing the size of particles in comparison to other solvents [253,254,257,259,260]. For example, Okubo et. al. showed that the particle size decreased from 500 to 170 nm when acetone concentration increased from 0.0 to 40.0 vol.%, respectively [254]. Camli et. al. also managed to synthesis sub-100 nm polymer particles using acetone [255].

All the aforementioned papers claimed that uniform polymer latexes could be obtained in the presence of acetone regardless of monomer concentration used. In most researches cited, dynamic light scattering (DLS), which is not a reliable technique for measuring the broadness of particle size distributions, was used to characterise the polymer latexes. This raises a serious concern about the statement that the presence of acetone always leads to the formation of uniform polymer latexes. In this chapter, therefore, we carried out series of experiments to investigate the impact of the presence of acetone dissolved in the aqueous phase on the kinetic of emulsifier-free emulsion polymerisation and uniformity of the resulting particles. The experiments were conducted using styrene as a model sparingly water-soluble monomer. The effects of the addition of acetone and also a water-soluble co-monomer on EFEP kinetic were also investigated. Polydispersity index (PDI) of latexes was measured using TEM micrographs.

8.3. EXPERIMENTAL

8.3.1. Materials

The styrene monomer, St, was supplied at 99.9% purity by VWR, with trace quantities of an inhibitor, which was removed using ion-exchange resins (inhibitor removal, disposal column, Sigma Aldrich), prior to use. Analytical grade potassium persulfate (KPS, Sigma Aldrich) was used as initiator. The co-monomer used was sodium p-styrenesulfonate

(NaSS, Sigma Aldrich). Mixtures of acetone (Sigma Aldrich) and deionized water at different volume ratios were used as the continuous phase.

8.3.2. Saturation level

Styrene was added to a number of glass bottles containing solutions made in different water-acetone ratios. The bottles were sealed and placed in the water bath at the same conditions used for polymerisation (80°C) for 1.0 h. Then after 1.0 hr, the presence of excess monomer phase on the top of the solution was checked. This procedure was repeated until such a layer was formed and the solubility level was found.

8.3.3. Preparation of polystyrene (PS) nanoparticles

The polymerisation was performed in a Pyrex glass bottle with screw cap (empty volume: 25.0 ml). Styrene was added into Pyrex glass bottle containing a mixture of acetone–water at different volume ratios to give a total reaction volume of 20.0 ml. The bottle was sealed and then placed in a shaking water bath (Julabo, SW23) with the reaction temperature controlled at T = 80°C and shaking speed at 150 rpm. After about 1 h, 4.0 mmol l^{-1} of KPS dissolved in 2.0 ml of deionised water from the overall recipe was injected into the sealed bottle using a plastic syringe to start polymerisation. Polymerisation reactions were carried out for 24 h. The resulting polystyrene latexes were then cooled down to room temperature and characterised. The experimental procedure was identical for all polymerisations performed in this work.

8.3.4. Determination of monomer conversion

The final conversions, *x*, were measured gravimetrically. Approximately 3.0 g of the latex was withdrawn from the glass bottle and placed in an aluminium foil dish. The samples were dried in a vacuum oven at 80°C for 24 h. The styrene conversion was calculated as the weight ratio of the polymer produced to the total monomer in the recipe:

$$x = \frac{\text{weight of polymer formed} - \text{residual weight}}{\text{weight of monomer in the recipe}} \quad (8.1)$$

The residue weight accounts for the weight of initiator and surfactant in the sample.

8.3.5. Latexes characterisation

Particles size was determined by Transmission Electron Microscopy (TEM; Nippon Denshi Co., Japan, 200 kV). Typically, a small quantity of latexes was diluted in deionised water (~1% mass), placed on a 200-mesh carbon film supported by a copper grid, and allowed to dry at room temperature. The average particle sizes were also examined by dynamic laser light scattering (DLS, Malvern sizer) to confirm the particle sizes determined by TEM.

The number of particles (N_p) was estimated using the following equation:

$$N_p = \frac{m \,.\, x}{\frac{\pi}{6} . D_v^3 . \rho_p} \quad (8.2)$$

where m is the mass of polymer, x is the overall conversion, ρ_p is the density of polymer (1.05 g cm^{-3}), and D_v is the volume average diameter defined by the following equation:

$$\left(D_V = \frac{\sum_{i=1}^{n} n_i {D_i}^3}{N} \right)^{1/3} \quad (8.3)$$

where n_i is the number of particles with diameter D_i and $N = \sum_{i=1}^{n} n_i$ is the total number of particles counted.

Polydispersity index (*PDI*) was calculated by the following equation:

$$PDI = \frac{D_w}{D_n} \quad (8.4)$$

where;

$$D_w = \frac{\sum_{i=1}^{n} n_i {D_i}^4}{\sum_{i=1}^{n} n_i {D_i}^3} \qquad \text{where} \qquad D_n = \frac{\sum_{i=1}^{n} n_i D_i}{N} \quad (8.5)$$

Zeta potentials were measured by Zetasizer (DLS, Zetasizer, Malvern) at 25.0°C by injecting approximately 1.0 ml of the diluted latex into the zeta potential cell.

8.4. RESULTS AND DISCUSSION

The concentrations of acetone [S] and monomer [M] were varied from 0 to 40.0 vol. % and 1.0 to 160 g l^{-1}, respectively. The concentration of the functional co-monomer NaSS [M_c] was varied from 0.5 to 16.0 mmol l^{-1}.

8.4.1. Physical properties of styrene in water-acetone mixture

We first conducted a series of experiment to explore the effect of acetone on the solubility of monomer in the aqueous phase. Figure 8.1a shows the solubility of styrene in acetone-water solutions. The solubility of styrene increases with increasing acetone concentration in the aqueous phase, as previously reported in [254].

One could see from Figure 8.1a that when the acetone content in the water phase increased from 0.0 to 40.0 % at 80.0°C, the solubility level increased from 0.7 g l^{-1} to 12.0 g l^{-1}. The increase in the monomer solubility with acetone concentration is also accompanied by a decrease in the surface tension σ, as shown in Figure 8.1b

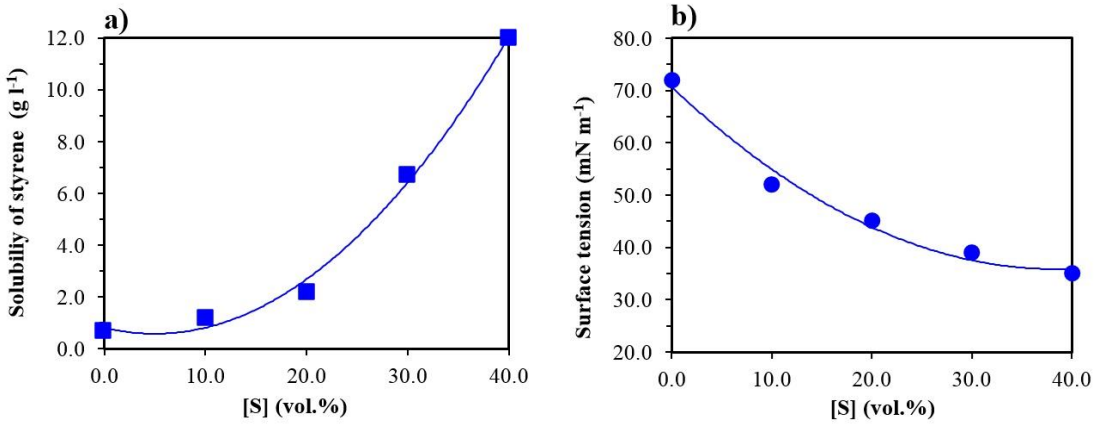

Figure 8.1 a) The solubility of styrene in acetone-water solution with different acetone ratio at 80°C and **b)** Surface tension of water-acetone solution at room temperature.

8.4.2. Conversion, particle size and stability

We monitored the effect of acetone content in a medium saturated with the monomer on the time evolution of conversion, volume-average diameter, zeta potential and conductivity. Note that the saturation level of styrene at 80.0 °C containing [S] = 0.0, 10.0, 20.0, 30.0 and 40.0 vol. % acetone is 0.7, 1.2, 2.2, 6.7 and 12.0 g l^{-1}, respectively (see Figure 8.1a).

Figure 8.2a shows the variations in conversion versus time for different acetone contents in the medium saturated with the monomer. The figure shows that the conversion increased with the reaction time, as expected. The reaction performed in the absence of acetone achieved much higher conversion with time than those carried out in the presence of acetone. After 20.0 min reaction, for example, the monomer conversion of the pure system was around 0.90 whereas the corresponding conversion for [S] = 40.0 vol. % was only 0.26. With the progress of the reaction, the conversion for all runs then slowly levelled off and reached as high as 0.90 within 60.0 min.

However, from the inset image shown in Figure 8.2a one could see that the amount of polymer produced *P*, which represents the rate of polymerisation R_P ($R_P = \frac{dp}{dt}$), increased with [S]. This is because the rate of particle growth increases with monomer concentration, taking into account that the initial monomer concentration for [S] = 40.0 vol. % is 12.0 g l^{-1} in comparison with only 0.70 g l^{-1} at [S] = 0.0 vol. %. Also, an enhanced solubility of styrene at [S] = 40.0 vol. % can increase the rate of particle generation resulting in more polymer produced (higher R_P).

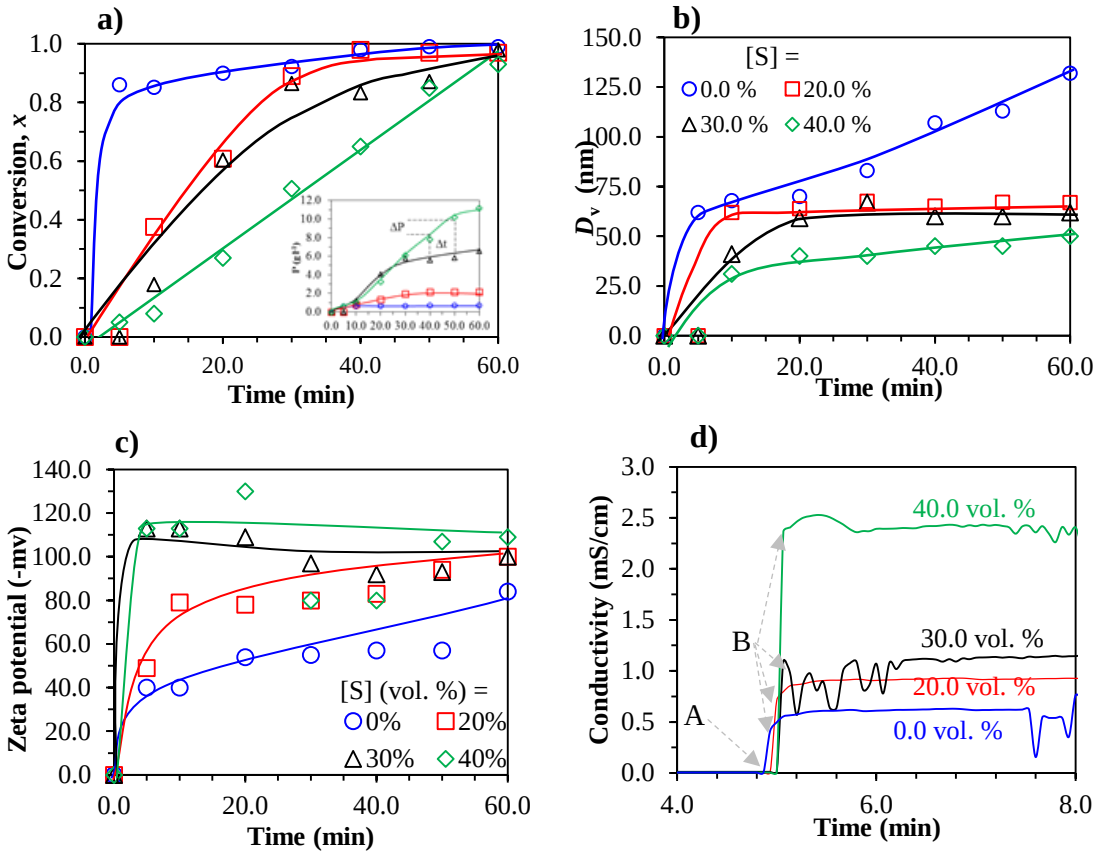

Figure 8.2 Time variations in **a)** conversions. Inset shows time evolution of polymer produced (P). **b)** volume-average diameter of particles D_V. **c)** Conductivity and **d)** Zeta potential for different acetone ratios in a medium saturated with the monomer (T = 80.0 °C).

The time evolution of the volume-average particle size in the course of reactions is shown in Figure 8.2b. The particle size increased with time for all runs, as expected. One could also see from Figure 8.2b that the particle size decreases with increasing acetone concentration, which is in agreement with the literature [252,253,254,255,256,257,258,259].

We also recorded the variations in zeta potential of latexes made at different acetone contents with time, as shown in Figure 8.2c. The curves clearly show that the zeta potential of particles increased with acetone concentration. As the stability of a latex is usually reflected by its zeta potential, with ≥ -30.0 mv for stable latexes, the data in

Figure 8.2c implies that particles achieved sufficient stability right after the start of the reaction. Also, the maximum particle stability was produced at [S] = 40.0 vol. %.

Figure 8.2d shows the conductivity-time curves measured during the initial period of the reaction in order to detect the onset of particle nucleation, as suggested by Tauer et. al. [262]. Point A corresponds to the time at which the initiator was injected into the reaction medium. The conductivity increased after injecting the initiator, but the response was different, depending on the acetone concentration. The figure shows that a sudden increase in conductivity occurred immediately after the addition of the initiator in the pure system (water), whereas the response was progressively delayed, by few seconds, with increasing acetone concentration. The A-B transition period indicates the pre-nucleation stage during which the reaction takes place in the homogeneous medium [262]. At point B, within few seconds after the addition of the initiator at corresponding point A, the slope of the conductivity-time curves suddenly changed. This deflection indicates the point where particle nucleation started to take place. The conductivity then remained almost constant during the course of reaction owning to the growth of particles. All runs followed the same pattern but the final value of the conductivity in the aqueous phase changed depending on the acetone concentration. From the data in Figure 8.2d one could see that the lowest conductivity's value 0.5 mS/cm was obtained in the absence of acetone. The conductivity increased with increasing acetone concentration and reached approximately 2.5 mS/cm at [S] = 40.0 vol. %. This deterministic feature of conductivity measurement assists us to explain the enhanced stability of the growing particles, which is supported by the high zeta potential of the particles obtained at high acetone content (see Figure 8.2c).

In a typical emulsifier-free emulsion polymerisation, particles formation occurs via homogeneous nucleation mechanism [237,238,263,264,265]. The radicals resulting from the decomposition of a water-soluble initiator in water react with monomer dissolved in the water phase to form surface-active oligomeric radicals. These radials can continue to propagate in the water phase until they reach a critical size and precipitate as a primary particle. The primary particles, which are extremely unstable, grow by coagulation with other primary particles and also by absorption of monomer from the monomer droplets, to the size they become sufficiently stable. Therefore, the increased solubility of monomer in the aqueous phase, in the presence of acetone, will increase the rate of propagation of radicals and reduce the rate of radical termination in the water phase. This means more oligomeric chains can reach the critical chain length to form primary particles. The terminated oligomeric radicals in the water phase, which failed to produce primary particles, can contribute to the stability of growing particles as *in-situ* oligomeric surfactants if they are of sufficient length [244]. This event is reflected by an increase in the conductivity. Therefore, a reduced rate of radical termination in the water-acetone phase cannot justify the increase in conductivity. This implies that other reasons should be sought to explain the increase in conductivity. One possible reason could be that acetone may have contributed to an increase in the decomposition rate of the initiator in the aqueous phase, as suggested by some investigators [266] This could result in the formation of more ionic radicals in the course of polymerisation with increasing [S], and enhanced generation of the particles. Furthermore the stability of particles in typical EFEP originates from the electrical charges induced by the ionisable initiator (KPS in the present study [263, 264].

8.4.3. Final conversion and particle size

Figure 8.3a-e shows the final conversion (reaction time = 24.0h) obtained at different monomer concentrations in the presence of different acetone contents. Note that for this set [M] was allowed to exceed the saturation level. The figure clearly shows that the final conversion increased with the monomer concentration regardless of the acetone content.

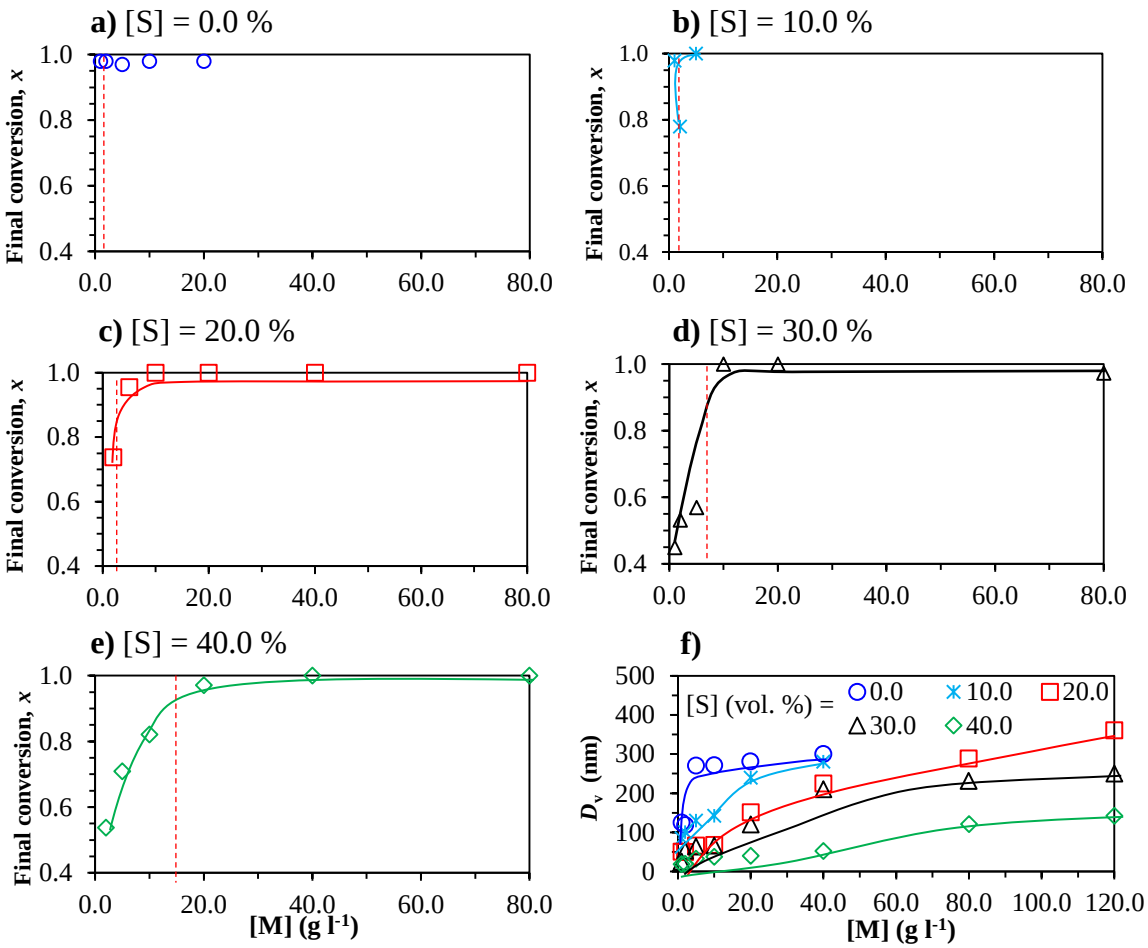

Figure 8.3 a-e) Effect of acetone concentration, [S] and monomer concentrations [M] on final conversion x and **f)** the volume-average diameter of particles D_V (T = 80°C). The dotted-line represents the saturation level.

One could also see from Figure 8.3a that the final conversion for [S] = 0.0 vol. % was generally high within the range of [M] studied. With increasing [S], the final conversion appears to be low at low [M]. The incomplete conversion at [M] < $[M]_{sat}$ is mainly due to dissolution of monomer in the aqueous phase (i.e. absence of monomer droplets), and the

associated diffusion-controlled monomer transport into growing polymer particles. One can also infer from Figure 8.3b-e that a complete conversion could be only achieved if $[M] > [M]_{sat}$, where monomer droplets formed and the amount of monomer dissolved in the aqueous phase became less important.

Figure 8.3f shows the effect of acetone and monomer concentration on the particle size. One can see from Figure 8.3f that the addition of acetone decreased the particle size. It also shows that the addition of only 10.0 vol. % acetone into the aqueous medium at a fixed styrene concentration of 10.0 g l^{-1} substantially decreased the particle size from 270.0 nm to 130.0 nm. An increase in the acetone content to 40.0 vol. % at the same styrene concentration (10.0 g l^{-1}) increased the particle size to approximately 40.0 nm. This is because the addition of solvent increased the monomer solubility. As a result, a faster rate of nucleation will generate more primary particles with smaller size. On the other hand, the latexes produced in water as the sole dispersion medium had the largest particles. One could also see from Figure 8.3f that further increase in [M] only increased the size of final particles until a critical size beyond which a massive coagulation occurred (at [M] = 400 g l^{-1} for [S]= 40.0 vol.%, as an example).

8.4.4. Particles uniformity

TEM micrographs of the latexes, produced by EFEP in the presence of various amounts of acetone at different monomer concentrations, are shown in Figure 8.4. The uniformity of particles obtained through EFEP is best reflected by their PDI, as shown in Figure 8.4a-e. For the pure system [S] = 0.0 vol. %, the polymer particles appeared to be uniform (U) at low [M], but degraded (N, non-uniform) thereafter when [M] > 20.0 g l^{-1} (column **A** in Figure 8.4).

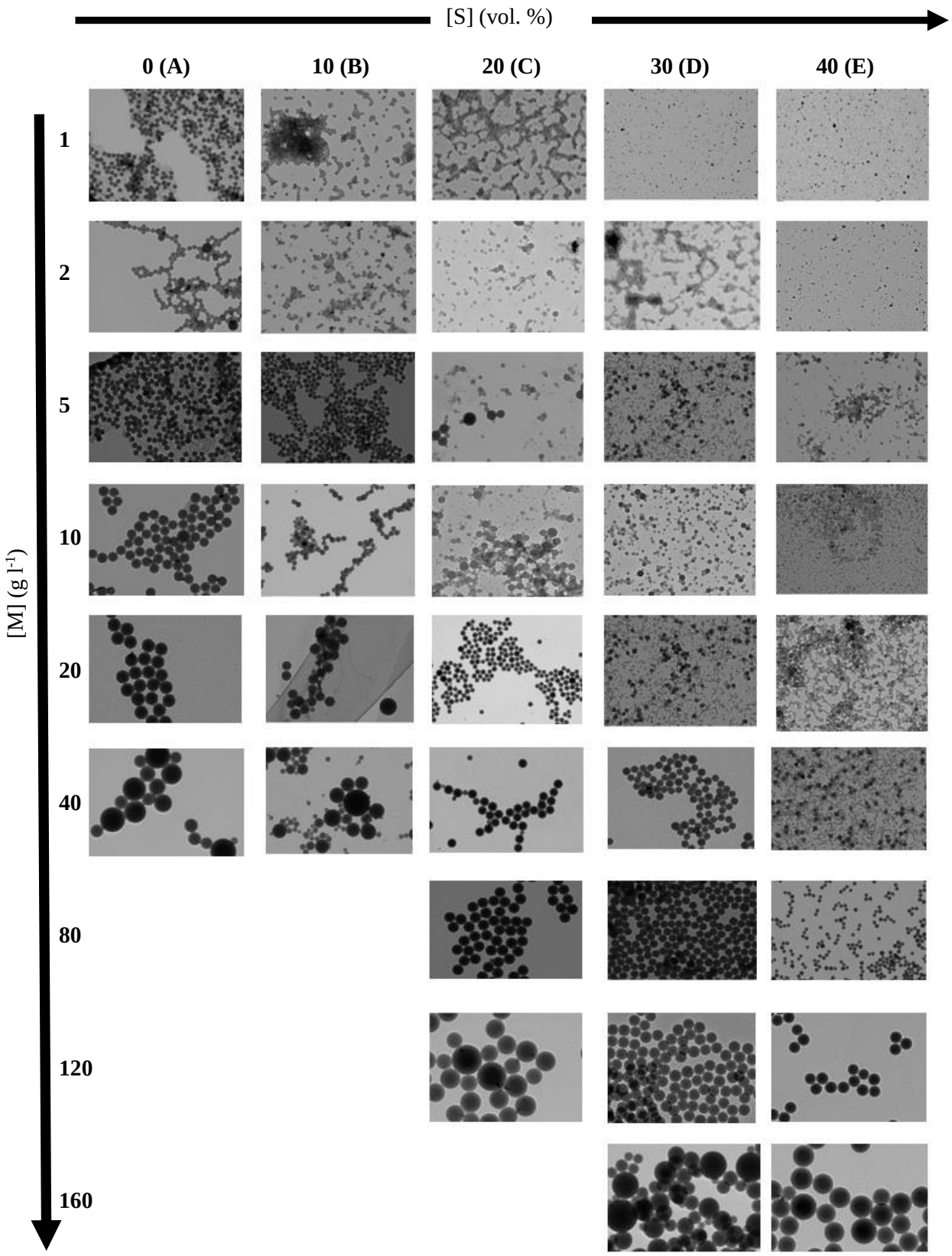

Figure 8.4 TEM micrographs of particles produced by EFEP in the presence of various amount of [S] at different monomer concentrations, [M], (T = 80°C).

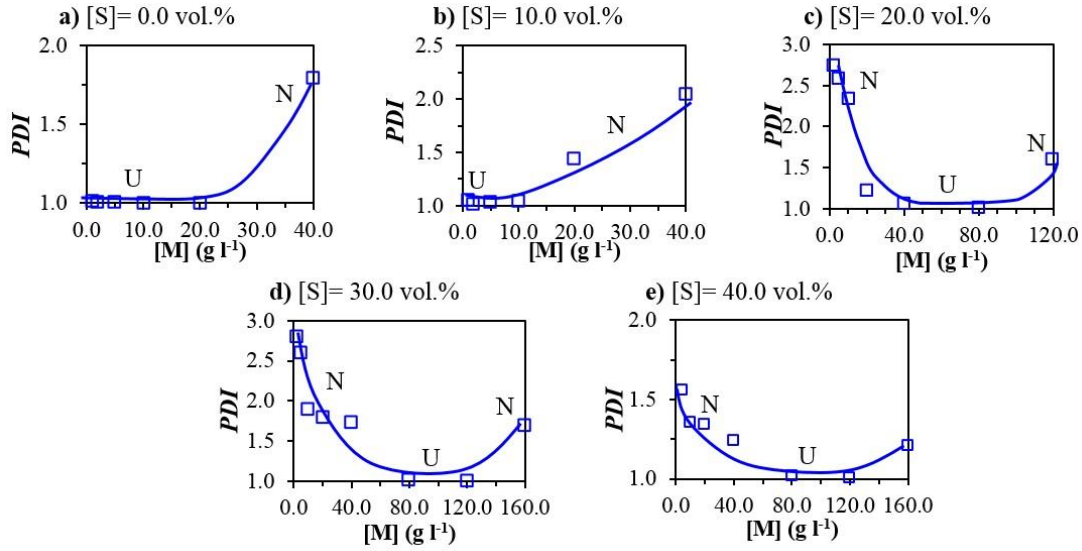

Figure 8.5a-e Effect of various amount of [M] at different acetone concentration, [S] on Polydispersity Indexes (*PDI*), (T = 80°C). N and U represent non-uniform and uniform particles. A rule of thumb for *PDI* of ≤ 1.07 is considered uniform.

Latexes produced at [S] = 10.0 vol. % (column **B)** followed the same UN pattern as the solvent-free emulsifier-free emulsion polymerisation but they started to become non uniform at a lower [M] ≥ 10.0 g l^{-1}. However, this UN trend changed to an NUN one when acetone concentration was increased to [S] ≥ 20.0 vol. % where solubility of the monomer in the continuous phase became significant. At a low styrene concentration (low solids content), the particles were small, but non-uniform (N). The reason for this is the increased monomer solubility in the medium that accelerates the rate of particle formation at the early stage of polymerisation and results in a higher number of primary particles with a smaller particle size (see Figure 8.3b) but with a higher polydisperse index (*PDI*), as shown in Figure 8.4a-e. The increase in polydispersity is because of the reduced rate of particle growth during nucleation, due to the slow rate of diffusion of monomer from the aqueous phase to the growing particles, which allows a longer nucleation time to happen [264]. Monodisperse particles started to emerge again at [M] = 20.0, 40.0 and 80.0 g l^{-1}, for [S] = 20.0, 30.0 and 40.0 vol. % respectively (Column **C**, **D** and **E** in

Figure 8.4). A high concentration of monomer was needed to enhance the rate of particles growth so that the primary particles formed during the early stage of polymerisation could capture all free radicals in the aqueous phase and prevent secondary nucleation. However, this finding should not allow us to draw a general conclusion that increasing the monomer concentration would always lead to the formation of uniform particles. At much higher styrene concentration, non-uniform particles again started to emerge due to an insufficient number of sulphate groups being available to stabilise the fast growing primary particles. Only non-uniform particles formed beyond [M] = 160 g l^{-1} within the range of [S] studied (see Figure 8.4).

8.4.5. Number of particles (N_p)

The number of particle N_p is the manifestation of the competition between the rate of generation R_{gen} and coagulation R_{coag} of primary particles as follows:

$$\frac{dN_p}{dt} = R_{gen} - R_{coag} \tag{8.6}$$

where

$$R_{gen} = k_{pw}^{j_{cr-1}}\left[M_{j_{cr-1}}^{o}\right][M]_w \tag{8.7}$$

where k_{pw} is the propagation rate constant in the water phase, $\left[M_{j_{cr-1}}^{o}\right]$ is the concentration of initiator derived radical with the chain length of j_{cr-1} (j_{cr} is the critical chain length for precipitation) and $[M]_w$ is monomer concentration in the water phase.

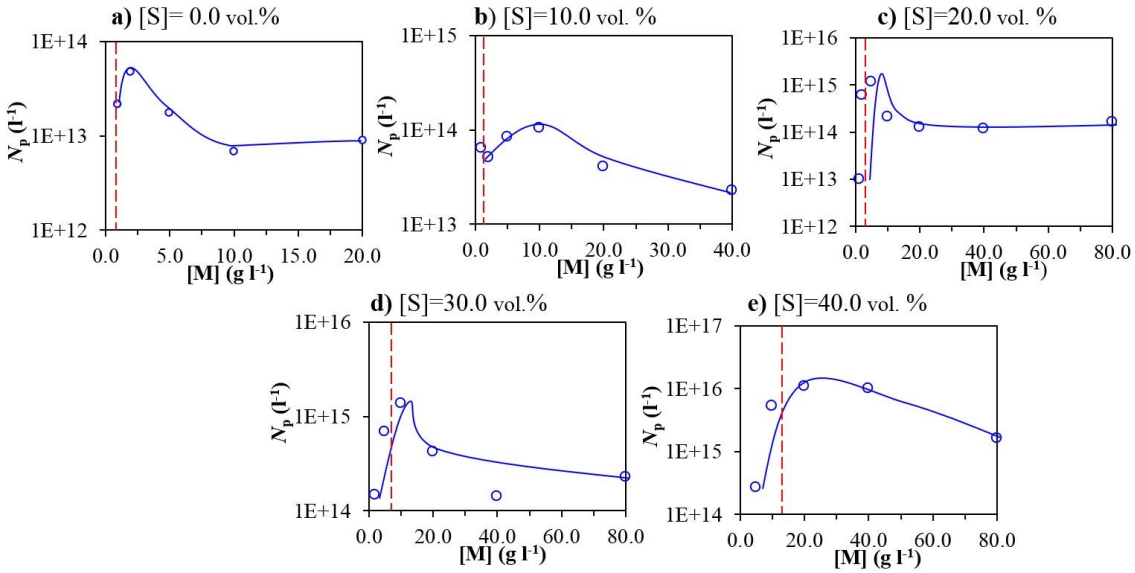

Figure 8.6a-e Effect of various amounts of [M] at different acetone concentrations [S] on the number of particles (N_p), [T = 80°C]. The dotted-line represents the saturation level.

The change in N_p with styrene concentration at different acetone contents is illustrated in Figure 8.6a-e. As eq. 8.7 suggests, N_p in all runs increased significantly with increasing [M] until it reached a maximum. The maximum N_p was produced at the highest acetone concentration explored (Figure 8.6a-e). This indicates that a higher solubility of monomer in the continuous phase, achieved at high acetone content, contributes to an extensive generation of particles with small size (see Figure 8.3b).

Another general observation from Figure 8.6a-e is that the maximum number of particles was always obtained when the medium was below the saturation level. A monomer concentration greater than the saturation level would insignificantly affect the rate of nucleation (see eq. 8.6), but substantially enhance the rate of particle coagulation R_{coag} by increasing the rate of particle growth. The generated primary particles grow by absorbing monomer droplets as well as coagulation with each other, to the size they become colloidally stable. This suggests that the rate of particle coagulation increases

with the size of the primary particles. The R_{coag} is function of surface charge density of the latexes so when there is a large quantity of monomer, the surface charged groups attached would not be sufficient to protect them against coagulation. This led to a large particles and thus a continuous reduction of N_p (with increasing [M]), as shown in Figure 8.6a-e Effect of co-monomer on particle size, PDI and N_p

We concluded from the previous results that polymerisations in the presence of acetone at high monomer concentration ([M] = 400 g l^{-1}) failed. In attempt to increase the solids content, we studied the copolymerisation of styrene with the functional co-monomer sodium p-styrenesulfonate (NaSS) in the presence of acetone using [M] = 400 g l^{-1}. Figure 8.7 shows the TEM micrographs of the final latexes, along with their volume-average particles size, *PDI* and N_p (Figure 8.7i-k). One comment worthy of note is that at a low [M_c] (0.5- 1.0 mmol l^{-1}), a mass coagulation occurred and the TEM micrographs in Figure 8.7a1 and Figure 8.7a2 are not representative and only represent particles that were not involved in the mass coagulations. However, stable latexes were formed at [M_c] = 2.0 mmol l^{-1} but they had a high polydispersity. One can also observe from the micrographs of the latexes in Figure 8.7a and their corresponding volume-average particles size in Figure 8.7i that the particle size decreases with increasing [M_c] upto = 8.0 mmol l^{-1} while their uniformity gradually improved (Figure 8.7j). One can also see from Figure 8.7k that N_p also progressively increased with [M_c] but changed little after [M_c] = 8.0 mmol l^{-1} within the range of [M_c] studied. This is consistent with the work of Kim et. al. [259] that emulsifier-free emulsion polymerisation of St and NaSS follows homogeneous nucleation mechanism at [M_c] ≤ 10.0 mmol l^{-1}.

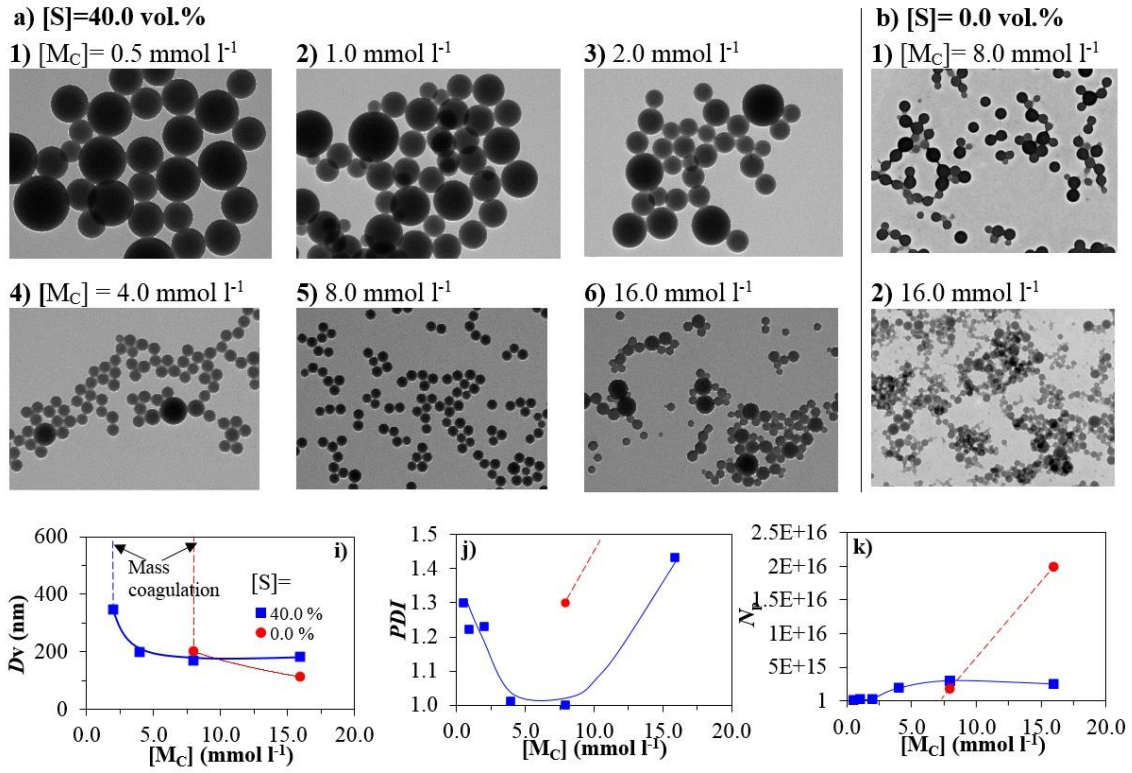

Figure 8.7 a-f) Particles obtained at different [M_C] at [S] = 40.0 vol. % and [M] = 400 g l^{-1}; **g)** and **h)** The morphology of particles obtained at different [M_C] at [S] = 0% and [M] = 400 g l^{-1}. **i), j)** and **k)** Effect of co-monomer concentration, [M_C] on the volume-average diameter of particles D_V, *PDI* and N_p., respectively. The *PDI* for [S] = 0.0 vol. % and [M_c] = 16.0 mmol l^{-1} was 2.5 and out of scale of plot J.

From Figure 8.7a6 one could also see non-uniform particles started to emerge at [M_c] = 16 mmol l^{-1}. The high polydispersity of particles at [M_c] = 160 mmol l^{-1}, together with a sudden rise in N_p as seen in the micrographs and Figure 8.7j may point to a micellar nucleation mechanism [259]. It has been suggested that at high NaSS concentration, homopolymerisation of NaSS may occur in the aqueous phase forming water-soluble polymer chains that can assemble to form micelles in a manner similar to conventional surfactants [259].

Similar runs were also carried out in the absence of acetone for comparisons. Within the range of [M_c] studied, latexes were only formed at [M_c] ≥ 8.0 mmol l^{-1}. Massive coagulation occurred at [M_c] < 8.0 mmol l^{-1}. This might seem in contrast with the results reported by Mike et.al. [250] that stable latexes were generated at relatively low [M_c] using a moderate solids content (22.0 wt. %). However, the current research used 40.0 wt. % solids content, which can explain the lack of particles stability at low [Mc]. The TEM micrographs of the latexes presented in Figure 8.7j show that the solvent-free polymerisation could only produce stable particles at [M_c] ≥ 16.0 mmol l^{-1} but they were quite polydisperse for the reasons explained before.

In the next section, we considered the effect of solids content [M] on particles uniformity at [M_c] = 8.0 mmol l^{-1}. This is the optimum concentration found from the previous section at which the smallest and most uniform particles could be produced via homogenous nucleation. The results are presented in Figure 8.8. One can observe from the micrographs in Figure 8.8a and Figure 8.8c that while particles size increased with increasing [M], their uniformity was further improved until [M] = 400 g l^{-1}, as seen in Figure 8.8d. While increasing the solid contents of the latex to 50.0 % ([M] = 500 g l^{-1}) slightly degraded the uniformity of the particles, though particles were still moderately uniform. Note that a sever coagulation occurred at [M] > 550 g l^{-1}.

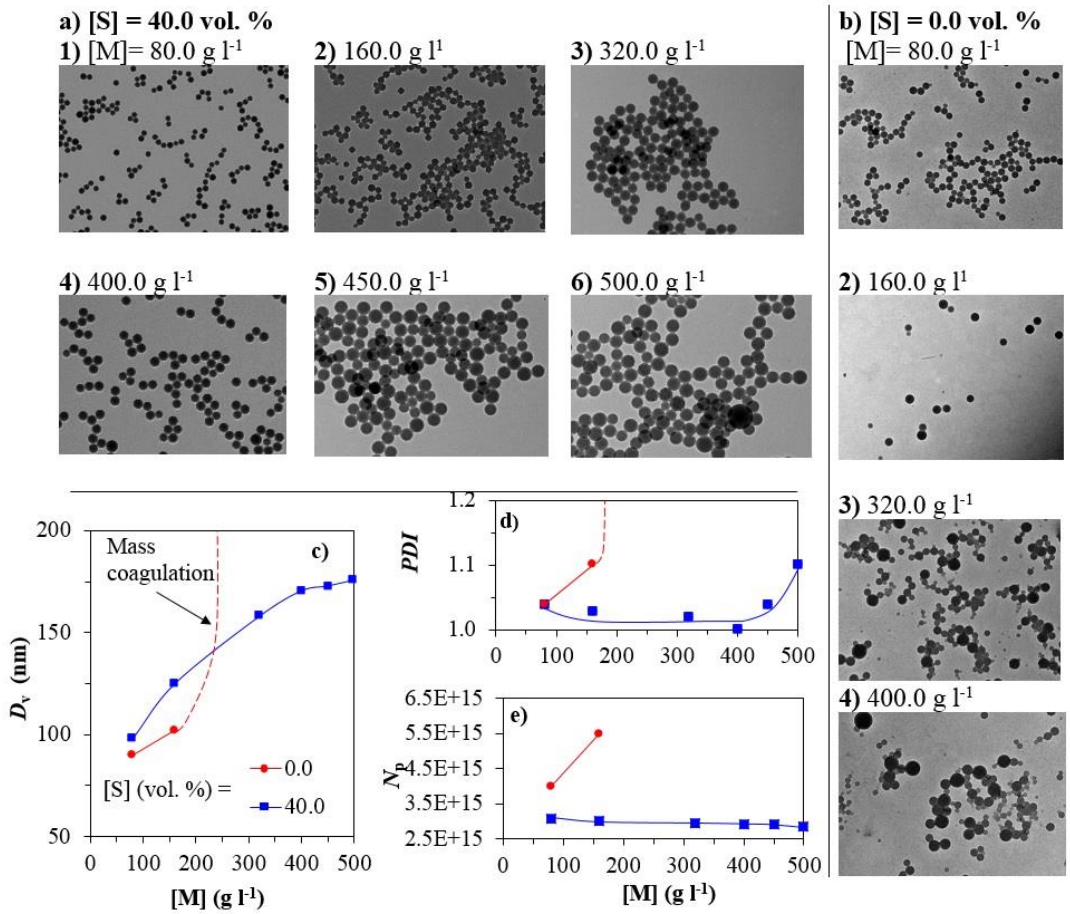

Figure 8.8 TEM micrographs of particles produced using different monomer concentrations obtained at **a)** in the presence of acetone [S] = 40.0 vol. % and **b)** in the absence of acetone [S] = 0.0 vol. %. **c), e)** and **d)** Effect of monomer concentration [M] on the volume-average diameter of particlesD_V, *PDI* and N_p, respectively. ([M_c] = 8.0 mmol l^{-1}). Sever coagulation occurred in the case of [M] =320 and 400 g l^{-1} in series (b) and therefore the micrographs are not representative.

The cross examination of micrographs in Figure 8.8a and Figure 8.8b indicates that in the absence of acetone average particles size was smaller (larger N_p, see Figure 8.8e) but polydispersity was higher (Figure 8.8d). Note that a significant coagulation occurred for [M] > 320 g l^{-1} in the absence of acetone (the TEM micrographs in Figure 8.8b2 and Figure 8.8b3 are not representative and only represent particles that were not involved in the mass coagulations). This indicates that the NaSS on its own cannot produced high solids contend latexes (max 16.0 %), but in the presence of acetone one can produce uniform latexes with solids content as high as 50.0 %.

8.5. CONCLUSION

In conclusion, we demonstrated the effect of acetone on the kinetic of emulsifier free emulsion polymerisation of styrene. Uniform polymer latexes with different sizes and solids content were produced. However, this statement is only valid at certain conditions and highly depends on the monomer content. The run in the absence of acetone or using low acetone concentration at a low monomer content produced rather monodisperse particles but they started to become polydisperse when acetone concentration increased above [S] = 10.0 %. Our results revealed that the addition of more acetone would require the addition of more monomers for the generation of monodisperse particles. The excessive amount of monomer droplets in the polymerisation system will only supply the growing particles feed for propagation, which explains the sharp *PDI* obtained at higher monomer concentrations. Therefore, it may be concluded that the range of styrene concentrations generating uniform particles can be extended somewhat by increasing the acetone concertation in the proportion to styrene concentration. This was necessary in order to achieve the required balance between nucleation and coagulation for the generation of monodisperse particles. The addition of co-monomer NaSS in the presence of acetone allowed the generation of particles with high solid contents where conventional approach failed to work.

Chapter 9 Conclusions and Recommendations for Future Studies

9.1. CONCLUSIONS

This thesis is the result of the research and development of different emulsification and polymerisation techniques for fabrication of a wide range of uniform polymeric materials. The first proposed idea of this research was to put forward ideas on how to improve the uniformity of polymer particles within conventional suspension polymerisation techniques.

In conjunction with the conventional techniques, the particle uniformity was further maximised by preserving the droplet identity formed by membrane emulsifications followed by a controlled-shear suspension polymerisation.

A microfluidic emulsification technique was also introduced as an alternative emulsification tool, which combined the operational advantages of producing high degree of drops uniformity, followed by photopolymerisation in order to produce a wide range of uniform polymeric particles and structures, such as porous particles and 3D structures. Finally, uniform nanoparticles with a high solids content were produced using emulsifier-free emulsion polymerisation in the presence of solvents. A summarised conclusion, highlighting the key findings from each case-study, is presented below.

Improving the Uniformity of Polymer Beads in Suspension Polymerisation via a Two-Stage Stirring Protocol:

- A two-stage stirring protocol was introduced for improving the uniformity of polymer beads produced in suspension polymerisation reactions.
- In the proposed study, the emulsification stage was carried out at an appropriate rpm followed by the polymerisation stage at reduced rpm in comparison to conventional techniques where the emulsification and polymerisation occur simultaneously in a single stirred vessel reactor at a constant rpm.
- The results showed that the two-stage protocol always produced narrower size distributions compared with those from conventional single-stage suspension polymerisation. The difference, however, broadened with decreasing stabiliser concentration, in a very similar way to the change in the average size of particles with stabiliser concentration.
- The advantage of the two-stage policy allowed to extend the operational range of rpm, particularly for [PVA] $\leq$ 0.25 g l^{-1}, while conventional single-stage suspension polymerisation failed to work.
- We also extended the application of the two-stage (agitation and stabiliser addition) hybrid protocol to further maximise the uniformity of the particles in comparison to the two-stage agitations protocol alone.

Uniform Polymer Beads by Membrane Emulsification-Assisted Suspension Polymerisation:

- A two-stage polymerisation process for the production of uniform polymer beads was introduced. Highly uniform monomer droplets were first obtained via stirred cell-flat membrane emulsification techniques, followed by a shear-controlled suspension polymerisation to convert the monomer droplets to polymer particles.
- We introduced a novel start-up method that did not allow intermixing of phases prior to emulsification and any associated mass transfer involved, thereby enhancing the uniformity of resulting droplets.
- The maximum droplets uniformity obtained via membrane emulsification were at an impeller speed range 500 -1500 rpm and flowrates within 1.0-3.0 ml min^{-1}.
- The droplet uniformity degraded at high impeller speed due to droplet break up in the emulsification vessel as well as low stabilise concentration. While the use of small amount of surfactants helped to stabilise the droplet, there was not any apparent advantage in increasing the amount of stabiliser above its CMC.
- Safe ranges of the reactor impeller speed and PVA concentration, within which the degree of uniformity of monomer droplets formed by membrane emulsification could be preserved during polymerisation, were found.
- Polymer particles with a one-one copy of the initial droplets with the same CV were obtained.

Fabrication of Highly-Ordered Interconnected Porous Microparticles:

- Uniform w/o/w emulsions, produced via glass-capillary based microfluidic technique, were first used as precursors to fabricate various shapes of porous microparticles via photopolymerisation. Three different shapes of uniform porous microparticles namely spherical, semi-spherical and plug-like shape, with highly ordered and well-defined interconnected windows, were produced.
- The size, porosity and the morphology of the resulting microparticles were controlled by the flow rate of individual phases, geometry of the microchannel and the packing structure of the inner droplets.
- Spherical porous microparticle made from critically-packed drops (critical phase ratio, ϕ_{cri}), were attempted. Different number of cores droplets, N from 1-8, were encapsulated and results showed that the windows did not form during polymerisation when $N \geq 6$.
- In contrast, highly packed drops where $\phi > \phi_{cri}$ showed consistent opening during polymerisation due to a significant stress applied on the over-stretched asymmetric interfaces during shrinking.
- We took an advantage of the confinement offered by the geometry of the microfluidic device to fabricate porous plug-like microparticles, which is the highlight of the present study. Furthermore, the fabrication of porous plug-like microparticles was reported for the first time.
- Osmosis policy was also introduced and could be used as an auxiliary method to enhance the internal phase ratio, where producing complex drops with a large number of internal droplets N at ϕ using microfluidic, remains experimentally challenging. This is because above certain N, only the size of would change.

Microfluidic Approach for Fabrication of Highly porous and Hierarchical polyHIPE Structures:

- Two polyHIPE scaffolds were prepared by means of different chemical formulations: acrylic-based and styrene-DVB polyHIPEs. They were produced by collecting a uniform w/o emulsion, produced via glass-capillary based microfluidic technique, in a hydrophobic glass vial followed by a subsequent polymerisation.
- It was experimentally challenging to simultaneously control the drop size while fixing the phase ratio (ϕ) as varying the size would always affect ϕ. Thus, centrifugal step was implemented to constitute HIPE ratio.
- The condition of relative centrifuge force (RCF) and time under which the uniform HIPE would remain stable, during centrifugation, were identified
- A precise control over physical properties of the polyHIPE, such as cavity size (originated from water drop), interconnecting window size and porosity, were manipulated by the flowrate.
- The mechanism of interconnecting windows formation during the polymerisation of HIPE was investigated. The results showed that the interconnecting windows can either form during or post polymerisation but this remarkably depends on the type of the surfactant, monomer and polymerisation techniques used for the preparation of polyHIPE.

Uniform Polymer Latex via Emulsifier free Emulsion Polymerisation in the presence of Solvent:

- In the last section, the effect of acetone on the kinetic of emulsifier free emulsion polymerisation was investigated. Uniform polymer latexes with different size and solid content, were obtained, unless otherwise indicated
- The results showed that polydisperse latexes were obtained at a higher acetone concentration and low monomer content or lower/absence of acetone concentration and high monomer content. The uniformity of the particles, however, depends on the concentration of acetone and monomer in the medium. Uniform nanoparticles with a low solid content were obtained at a low acetone and styrene concentration. A reverse order was produced using a high acetone and monomer concentration.
- The maximum number of particles was obtained at the highest acetone concentration explored and when the medium, for different acetone contents, was slightly above the saturation level with the monomer
- The boundary between particle nucleation and coagulation in order to produce uniform polymer nanoparticles in the presence of acetone was identified.
- The effect of the addition of a water-soluble co-monomer such as NaSS in the presence acetone on EFEP was also investigated. The results showed that the addition of co-monomer in the presence of acetone increased the solid content up to 40.0% while maintaining a latex size of approximately less than 100nm.

9.2. RECOMMENDATIONS FOR FUTURE STUDIES

This thesis demonstrated a proof of concept of different approaches for fabrication of uniform polymeric materials. The research presented in this thesis seems to have opened up a new vista for more adaptations, tests, and experiments that could be pursued for the future considerations, as follows below:

- It could be interesting to consider the application of the two-stage stirring protocol, where the emulsification and polymerisation stage are carried out at an impeller speed of more than 700 (i.e. 1000) and 250 (i.e. 500) rpm, respectively, in order to see their impacts on the particles uniformity. Also, the use of more commercial monomers such as styrene or vinyl acetate could also be tested.

- In addition to the optimisation of membrane emulsification-assisted suspension polymerisation, the potential to become a platform technology for increasing the production outcome of uniform polymer particles could be exploited. This could be achieved via an instant photpolymerisation of the drops once existing the membrane vessel. Obviously, the use of fast reactive monomers such as acrylic-based monomers is mandatory. This mechanism would also aid to further improve the uniformity of the resultant polymer particles, as the drops may not face an additional breakage or coalescence in the membrane vessel during monomer feeding.

- New polymer structures can be induced from the production of uniform double emulsion using microfluidics techniques. In comparison to the current study, the polymerisation of inverse double emulsion (monomer/water/oil) can led to the formation of a small clusters of microparticles. The size, number and cluster configuration of the microparticles could be precisely tuned by the flowrate,

confinement offered by the geometry of the channel and by packing structure of the inner monomer droplets.

- The development of the porous materials such as microparticles and 3D PolyHIPE structures requires deeper analysis and characterisations. These unique features of porous materials could also be a promising choice as absorption of oil spills or CO_2 captures for the preservation of environment.
- Regarding the emulsifier-free emulsion polymerisation in the presence of acetone, the work can be extended to test monomers with a wide difference in water solubility. It would also be interesting to conduct the experiment with different solvents in order to have a profound and comprehensive understanding on the kinetic of emulsifier-free emulsion polymerisation.

Appendix A

1. Experimental Set-up

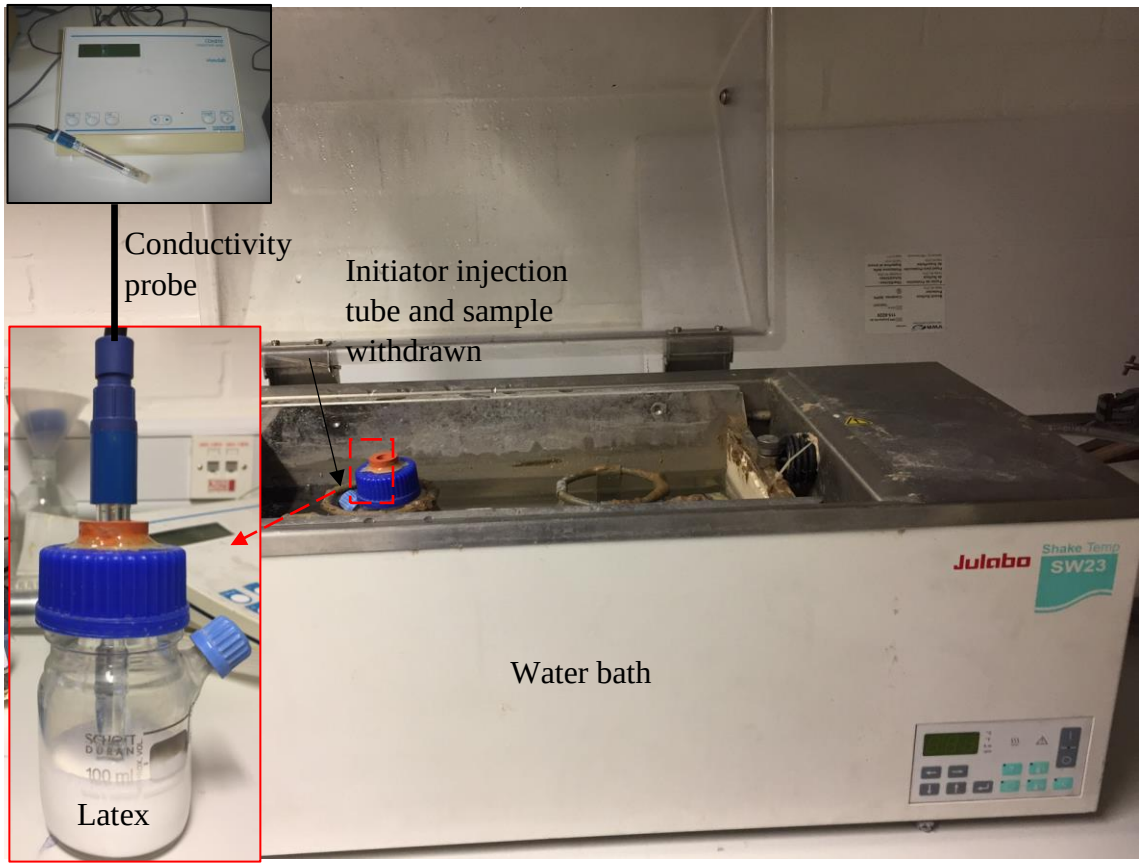

Figure A. 1 Emulsifier-free emulsion polymerisation set-up

2. Instruments

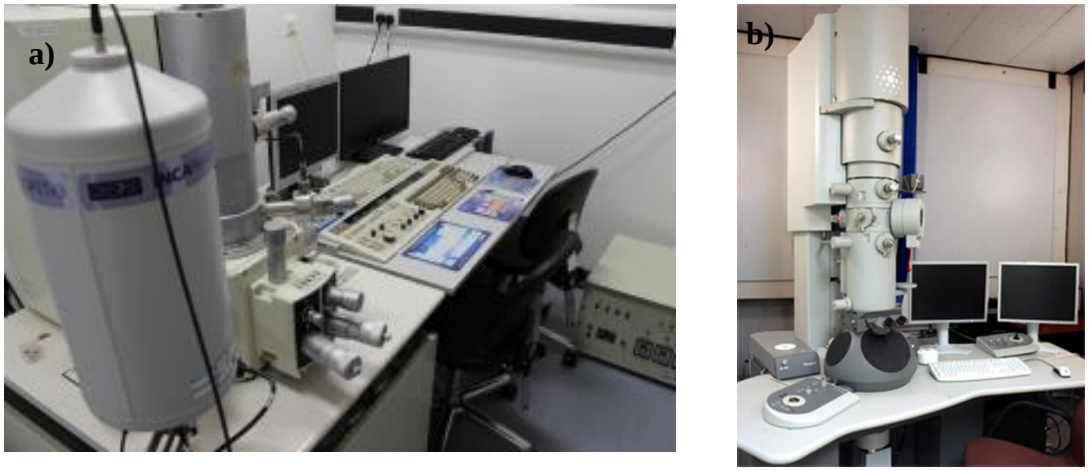

Figure A.2 a) Scanning Electron Microscope (SEM; Hitachi, S4000) and **b)** Transmission Electron Microscope (TEM; Nippon Denshi Co., Japan, 200 kV).

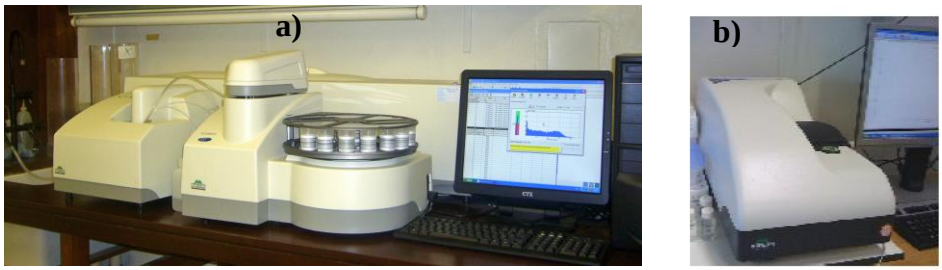

Figure A.3 a) Laser Diffraction Particle Size Analyser (Malvern, Coulter LS130) and **b)** Dynamic Light Scattering (Malvern Zetasizer nano ZS, particle size and zeta potential measurements)

3. Auxiliary Equipment

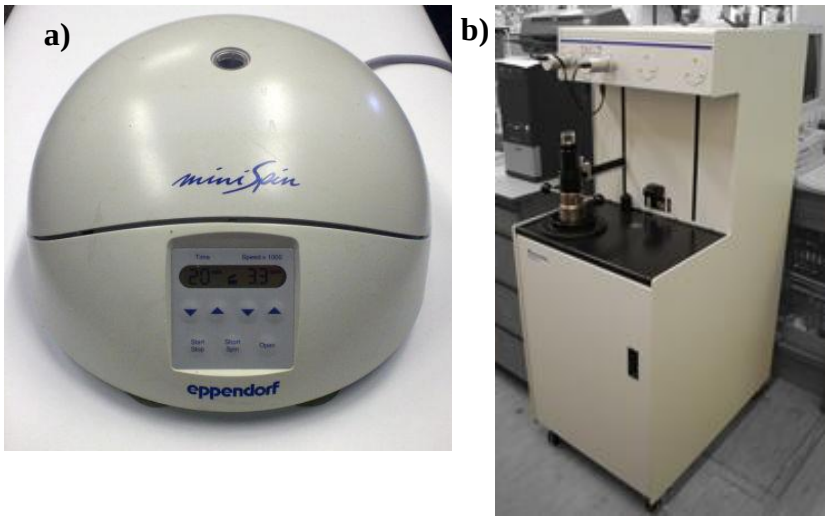

Figure A. 4 a) Eppendorf MiniSpin Microcentrifuges and **b)** Mercury intrusion porosimetry

Appendix B

1. Calculation of critical phase ratio ϕ_{cri}

The critical phase ratio ϕ_{cri} of sphere packing in a sphere can be calculated using the following equation. Note that the d/D values were found from the literature:

$$\phi = (d/D)^3 \; ; \qquad \text{where d=1}$$

N	d/D	D	ϕ
2	0.5	2	0.25
3	0.4641	2.154708	0.299886
4	0.4494	2.225189	0.363044
5	0.4142	2.414293	0.355304
6	0.4142	2.414293	0.426365
7	0.3859	2.591345	0.402274
8	0.378	2.645503	0.432081
9	0.366	2.73224	0.441251
10	0.353	2.832861	0.43987
11	0.3445	2.902758	0.449739
12	0.3445	2.902758	0.490624

The theoretical values of ϕ_{cri} versus the number of uniform internal droplets, *N*, are shown in **Figure B. 1**. Frome **Figure B. 1**, two different scenarios can be assumed in order to calculate ϕ_{cri}; 1) keeping size of internal droplets, ***d***, constant or 2) the external drops, **D**, constant. In both scenarios, the critical phase ratio ϕ_{cri} increases with the number of internal droplets, as shown in **Figure B. 1**.

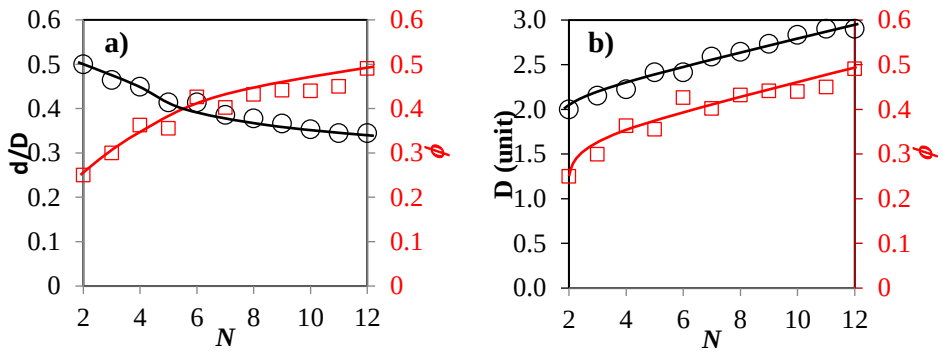

Figure B. 1 The calculated theoretical values of ϕ_{cri} obtained at **a)** constant D and **b)** constant d.

The critical phase ratio ϕ_{cri} of a sphere containing N = 2 and 3 can be calculated theoretically as described below:

For N =2

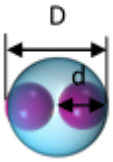

$$\phi_{cri} = \frac{\frac{\pi d^3}{6} \times N}{\frac{\pi D^3}{6}}$$

where N =2 and D= $2d$

$$\phi_{cri} = \frac{2d^3}{(2d)^3} = 0.25$$

For N =3

$$\frac{D}{2} = \frac{d}{2} + \frac{d}{\sqrt{3}}$$

$$\frac{D}{2} = d\left(\frac{1}{2} + \frac{1}{\sqrt{3}}\right)$$

$$\frac{D}{2} = d\left(\frac{2+\sqrt{3}}{2\sqrt{3}}\right)$$

$$\frac{D}{2} = d\left(\frac{2+\sqrt{3}}{2\sqrt{3}}\right) = 2.15d$$

$$\phi_{cri} = \frac{\frac{\pi d^3}{6} \times N}{\frac{\pi D^3}{6}}$$ where N =3 and D= $2.15d$

$$\phi_{cri} = \frac{3d^3}{(2.15d)^3} = 0.29$$

2. Evolution of drops morphology

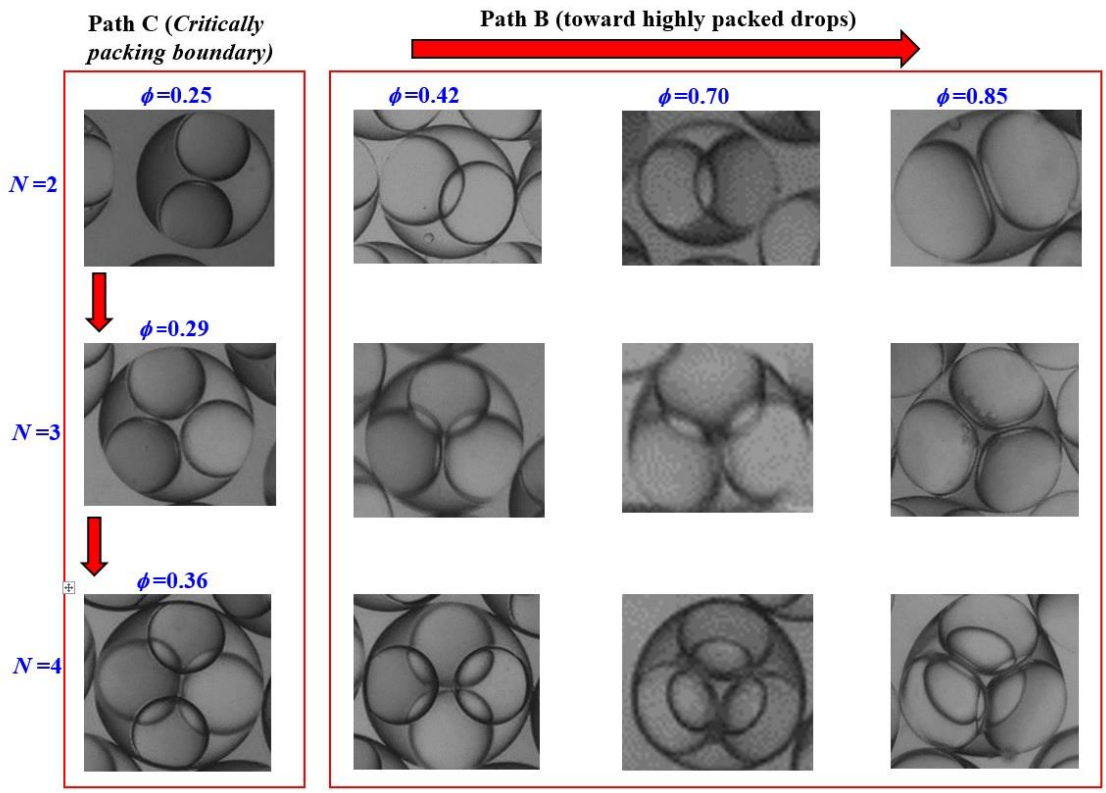

Figure B. 2 Optical micrographs images of w/o/w drops undergoing Path **A** and **B**. The downward arrow shows how the phase ratio increases with the number of core droplets. The Rightward arrow shows how the shape of the drops are transformed to critically packed drops with increasing the phase ratio.

3. Effect of KCl concentration on the drops morphology

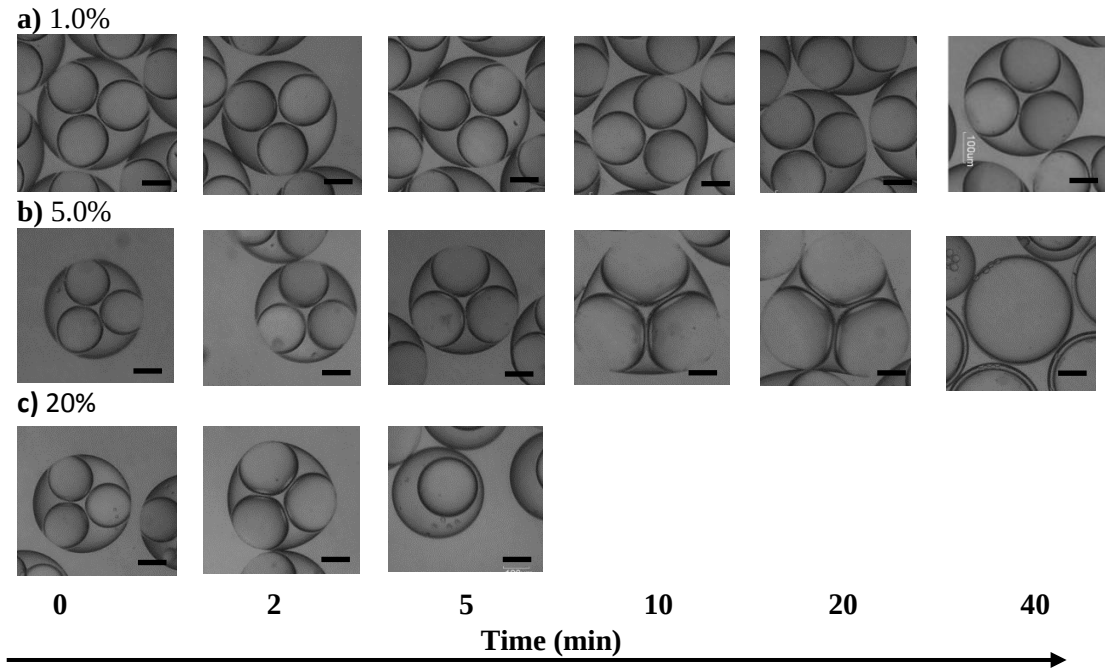

Figure B. 3 Optical images show the time-dependent change in the drop shape, containing three core droplets, at different KCl concentrations. The scale bar is 100 μm.

4. Effect of ϕ on the opening of the micoparticles during polymerisation

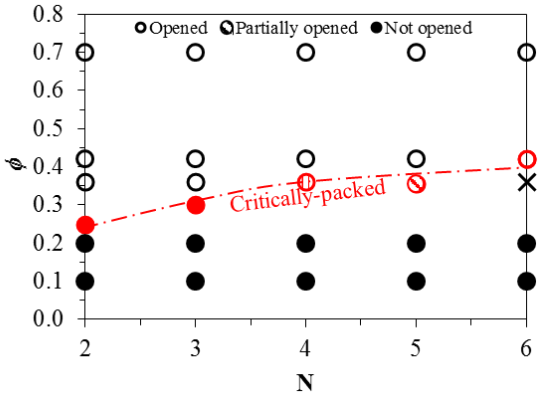

Figure B. 4 a) Symbols showing the opening of the micoparticles during polymerisation with ϕ at different N.

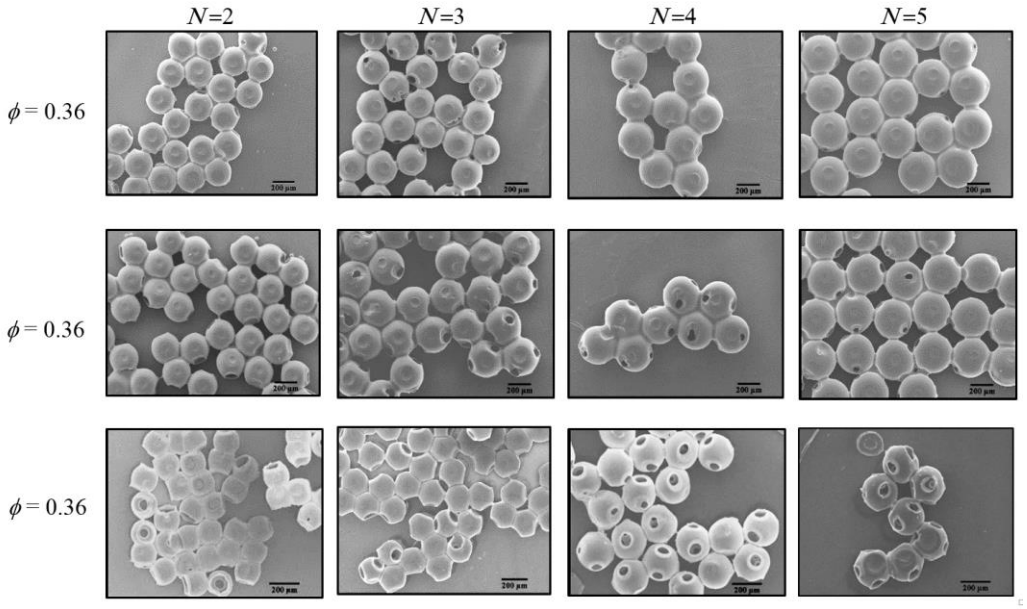

Figure B. 5 SEM images shows the comparison of porous microparticles, with a given number of core droplets (N) obtained at different ϕ. The scale bar is 200 μm. The experimental conditions for each category are given in Chapter 6.

5. Effect of oil surfactant

The effect of oil surfactant concentrations on drop and core size shown in **Figure B. 6** were obtained under a fixed condition. The drop and core sizes remained almost unchangeable with increasing the surfactant concentration from 2.5% to 5.0%. When the surfactant concentration was increased to 7.5%, however, a jetting regime was observed which resulted in a sudden fall in drop and core size. Such a reduced in the size immediately after the transition from dripping to jetting regime in a co-flow system was attributed to the high shear exerted by the more viscous continuous phase. The uniformity of both drop and core were also affected. This agrees with the literature that jetting produces less monodisperse drops than dripping. **Figure B. 6** shows the effect of surfactant concentration on the dimensionless number of dw/d. As can be seen from the figure that no considerable difference were noticed on dw/d with increasing surfactant concentration. We, therefore, concluded that surfactant concentration of 5.0% would be the optimum condition for the present study as it also enhanced the stability of the emulsion.

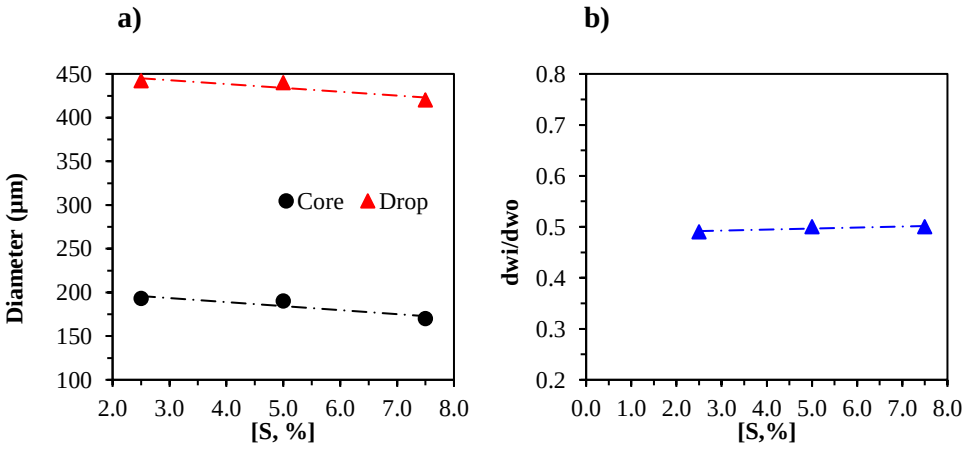

Figure B. 6 Effect of oil surfactant on **a)** drops diameter and **b)** degree of opening.

6. Effect of different flow conditions on the formation of drops

a) Q_i= 25 ul hr^{-1}

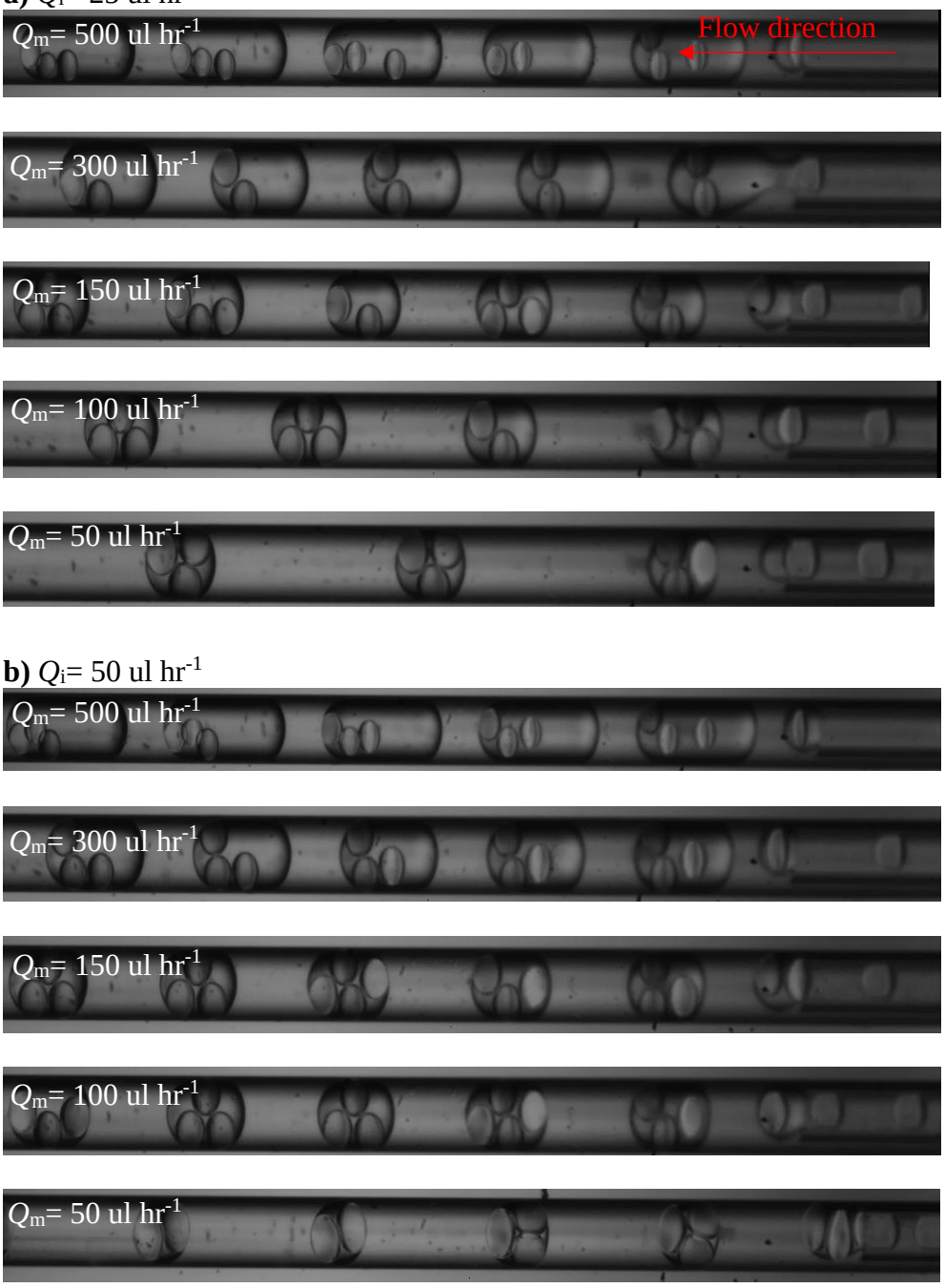

b) Q_i= 50 ul hr^{-1}

c) Q_i= 100 ul hr^{-1}

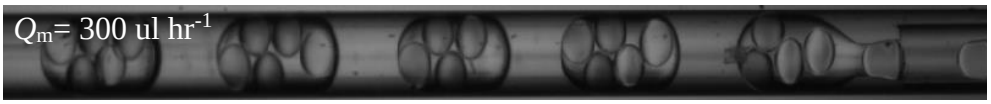

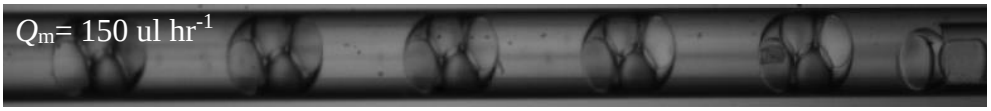

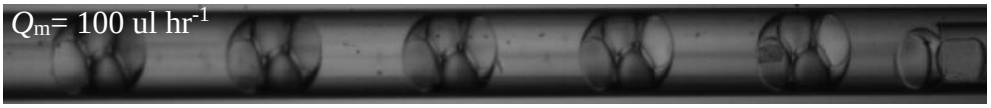

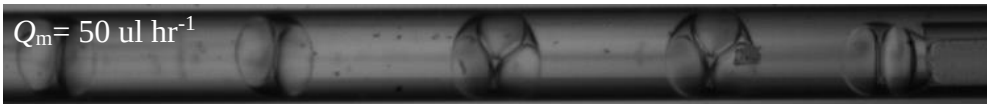

d) Q_i= 150 ul hr^{-1}

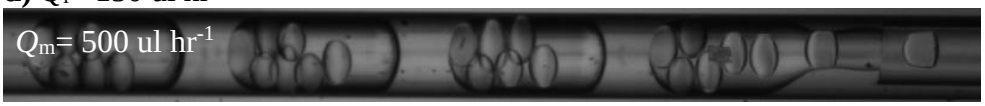

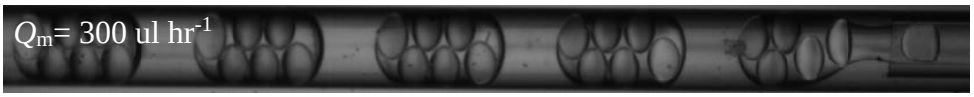

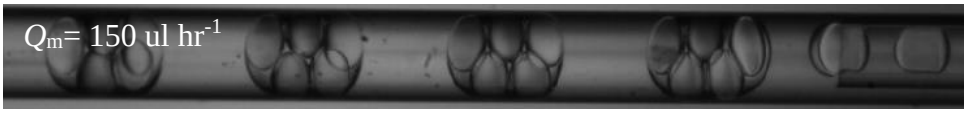

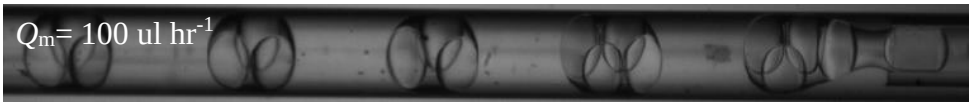

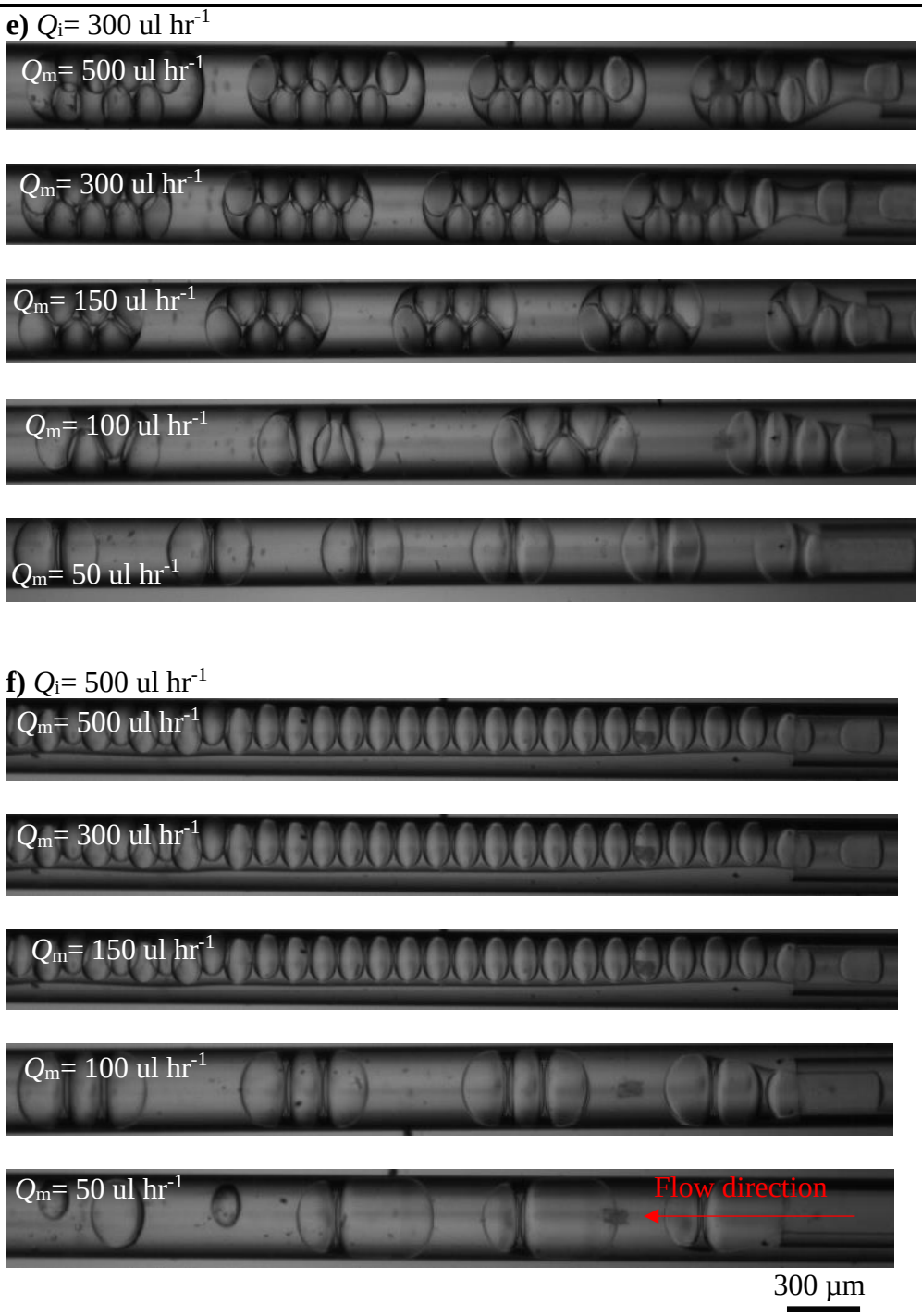

Figure B. 7a-f) Optical images taken at the tip of the capillary, showing the formation of droplets, with different configurations, obtained at different flow conditions. The scale bar is 300 µm.

7. Microfluidics approach towards nonspherical ultra-thin core-shell micoparticles

Core-shell microparticles with ultra-thin shell are developed for a wide range of applications such as pharmaceutical and biotechnological applications. The literature clearly cited that the material, geometry and shell thickness of the core-shell microparticles have a significant influence on their applications and are therefore crucial to be controlled. To date, most core-shell microparticles produced by microfluidics have been spherical in shape due to the relative ease in their fabrication. To fabricate nonspherical ultra-thin core-shell micoparticles, similar microfluidics device to the one shown in **Figure 6.1** were used but with the tip of the middle closer to the outer one (see FigB7). In brief, uniform w/o/w drops with high phase ratio (ϕ>0.90) were generated by microfluidics. The size of the drops were larger than the width of the outer channel. The length and thickness of the core-shell drops were controlled by the outer flowrate, Q_o. In the next stage, the polymerisation of the core-shell drops via UV irradiation was attempted with results shown in **Figure 6.11**. Figure 6.11a-e shows a range of core-shell microparticles with different shell thickness.

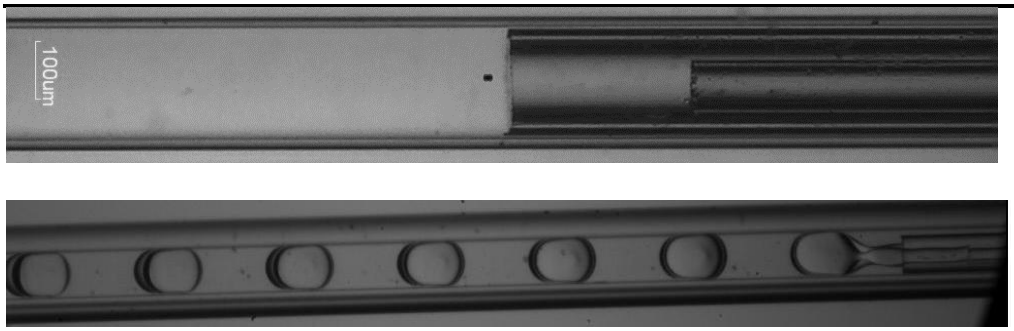

Figure B. 8 Optical images of the micro-capillary **a)** taken at the tip of the capillary, showing the fabrication of the device and **b)** formation of non-spherical core-shell. The scale bar is 100 µm.

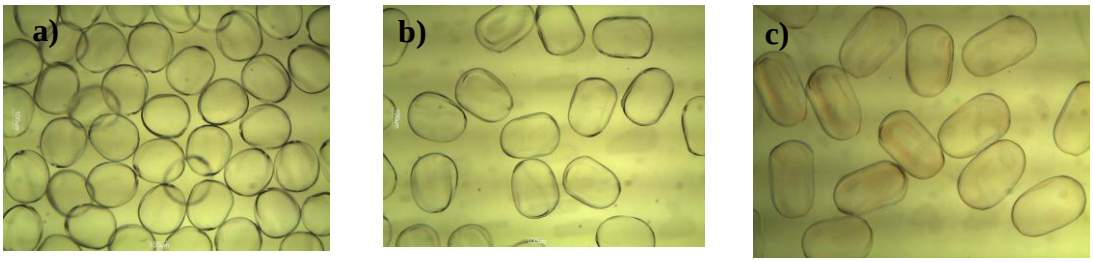

Figure B. 9 a-c) Optical micrographs images showing the ultra-thin core-shell drops with various morphologies. The scale bar is 100 µm.

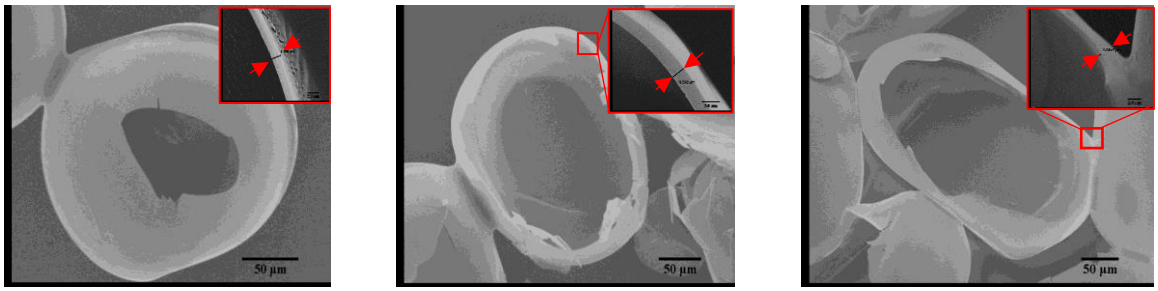

Figure B. 10 SEM images showing the evolution of particles from spherical to non-spherical ultra-thin core-shell.

8. Porous Fibre

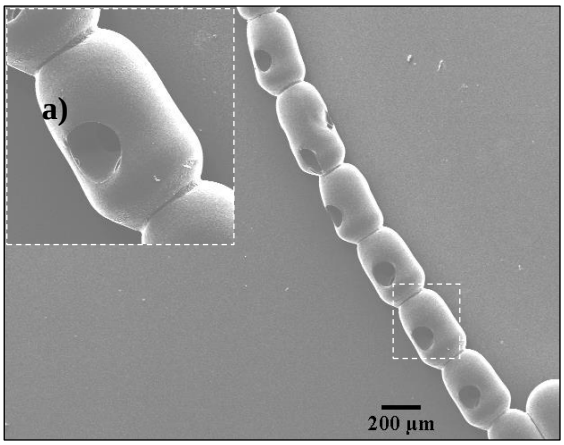

Figure B. 11 SEM images showing the porous fibres

Appendix C

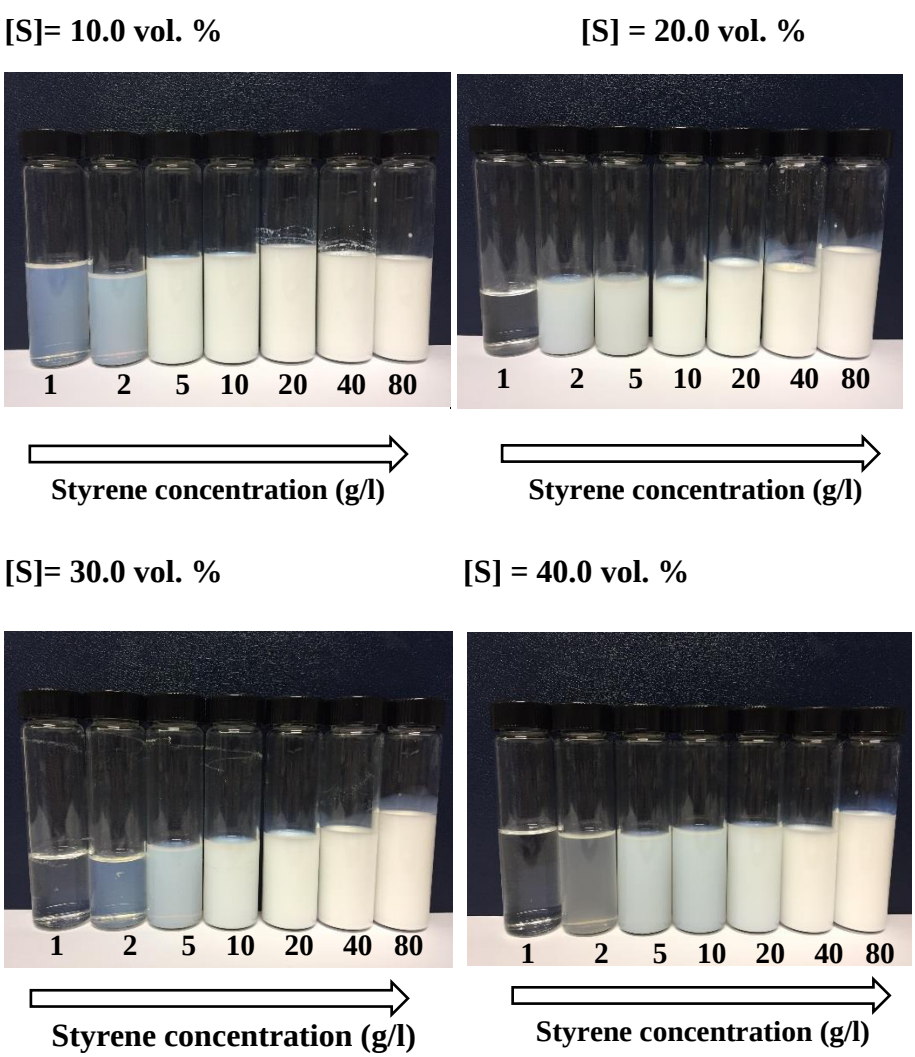

Figure C.1 Images of polystyrene latexes produced by emulsifier-free emulsion polymerisation in the presence of solvent [S].

References

[1] Arshady, R., 1992. Suspension, emulsion, and dispersion polymerisation: A methodological survey. Colloid & Polymer Science, 270(8), pp.717-732.

[2] Chern, C.S., 2006. Emulsion polymerization mechanisms and kinetics. Progress in polymer science, 31(5), pp.443-486.

[3] Bovey, F.A., Kolthoff, I.M., Medalia, A.I. and Meehan, E.J., Emulsion Polymerization,(1955). Interscience, New York.

[4] Prince, L. ed., 2012. Microemulsions theory and practice. Elsevier.

[5] Eliseeva, V.I., Ivanchev, S.S., Kuchanov, S.I. and Lebedev, A.V., 2012. Emulsion polymerization and its applications in industry. Springer Science & Business Media.

[6] Maaß, S., Metz, F., Rehm, T. and Kraume, M., 2010. Prediction of drop sizes for liquid–liquid systems in stirred slim reactors—Part I: Single stage impellers. Chemical Engineering Journal, 162(2), pp.792-801.

[7] Maaß, S., Rehm, T. and Kraume, M., 2011. Prediction of drop sizes for liquid–liquid systems in stirred slim reactors—part II: multi stage impellers. Chemical engineering journal, 168(2), pp.827-838.

[8] Uchida, T., Shiosaki, K., Nakada, Y., Fukada, K., Eda, Y., Tokiyoshi, S., Nagareya, N. and Matsuyama, K., 1998. Microencapsulation of hepatitis B core antigen for vaccine preparation. *Pharmaceutical research*, *15*(11), pp.1708-1713.

[9] Cleland, J.L., Lim, A., Daugherty, A., Barron, L., Desjardin, N., Duenas, E.T., Eastman, D.J., Vennari, J.C., Wrin, T., Berman, P. and Murthy, K.K., 1998. Development

of a single-shot subunit vaccine for HIV-1. 5. Programmable in vivo autoboost and long lasting neutralizing response. *Journal of pharmaceutical sciences*, *87*(12), pp.1489-1495.

[10] Brahim, S., Narinesingh, D. and Guiseppi-Elie, A., 2002. Kinetics of glucose oxidase immobilized in p (HEMA)-hydrogel microspheres in a packed-bed bioreactor. *Journal of Molecular Catalysis B: Enzymatic*, *18*(1), pp.69-80.

[11] Tang, M., Cao, X., Liu, Z., Wu, X. and Gance, D., 1999. Synthesis of glycidyl methacrylate-based matrix and its application in affinity chromatography of urokinase. *Process Biochemistry*, *34*(8), pp.857-862.

[12] Asua, J.M. ed., 2012. *Polymeric dispersions: principles and applications* (Vol. 335). Springer Science & Business Media.

[13] Tadros, T.F. ed., 2013. *Emulsion formation and stability*. John Wiley & Sons.pp. 1-75.

[14] Chaurasia, A.S., 2016. *Buoyancy-assisted microfluidics* (Doctoral dissertation, King's College London).

[15] Sander, J.S., Isa, L., Rühs, P.A., Fischer, P. and Studart, A.R., 2012. Stabilization mechanism of double emulsions made by microfluidics. *Soft Matter*, *8*(45), pp.11471-11477.

[16] Sonneville-Aubrun, O., Bergeron, V., Gulik-Krzywicki, T., Jönsson, B., Wennerström, H., Lindner, P. and Cabane, B., 2000. Surfactant films in biliquid foams. *Langmuir*, *16*(4), pp.1566-1579.

[17] Domínguez, A., Fernández, A., González, N., Iglesias, E. and Montenegro, L., 1997. Determination of critical micelle concentration of some surfactants by three techniques. *J. Chem. Educ*, *74*(10), p.1227.

[18] Nusselder, J.J.H. and Engberts, J.B., 1992. Toward a better understanding of the driving force for micelle formation and micellar growth. *Journal of colloid and interface science*, *148*(2), pp.353-361.

[19] Harkins, W.D., 1945. A general theory of the reaction loci in emulsion polymerization. *The Journal of Chemical Physics*, *13*(9), pp.381-382.

[20] Smith, W.V. and Ewart, R.H., 1948. Kinetics of emulsion polymerization. *The journal of chemical physics*, *16*(6), pp.592-599.

[21] Griffin, W.C. and Lynch, M.J., 1968. Surface active agents. *Handbook of food additives, 2nd edn.(Ed.: Furia, TE)*, p.397.

[22] van Aken, G.A. and Zoet, F.D., 2000. Coalescence in highly concentrated coarse emulsions. *Langmuir*, *16*(18), pp.7131-7138.

[23] Dickinson, E., 2010. Flocculation of protein-stabilized oil-in-water emulsions. *Colloids and Surfaces B: Biointerfaces*, *81*(1), pp.130-140.

[24] Voorhees, P.W., 1985. The theory of Ostwald ripening. *Journal of Statistical Physics*, *38*(1), pp.231-252.

[25] Karbstein, H. and Schubert, H., 1995. Developments in the continuous mechanical production of oil-in-water macro-emulsions. *Chemical Engineering and Processing: Process Intensification*, *34*(3), pp.205-211.

[26] Lambrich, U. and Schubert, H., 2005. Emulsification using microporous systems. *Journal of Membrane Science*, *257*(1), pp.76-84.

[27] Egidi, E., Gasparini, G., Holdich, R.G., Vladisavljević, G.T. and Kosvintsev, S.R., 2008. Membrane emulsification using membranes of regular pore spacing: Droplet size and uniformity in the presence of surface shear. *Journal of Membrane Science*, *323*(2), pp.414-420.

[28] Fuchigami, T., Toki, M. and Nakanishi, K., 2000. Membrane emulsification using sol-gel derived macroporous silica glass. *Journal of Sol-Gel Science and Technology*, *19*(1), pp.337-341.

[29] Kosvintsev, S.R., Gasparini, G., Holdich, R.G., Cumming, I.W. and Stillwell, M.T., 2005. Liquid− Liquid Membrane Dispersion in a Stirred Cell with and without Controlled Shear. *Industrial & engineering chemistry research*, *44*(24), pp.9323-9330.

[30] Ito, F. and Makino, K., 2004. Preparation and properties of monodispersed rifampicin-loaded poly (lactide-co-glycolide) microspheres. *Colloids and Surfaces B: Biointerfaces*, *39*(1), pp.17-21.

[31] Stillwell, M.T., Holdich, R.G., Kosvintsev, S.R., Gasparini, G. and Cumming, I.W., 2007. Stirred cell membrane emulsification and factors influencing dispersion drop size and uniformity. *Industrial & engineering chemistry research*, *46*(3), pp.965-972.

[32] Vladisavljević, G.T., Kobayashi, I. and Nakajima, M., 2012. Production of uniform droplets using membrane, microchannel and microfluidic emulsification devices. *Microfluidics and nanofluidics*, *13*(1), pp.151-178.

[33] Vladisavljević, G.T. and Williams, R.A., 2006. Manufacture of large uniform droplets using rotating membrane emulsification. *Journal of colloid and interface science*, *299*(1), pp.396-402.

[34] Zhu, J. and Barrow, D., 2005. Analysis of droplet size during crossflow membrane emulsification using stationary and vibrating micromachined silicon nitride membranes. *Journal of membrane science*, *261*(1), pp.136-144.

[35] Whitesides, G.M., 2006. The origins and the future of microfluidics. *Nature*, *442*(7101), pp.368-373.

[36] Zhang, M., Wang, W., Xie, R., Ju, X., Liu, Z., Jiang, L., Chen, Q. and Chu, L., 2016. Controllable microfluidic strategies for fabricating microparticles using emulsions as templates. *Particuology*, *24*, pp.18-31.

[37] Kumacheva, E. and Garstecki, P., 2011. Microfluidic Synthesis of Polymer Particles with Non-Conventional Shapes. *Microfluidic Reactors for Polymer Particles*, pp.192-214.

[38] Takeuchi, S., Garstecki, P., Weibel, D.B. and Whitesides, G.M., 2005. An axisymmetric Flow-Focusing microfluidic device. *Advanced materials*, *17*(8), pp.1067-1072.

[39] Chu, L.Y., Utada, A.S., Shah, R.K., Kim, J.W. and Weitz, D.A., 2007. Controllable monodisperse multiple emulsions. *Angewandte Chemie International Edition*, *46*(47), pp.8970-8974.

[40] Utada, A.S., Lorenceau, E., Link, D.R., Kaplan, P.D., Stone, H.A. and Weitz, D.A., 2005. Monodisperse double emulsions generated from a microcapillary device. *Science*, *308*(5721), pp.537-541.

[41] Abate, A.R. and Weitz, D.A., 2009. High-order multiple emulsions formed in poly (dimethylsiloxane) microfluidics. *Small*, *5*(18), pp.2030-2032.

[42] Matyjaszewski, K. and Davis, T.P., 2003. *Handbook of radical polymerization*. John Wiley & Sons.

[43] F. Hoffman, K. Delbruch, Patent (Ger.) No. 250 690, Farbenfabriken Bayer, Germany, 1909.

[44] W. Bauer, H. Lauth, Patent (Ger.) No. 656,134, Rohm and Haas, Darmstadt, 1931.

[45] Mlynek, Y. and Resnick, W., 1972. Drop sizes in an agitated liquid-liquid system. *AIChE Journal*, *18*(1), pp.122-127.

[46] Tanaka, M. and Oshima, E., 1983. Spatial Differences in Droplet Sizes in the Reactor in Suspension Polymerization. *Kagaku Kogaku Ronbunshu*, *9*(1), pp.72-75.

[47] Gökmen, M., 2011. *Complex polymer particles via microfluidics* (Doctoral dissertation, Ghent University).

[48] Petro, M., Svec, F. and Fréchet, J.M., 1996. Molded continuous poly (styrene-co-divinylbenzene) rod as a separation medium for the very fast separation of polymers Comparison of the chromatographic properties of the monolithic rod with columns packed with porous and non-porous beads in high-performance liquid chromatography of polystyrenes. *Journal of Chromatography A*, *752*(1-2), pp.59-66.

[49] Vivaldo-Lima, E., Wood, P.E., Hamielec, A.E. and Penlidis, A., 1997. An updated review on suspension polymerization. *Industrial & engineering chemistry research*, *36*(4), pp.939-965.

[50] Cunningham, M.F., 2008. Controlled/living radical polymerization in aqueous dispersed systems. *Progress in polymer science*, *33*(4), pp.365-398.

[51] Johnson, G.R., 1980. Effects of agitation during VCM suspension polymerization. *Journal of Vinyl Technology*, *2*(3), pp.138-140.

[52] Dowding, P.J., Vincent, B., 2000. Suspension polymerisation to form polymer beads. Colloids and Surfaces A: Physicochemical and Engineering Aspects 161, 259–269.

[53] Jahanzad, F., 2004. Evolution of particle size distribution in suspension polymerisation reactions. Ph.D. Thesis, Loughborough University, Loughborough, UK

[54] Jahanzad, F., Sajjadi, S., Brooks, B.W., 2004. On the evolution of particle size average and size distribution in suspension polymerisation processes. Macromolecular Symposia 206, 255–262.

[55] Nisisako, T., Torii, T. and Higuchi, T., 2004. Novel microreactors for functional polymer beads. *Chemical Engineering Journal*, *101*(1), pp.23-29.

[56] Xu, S., Nie, Z., Seo, M., Lewis, P., Kumacheva, E., Stone, H.A., Garstecki, P., Weibel, D.B., Gitlin, I. and Whitesides, G.M., 2005. Generation of monodisperse particles by using microfluidics: control over size, shape, and composition. *Angewandte Chemie*, *117*(5), pp.734-738.

[57] Dendukuri, D., Pregibon, D.C., Collins, J., Hatton, T.A. and Doyle, P.S., 2006. Continuous-flow lithography for high-throughput microparticle synthesis. *Nature materials*, *5*(5), pp.365-369.

[58] Controlled Synthesis of Nonspherical Microparticles Using Microfluidics

[59] Shim, T.S., Yang, S.M. and Kim, S.H., 2015. Dynamic designing of microstructures by chemical gradient-mediated growth. *Nature communications*, *6*.

[60] Kumacheva, E. and Garstecki, P., 2011. *Microfluidic reactors for polymer particles*. John Wiley & Sons.

[61] Garti, N. and Bisperink, C., 1998. Double emulsions: progress and applications. *Current Opinion in Colloid & Interface Science*, *3*(6), pp.657-667.

[62] Utada, A.S., Lorenceau, E., Link, D.R., Kaplan, P.D., Stone, H.A. & Weitz, D.A. 2005, "Monodisperse double emulsions generated from a microcapillary device", *Science*, vol. 308, no. 5721, pp. 537-541.

[63] Kim, S.H., Kim, J.W., Cho, J.C. and Weitz, D.A., 2011. Double-emulsion drops with ultra-thin shells for capsule templates. *Lab on a Chip*, *11*(18), pp.3162-3166.

[64] Abbaspourrad, A., Carroll, N.J., Kim, S.H. and Weitz, D.A., 2013. Polymer microcapsules with programmable active release. *Journal of the American Chemical Society*, *135*(20), pp.7744-7750.

[65] Chaurasia, A.S., Josephides, D.N. and Sajjadi, S., 2015. Large Ultrathin Shelled Drops Produced via Non-Confined Microfluidics. *ChemPhysChem*, *16*(2), pp.403-411.

[66] Kim, S.H., Hwang, H., Lim, C.H., Shim, J.W. and Yang, S.M., 2011. Packing of Emulsion Droplets: Structural and Functional Motifs for Multi-Cored Microcapsules. *Advanced Functional Materials*, *21*(9), pp.1608-1615.

[67] Zhang, M.J., Wang, W., Yang, X.L., Ma, B., Liu, Y.M., Xie, R., Ju, X.J., Liu, Z. and Chu, L.Y., 2015. Uniform microparticles with controllable highly interconnected hierarchical porous structures. *ACS applied materials & interfaces*, *7*(25), pp.13758-13767.

[68] Wang, J., Cheng, Y., Yu, Y., Fu, F., Chen, Z., Zhao, Y. and Gu, Z., 2015. Microfluidic Generation of Porous Microcarriers for Three-Dimensional Cell Culture. *ACS applied materials & interfaces*, *7*(49), pp.27035-27039.

[69] San Manley, S., Graeber, N., Grof, Z., Menner, A., Hewitt, G.F., Stepanek, F. and Bismarck, A., 2009. New insights into the relationship between internal phase level of emulsion templates and gas–liquid permeability of interconnected macroporous polymers. *Soft Matter*, *5*(23), pp.4780-4787.

[70] Jiang, J.X., Trewin, A., Su, F., Wood, C.D., Niu, H., Jones, J.T., Khimyak, Y.Z. and Cooper, A.I., 2009. Microporous poly (tri (4-ethynylphenyl) amine) networks: synthesis, properties, and atomistic simulation. *Macromolecules*, *42*(7), pp.2658-2666.

[71] Ben, T., Ren, H., Ma, S., Cao, D., Lan, J., Jing, X., Wang, W., Xu, J., Deng, F., Simmons, J.M. and Qiu, S., 2009. Targeted synthesis of a porous aromatic framework with high stability and exceptionally high surface area. *Angewandte Chemie*, *121*(50), pp.9621-9624.

[72] Silverstein, M.S. and Cameron, N.R., 2010. PolyHIPEs—Porous Polymers from High Internal Phase Emulsions. *Encyclopedia of Polymer Science and Technology*.

[73] Carnachan, R.J., Bokhari, M., Przyborski, S.A. and Cameron, N.R., 2006. Tailoring the morphology of emulsion-templated porous polymers. *Soft Matter*, *2*(7), pp.608-616.

[74] Pulko, I. and Krajnc, P., 2012. High internal phase emulsion templating–a path to hierarchically porous functional polymers. *Macromolecular rapid communications*, *33*(20), pp.1731-1746.

[75] Silverstein, M.S., 2014. PolyHIPEs: Recent advances in emulsion-templated porous polymers. *progress in Polymer Science*, *39*(1), pp.199-234.

[76] Bokhari MA, Akay G, Zhang SG, Birch MA. Biomaterials 2005;26:5198-208.

[77] Cameron, N.R. and Sherrington, D.C., 1996. High internal phase emulsions (HIPEs)—structure, properties and use in polymer preparation. In *Biopolymers liquid crystalline polymers phase emulsion* (pp. 163-214). Springer Berlin Heidelberg.

[78] Schacher, F., Ulbricht, M. and Müller, A.H., 2009. Self-Supporting, Double Stimuli-Responsive Porous Membranes From Polystyrene-block-poly (N, N-dimethylaminoethyl methacrylate) Diblock Copolymers. *Advanced Functional Materials*, *19*(7), pp.1040-1045.

[79] Zhang, H. and Cooper, A.I., 2005. Synthesis and applications of emulsion-templated porous materials. *Soft Matter*, *1*(2), pp.107-113.

[80] Livshin, S. and Silverstein, M.S., 2008. Crystallinity and cross-linking in porous polymers synthesized from long side chain monomers through emulsion templating. *Macromolecules*, *41*(11), pp.3930-3938.

[81] Pierre, S.J., Thies, J.C., Dureault, A., Cameron, N.R., van Hest, J.C., Carette, N., Michon, T. and Weberskirch, R., 2006. Covalent enzyme immobilization onto photopolymerized highly porous monoliths. *Advanced Materials*, *18*(14), pp.1822-1826.

[82] Martín, C.F., Stöckel, E.V., Clowes, R., Adams, D.J., Cooper, A.I., Pis, J.J., Rubiera, F. and Pevida, C., 2011. Hypercrosslinked organic polymer networks as potential adsorbents for pre-combustion CO 2 capture. *Journal of Materials Chemistry*, *21*(14), pp.5475-5483.

[83] Trewin, A., Willock, D.J. and Cooper, A.I., 2008. Atomistic simulation of micropore structure, surface area, and gas sorption properties for amorphous microporous polymer networks. *The Journal of Physical Chemistry C*, *112*(51), pp.20549-20559.

[84] Makhseed, S. and Samuel, J., 2008. Hydrogen adsorption in microporous organic framework polymer. *Chemical Communications*, (36), pp.4342-4344.

[85] Budd, P.M., Msayib, K.J., Tattershall, C.E., Ghanem, B.S., Reynolds, K.J., McKeown, N.B. and Fritsch, D., 2005. Gas separation membranes from polymers of intrinsic microporosity. *Journal of Membrane Science*, *251*(1), pp.263-269.

[86] Du, N., Robertson, G.P., Song, J., Pinnau, I., Thomas, S. and Guiver, M.D., 2008. Polymers of intrinsic microporosity containing trifluoromethyl and phenylsulfone groups as materials for membrane gas separation. *Macromolecules*, *41*(24), pp.9656-9662.

[87] Meng, Y., Gu, D., Zhang, F., Shi, Y., Yang, H., Li, Z., Yu, C., Tu, B. and Zhao, D., 2005. Ordered mesoporous polymers and homologous carbon frameworks: amphiphilic surfactant templating and direct transformation. *Angewandte Chemie*, *117*(43), pp.7215-7221.

[88] Kou, Y., Xu, Y., Guo, Z. and Jiang, D., 2011. Supercapacitive Energy Storage and Electric Power Supply Using an Aza-Fused π-Conjugated Microporous Framework. *Angewandte Chemie*, *123*(37), pp.8912-8916.

[89] Liu, R., Cho, S.I. and Lee, S.B., 2008. Poly (3, 4-ethylenedioxythiophene) nanotubes as electrode materials for a high-powered supercapacitor. *Nanotechnology*, *19*(21), p.215710.

[90] Rose, M., Klein, N., Senkovska, I., Schrage, C., Wollmann, P., Böhlmann, W., Böhringer, B., Fichtner, S. and Kaskel, S., 2011. A new route to porous monolithic organic frameworks via cyclotrimerization. *Journal of Materials Chemistry*, *21*(3), pp.711-716.

[91] Svec, F., 2010. Porous polymer monoliths: amazingly wide variety of techniques enabling their preparation. *Journal of Chromatography A*, *1217*(6), pp.902-924.

[92] Zhang, R., Qi, L., Xin, P., Yang, G. and Chen, Y., 2010. Preparation of macroporous monolith with three dimensional bicontinuous skeleton structure by atom transfer radical polymerization for HPLC. *Polymer*, *51*(8), pp.1703-1708.

[93] Cai, Y., Chen, Y., Hong, X., Liu, Z. and Yuan, W., 2013. Porous microsphere and its applications. *International journal of nanomedicine*, *8*, p.1111.

[94] Coutinho, F.M., Neves, M.A.F.S. and Dias, M.L., 1997. Porous structure and swelling properties of styrene-divinylbenzene copolymers for size exclusion chromatography. *Journal of applied polymer science*, *65*(7), pp.1257-1262..

[95] Lovell, P.A. and El-Aasser, M.S. eds., 1997. *Emulsion polymerization and emulsion polymers*. Wiley.

[96] Bovey FA, Kolthoff IM, Medalia AI, Meehan EJ. Emulsion polymerization. New York: Interscience Publishers; 1965.

[97] Smith WV, Ewart RH. Kinetics of emulsion polymerization. J Chem Phys 1948;16:592–9.

[98] Priest WJ. Particle growth in the aqueous polymerization of vinyl acetate. J Phys Chem 1952;56:1077–83.

[99] Roe CP. Surface chemistry aspects of emulsion polymerization. Ind Eng Chem 1968;60:20–33.

[100] Fitch RM, Tsai CH. Particle formation in polymer colloids. III. Prediction of the number of particles by a homogeneous nucleation theory. In: Fitch RM, editor. Polymer colloids. New York: Plenum Press; 1971. p. 73–102.

[101] Fitch RM, Tsai CH. Homogeneous nucleation of polymer colloids. IV. The role of soluble oligomeric radicals. In: Fitch RM, editor. Polymer colloids. New York: Plenum Press; 1971. p. 103–16.

[102] Chen, Y., 2012. Comprehensive study of semicontinuous emulsion polymerisation processes for producing nanoparticles (Doctoral dissertation, King's College London (University of London)).

[103] Bartoň, J. and Capek, I., 1994. *Radical polymerization in disperse systems*. Ellis Horwood Ltd.

[104] Chern CS.,2002. Polymerization of monomer emulsions. In: Hubbard A, editor. Encyclopedia of surface and colloid science. pp. 4220–41.

[105] Sato, T. and Ruch, R., 1980. Stabilization of colloidal dispersions by polymer adsorption. Dekker.

[106] Chern, C.S., 2006. Emulsion polymerization mechanisms and kinetics. *Progress in polymer science*, *31*(5), pp.443-486.

[107] Tauer, K., Deckwer, R., Kühn, I. and Schellenberg, C., 1999. A comprehensive experimental study of surfactant-free emulsion polymerization of styrene. *Colloid & Polymer Science*, *277*(7), pp.607-626.

[108] Wang, Y.M. and Pan, C.Y., 1999. Study of the mechanism of the emulsifier-free emulsion polymerization of the styrene/4-vinylpyridine system. *Colloid & Polymer Science*, *277*(7), pp.658-665.

[109] Wang, Y.M. and Pan, C.Y., 1999. Study of the mechanism of the emulsifier-free emulsion polymerization of the styrene/4-vinylpyridine system. *Colloid & Polymer Science*, *277*(7), pp.658-665.

[110] Ni, H., Ma, G., Nagai, M. and Omi, S., 2001. Effects of ethyl acetate on the soap-free emulsion polymerization of 4-vinylpyridine and styrene. II. Aspects of the mechanism. *Journal of applied polymer science*, *82*(11), pp.2692-2708.

[111] Ou, J.L., Yang, J.K. and Chen, H., 2001. Styrene/potassium persulfate/water systems: effects of hydrophilic comonomers and solvent additives on the nucleation mechanism and the particle size. *European polymer journal*, *37*(4), pp.789-799.

[112] Yan, C.E., Cheng, S. and Feng, L., 1999. Kinetics and mechanism of emulsifier-free emulsion copolymerization: Styrene-methyl methacrylate-acrylic acid system. *Journal of Polymer Science Part A: Polymer Chemistry*, *37*(14), pp.2649-2656.

[113] Mahdavian, A.R. and Abdollahi, M., 2004. Investigation into the effect of carboxylic acid monomer on particle nucleation and growth in emulsifier-free emulsion copolymerization of styrene–butadiene–acrylic acid. *Polymer*, *45*(10), pp.3233-3239.

[114] Vivaldo-Lima, E., Wood, P.E., Hamielec, A.E. and Penlidis, A. An updated review on suspension polymerization. *Ind. Eng. Chem. Res.* 1997, ***36,*** (4), 939-965.

[115] Brooks, B.W. Basic Aspects and Recent Developments in Suspension Polymerisation. *Makromolekulare Chemie-Macromolecular Symposia.* 1990, **35-6** (1), 121-140.

[116] Konno, M., Arai, K., and Saito, S., The Effect of Stabilizer on Coalescence of Dispersed Drops in Suspension Polymerization of Styrene, *J. Chem. Eng. Jpn.*, 1982, **15** (2), 131.

[117] Nikolaeva, V.F., Kazanskaya, V.F., Vinogradskii, V.O., and Usacheva, V.T., Technological Features of Suspension Polymerization of Styrene, *Plastmassy*, **1980**, 6, 11.

[118] Langner, F., Moritz, N.-U., and Reichert, K.-H., Reactor Scale-up for Polymerization in Suspension, *Chem. Eng. Sci.*, 1980, **35** (1-2), 1519.

[119] Ni, X., Zhang, Y., and Mustafa, I., Correlation of Polymer Particle Size with Drop Size in Suspension Polymerization of Methylmethacrylate in a Batch Oscillatory- Baffled Reactor, *Chem. Eng. Sci.*, 1999, **54** (6), 841.

[120] Wang, R., Zhang, Y., Ma, G. and Su, Z. Preparation of uniform poly (glycidyl methacrylate) porous microspheres by membrane emulsification-polymerisation technology. *J. Appl. Polym. Sci.* 2006, **102** (5), 5018-5027.

[121] Ma, G.H., An, C.J., Yuyama, H., Su, Z.G. and Omi, S. Synthesis and characterization of polyurethaneurea-vinyl polymer (PUU-VP) uniform hybrid microspheres by SPG emulsification technique and subsequent suspension polymerisation. *J. Appl. Polym. Sci.*. 2003, **89** (1), pp. 163-178.

[122] Nuisin, R., Omi, S. and Kiatkamjornwong, S. Synthesis and property behavior of dioctyl phthalate plasticized styrene-acrylate particles by Shirasu porous glass

emulsification and subsequent suspension copolymerisation. *J. Appl. Polym. Sci.*. 2003, **90** (11), 3037-3050.

[123] Omi, S. Preparation of monodisperse microspheres using the Shirasu porous glass emulsification technique. *Colloids and Surfaces A: Physicochemical and Engineering Aspects*. 1996 (109), 97-107

[124] Jahanzad, F., Sajjadi, S. and Brooks, B.W. Characteristic intervals in suspension polymerisation reactors: An experimental and modelling study. *Chem. Eng. Sci*. 2005, **60** (20), 5574-5589.

[125] Erbay, E., B [Idot]Lg[Idot]Ç, T., Karali, M. and Savaşçi, Ö.T.,. Polystyrene Suspension Polymerization: The Effect of Polymerization Parameters on Particle Size and Distribution. *Polymer-Plastics Technology and Engineering*, 1992, **31** (7-8), 589-605.

[126] Yang, B., Takahashi, K. and Takeishi, M. Unsteady stirring method staged used in suspension polymerisation of styrene. *J. Appl. Polym. Sci.* 2001, **82** (8), 1873-1881.

[127] Shinnar, R and Church, J.M. "Predicting particle size in agitated dispersions. *Ind. Eng. Chem. Res* 1960, **52** (3), 253-256

[128] Jahanzad, F. and Sajjadi, S. Two-stage stabilizer addition protocol as a means to reduce the size and improve the uniformity of polymer beads in suspension polymerization. *J. Appl. Polym. Sci*. 2017, (134), 1097-4628.

[129] Coulaloglou, CA and Tavlarides, L.L. "Description of interaction processes in agitated Liquid-liquid dispersions. *Chem. Eng. Sci*. 1977, **32** (1), 1289-1297

[130] Liu, S., and Li, D. "Drop coalescence in turbulent dispersions. *Chem. Eng. Sci*. 1999, 54,5667-5675.

[131] Hong, P.O. Lee, J.M. "Changes of the average drop sizes during the initial period of liquid-liquid dispersions in agitated vessels. *Ind. Eng. Chem. Res.* 1985, **24**, 868-872.

[132] Alroaithi, M. and Sajjadi, S. Uniform polymer beads by membrane emulsification-assisted suspension polymerisation. *RSC Advances*. 2016 *6* (83), 79745-79754.

[133] Yao, W.G., Sato, H., Takahashi, K. and Koyama, K., 1998. Mixing performance experiments in impeller stirred tanks subjected to unsteady rotational speeds. *Chem. Eng. Sci*. 1996, ***53*** (17), 3031-3040.

[134] Ogawa, K., Kuroda, C., Mizumori, H. and Yoshikawa, S. Effects of unsteady agitation by reversing revolution of an impeller in an agitated vessel with aeration. *Kagaku Kogaku Ronbunshu*. 1996, ***22***, 91-97.

[135] Rajapakse, A., Parthasarathy, R. and Bhattacharya, S.N. Effect of dispersed phase volume fraction on drop size distribution in a stirred reactor. In *Chemeca 2004: 32nd Australasian Chemical Engineering Conference: Sustainable Processes* (p. 59). Engineers Australia.

[136] Jahanzad, F., Sajjadi, S., Yianneskis, M. and Brooks, B.W. In situ mass-suspension polymerisation. *Chem. Eng. Sci*. 2008, **63** (17), 4412-4417.

[137] Tanaka, M., 1989. Effect of Sudden Reduction of Impeller Speed on Particle Size Distribution in Suspension Polymerization of Styrene. *Journal Of Chemical Engineering Of Japan*, *22*(5), pp.559-561.

[138] Olayo, R., Garcia, E., Garcia-Corichi, B., Sanchez-Vazquez, L. and Alvarez, J., 1998. Poly (vinyl alcohol) as a Stabilizer in the Suspension Polymerization of Styrene: The Effect of the Molecular Weight. *Journal of applied polymer science*, *67*(1), pp.71-77.

[139] Sinnott, R.K., 1999. Coulson & Richardson's Chemical Enginering: Volume 6/Chemical Engineering Design. Elsevier Butterworth Heinemann.

[140]Maaß, S., Metz, F., Rehm, T. and Kraume, M., 2010. Prediction of drop sizes for liquid–liquid systems in stirred slim reactors—Part I: Single stage impellers. *Chemical Engineering Journal*, *162*(2), pp.792-801.

[141] Uchida, T., Shiosaki, K., Nakada, Y., Fukada, K., Eda, Y., Tokiyoshi, S., Nagareya, N. and Matsuyama, K., 1998. Microencapsulation of hepatitis B core antigen for vaccine preparation. *Pharmaceutical research*, *15*(11), pp.1708-1713.

[142] Cleland, J.L., Lim, A., Daugherty, A., Barron, L., Desjardin, N., Duenas, E.T., Eastman, D.J., Vennari, J.C., Wrin, T., Berman, P. and Murthy, K.K., 1998. Development of a single-shot subunit vaccine for HIV-1. 5. Programmable in vivo autoboost and long lasting neutralizing response. *Journal of pharmaceutical sciences*, *87*(12), pp.1489-1495.

[143] Brahim, S., Narinesingh, D. and Guiseppi-Elie, A., 2002. Kinetics of glucose oxidase immobilized in p (HEMA)-hydrogel microspheres in a packed-bed bioreactor. *Journal of Molecular Catalysis B: Enzymatic*, *18*(1), pp.69-80.

[144] M. Tang, X.J. Cao, Z.Z. Liu, X.Y. Wu, and D. Gance, 1999, 34, 857-862.

[145] Mitragotri, S. and Lahann, J., 2009. Physical approaches to biomaterial design. *Nature materials*, *8*(1), pp.15-23.

[146] B.W. Brooks, Angew. Makromol. Chem., 1990, 35-6, 121-140.

[147] Vivaldo-Lima, E., Wood, P.E., Hamielec, A.E. and Penlidis, A., 1997. An updated review on suspension polymerization. *Industrial & engineering chemistry research*, *36*(4), pp.939-965.

[148] J. Alvarez, and R.E. Martinez, J Appl Polym Sci., 1999, 209–221.

[149] Dowding, P.J., Goodwin, J.W. and Vincent, B., 2001. Production of porous suspension polymer beads with a narrow size distribution using a cross-flow membrane and a continuous tubular reactor. *Colloids and Surfaces A: Physicochemical and Engineering Aspects*, *180*(3), pp.301-309.

[150] Konno, M., Arai, K. and SAITO, S., 1982. The effect of stabilizer on coalescence of dispersed drops in suspension polymerization of styrene. *Journal of Chemical Engineering of Japan*, *15*(2), pp.131-135.

[151] Maggioris, D., Goulas, A., Alexopoulos, A.H., Chatzi, E.G. and Kiparissides, C., 2000. Prediction of particle size distribution in suspension polymerization reactors: effect of turbulence nonhomogeneity. *Chemical Engineering Science*, *55*(20), pp.4611-4627.

[152] Jahanzad, F., Sajjadi, S. and Brooks, B.W., 2005. Comparative Study of Particle Size in Suspension Polymerization and Corresponding Monomer− Water Dispersion. *Industrial & engineering chemistry research*, *44*(11), pp.4112-4119.

[153] Joscelyne, S.M. and Trägårdh, G., 2000. Membrane emulsification—a literature review. *Journal of Membrane Science*, *169*(1), pp.107-117.

[154] Kosvintsev, S.R., Gasparini, G., Holdich, R.G., Cumming, I.W. and Stillwell, M.T., 2005. Liquid− Liquid Membrane Dispersion in a Stirred Cell with and without Controlled Shear. *Industrial & engineering chemistry research*, *44*(24), pp.9323-9330.

[155] Vladisavljević, G.T., Kobayashi, I. and Nakajima, M., 2012. Production of uniform droplets using membrane, microchannel and microfluidic emulsification devices. *Microfluidics and nanofluidics*, *13*(1), pp.151-178.

[156] Kosvintsev, S.R., Gasparini, G. and Holdich, R.G., 2008. Membrane emulsification: droplet size and uniformity in the absence of surface shear. *Journal of Membrane Science*, *313*(1), pp.182-189.

[157] Peng, S.J. and Williams, R.A., 1998. Controlled production of emulsions using a crossflow membrane: Part I: Droplet formation from a single pore. *Chemical Engineering Research and Design*, *76*(8), pp.894-901.

[158] Vladisavljević, G.T. and Schubert, H., 2003. Influence of process parameters on droplet size distribution in SPG membrane emulsification and stability of prepared emulsion droplets. *Journal of Membrane Science*, *225*(1), pp.15-23.

[159] Wang, R., Zhang, Y., Ma, G. and Su, Z., 2006. Preparation of uniform poly (glycidyl methacrylate) porous microspheres by membrane emulsification–polymerization technology. *Journal of applied polymer science*, *102*(5), pp.5018-5027.

[160] Ma, G.H., An, C.J., Yuyama, H., Su, Z.G. and Omi, S., 2003. Synthesis and characterization of polyurethaneurea–vinyl polymer (PUU–VP) uniform hybrid microspheres by SPG emulsification technique and subsequent suspension polymerization. *Journal of applied polymer science*, *89*(1), pp.163-178.

[161] Nuisin, R., Omi, S. and Kiatkamjornwong, S., 2003. Synthesis and property behavior of dioctyl phthalate plasticized styrene–acrylate particles by Shirasu porous glass emulsification and subsequent suspension copolymerization. *Journal of applied polymer science*, *90*(11), pp.3037-3050.

[162] Omi, S., 1996. Preparation of monodisperse microspheres using the Shirasu porous glass emulsification technique. *Colloids and Surfaces A: Physicochemical and Engineering Aspects*, *109*, pp.97-107.

[163] Kobayashi, I., Yasuno, M., Iwamoto, S., Shono, A., Satoh, K. and Nakajima, M., 2002. Microscopic observation of emulsion droplet formation from a polycarbonate membrane. *Colloids and Surfaces A: Physicochemical and Engineering Aspects*, *207*(1), pp.185-196.

[164] Schröder, V., Behrend, O. and Schubert, H., 1998. Effect of dynamic interfacial tension on the emulsification process using microporous, ceramic membranes. *Journal of Colloid and Interface Science*, *202*(2), pp.334-340.

[165] Kandori, K., Kishi, K. and Ishikawa, T., 1991. Formation mechanisms of monodispersed W/O emulsions by SPG filter emulsification method. *Colloids and surfaces*, *61*, pp.269-279.

[166] Kandori, K., Kishi, K. and Ishikawa, T., 1991. Preparation of monodispersed W/O emulsions by Shirasu-porous-glass filter emulsification technique. *Colloids and surfaces*, *55*, pp.73-78.

[167] Yuyama, H., Watanabe, T., Ma, G.H., Nagai, M. and Omi, S., 2000. Preparation and analysis of uniform emulsion droplets using SPG membrane emulsification technique. *Colloids and Surfaces A: Physicochemical and Engineering Aspects*, *168*(2), pp.159-174.

[168] Zerfa, M. and Brooks, B.W., 1996. Prediction of vinyl chloride drop sizes in stabilised liquid-liquid agitated dispersion. *Chemical Engineering Science*, *51*(12), pp.3223-3233.

[169] Cheremisinoff, P., 1997. Handbook of engineering polymeric materials. CRC Press.

[170] Dowding, P.J. and Vincent, B., 2000. Suspension polymerisation to form polymer beads. *Colloids and Surfaces A: Physicochemical and Engineering Aspects*, *161*(2), pp.259-269.

[171] San Manley, S., Graeber, N., Grof, Z., Menner, A., Hewitt, G.F., Stepanek, F. and Bismarck, A., 2009. New insights into the relationship between internal phase level of emulsion templates and gas–liquid permeability of interconnected macroporous polymers. *Soft Matter*, *5*(23), pp.4780-4787.

[172] Jiang, J.X., Trewin, A., Su, F., Wood, C.D., Niu, H., Jones, J.T., Khimyak, Y.Z. and Cooper, A.I., 2009. Microporous poly (tri (4-ethynylphenyl) amine) networks: synthesis, properties, and atomistic simulation. *Macromolecules*, *42*(7), pp.2658-2666.

[173] Ben, T., Ren, H., Ma, S., Cao, D., Lan, J., Jing, X., Wang, W., Xu, J., Deng, F., Simmons, J.M. and Qiu, S., 2009. Targeted synthesis of a porous aromatic framework with high stability and exceptionally high surface area. *Angewandte Chemie*, *121*(50), pp.9621-9624.

[174] Schacher, F., Ulbricht, M. and Müller, A.H., 2009. Self-Supporting, Double Stimuli-Responsive Porous Membranes From Polystyrene-block-poly (N, N-dimethylaminoethyl methacrylate) Diblock Copolymers. *Advanced Functional Materials*, *19*(7), pp.1040-1045.

[175] Zhang, H. and Cooper, A.I., 2005. Synthesis and applications of emulsion-templated porous materials. *Soft Matter*, *1*(2), pp.107-113.

[176] Livshin, S. and Silverstein, M.S., 2008. Crystallinity and cross-linking in porous polymers synthesized from long side chain monomers through emulsion templating. *Macromolecules*, *41*(11), pp.3930-3938.

[177] Pierre, S.J., Thies, J.C., Dureault, A., Cameron, N.R., van Hest, J.C., Carette, N., Michon, T. and Weberskirch, R., 2006. Covalent enzyme immobilization onto photopolymerized highly porous monoliths. *Advanced Materials*, *18*(14), pp.1822-1826.

[178] Martín, C.F., Stöckel, E.V., Clowes, R., Adams, D.J., Cooper, A.I., Pis, J.J., Rubiera, F. and Pevida, C., 2011. Hypercrosslinked organic polymer networks as potential adsorbents for pre-combustion CO 2 capture. *Journal of Materials Chemistry*, *21*(14), pp.5475-5483.

[179] Trewin, A., Willock, D.J. and Cooper, A.I., 2008. Atomistic simulation of micropore structure, surface area, and gas sorption properties for amorphous microporous polymer networks. *The Journal of Physical Chemistry C*, *112*(51), pp.20549-20559.

[180] Makhseed, S. and Samuel, J., 2008. Hydrogen adsorption in microporous organic framework polymer. *Chemical Communications*, (36), pp.4342-4344.

[181] Budd, P.M., Msayib, K.J., Tattershall, C.E., Ghanem, B.S., Reynolds, K.J., McKeown, N.B. and Fritsch, D., 2005. Gas separation membranes from polymers of intrinsic microporosity. *Journal of Membrane Science*, *251*(1), pp.263-269.

[182] Rose, M., Klein, N., Senkovska, I., Schrage, C., Wollmann, P., Böhlmann, W., Böhringer, B., Fichtner, S. and Kaskel, S., 2011. A new route to porous monolithic organic frameworks via cyclotrimerization. *Journal of Materials Chemistry*, *21*(3), pp.711-716.

[183] Svec, F., 2010. Porous polymer monoliths: amazingly wide variety of techniques enabling their preparation. *Journal of Chromatography A*, *1217*(6), pp.902-924.

[184] Cai, Y., Chen, Y., Hong, X., Liu, Z. and Yuan, W., 2013. Porous microsphere and its applications. *International journal of nanomedicine*, *8*, p.1111.

[185] Coutinho, F.M., Neves, M.A.F.S. and Dias, M.L., 1997. Porous structure and swelling properties of styrene-divinylbenzene copolymers for size exclusion chromatography. *Journal of applied polymer science*, *65*(7), pp.1257-1262.

[186] De La Vega, J.C., Elischer, P., Schneider, T. and Häfeli, U.O., 2013. Uniform polymer microspheres: monodispersity criteria, methods of formation and applications. *Nanomedicine*, *8*(2), pp.265-285.

[187] Xu, Q., Hashimoto, M., Dang, T.T., Hoare, T., Kohane, D.S., Whitesides, G.M., Langer, R. and Anderson, D.G., 2009. Preparation of monodisperse biodegradable polymer microparticles using a microfluidic flow-focusing device for controlled drug delivery. *Small*, *5*(13), pp.1575-1581.

[188] Gokmen, M.T., Dereli, B., De Geest, B.G. and Du Prez, F.E., 2013. Complexity from simplicity: Unique polymer capsules, rods, monoliths, and liquid marbles prepared via HIPE in microfluidics. *Particle & Particle Systems Characterization*, *30*(5), pp.438-444.

[189] Zhang, M.J., Wang, W., Yang, X.L., Ma, B., Liu, Y.M., Xie, R., Ju, X.J., Liu, Z. and Chu, L.Y., 2015. Uniform microparticles with controllable highly interconnected hierarchical porous structures. *ACS applied materials & interfaces*, *7*(25), pp.13758-13767.

[190] Wang, J., Cheng, Y., Yu, Y., Fu, F., Chen, Z., Zhao, Y. and Gu, Z., 2015. Microfluidic Generation of Porous Microcarriers for Three-Dimensional Cell Culture. *ACS applied materials & interfaces*, *7*(49), pp.27035-27039.

[191] Shum, H.C., Abate, A.R., Lee, D., Studart, A.R., Wang, B., Chen, C.H., Thiele, J., Shah, R.K., Krummel, A. and Weitz, D.A., 2010. Droplet microfluidics for fabrication of non-spherical particles. *Macromolecular rapid communications*, *31*(2), pp.108-118.

[192] Xu, S., Nie, Z., Seo, M., Lewis, P., Kumacheva, E., Stone, H.A., Garstecki, P., Weibel, D.B., Gitlin, I. and Whitesides, G.M., 2005. Generation of monodisperse particles by using microfluidics: control over size, shape, and composition. *Angewandte Chemie*, *117*(5), pp.734-738.

[193] Donev, A., Cisse, I., Sachs, D., Variano, E.A., Stillinger, F.H., Connelly, R., Torquato, S. and Chaikin, P.M., 2004. Improving the density of jammed disordered packings using ellipsoids. *Science*, *303*(5660), pp.990-993.

[194] Yamamoto, S. and Matsuoka, T., 1994. Viscosity of dilute suspensions of rodlike particles: A numerical simulation method. *The Journal of chemical physics*, *100*(4), pp.3317-3324.

[195] Hwang, D.K., Dendukuri, D. and Doyle, P.S., 2008. Microfluidic-based synthesis of non-spherical magnetic hydrogel microparticles. *Lab on a Chip*, *8*(10), pp.1640-1647.

[196] Gupta, S., Zhang, Q., Emrick, T. and Russell, T.P., 2006. "Self-corralling" nanorods under an applied electric field. *Nano letters*, *6*(9), pp.2066-2069.

[197] Glotzer, S.C. and Solomon, M.J., 2007. Anisotropy of building blocks and their assembly into complex structures. *Nature materials*, *6*(8), pp.557-562.

[198] Chaurasia, A.S., Josephides, D.N. and Sajjadi, S., 2015. Large Ultrathin Shelled Drops Produced via Non-Confined Microfluidics. *ChemPhysChem*, *16*(2), pp.403-411.

[199] Khan, I.U., Stolch, L., Serra, C.A., Anton, N., Akasov, R. and Vandamme, T.F., 2015. Microfluidic conceived pH sensitive core–shell particles for dual drug delivery. *International journal of pharmaceutics*, *478*(1), pp.78-87.

[200] Kim, S.H., Hwang, H., Lim, C.H., Shim, J.W. and Yang, S.M., 2011. Packing of Emulsion Droplets: Structural and Functional Motifs for Multi-Cored Microcapsules. *Advanced Functional Materials*, *21*(9), pp.1608-1615.

[201] Guzowski, J. and Garstecki, P., 2015. Droplet clusters: Exploring the phase space of soft mesoscale atoms. *Physical review letters*, *114*(18), p.188302.

[202] Cameron, N.R., Sherrington, D.C., Albiston, L. and Gregory, D.P., 1996. Study of the formation of the open-cellular morphology of poly (styrene/divinylbenzene) polyHIPE materials by cryo-SEM. *Colloid & Polymer Science*, *274*(6), pp.592-595.

[203] Teich, E.G., van Anders, G., Klotsa, D., Dshemuchadse, J. and Glotzer, S.C., 2016. Clusters of polyhedra in spherical confinement. *Proceedings of the National Academy of Sciences*, *113*(6), pp.E669-E678.

[204] Fleischmann, E.K., Liang, H.L., Kapernaum, N., Giesselmann, F., Lagerwall, J. and Zentel, R., 2012. One-piece micropumps from liquid crystalline core-shell particles. *Nature communications*, *3*, p.1178.

[205] Lissant KJ, editor. Emulsions and emulsion technology part 1. New York: Marcel Dekker Inc.; 1974.

[206] Bamfield HA, Copper J. In: Becher P, Dekker Marcel, editors. In Encyclopedia of emulsion tech, vol. 3; 1988. p. 281e306. New York.

[207] Silverstein MS, Cameron NR. PolyHIPEs – porous polymers fromhigh internal phase emulsions. In: Encyclopedia of polymer sci-ence and technology. New York: John Wiley & Sons; 2010,

[208] Cooper AI, Bray CL, Su F, Carter BO, Wang W, Adams DJ. Clathratesfor gas storage in the presence of emulsion-templated porous sup-port. WO 2009 068912, Ulive Enterprises Limited, UK, 2009

[209] Jonschker G, Koch M, Pahnke J, Schwab M. Monolithic polymermaterials for gas storage. WO 2009 095153, Merck Patent GmbH,Germany, 2009.

[210] Tailoring the morphology of emulsion-templated porous polymers Ross J. Carnachan,a Maria Bokhari,ab Stefan A. Przyborskibc and Neil R. Cameron*a

[211] High Internal Phase Emulsion Templating A Path To Hierarchically Porous Functional Polymers Irena Pulko , Peter Krajnc

[212] D. Barby and Z. Haq, Eur. Pat. Appl., 1982, 60138; N. R. Cameron and D. C. Sherrington, Adv. Polym. Sci., 1996, 126, 163; N. R. Cameron, Polymer, 2005, 46, 1439; H. Zhang and A. I. Cooper, Soft Matter, 2005, 1, 107.

[213] Silverstein, M.S., 2014. PolyHIPEs: Recent advances in emulsion-templated porous polymers. *progress in Polymer Science*, *39*(1), pp.199-234.

[214] Krajnc, P., Leber, N., Štefanec, D., Kontrec, S. and Podgornik, A., 2005. Preparation and characterisation of poly (high internal phase emulsion) methacrylate monoliths and their application as separation media. *Journal of Chromatography A*, *1065*(1), pp.69-73.Peter

[215] Zhang, S., Chen, J. and Perchyonok, V.T., 2009. Stability of high internal phase emulsions with sole cationic surfactant and its tailoring morphology of porous polymers based on the emulsions. *Polymer*, *50*(7), pp.1723-1731.

[216] He, H., Li, W., Lamson, M., Zhong, M., Konkolewicz, D., Hui, C.M., Yaccato, K., Rappold, T., Sugar, G., David, N.E. and Damodaran, K., 2014. Porous polymers prepared via high internal phase emulsion polymerization for reversible CO 2 capture. *Polymer*, *55*(1), pp.385-394.

[217] Costantini, M., Colosi, C., Guzowski, J., Barbetta, A., Jaroszewicz, J., Święszkowski, W., Dentini, M. and Garstecki, P., 2014. Highly ordered and tunable polyHIPEs by using microfluidics. *Journal of Materials Chemistry B*, *2*(16), pp.2290-2300.

[218] Elsing, J., Stefanov, T., Gilchrist, M.D. and Stubenrauch, C., 2017. Monodisperse polystyrene foams via polymerization of foamed emulsions: structure and mechanical properties. *Physical Chemistry Chemical Physics*, *19*(7), pp.5477-5485.

[219] Quell, A., Elsing, J., Drenckhan, W. and Stubenrauch, C., 2015. Monodisperse Polystyrene Foams via Microfluidics–A Novel Templating Route. *Advanced Engineering Materials*, *17*(5), pp.604-609.

[220] Costantini, M., Colosi, C., Mozetic, P., Jaroszewicz, J., Tosato, A., Rainer, A., Trombetta, M., Święszkowski, W., Dentini, M. and Barbetta, A., 2016. Correlation between porous texture and cell seeding efficiency of gas foaming and microfluidic foaming scaffolds. *Materials Science and Engineering: C*, *62*, pp.668-677.

[221] Choi, J.S., Chun, B.C. and Lee, S.J., 2003. Effect of rubber on microcellular structures from high internal phase emulsion polymerization. *Macromolecular research*, *11*(2), pp.104-109.

[222] Cameron, N.R. and Sherrington, D.C., 1996. High internal phase emulsions (HIPEs)—structure, properties and use in polymer preparation. In *Biopolymers liquid crystalline polymers phase emulsion* (pp. 163-214). Springer Berlin Heidelberg.

[223] San Manley, S., Graeber, N., Grof, Z., Menner, A., Hewitt, G.F., Stepanek, F. and Bismarck, A., 2009. New insights into the relationship between internal phase level of emulsion templates and gas–liquid permeability of interconnected macroporous polymers. *Soft Matter*, *5*(23), pp.4780-4787.

[224] Wu, R., Menner, A. and Bismarck, A., 2010. Tough interconnected polymerized medium and high internal phase emulsions reinforced by silica particles. *Journal of Polymer Science Part A: Polymer Chemistry*, *48*(9), pp.1979-1989.

[225] Menner, A., Verdejo, R., Shaffer, M. and Bismarck, A., 2007. Particle-stabilized surfactant-free medium internal phase emulsions as templates for porous nanocomposite materials: poly-pickering-foams. *Langmuir*, *23*(5), pp.2398-2403.

[226] Tadros, T.F., Vandamme, A., Levecke, B., Booten, K. and Stevens, C.V., 2004. Stabilization of emulsions using polymeric surfactants based on inulin. *Advances in colloid and interface science*, *108*, pp.207-226.

[227] Nunes, J.K., Tsai, S.S.H., Wan, J. and Stone, H.A., 2013. Dripping and jetting in microfluidic multiphase flows applied to particle and fibre synthesis. *Journal of physics D: Applied physics*, *46*(11), p.114002.

[228] Cameron, N.R., Sherrington, D.C., Albiston, L. and Gregory, D.P., 1996. Study of the formation of the open-cellular morphology of poly (styrene/divinylbenzene) polyHIPE materials by cryo-SEM. *Colloid & Polymer Science*, *274*(6), pp.592-595.

[229] Cameron, N.R., Sherrington, D.C., Albiston, L. and Gregory, D.P., 1996. Study of the formation of the open-cellular morphology of poly (styrene/divinylbenzene) polyHIPE materials by cryo-SEM. *Colloid & Polymer Science*, *274*(6), pp.592-595.

[230] Cameron, N.R., 2005. High internal phase emulsion templating as a route to well-defined porous polymers. *Polymer*, *46*(5), pp.1439-1449.

[231] Menner, A. and Bismarck, A., 2006, October. New evidence for the mechanism of the pore formation in polymerising high internal phase emulsions or why polyHIPEs have an interconnected pore network structure. In *Macromolecular symposia* (Vol. 242, No. 1, pp. 19-24). WILEY-VCH Verlag.

[232] Williams, J.M., 1988. Toroidal microstructures from water-in-oil emulsions. *Langmuir*, *4*(1), pp.44-49.

[233] Williams, J.M. and Wrobleski, D.A., 1988. Spatial distribution of the phases in water-in-oil emulsions. Open and closed microcellular foams from cross-linked polystyrene. *Langmuir*, *4*(3), pp.656-662.

[234] Williams, J.M., Gray, A.J. and Wilkerson, M.H., 1990. Emulsion stability and rigid foams from styrene or divinylbenzene water-in-oil emulsions. *Langmuir*, *6*(2), pp.437-444.

[235] Williams, J.M., 1991. High internal phase water-in-oil emulsions: influence of surfactants and cosurfactants on emulsion stability and foam quality. *Langmuir*, *7*(7), pp.1370-1377.

[236] Goodwin, J.W., Ottewill, R.H., Pelton, R., Vianello, G. and Yates, D.E., 1978. Control of particle size in the formation of polymer latices. *Polymer International*, *10*(3), pp.173-180.

[237] Goodall, A.R., Wilkinson, M.C. and Hearn, J., 1977. Mechanism of emulsion polymerization of styrene in soap-free systems. *Journal of polymer science: Polymer chemistry edition*, *15*(9), pp.2193-2218.

[238] Hearn, J., Wilkinson, M.C., Goodall, A.R. and Chainey, M., 1985. Kinetics of the surfactant-free emulsion polymerization of styrene:-The post nucleation stage. *Journal of Polymer Science: Polymer Chemistry Edition*, *23*(7), pp.1869-1883.

[239] Zou, D., Derlich, V., Gandhi, K., Park, M., Sun, L., Kriz, D., Lee, Y.D., Kim, G., Aklonis, J.J. and Salovey, R., 1990. Model filled polymers. I. Synthesis of crosslinked monodisperse polystyrene beads. *Journal of Polymer Science Part A: Polymer Chemistry*, *28*(7), pp.1909-1921.

[240] Van den Hul, H.J. and Vanderhoff, J.W., 1972. The characterization of latex particle surfaces by ion exchange and conductometric titration. *Journal of Electroanalytical Chemistry and Interfacial Electrochemistry*, *37*(1), pp.161-182.

[241] Stevens, R.W., 1965. Agglutination of Reiter Protein-Coated Latex Particles. *American Journal of Clinical Pathology*, *43*(5), pp.490-93.

[242] Hansen, F.K., Ugelstad, J. and Piirma, I., 1982. Emulsion polymerization. *Piirma, I., Ed*, p.51.

[243] Kim, S.H., Lee, S.Y., Yang, S.M. and Yi, G.R., 2011. Self-assembled colloidal structures for photonics. *NPG Asia Materials*, *3*(1), pp.25-33.

[244] Sajjadi, S., 2015. Extending the limits of emulsifier-free emulsion polymerization to achieve small uniform particles. *RSC Advances*, *5*(72), pp.58549-58560.

[245] Song, Z. and Poehlein, G.W., 1990. Kinetics of emulsifier-free emulsion polymerization of styrene. *Journal of Polymer Science Part A: Polymer Chemistry*, *28*(9), pp.2359-2392.

[246] Tanrisever, T., Okay, O. and Soenmezoğlu, I.C., 1996. Kinetics of emulsifier-free emulsion polymerization of methyl methacrylate. *Journal of applied polymer science*, *61*(3), pp.485-493.

[247] Hill, D.J.T. and O'Donnell, J.H., 1984. The dead-end polymerization experiment: A modified treatment. *J. Chem. Educ*, *61*(10), p.881.

[248] Litt, M., Patsiga, R. and Stannett, V., 1970. Emulsion polymerization of vinyl acetate. II. *Journal of Polymer Science Part A-1: Polymer Chemistry*, *8*(12), pp.3607-3649.

[249] Kim, J.H., Chainey, M., El-Aasser, M.S. and Vanderhoff, J.W., 1992. Emulsifier-free emulsion copolymerization of styrene and sodium styrene sulfonate. *Journal of Polymer Science Part A: Polymer Chemistry*, *30*(2), pp.171-183..

[250] Juang, M.S.D. and Krieger, I.M., 1976. Emulsifier-free emulsion polymerization with ionic comonomer. *Journal of Polymer Science: Polymer Chemistry Edition*, *14*(9), pp.2089-2107.

[251] Sajjadi, S. and Yianneskis, M., 2004, February. Analysis of particle formation under monomer-starved conditions in emulsion polymerization reactors. In *Macromolecular Symposia* (Vol. 206, No. 1, pp. 201-214). WILEY-VCH Verlag.

[252] Homola, A.M., Inoue, M. and Robertson, A.A., 1975. Experiments with soap-free polymerization of styrene in the presence of alcohols. *Journal of Applied Polymer Science*, *19*(11), pp.3077-3086.

[253] J. Laaksonen, K. Nurmi, P. Stenius et al., *Kern.-Kemi*, *5* (1978) 143.

[254] Okubo, M., Yamada, A., Shibao, S., Nakamae, K. and Matsumoto, T., 1981. Studies on suspension and emulsion. XLVI. Emulsifier-free emulsion polymerization of styrene in acetone–water. *Journal of Applied Polymer Science*, *26*(5), pp.1675-1679.

[255] Camli, S.T., Buyukserin, F., Balci, O. and Budak, G.G., 2010. Size controlled synthesis of sub-100nm monodisperse poly (methylmethacrylate) nanoparticles using surfactant-free emulsion polymerization. *Journal of colloid and interface science*, *344*(2), pp.528-532.

[256] Liu, Z. and Xiao, H., 2000. Soap-free emulsion copolymerisation of styrene with cationic monomer: effect of ethanol as a cosolvent. *Polymer*, *41*(19), pp.7023-7031.

[257] OU, J.L., YANG, J.K. and CHEN, H., 2001. Styrene/potassium persulfate/water systems: effects of hydrophilic comonomers and solvent additives on the nucleation mechanism and the particle size. *European Polymer Journal*, 37(4), pp. 789-799.

[258] Ngai, T. and Wu, C., 2005. Double roles of stabilization and destabilization of initiator potassium persulfate in surfactant-free emulsion polymerization of styrene under microwave irradiation. *Langmuir*, *21*(18), pp.8520-8525.

[259] Kim, G., Lim, S., Lee, B.H., Shim, S.E. and Choe, S., 2010. Effect of homogeneity of methanol/water/monomer mixture on the mode of polymerization of MMA: soap-free

emulsion polymerization versus dispersion polymerization. *Polymer*, *51*(5), pp.1197-1205.

[260] Bao, J. and Zhang, A., 2004. Poly (methyl methacrylate) nanoparticles prepared through microwave emulsion polymerization. *Journal of applied polymer science*, *93*(6), pp.2815-2820.

[261] An, Z., Tang, W., Hawker, C.J. and Stucky, G.D., 2006. One-step microwave preparation of well-defined and functionalized polymeric nanoparticles. Journal of the American Chemical Society, 128(47), pp.15054-15055.

[262] Tauer, K., Hernandez, H., Kozempel, S., Lazareva, O. and Nazaran, P., 2008. Towards a consistent mechanism of emulsion polymerization—new experimental details. Colloid and polymer science, 286(5), pp.499-515.

[263] Fitch, R.M., Palmgren, T.H., Aoyagi, T. and Zuikov, A., 1984. Kinetics of particle nucleation and growth in the emulsion polymerization of acrylic monomers. *Die Angewandte makromolekulare Chemie*, *123*(1), pp.261-283.

[264] Fitch, R.M., Palmgren, T.H., Aoyagi, T. and Zuikov, A., 1985, January. Kinetics of particle nucleation and growth in the emulsion polymerization of acrylic monomers. In *Journal of Polymer Science: Polymer Symposia* (Vol. 72, No. 1, pp. 221-224). Wiley Subscription Services, Inc., A Wiley Company.

[265] Yan, C.E., Cheng, S. and Feng, L., 1999. Kinetics and mechanism of emulsifier-free emulsion copolymerization: Styrene-methyl methacrylate-acrylic acid system. *Journal of Polymer Science Part A: Polymer Chemistry*, *37*(14), pp.2649-2656.

[266] Aslamazova, T.R., 1995. Emulsifier-free latexes and polymers on their base. *Progress in Organic Coatings*, *25*(2), pp.109-167.